THE UNIVERSITY OF CHICAGO

RESTORING THE SENSE OF TOUCH WITH ELECTRICAL STIMULATION OF THE NERVE AND BRAIN

A DISSERTATION SUBMITTED TO
THE FACULTY OF THE DIVISION OF THE BIOLOGICAL SCIENCES
AND THE PRITZKER SCHOOL OF MEDICINE
IN CANDIDACY FOR THE DEGREE OF
DOCTOR OF PHILOSOPHY

COMMITTEE ON COMPUTATIONAL NEUROSCIENCE

BY
THIERRI CALLIER

CHICAGO, ILLINOIS
DECEMBER 2021

Table of Contents

List of Figures

List of Tables

Acknowledgments

Advisor

Sliman Bensmaia

Thesis Committee

John Maunsell

Nicho Hatsopoulos

Lee Miller

Abstract

Prosthetic limbs controlled with brain-machine interfaces have the potential to confer to patients with tetraplegia the ability to physically interact with the world and regain a level of independence, but the dexterity of prosthetic hands is severely limited without sensory feedback. Accordingly, efforts are underway to restore tactile sensation through prosthetic limbs. Current attempts to convey sensory feedback focus on conveying basic information about object interactions to support simple manual behaviors such as grasping. This includes which part of the hand is touching the object, how much pressure is exerted, and when contact occurs. To convey information about the object itself – its texture and compliance for example – would improve the dexterity of bionic hands, but it is much more challenging. One of the principles that guides sensory encoding algorithms is that of biomimicry: to the extent that the patterns of neuronal activation elicited through electrical stimulation mimic natural patterns, the resulting sensations will be natural and thus intuitive. General principles of tactile neural coding can be invoked to produce patterns that are as natural as possible. One unresolved coding principle is whether spike timing in the central nervous system shapes tactile sensations. Neurons throughout the nervous system exhibit patterns of activation that contain information not only in the strength of their response but also in the distribution of spikes across time at single-digit millisecond time scales, and it has proven extremely difficult to disentangle the effects of spike timing and rate. The objective of the study presented in chapter 2 was to assess the degree to which spike timing shapes pitch perception. To this end, we trained monkeys to discriminate the frequency of vibrations delivered to the skin while we recorded the responses of neurons in somatosensory cortex (SC). To disentangle the contribution of rate and timing to frequency perception, we varied the amplitude of the vibrations such that the firing rates of the SC response – and the intensity of the stimulus – would vary independently of the behaviorally relevant parameter, frequency. We found that a rate-based code could not account for the ability to discriminate

frequency, implicating phase-locking in pitch perception. We conclude that temporal spiking patterns play a key role in tactile pitch perception, and that the temporal patterning of ICMS pulses could, in principle, be manipulated to shape artificial touch. However, whether the manipulations of ICMS temporal patterning will result in interpretable sensations is unclear. This question can be addressed empirically by studying the perceptual correlates of ICMS timing. Chapter 3 presents a behavioral assessment of the perceptual effects of stimulation frequency in SC. The results show that animals can discriminate ICMS frequency despite concomitant and uninformative variations in amplitude, demonstrating that frequency has a distinct impact on sensation from amplitude. These experiments add to a growing body of evidence showing that temporal spiking patterns in somatosensory cortex shape tactile perception. Accordingly, modulation of pulse timing – which in turn shapes spike timing in the activated population – can be used to convey stimulus information in a biomimetic way.

Chapter 1 | Introduction

1.1 The importance of touch in manual behavior

State-of-the-art bionic hands are highly sophisticated, approaching the complexity of the human hand, and algorithms to infer intended movements from patterns of activity in residual muscles or neurons have improved (Ajiboye et al., 2017; Collinger et al., 2013; Gilja et al., 2012; Hochberg et al., 2012; Wodlinger et al., 2015). However, prosthetic hands can never confer to their user the dexterity with which natural hands are endowed without restoring somatosensory feedback (Bensmaia, 2015). Indeed, manual interactions with objects rely on a barrage of sensory signals from the hand that convey information about the object itself – its size, shape, texture, etc. – and about the interactions themselves – contact timing, contact force, contact location, etc. Individuals who have lost somatosensation due to a neuropathy struggle to perform activities of daily living because their movements are slow, clumsy, and effortful (Sainburg et al., 1993). Without sensation, not only is the functionality of a bionic hand compromised, but the hand seems disembodied. Indeed, prosthetics users who can volitionally control an arm without being able to feel through it experience the limb as a tool rather than a body part (Page et al., 2018; Valle et al., 2018), which makes it far less appealing. The restoration of touch has the potential to lead to greater embodiment of the prosthetic arm (Flesher et al., 2019; Valle et al., 2018).

1.2 Electrical activation of neurons

Two observations in neuroscience that predate even the discovery of the neuron and the action potential (Hodgkin & Huxley, 1952; Ramon y Cajal, 1888) set the stage for current efforts to sensitize bionic hands. The first is that nervous tissue can be activated by delivering electrical currents (Galvani, 1791). The second is that certain regions of the brain are implicated in specific sensory functions (Gennari, 1782; Glickstein, 1988; Glickstein &

Whitteridge, 1987; Munk, 1881). These phenomena converged in a pivotal way in the 1930s when, searching for the foci of elliptical seizures, Wilder Penfield and colleagues electrically stimulated the brains of awake patients and discovered that stimulating somatosensory cortex elicits sensations of touch localized to restricted regions of the body (Penfield & Boldrey, 1937). This opened the possibility that artificial sensations might be systematically elicited by electrically activating the sensory apparatus of the nervous system. This phenomenon has been harnessed with great success in the restoration of hearing using cochlear implants and, as discussed herein, is key to the restoration of the sense of touch through bionic hands (Figure 1.1).

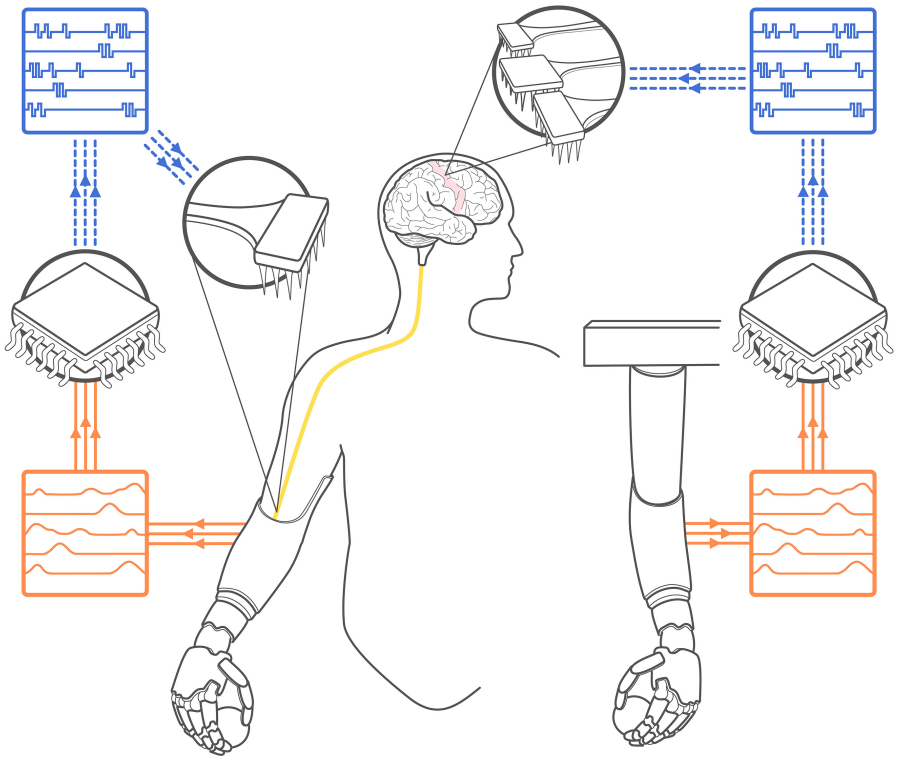

Figure 1.1: Diagram of somatosensory neuroprostheses with a peripheral interface (left) and a cortical interface (right). Signals from sensors in the bionic hand (orange) are converted by sensory encoding algorithms into pulse trains of electrical stimulation delivered to the nerve or somatosensory cortex (blue). These are designed to elicit meaningful sensations that convey information about the object grasped by the hand.

1.3 Neural coding – the language of the nervous system

At every level of processing in the nervous system, from the peripheral nerves through cortex, neurons communicate with each other via action potentials, also known as spikes, and the output of a neuron can be described by its spike times. Sensory neurons can convey information about stimulus features in different ways, according to a so-called neural code. Information can be encoded in the number of spikes emitted per unit time – a rate code. For example, the perceived intensity of a touch is determined by the firing rate of all the activated tactile nerve fibers (Muniak et al., 2007). Alternatively, information can be encoded in the spatial pattern of activation over a population of neurons: the location of the active neurons within a brain area determines what is experienced. For example, the perceived location of a touch is determined by such a spatial code (Tabot et al., 2013). Finally, information can be encoded in the temporal pattern of spiking over short time scales (milliseconds or tens of milliseconds). For example, the perceived texture of a surface is determined in part by the precise timing of neural responses evoked in the nerve (Mackevicius et al., 2012; Talbot et al., 1968) and in the brain (Harvey et al., 2013).

As is perhaps obvious, if one could artificially recreate a natural pattern of neuronal activation evoked by a given stimulus, the evoked sensation would be completely natural. Unfortunately, perfect biomimicry cannot be achieved because current stimulation technology is not selective enough to activate individual neurons independently and because our understanding of sensory coding in the central nervous system is not sufficiently detailed. Nonetheless, mimicking natural patterns of activation to the extent possible may lead to more meaningful sensations than would ignoring the native neural code altogether. Indeed, cochlear implants – which convert sounds into patterns of electrical stimulation of the basilar membrane in the inner ear – are built on the principle that the cochlea splits incoming sounds into their component frequencies, which leads to neural activation at locations on the membrane that depend on the frequency. The sensory encoding algorithms in cochlear implants

split acoustic signals into component frequency bands and electrically stimulate the basilar membrane accordingly. While the resulting neural signals are not completely biomimetic, they nonetheless mimic key aspects of natural patterns of activation that preserve their information content. Biomimicry – one of the guiding principles of the development of artificial touch – requires an understanding of the neural mechanisms that mediate natural touch. A brief review of the somatosensory neuraxis, excerpt from Callier and Bensmaia, 2021, is presented in appendix A.

1.4 Electrical interfaces with the nervous system

Delivering currents to nervous tissue results in the activation thereof. While the effect of electrical stimulation on neurons depends on distance to the electrode, the parameters of stimulation, and the metallization of the electrode, it follows several general principles. First, the probability that an electrical pulse will directly activate a neuron increases with charge but decreases with distance between electrode and neuron (Tehovnik et al., 2006) (Figure 1.2). Second, every activated neuron spikes synchronously in response to each electrical pulse. Thus, a periodic train of electrical pulses will produce synchronized periodic spiking in a volume of neurons. Because axons are more sensitive to electrical stimulation than are cell bodies, electrical stimulation also produces a distributed activity beyond the expected volume (Histed et al., 2009) but its principle effect is confined to this volume (Aberra et al., 2018). Thus, electrical stimulation of the nerve or the brain through a single electrode enables the activation of a pool of neurons the size of which depends on the amount of charge per pulse, and the timing of which depends on the distribution of pulses over time. However, the pattern of activation within the population of activated neurons cannot be further sculpted, which considerably limits the ability of electrical stimulation to reproduce natural patterns of neuronal activation, in which neurons in a given volume each respond idiosyncratically.

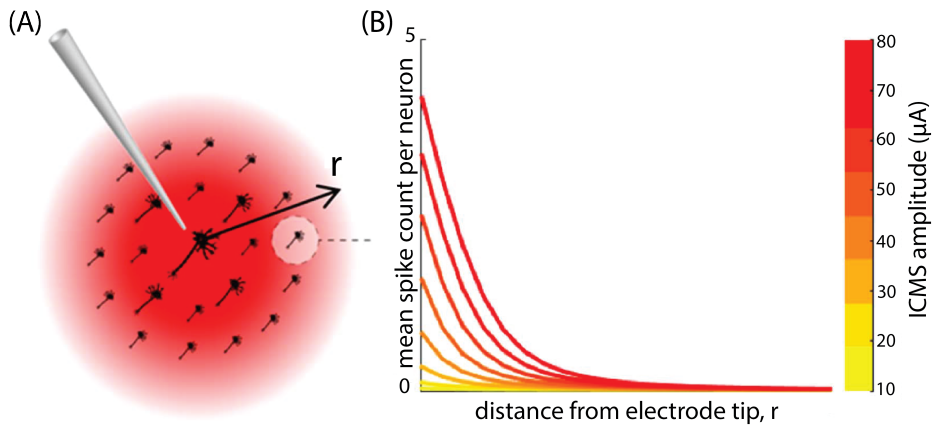

Figure 1.2: Electrical stimulation recruits nearby neurons A) Electrical stimulation through a penetrating microelectrode primarily activates neurons in a restricted volume surrounding the electrical contact. B) The stimulation-evoked firing rate of a neuron increases with pulse amplitude but decreases with distance from the electrode tip. Modified from (S. Kim et al., 2017).

The neural target for an electrical interface depends on the location of the injury that caused the deafferentation. For an amputee, the residual nerve is the preferred target, because all downstream structures are intact. For a spinal cord injury patient, the nerve is not an option because its connection to downstream structures has been compromised, so an interface with the central nervous system is required. In addition to being more or less suited for different user populations, interfaces with the peripheral and central nervous systems each present advantages and disadvantages.

The advantages of peripheral nerve interfaces are that (1) the required surgery is less invasive in that it does not involve the brain; (2) neural coding in the nerve is simpler and better understood; (3) nerve fibers carry parallel signals to the brain, so nerve stimulation avoids the complexities associated with stimulating the complex circuitry of the brain; (4) peripheral nerve stimulation has the potential to engage sensory pathways that are bypassed with more central interfaces, for example spinal reflexes (Schouenborg, 2008). The principal advantage of interfaces with the central nervous system is that they can be applied to patients

with spinal cord injury or suffering from neuropathies that affect more peripheral structures. The cortex offers the additional advantages that (1) it is much larger than is the nerve and thus offers the possibility of more selective activation via electrical stimulation and (2) it features functional topographies – notably somatopic organization – that can be exploited. A brief overview of neural interfaces with the peripheral and central nervous systems most commonly used for sensory neuroprostheses, excerpt from Callier and Bensmaia, 2021, is presented in appendix B. A key consideration for any interface is its durability and ability to deliver stable, persistent sensations over years.

1.5 Shaping artificial touch sensations

When we interact with an object, sensory signals from the hand convey information about the object and about our interactions with it. Tactile sensibility is rich and multidimensional, and to restore it completely would require the ability to selectively activate each of thousands of neurons in the nerve or each of hundreds of thousands of neurons in the brain, which is currently impossible. Rather, current attempts to convey sensory feedback focus on conveying the basic information about object interactions to support simple manual behaviors such as grasping. To grasp an object requires sensing which part of the hand is touching the object – minimally the thumb and one of the fingers –, how much pressure is exerted on the object – enough to pick it up without breaking it –, and when contact is established – to signal the end of the reach and the completion of the grasp. To convey information about the object itself – its texture and compliance for example – would improve the dexterity of bionic hands, but it is much more challenging with current neural interfaces.

One of the principles that guides sensory encoding algorithms is that of biomimicry: to the extent that the patterns of neuronal activation elicited through electrical stimulation mimic natural patterns of activation, the resulting sensations will be natural and thus intuitive. As mentioned above, the naturalness of electrically evoked neuronal activation is severely

limited given the available technology, but general principles of neural coding can be invoked to produce patterns that are as natural as possible. The neural mechanisms behind some aspects of touch are well understood, offering clear road maps for the implementation of biomimetic approaches. The neural basis of many other aspects of touch remain poorly understood, particularly in the central nervous system; for these, further scientific inquiry will be required to develop biomimetic approaches.

1.5.1 Does the precise timing of neural activity shape the tactile experience?

One such unresolved question is whether spike timing in central nervous system shapes tactile sensations. Neurons throughout the nervous system exhibit patterns of activation that contain information not only in the strength of their response – the rate at which they emit spikes – but also in the distribution of these spikes across time, at time scales measured in single-digit milliseconds. Early areas of somatosensory cortex prominently feature such spike timing, reflecting temporal patterns of nerve activity at the periphery which have been shown to play an important role in how we perceive texture (Birznieks & Vickery, 2017; Lieber et al., 2017; Mackevicius et al., 2012; Weber et al., 2013). However, whether spike timing at those temporal resolutions contributes to the transmission of information in the central nervous system remains controversial, because it has proven extremely difficult to disentangle the timing and strength of neural responses. Chapter 2 presents an in-depth investigation of this question. Our results strongly support the contribution of spike timing to perception and suggest that the temporal patterning of ICMS pulses could, in principle be manipulated to shape artificial touch.

However, whether the manipulations of the temporal patterning of ICMS will result in interpretable sensations is unclear given that electrically-evoked neural activity is highly unnatural. This question can be addressed empirically by studying the perceptual correlates of manipulating ICMS timing, for example the frequency at which pulse trains are delivered.

However, as with vibrations, changing the frequency of ICMS changes the strength and spatial pattern of the response in ways that are impossible to observe or predict. Indeed, computational models of stimulation-evoked activity run the gamut from simple probabilistic models based on spherical current spread to complex biophysically-based models of multi-compartment cortical neurons connected in layers and trained on responses to natural stimuli, but none has been developed that allows reliable in silico exploration of the effects of ICMS frequency manipulations. Chapter 3 presents a behavioral assessment of the perceptual effects of stimulation frequency in somatosensory cortex. The results show that animals can discriminate the ICMS frequency despite concomitant and uninformative variations in ICMS amplitude, demonstrating that frequency has a distinct impact on the artificial sensation from amplitude. The use of timing to shape touch feedback remains an active area of research not only in animals but in human subjects (Graczyk et al., 2020; Hughes et al., 2021). In Chapter 4, we offer some final thoughts on next steps in the investigation of timing and touch in cortex and on the potential implications for neuroprosthetics.

1.5.2 Contact location – leveraging somatotopic maps

In early studies, electrical activation of individual nerve fibers (Marchettini et al., 1990; Ochoa & Torebjörk, 1983) or of neurons in different locations within somatosensory cortex (Penfield & Boldrey, 1937) was shown to elicit sensations that are localized to specific locations on the body. The principle that emerges from this work is that contact location is encoded with a spatial code along the entire neuraxis, at least through somatosensory cortex (electrical stimulation of S2 and PV has not yet been attempted). That is, where on the body a tactile sensation is experienced – the projected field – depends on which neurons are activated. Nerve fibers confined to a given fascicle typically innervate a specific patch of skin and activation of these nerve fibers gives rise to a sensation experienced at that location (Davis et al., 2016; Marchettini et al., 1990; Ochoa & Torebjörk, 1983; Ortiz-Catalan,

Mastinu, Sassu, et al., 2020; Raspopovic et al., 2014; Tan et al., 2014). Similarly, neurons within a given volume of cortex innervate a specific patch of skin and their activity results in a sensation experience there (Armenta Salas et al., 2018; Fifer et al., 2020; Flesher et al., 2016; Graczyk et al., 2016; Tabot et al., 2013).

This phenomenon can then be leveraged to convey information about where on the bionic hand contact is established. For example, if the bionic index fingertip makes contact with an object, the output of the index fingertip sensor triggers electrical stimulation of a nerve fascicle or cortical neurons with index fingertip projection fields (Figure 1.3). The user then experiences a sensation on his or her index fingertip. This somatotopic mapping between sensors and electrodes is an example of biomimicry: by leveraging the way the nervous system naturally encodes information about location, the resulting sensory feedback is highly intuitive.

Nerve stimulation through a given electrode evokes sensations spanning one or two phalanges or similar-sized patches of skin on the palm, and a single implant can yield 10 to 15 unique projection fields (Ortiz-Catalan et al., 2014; Raspopovic et al., 2014; Rijnbeek et al., 2018; Tan et al., 2014). While intrafascicular electrodes in principle enable selective activation of a smaller number of nerve fibers, projected fields tend to be similar to those achieved with extrafascicular electrodes with the currents that are typically delivered (Raspopovic et al., 2014; Rijnbeek et al., 2018; Tan et al., 2015; Wendelken et al., 2017). Given that projected fields are determined by which population of neurons is activated, the projected field of an electrode remains stable to the extent that its position within the tissue is stable (Ortiz-Catalan, Mastinu, Greenspon, et al., 2020; Tan et al., 2015).

Microstimulation of somatosensory cortex – Brodmann's areas 3b and 1 – evokes sensations that are restricted to a small patch of skin, spanning a phalange or two (Armenta Salas et al., 2018; Fifer et al., 2020; Flesher et al., 2016; Tabot et al., 2013). Studies in monkeys suggest that the projected fields of electrodes in area 3b are smaller than are their

counterparts in area 1, as might be expected given the respective sizes of the receptive field in these cortical areas. (Tabot et al., 2014). However, area 1 is the target for implantation in human subjects because its location on the gyrus makes it more surgically accessible. Indeed, area 3b lies in the posterior bank of the central sulcus and thus cannot be accessed with technologies that are currently approved for human use (see Appendix A). In contrast to ICMS, ECoG stimulation activates populations of neurons over large swaths of cortex, so the evoked sensations are referred to large swaths of skin, often the entire hand (Collins et al., 2017; Hiremath et al., 2017; Johnson et al., 2013; Lee et al., 2018). ECoG stimulation thus provides limited information about contact location.

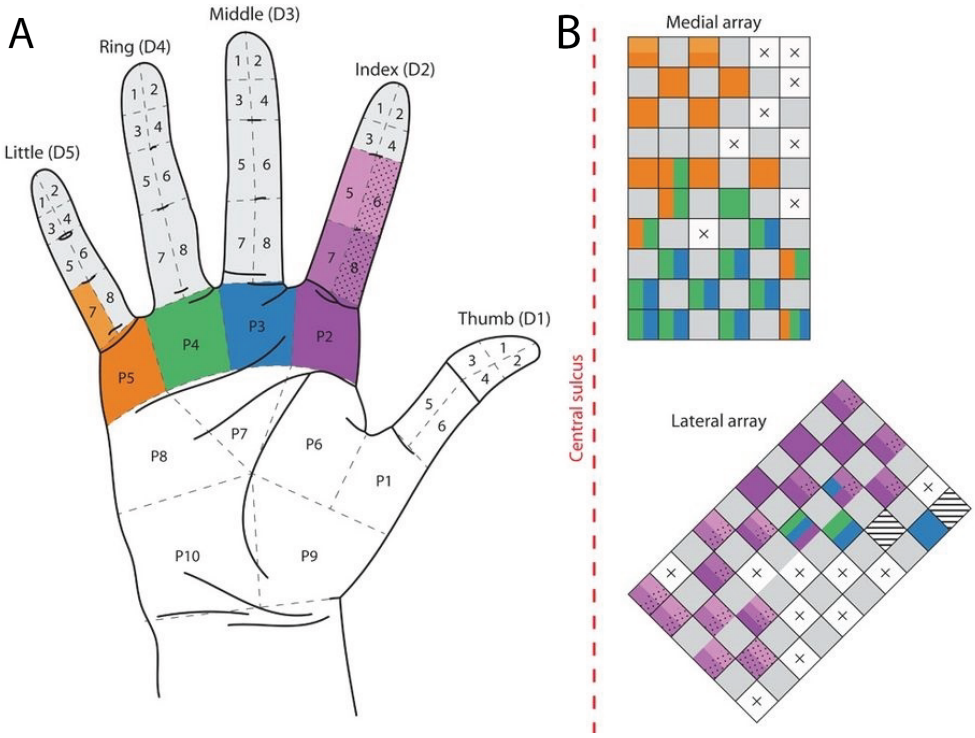

Figure 1.3: Projected fields of electrodes on two microelectrode arrays implanted in somatosensory cortex of a human subject. Contact location is encoded with a spatial code in the nerve and in somatosensory cortex, and stimulation of neurons that innervate (or used to innervate before deafferentation) a specific skin location results in a sensation experienced there: stimulation through electrodes of a given color in B) elicited a tactile percept at the corresponding colored path of skin on the hand in A). This can be leveraged to intuitively convey information about contact location on a bionic hand. Reproduced from (Flesher et al., 2016).

1.5.3 Contact pressure

When we grasp and transport an object, we exert enough force so that it will not slip from our grasp, and not much more. While proprioceptive signals also convey information about the muscular effort deployed during grasping, the fine control of applied force is mediated by the sense of touch, as evidenced by the deficits that are incurred when touch is abolished, for example when the hand is anesthetized (Augurelle et al., 2003). Light pressure results in a faint tactile sensation, forceful pressure in a strong sensation. In the nerve and in the brain, this sensory continuum is associated with an increase in the evoked neuronal activity (Callier et al., 2019; Muniak et al., 2007). Higher pressure results in stronger responses in activated neurons and in the recruitment of additional neurons (Callier et al., 2019) (Figure 1.4 A). Accordingly, information about pressure can be conveyed by modulating the strength of the neuronal activity evoked in the nerve or in the brain (Figure 1.4 A, B).

The population response rate can be modulated by modulating stimulation frequency or amplitude. Changes in frequency result in changes in the firing rates of the activated neuron, in a nearly one-to-one fashion: each stimulating pulse produces an action potential in the volume of neurons over which that pulse exceeds absolute threshold, so more pulses result in more spikes in these neurons. Note, however, that the one-to-one relationship between pulse frequency and spike rate breaks down at higher frequencies, when the inter-pulse interval is shorter than the refractory period (S. Kim et al., 2017). Indeed, neurons that have been recently activated are more difficult to reactivate within a short window of time, measured in single-digit milliseconds. In contrast, changes in stimulation amplitude result in changes in the activated volume, which also results in a higher overall response. The greater the amplitude, the more current spreads, which recruits neurons away from the stimulating electrode (Butovas & Schwarz, 2003; Stoney et al., 1968; Tehovnik et al., 2006). Accordingly, information about contact pressure has been modulated by varying stimulation frequency and amplitude, with higher frequencies/amplitudes signaling higher pressures.

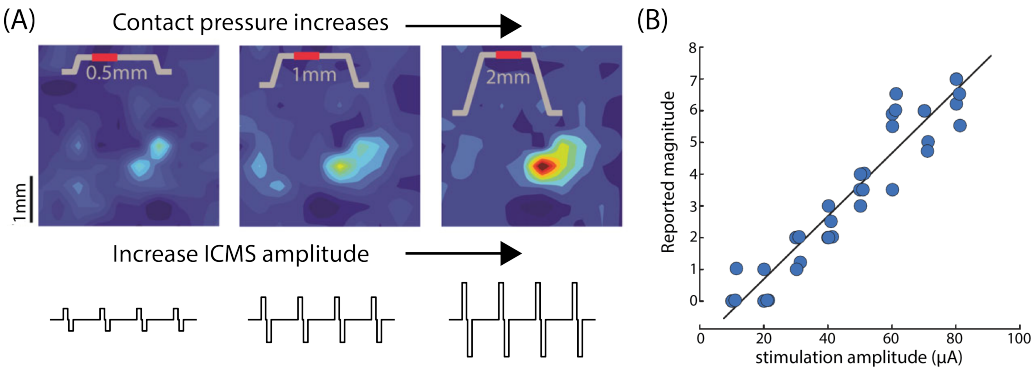

Figure 1.4: Pressure coding A) Higher pressure results in stronger responses in activated neurons and in the recruitment of additional neurons. Top: spatial layout of the response in somatosensory cortex during the sustained portion of indentations (red on the trace) of increasing pressure from left to right. Bottom: the population response can be modulated by modulating stimulation amplitude (or frequency) to convey information about contact pressure. Modified from (Callier et al., 2019). B) Increases in stimulation amplitude (or frequency) elicit a more intense sensation. Shown here, reports from a human subject of sensation magnitude (on an arbitrary scale) as a function of the amplitude of ICMS delivered to somatosensory cortex. Reproduced from (Flesher et al., 2016).

Experiments with peripheral nerve interfaces have shown that increases in both stimulation amplitude (Graczyk et al., 2016; Raspopovic et al., 2014; Tan et al., 2014) or frequency (Dhillon & Horch, 2005; George et al., 2019) result in increases in the perceived magnitude of an electrically evoked sensation. In fact, greater afferent activation elicits a more intense sensation regardless of whether it is achieved by increasing the stimulation amplitude or frequency (Graczyk et al., 2016). The perceived magnitude of the sensation elicited by a given pulse train can be predicted from the amount of current injected into the nerve after correcting for the activation threshold. Pressure-dependent frequency or amplitude modulation improves the ability of prosthetic users to sense the stiffness of objects (Raspopovic et al., 2014), control grasp force (Raspopovic et al., 2014), and perform tasks requiring dexterity such as picking up and moving a wooden block (Schiefer et al., 2016), picking the stems off cherries (Tan et al., 2014), and transferring a fragile object without breaking it (Valle et al., 2018).

Experiments with cortical interfaces in macaques have shown that the same general prin-

ciples apply to ICMS-based artificial touch. Indeed, as is the case in the nerve, increases in stimulation amplitude result in a consistent increase in the perceived magnitude of an electrically evoked sensation (Flesher et al., 2016; S. Kim et al., 2015) (Figure 1.4 B). Similarly, increasing ICMS frequency leads to an increase in perceived magnitude (Callier et al., 2020) but this effect is complicated by concomitant changes in quality (Hughes et al., 2021). As with peripheral nerve interfaces, sensory feedback consisting of modulating ICMS amplitude in a pressure-dependent way improved a human subject's ability to grasp and transport objects (Flesher et al., 2019).

1.5.4 Timing of contact events

When we reach for an object, we terminate our reach and complete our grasp as soon as we make contact with the object (Johansson & Flanagan, 2009). When we handle an object, slip rapidly triggers a grip adjustment (Johansson & Flanagan, 2009). The abolition of touch results in overreaching and in allowing objects to slip from one's grasp. As these examples illustrate, information about the timing of contact events is critical to dexterous manual behavior.

Tracking pressure does not result in precise information about contact timing. Indeed, the pressure experienced by the skin increases slowly during grasp, so a pressure-tracking sensory encoding algorithm will lead to delayed detection of contact, as detection can only occur when stimulation levels exceed threshold. In the intact nerve, RA and PC fibers produce a strong phasic response at the onset and offset of contact, and this signal is well suited to convey information about the timing of contact events (see appendix A). This sensitivity to contact transients can be accounted for by the fact that some nerve fibers are primarily sensitive to changes in pressure (RA, PC) (Dong et al., 2013; Kim et al., 2010; Saal et al., 2017) and thus carry a signal that emphasizes contact transients (Callier et al., 2019) (Figure 1.5). Another population of nerve fibers (SA1 fibers) carry information about

pressure during maintained contact, but this sustained signal tends to be weaker and more localized than its phasic counterpart during contact transients.

A straightforward way to mimic these two aspects of the neural response – strong response during contact transients, weaker sustained response during maintained contact – consists of modulating the intensity of electrical stimulation (frequency and/or amplitude) according to a combination of instantaneous pressure and its derivative (Saal & Bensmaia, 2015) (Figure 1.5). This way, contact transients lead to greater stimulation – driven by the derivative term –, but pressure is also tracked during maintained contact. The resulting signals can approximate the aggregate behavior of nerve fibers during activities of daily living (Okorokova et al., 2018). This biomimetic strategy leads to an improved ability to transport fragile objects (George et al., 2019; Valle et al., 2018), a task that requires sensory feedback, and to an improved ability to sense the properties of grasped objects, for example their compliance (George et al., 2019).

At the aggregate level, responses in somatosensory cortex resemble their peripheral counterparts: onset and offset of contact are signaled by precisely timed phasic responses – driven by RA and PC fibers (Johansson & Flanagan, 2009; Pei et al., 2009) – and maintained contact by a weaker response – driven by SA1 fibers (Figure 1.5). Appendix D, a study of the responses of somatosensory cortex to contact events, reports that phasic responses associated with contact transients dwarf the tonic response during maintained contact and result in a neuronal representations that rapidly convey information about contact parameters, for example timing and location. Thus, biomimetic encoding algorithms designed for the nerve could in principle be applied directly to ICMS-based feedback (Callier et al., 2019; Okorokova et al., 2018) but the efficacy of such algorithms has yet to be tested.

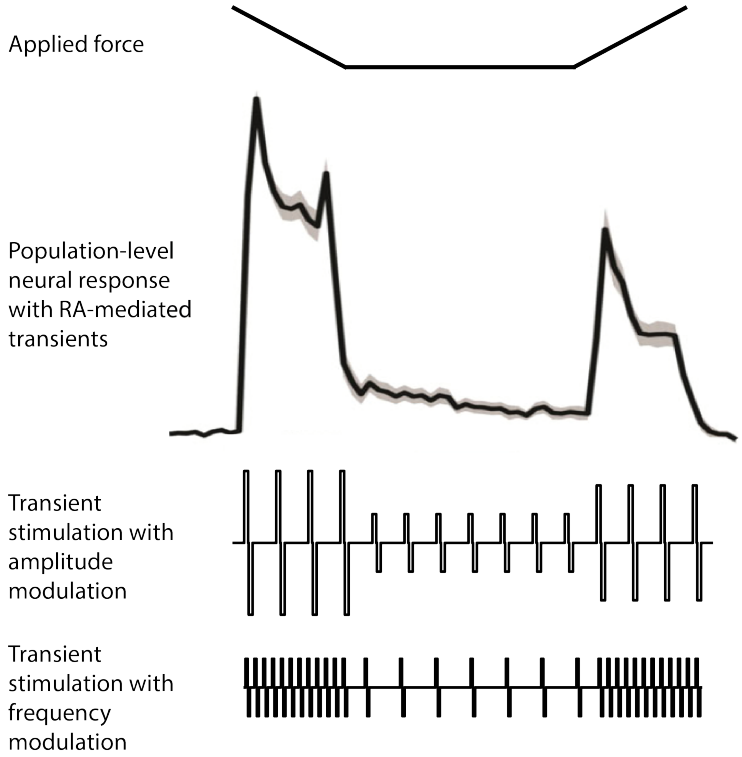

Figure 1.5: Spatiotemporal dynamics of the neural response to contact events: strong phasic responses to force transients are well suited to rapidly convey the timing of those events. The population-level neural response in somatosensory cortex to a simple indentation (top trace) is shown here. The aggregate response in the nerve is similar. This neural response can be mimicked by modulating the intensity of electrical stimulation according to instantaneous pressure (the sole factor during the sustained portion of the indentation) and its derivative (during transients). The increased intensity during transients can be modulated with stimulation frequency and/or amplitude. Modified from (Callier et al., 2019).

1.5.5 Sensory quality

Tactile sensations can be described in terms of their location on the body, their strength, and their timing, and our understanding of the neural coding of these perceptual features can be leveraged in designing sensory encoding algorithms. However, touch conveys far more detailed information about objects and about contact events than these three features. For example, we can sense the size, shape, and texture of an object, and its movement across the skin, via cutaneous signals. These different sensations are characterized by different qualities. The sensation of an edge indented into the skin has a different quality than the

sensation of a texture scanned across the skin. The sensory space of touch is very complex. Even specific domains of touch – texture, e.g. – are encoded in a high dimensional space (Lieber & Bensmaia, 2019). Sensory quality thus encompasses the bulk of the information about objects and contact events. The quality of a sensory percept is shaped by the specific pattern of a neuronal activation that gave rise to it. Indeed, a specific texture produces a specific spatiotemporal pattern of activation and the quality of the evoked sensation is the outcome of this spatiotemporal pattern. An indented edge produces a different spatiotemporal pattern of activation, one that depends in part on its orientation, and gives rise to a different sensation. To elicit sensations endowed with specific qualities would require reproducing these spatiotemporal patterns of activation, which is impossible given existing technologies and will probably remain so in the foreseeable future. However, the quality of an electrically evoked sensation can be systematically manipulated, albeit in a limited way.

First, one might ask whether electrically evoked sensations resemble those that are mechanically evoked through interactions with objects. The answer depends on whether the stimulus is applied to the nerve or the brain. Electrical stimulation of the nerve typically results in paresthesias – tingling sensations that feel unnatural – but sensations of vibration, pressure, or tapping have also been described (Ackerley et al., 2018; Davis et al., 2016; George et al., 2019; Ortiz-Catalan et al., 2019; Tan et al., 2014). In contrast, ICMS evokes sensations that are described as natural or nearly so (Armenta Salas et al., 2018; Flesher et al., 2016).

Second, one might ask to what extent electrically evoked sensations depend on which subpopulations of neurons are activated. In the nerve, evoked sensations are relatively independent of which electrode delivers the stimulation (Graczyk et al., n.d.), likely due to the relatively consistent submodality composition of fascicles across the nerve. Indeed, the only way for the quality of electrically evoked sensations to differ across electrodes would be if different fascicles contained different proportions of SA1, RA, and PC fibers. Given that

these differences are minimal, the resulting variability in the quality of electrically evoked sensations across electrodes is also minimal. In contrast, the quality of ICMS-evoked sensations is strongly electrode dependent. Indeed, subjects report different types of sensations – pressure, tapping, pulsing, light movement, e.g. – depending on the stimulating electrode, even though these are in the same cortical area (Armenta Salas et al., 2018; Flesher et al., 2016; Hughes et al., 2020). The dependence of quality on electrode likely reflects differences in the functional roles of different neuronal subpopulations. If one volume of cortex contains a preponderance of neurons involved in motion analysis, activating these neurons may result in a percept of tactile motion. If another volume contains texture-sensitive neurons, stimulation thereof may evoke texture-like sensations. While sensory quality can be manipulated by activating different electrodes, this phenomenon cannot be leveraged meaningfully because (1) both quality and projected field vary with electrodes so quality and location are inextricably linked and (2) quality depends idiosyncratically and unpredictably on the brain area in which the electrodes are implanted.

Third, one might ask how the parameters of stimulation change the quality of the sensation. In both the nerve and the brain, changes in stimulation amplitude lead to an increase in the magnitude of the sensation (Flesher et al., 2016; Graczyk et al., 2016; Kim et al., 2015). In the nerve, increases in amplitude can also result in an increase in the size of the projected field (Davis et al., 2016; Ortiz-Catalan, Mastinu, Sassu, et al., 2020; Tan et al., 2014). In neither the nerve nor the brain does the quality of the sensation systematically change with changes in amplitude. In contrast, changes in the timing of pulses can impact the quality, as evidenced by the effect of changes in stimulation frequency on the evoked percept. Indeed, changes in stimulation frequency result in changes in the quality of the percept in both the nerve (Graczyk et al., n.d.) and the brain (Callier et al., 2020; Hughes et al., 2020). In the nerve, changes in frequency have an effect on quality that is consistent across electrodes and even across subjects (Graczyk et al., n.d.). Indeed, the perceived frequency increases

with increases in pulse frequency up to about 100 Hz. Increases in frequency beyond 100 Hz result in increases in magnitude but not quality. In cortex, changes in microstimulation frequency also result in a change in quality (Callier et al., 2020; Hughes et al., 2020), but the specific relationship between stimulation frequency and quality depends on the stimulation electrode (Hughes et al., 2020). In both the nerve and the brain, low-frequency stimulation typically results in intermittent sensations, such as tapping, whereas high-frequency stimulation results in fused events, such as pressure.

As summarized above, sensory quality is determined by the specific spatiotemporal pattern of activation evoked by a stimulus. Accordingly, the ability to electrically evoke sensations endowed with a specific quality is limited by the inability to activate individual neurons in a selective manner. In Chapter 4, we offer some final thoughts on surmounting this limitation and on the future horizons of touch neuroprosthetics.

1.6 References

Aberra, A. S., Peterchev, A. V., & Grill, W. M. (2018). Biophysically realistic neuron models for simulation of cortical stimulation. Journal of Neural Engineering, 15(6), 066023. https://doi.org/10.1088/1741-2552/aadbb1

Ackerley, R., Backlund Wasling, H., Ortiz-Catalan, M., Brånemark, R., & Wessberg, J. (2018). Case Studies in Neuroscience: Sensations elicited and discrimination ability from nerve cuff stimulation in an amputee over time. Journal of Neurophysiology, 120(1), 291–295. https://doi.org/10.1152/jn.00909.2017

Ajiboye, A. B., Willett, F. R., Young, D. R., Memberg, W. D., Murphy, B. A., Miller, J. P., Walter, B. L., Sweet, J. A., Hoyen, H. A., Keith, M. W., Peckham, P. H., Simeral, J. D., Donoghue, J. P., Hochberg, L. R., & Kirsch, R. F. (2017). Restoration of reaching and grasping movements through brain-controlled muscle stimulation in a person with tetraplegia: A proof-of-concept demonstration. The Lancet, 389(10081), 1821–1830.

Armenta Salas, M., Bashford, L., Kellis, S., Jafari, M., Jo, H., Kramer, D., Shanfield, K., Pejsa, K., Lee, B., Liu, C. Y., & Andersen, R. A. (2018). Proprioceptive and cutaneous sensations in humans elicited by intracortical microstimulation. ELife, 7, e32904. https://doi.org/10.7554/eLife.32904 Augurelle, A.-S., Smith, A. M., Lejeune, T., & Thonnard, J.-L. (2003). Importance of cutaneous feedback in maintaining a secure grip during manipulation of hand-held objects. Journal of Neurophysiology, 89(2), 665–671.

Bensmaia, S. J. (2015). Biological and bionic hands: Natural neural coding and artificial perception. Philosophical Transactions of the Royal Society B: Biological Sciences, 370(1677), 20140209. https://doi.org/10.1098/rstb.2014.0209

Birznieks, I., & Vickery, R. M. (2017). Spike Timing Matters in Novel Neuronal Code Involved in Vibrotactile Frequency Perception. Current Biology, 27(10), 1485-1490.e2.

Butovas, S., & Schwarz, C. (2003). Spatiotemporal Effects of Microstimulation in Rat Neocortex: A Parametric Study Using Multielectrode Recordings. Journal of Neurophysiology, 90(5), 3024–3039. https://doi.org/10.1152/jn.00245.2003

Callier, T., Brantly, N. W., Caravelli, A., & Bensmaia, S. J. (2020). The frequency of cortical microstimulation shapes artificial touch. Proceedings of the National Academy of Sciences, 117(2), 1191–1200.

Callier, T., Suresh, A. K., & Bensmaia, S. J. (2019). Neural Coding of Contact Events in Somatosensory Cortex. Cerebral Cortex, 29(11), 4613–4627.

Collinger, J. L., Wodlinger, B., Downey, J. E., Wang, W., Tyler-Kabara, E. C., Weber, D. J., McMorland, A. J., Velliste, M., Boninger, M. L., & Schwartz, A. B. (2013). High-performance neuroprosthetic control by an individual with tetraplegia. The Lancet, 381(9866), 557–564. https://doi.org/10.1016/S0140-6736(12)61816-9

Collins, K. L., Guterstam, A., Cronin, J., Olson, J. D., Ehrsson, H. H., & Ojemann, J. G. (2017). Ownership of an artificial limb induced by electrical brain stimulation. Proceedings of the National Academy of Sciences, 114(1), 166–171.

Davis, T. S., Wark, H. A. C., Hutchinson, D. T., Warren, D. J., O'Neill, K., Scheinblum, T., Clark, G. A., Normann, R. A., & Greger, B. (2016). Restoring motor control and sensory feedback in people with upper extremity amputations using arrays of 96 microelectrodes implanted in the median and ulnar nerves. Journal of Neural Engineering, 13(3), 036001. https://doi.org/10.1088/1741-2560/13/3/036001

Dhillon, G. S., & Horch, K. W. (2005). Direct Neural Sensory Feedback and Control of a Prosthetic Arm. IEEE Transactions on Neural Systems and Rehabilitation Engineering, 13(4), 468–472. https://doi.org/10.1109/TNSRE.2005.856072

Dong, Y., Mihalas, S., Kim, S. S., Yoshioka, T., Bensmaia, S. J., & Niebur, E. (2013). A simple model of mechanotransduction in primate glabrous skin. Journal of Neurophysiology, 109(5), 1350–1359. https://doi.org/10.1152/jn.00395.2012

Fifer, M. S., McMullen, D. P., Thomas, T. M., Osborn, L. E., Nickl, R. W., Candrea, D. N., Pohlmeyer, E. A., Thompson, M. C., Anaya, M., Schellekens, W., Ramsey, N. F., Bensmaia, S. J., Anderson, W. S., Wester, B. A., Crone, N. E., Celnik, P. A., Cantarero, G. L., & Tenore, F. V. (2020). Intracortical Microstimulation Elicits Human Fingertip Sensations. MedRxiv, 2020.05.29.20117374. https://doi.org/10.1101/2020.05.29.20117374

Flesher, S. N., Collinger, J. L., Foldes, S. T., Weiss, J. M., Downey, J. E., Tyler-Kabara, E. C., Bensmaia, S. J., Schwartz, A. B., Boninger, M. L., & Gaunt, R. A. (2016). Intracortical microstimulation of human somatosensory cortex. Science Translational Medicine, 8(361), 361ra141-361ra141. https://doi.org/10.1126/scitranslmed.aaf8083

Flesher, S. N., Downey, J. E., Weiss, J. M., Hughes, C. L., Herrera, A. J., Tyler-Kabara, E. C., Boninger, M. L., Collinger, J. L., & Gaunt, R. A. (2019). Restored tactile sensation improves neuroprosthetic arm control [Preprint]. Clinical Trials. https://doi.org/10.1101/653428

Galvani, L. (1791). De viribus electricitatis in motu musculari commentarius. Ex Typographia Instituti Scientiarium. https://doi.org/10.5479/sil.324681.39088000932442

Gennari, F. (1782). De Peculiari Structura Cerebri Nonnuliaque Ejus Morbis. Parma Ex

Regio Typographeo.

George, J. A., Kluger, D. T., Davis, T. S., Wendelken, S. M., Okorokova, E. V., He, Q., Duncan, C. C., Hutchinson, D. T., Thumser, Z. C., Beckler, D. T., Marasco, P. D., Bensmaia, S. J., & Clark, G. A. (2019). Biomimetic sensory feedback through peripheral nerve stimulation improves dexterous use of a bionic hand. Science Robotics, 4(32). https://doi.org/10.1126/scirobotics.aax2352

Gilja, V., Nuyujukian, P., Chestek, C. A., Cunningham, J. P., Yu, B. M., Fan, J. M., Churchland, M. M., Kaufman, M. T., Kao, J. C., Ryu, S. I., & Shenoy, K. V. (2012). A high-performance neural prosthesis enabled by control algorithm design. Nature Neuroscience, 15(12), 1752–1757. https://doi.org/10.1038/nn.3265

Glickstein, M. (1988). The Discovery of the Visual Cortex. Scientific American, 259(3), 118–127. https://doi.org/10.1038/scientificamerican0988-118

Glickstein, M., & Whitteridge, D. (1987). Tatsuji Inouye and the mapping of the visual fields on the human cerebral cortex. Trends in Neurosciences, 10(9), 350–353.

Graczyk, E. L., Christie, B. P., He, Q., Tyler, D. J., & Bensmaia, S. J. (2020). Frequency shapes the quality of tactile percepts evoked through electrical stimulation of the nerves [Preprint]. Bioengineering. https://doi.org/10.1101/2020.08.24.263822

Graczyk, E. L., Christie, Breanne, He, Q., Tyler, D. J., & Bensmaia, S. J. (n.d.). Frequency shapes the quality of tactile percepts evoked through electrical stimulation of the nerves. BioRxiv.

Graczyk, E. L., Schiefer, M. A., Saal, H. P., Delhaye, B. P., Bensmaia, S. J., & Tyler, D. J. (2016). The neural basis of perceived intensity in natural and artificial touch. Science Translational Medicine, 8(362), 362ra142-362ra142. https://doi.org/10.1126/scitranslmed.aaf5187

Harvey, M. A., Saal, H. P., Dammann, J. F., & Bensmaia, S. J. (2013). Multiplexing Stimulus Information through Rate and Temporal Codes in Primate Somatosensory Cortex. PLoS Biology, 11(5), e1001558. https://doi.org/10.1371/journal.pbio.1001558

Hiremath, S. V., Tyler-Kabara, E. C., Wheeler, J. J., Moran, D. W., Gaunt, R. A., Collinger, J. L., Foldes, S. T., Weber, D. J., Chen, W., Boninger, M. L., & Wang, W. (2017). Human perception of electrical stimulation on the surface of somatosensory cortex. PLOS ONE, 12(5), e0176020. https://doi.org/10.1371/journal.pone.0176020

Histed, M. H., Bonin, V., & Reid, R. C. (2009). Direct Activation of Sparse, Distributed Populations of Cortical Neurons by Electrical Microstimulation. Neuron, 63(4), 508–522. https://doi.org/10.1016/j.neuron.2009.07.016

Hochberg, L. R., Bacher, D., Jarosiewicz, B., Masse, N. Y., Simeral, J. D., Vogel, J., Haddadin, S., Liu, J., Cash, S. S., van der Smagt, P., & Donoghue, J. P. (2012). Reach and grasp by people with tetraplegia using a neurally controlled robotic arm. Nature, 485(7398), 372–375. https://doi.org/10.1038/nature11076

Hodgkin, A. L., & Huxley, A. F. (1952). A quantitative description of membrane current and its application to conduction and excitation in nerve. The Journal of Physiology, 114(4), 500–544. https://doi.org/10.1113/jphysiol.1952.sp004764

Hughes, C. L., Flesher, S. N., Weiss, J. M., Boninger, M., Collinger, J. L., & Gaunt, R. (2020). Perceptual responses to microstimulation frequency are spatially organized in human somatosensory cortex [Preprint]. Neuroscience. https://doi.org/10.1101/2020.07.16.207506

Hughes, C. L., Flesher, S. N., Weiss, J. M., Boninger, M., Collinger, J. L., & Gaunt, R. A. (2021). Perception of microstimulation frequency in human somatosensory cortex. ELife, 10, e65128. https://doi.org/10.7554/eLife.65128

Johansson, R. S., & Flanagan, J. R. (2009). Coding and use of tactile signals from the fingertips in object manipulation tasks. Nature Reviews Neuroscience, 10(5), 345–359. https://doi.org/10.1038/nrn2621

Johnson, L. A., Wander, J. D., Sarma, D., Su, D. K., Fetz, E. E., & Ojemann, J. G. (2013). Direct electrical stimulation of the somatosensory cortex in humans using electrocorticography electrodes: A qualitative and quantitative report. Journal of Neural Engineering, 10(3),

036021. https://doi.org/10.1088/1741-2560/10/3/036021

Kim, S., Callier, T., & Bensmaia, S. J. (2017). A computational model that predicts behavioral sensitivity to intracortical microstimulation. Journal of Neural Engineering, 14(1), 016012. https://doi.org/10.1088/1741-2552/14/1/016012

Kim, S., Callier, T., Tabot, G. A., Gaunt, R. A., Tenore, F. V., & Bensmaia, S. J. (2015). Behavioral assessment of sensitivity to intracortical microstimulation of primate somatosensory cortex. Proceedings of the National Academy of Sciences, 112(49), 15202–15207. https://doi.org/10.1073/pnas.1509265112

Kim, S. S., Sripati, A. P., & Bensmaia, S. J. (2010). Predicting the Timing of Spikes Evoked by Tactile Stimulation of the Hand. Journal of Neurophysiology, 104(3), 1484–1496. https://doi.org/10.1152/jn.00187.2010

Lee, B., Kramer, D., Armenta Salas, M., Kellis, S., Brown, D., Dobreva, T., Klaes, C., Heck, C., Liu, C., & Andersen, R. A. (2018). Engineering Artificial Somatosensation Through Cortical Stimulation in Humans. Frontiers in Systems Neuroscience, 12, 24.

Lieber, J. D., & Bensmaia, S. J. (2019). High-dimensional representation of texture in somatosensory cortex of primates. Proceedings of the National Academy of Sciences, 116(8), 3268–3277. https://doi.org/10.1073/pnas.1818501116

Lieber, J. D., Xia, X., Weber, A. I., & Bensmaia, S. J. (2017). The neural code for tactile roughness in the somatosensory nerves. Journal of Neurophysiology, 118(6), 3107–3117. https://doi.org/10.1152/jn.00374.2017

Mackevicius, E. L., Best, M. D., Saal, H. P., & Bensmaia, S. J. (2012). Millisecond Precision Spike Timing Shapes Tactile Perception. Journal of Neuroscience, 32(44), 15309–15317. https://doi.org/10.1523/JNEUROSCI.2161-12.2012

Marchettini, P., Cline, M., & Ochoa, J. L. (1990). Innervation territories for touch and pain afferents of single fascicles of the human ulnar nerve: mapping through intraneural microrecording and microstimulation. Brain, 113(5), 1491–1500.

Muniak, M. A., Ray, S., Hsiao, S. S., Dammann, J. F., & Bensmaia, S. J. (2007). The Neural Coding of Stimulus Intensity: Linking the Population Response of Mechanoreceptive Afferents with Psychophysical Behavior. Journal of Neuroscience, 27(43), 11687–11699. https://doi.org/10.1523/JNEUROSCI.1486-07.2007

Munk, H. (1881). Uber die Funktionen der Grosshimrinde. A. Hirshwald. Ochoa, J., & Torebjörk, E. (1983). Sensations evoked by intraneural microstimulation of single mechanoreceptor units innervating the human hand. The Journal of Physiology, 342(1), 633–654. https://doi.org/10.1113/jphysiol.1983.sp014873

Okorokova, E. V., He, Q., & Bensmaia, S. J. (2018). Biomimetic encoding model for restoring touch in bionic hands through a nerve interface. Journal of Neural Engineering, 15(6), 066033. https://doi.org/10.1088/1741-2552/aae398

Ortiz-Catalan, M., Hakansson, B., & Branemark, R. (2014). An osseointegrated human-machine gateway for long-term sensory feedback and motor control of artificial limbs. Science Translational Medicine, 6(257), 257re6-257re6. https://doi.org/10.1126/scitranslmed.3008933

Ortiz-Catalan, M., Mastinu, E., Greenspon, C., & Bensmaia, S. (2020). Chronic use of a sensitized bionic hand does not remap the sense of touch. Cell Reports.

Ortiz-Catalan, M., Mastinu, E., Sassu, P., Aszmann, O., & Brånemark, R. (2020). Self-Contained Neuromusculoskeletal Arm Prostheses. New England Journal of Medicine, 382(18), 1732–1738. https://doi.org/10.1056/NEJMoa1917537

Ortiz-Catalan, M., Wessberg, J., Mastinu, E., Naber, A., & Branemark, R. (2019). Patterned Stimulation of Peripheral Nerves Produces Natural Sensations With Regards to Location but Not Quality. IEEE Transactions on Medical Robotics and Bionics, 1(3), 199–203. https://doi.org/10.1109/TMRB.2019.2931758

Page, D. M., George, J. A., Kluger, D. T., Duncan, C., Wendelken, S., Davis, T., Hutchinson, D. T., & Clark, G. A. (2018). Motor Control and Sensory Feedback Enhance Prosthesis Embodiment and Reduce Phantom Pain After Long-Term Hand Amputation. Frontiers in

Human Neuroscience, 12, 352. https://doi.org/10.3389/fnhum.2018.00352

Pei, Y.-C., Denchev, P. V., Hsiao, S. S., Craig, J. C., & Bensmaia, S. J. (2009). Convergence of Submodality-Specific Input Onto Neurons in Primary Somatosensory Cortex. Journal of Neurophysiology, 102(3), 1843–1853. https://doi.org/10.1152/jn.00235.2009

Penfield, W., & Boldrey, E. (1937). Somatic motor and sensory representation in the cerebral cortex of man as studied by electrical stimulation. Brain, 60(4), 389–443.

Ramon y Cajal, S. (1888). Estructura de los centros nerviosos de las aves. Revista Trimestral de Histologia Normal y Patologica, 1.

Raspopovic, S., Capogrosso, M., Petrini, F. M., Bonizzato, M., Rigosa, J., Di Pino, G., Carpaneto, J., Controzzi, M., Boretius, T., Fernandez, E., Granata, G., Oddo, C. M., Citi, L., Ciancio, A. L., Cipriani, C., Carrozza, M. C., Jensen, W., Guglielmelli, E., Stieglitz, T., ... Micera, S. (2014). Restoring Natural Sensory Feedback in Real-Time Bidirectional Hand Prostheses. Science Translational Medicine, 6(222).

Rijnbeek, E. H., Eleveld, N., & Olthuis, W. (2018). Update on Peripheral Nerve Electrodes for Closed-Loop Neuroprosthetics. Frontiers in Neuroscience, 12, 350.

Saal, H. P., & Bensmaia, S. J. (2015). Biomimetic approaches to bionic touch through a peripheral nerve interface. Neuropsychologia, 79, 344–353.

Saal, H. P., Delhaye, B. P., Rayhaun, B. C., & Bensmaia, S. J. (2017). Simulating tactile signals from the whole hand with millisecond precision. Proceedings of the National Academy of Sciences, 114(28), E5693–E5702.

Sainburg, R. L., Poizner, H., & Ghez, C. (1993). Loss of proprioception produces deficits in interjoint coordination. Journal of Neurophysiology, 70(5), 2136–2147.

Schiefer, M., Tan, D., Sidek, S. M., & Tyler, D. J. (2016). Sensory feedback by peripheral nerve stimulation improves task performance in individuals with upper limb loss using a myoelectric prosthesis. Journal of Neural Engineering, 13(1), 016001. https://doi.org/10.1088/1741-2560/13/1/016001

Schouenborg, J. (2008). Action-based sensory encoding in spinal sensorimotor circuits. Brain Research Reviews, 57(1), 111–117. https://doi.org/10.1016/j.brainresrev.2007.08.007

Stoney, S. D., Thompson, W. D., & Asanuma, H. (1968). Excitation of pyramidal tract cells by intracortical microstimulation: Effective extent of stimulating current. Journal of Neurophysiology, 31(5), 659–669. https://doi.org/10.1152/jn.1968.31.5.659

Tabot, G. A., Damman, J. F., Berg, J. A., Tenore, F. V., Boback, J. L., Vogelstein, R. J., & Bensmaia, S. J. (2014). Restoring the sense of touch with a prosthetic hand through a brain interface. Proceedings of the National Academy of Sciences, 111(2), 875–875. https://doi.org/10.1073/pnas.1322627111

Tabot, G. A., Dammann, J. F., Berg, J. A., Tenore, F. V., Boback, J. L., Vogelstein, R. J., & Bensmaia, S. J. (2013). Restoring the sense of touch with a prosthetic hand through a brain interface. Proceedings of the National Academy of Sciences of the United States of America, 110(45), 18279–18284. https://doi.org/10.1073/pnas.1221113110

Talbot, W. H., Darian-Smith, I., Kornhuber, H. H., & Mountcastle, V. B. (1968). The sense of flutter-vibration: Comparison of the human capacity with response patterns of mechanoreceptive afferents from the monkey hand. Journal of Neurophysiology, 31(2), 301–334. https://doi.org/10.1152/jn.1968.31.2.301

Tan, D. W., Schiefer, M. A., Keith, M. W., Anderson, J. R., & Tyler, D. J. (2015). Stability and selectivity of a chronic, multi-contact cuff electrode for sensory stimulation in human amputees. Journal of Neural Engineering, 12(2), 026002. https://doi.org/10.1088/1741-2560/12/2/026002

Tan, D. W., Schiefer, M. A., Keith, M. W., Anderson, J. R., Tyler, J., & Tyler, D. J. (2014). A neural interface provides long-term stable natural touch perception. Science Translational Medicine, 6(257), 257ra138-257ra138. https://doi.org/10.1126/scitranslmed.3008669

Tehovnik, E. J., Tolias, A. S., Sultan, F., Slocum, W. M., & Logothetis, N. K. (2006). Direct and Indirect Activation of Cortical Neurons by Electrical Microstimulation. Journal of

Neurophysiology, 96(2), 512–521. https://doi.org/10.1152/jn.00126.2006

Valle, G., Mazzoni, A., Iberite, F., D'Anna, E., Strauss, I., Granata, G., Controzzi, M., Clemente, F., Rognini, G., Cipriani, C., Stieglitz, T., Petrini, F. M., Rossini, P. M., & Micera, S. (2018). Biomimetic Intraneural Sensory Feedback Enhances Sensation Naturalness, Tactile Sensitivity, and Manual Dexterity in a Bidirectional Prosthesis. Neuron, 100(1), 37-45.e7. https://doi.org/10.1016/j.neuron.2018.08.033

Weber, A. I., Saal, H. P., Lieber, J. D., Cheng, J.-W., Manfredi, L. R., Dammann, J. F., & Bensmaia, S. J. (2013). Spatial and temporal codes mediate the tactile perception of natural textures. Proceedings of the National Academy of Sciences, 110(42), 17107–17112. https://doi.org/10.1073/pnas.1305509110

Wendelken, S., Page, D. M., Davis, T., Wark, H. A. C., Kluger, D. T., Duncan, C., Warren, D. J., Hutchinson, D. T., & Clark, G. A. (2017). Restoration of motor control and proprioceptive and cutaneous sensation in humans with prior upper-limb amputation via multiple Utah Slanted Electrode Arrays (USEAs) implanted in residual peripheral arm nerves. Journal of NeuroEngineering and Rehabilitation, 14(1), 121. https://doi.org/10.1186/s12984-017-0320-4

Wodlinger, B., Downey, J. E., Tyler-Kabara, E. C., Schwartz, A. B., Boninger, M. L., & Collinger, J. L. (2015). Ten-dimensional anthropomorphic arm control in a human brain-machine interface: Difficulties, solutions, and limitations. Journal of Neural Engineering, 12(1), 016011. https://doi.org/10.1088/1741-2560/12/1/016011

Chapter 2 | Spike timing in somatosensory cortex supports frequency perception

2.1 Abstract

The temporal patterning of spikes – on the scale of milliseconds – often carries task-relevant information. In sensory systems, temporal spiking patterns in the periphery have been shown to be relevant for perception, but their role in the central nervous system remains controversial. The neuronal processing of skin vibrations and its perceptual correlates constitutes a fruitful model of the role of spike timing in cortex. Indeed, vibratory responses in somatosensory cortex (SC) exhibit phase-locking that faithfully carry information about the frequency composition of the vibrations. However, under certain conditions, frequency information is also conveyed in the response rates. The respective roles of timing and rate to frequency encoding in cortex is compounded by the facts that changes in frequency (1) result in changes in both vibratory pitch and magnitude; and (2) modulate both the temporal patterning and the response rates. To disentangle the contributions of timing and rate to the vibrotactile pitch perception, we trained monkeys to discriminate the frequency of vibrations – ranging from 10 to 200 Hz – in the presence of concomitant and uninformative variations in stimulus amplitude. The manipulation of amplitude was designed to eliminate intensive cues in pitch discrimination and to introduce a parameter that modulates firing rates. We could then assess the degree to which the strength and timing of populations of SC neurons account for the animals' ability to perform the frequency discrimination task in the presence of intensity confounds. First, we show that animals can discriminate pitch, but their performance is biased by stimulus amplitude. Second, we show that rate-based representations of frequency are far more dependent on vibratory amplitude than is the animals' behavior. In contrast, timing-based representations are impervious to changes in amplitude. We conclude that temporal spiking patterns play a key role in tactile pitch perception but

that rate drives pitch judgments, albeit to a lesser extent.

2.2 Introduction

Neurons throughout the nervous system exhibit patterns of activation that contain information not only in the strength of their response – the rate at which they emit spikes – but also in the distribution of these spikes across time, at time scales measured in single-digit milliseconds. Whether spike timing at those temporal resolutions contributes to the transmission of information in the central nervous system remains controversial. The somatosensory system is a fertile model to study the role of temporal coding in nervous system function given the exquisitely precise temporal patterning in the spiking responses of neurons across large swaths of its neuraxis. Indeed, skin vibrations delivered to the skin or textured surfaces scanned across the skin elicit highly repeatable and precise spiking patterns in tactile nerve fibers. These patterns have been shown to be highly informative about the frequency composition of the vibration (Mackevicius et al., 2012; Talbot et al., 1968) or the identity of the texture (Weber et al., 2013). Temporal spiking patterns have also been shown to shape the way the vibrations or textures are perceived (Birznieks and Vickery, 2017; Lieber et al., 2017; Mackevicius et al., 2012; Weber et al., 2013).

Informative temporal spiking patterns have also been observed in the central nervous system, including the cuneate nucleus (Suresh et al., 2021), thalamus (Moore et al., 2015; Urbain et al., 2015), and somatosensory cortex (SC) (Harvey et al., 2013; Hernandez et al., 2000; Lieber and Bensmaia, 2019; Long et al., 2021; Luna et al., 2005; Mountcastle and Steinmetz, 1990; Mountcastle et al., 1990, 1969; Romo and Salinas, 2003; Salinas et al., 2000). Unlike at the periphery, however, the role of spike timing in downstream neurons is more difficult to ascertain because, unlike tactile nerve fibers, which can be divided into a handful of clearly delineated neuronal classes, central neurons exhibit highly heterogeneous responses. Each neuron affects computations on input signals from multiple nerve fibers,

often of different classes, conferring to it a preference for a spatiotemporal feature in the input (DiCarlo et al., 1998; Lieber and Bensmaia, 2019; Saal et al., 2015; Suresh et al., 2021). A large population of such neurons can thus, in principle, encode any spatiotemporal input pattern in its rate response (Lieber and Bensmaia, 2019).

The most direct and compelling inquiries of the role of spike timing in SC have been in the context of sinusoidal vibrations, which vary in only two parameters – frequency and amplitude – and produce sensations that varies along two perceptual continua – pitch and intensity. SC responses have been shown to phase lock to the vibrations, (Harvey et al., 2013; Hernandez et al., 2000; Luna et al., 2005; Mountcastle and Steinmetz, 1990; Mountcastle et al., 1990, 1969; Salinas et al., 2000), though the phase locking drops sharply at higher frequencies (Harvey et al., 2013; Mountcastle and Steinmetz, 1990). As the phase locked responses faithfully reflect the stimulus frequency, this temporal code was put forth as a candidate neural signal for encoding pitch (Mountcastle and Steinmetz, 1990). However, changes in frequency are accompanied by changes in firing rate, and this rate-based signal– under some conditions – is also highly informative about frequency and can account for pitch perception (Harvey et al., 2013; Luna et al., 2005; Mountcastle et al., 1969; Salinas et al., 2000). The viability of the rate code breaks down at high frequencies ($>$ 50 Hz) as the relationship between firing rate and frequency breaks down (Harvey et al., 2013). Even at the low frequencies, the rate code for frequency is, in principle at least, susceptible to large amplitude-dependent distortions given the strong and nearly universal impact amplitude has on SC firing rates. To further muddle the issue, changes in frequency do not only change the perceived pitch of a vibration, but also its perceived intensity, likely resulting from the frequency-dependent changes in cortical rates.

The objective of the present study was to disentangle the various factors that shape pitch perception and the neuronal representation of vibration to assess the degree to which spike timing shapes pitch perception. To this end, we trained monkeys to discriminate the

frequency of sinusoidal vibrations delivered to skin while we recorded the responses of neurons in SC. To disentangle the contribution of rate and timing to frequency perception, we varied the amplitude of the vibrations from trial to trial, such that the firing rate of the SC population response – and the intensity of the stimulus – would vary independently of the behaviorally relevant parameter, namely frequency. To disentangle the seemingly disparate codes in the flutter (< 50 Hz) and vibration (> 50 Hz) ranges, we had the animals perform the discrimination task across frequencies up to 200 Hz. We found, under these experimental conditions, that a rate-based code could not account for the ability to discriminate frequency, implicating phase-locking in pitch perception. However, our results also suggest that rate information may also contribute to pitch perception, or at least influence frequency judgments.

2.3 Results

2.3.1 Frequency discrimination

Human subjects can discriminate the frequency of vibrations applied to the skin even in the presence of concomitant and uninformative variations in amplitude (Harvey et al., 2013). To assess the degree to which monkeys were also capable of frequency discrimination, we had them perform a frequency discrimination task. In one version of the task, animals were sequentially presented with a pair of vibrations and reported which of the two was higher in frequency. In another version of the task, they were presented a single vibration and classified it as higher or lower than a separatrix, which they learned via trial and error over a few hundred trials (Figure 2.1B). The latter paradigm tended to yield higher accuracy than the former, but the results were qualitatively similar. In both cases, the amplitude of each stimulus varied from trial to trial to preclude performing the task on the basis of intensive cues, as sensation intensity increases with both frequency and amplitude (LaMotte

and Mountcastle, 1975; Mountcastle et al., 1990; Verrillo et al., 1969).

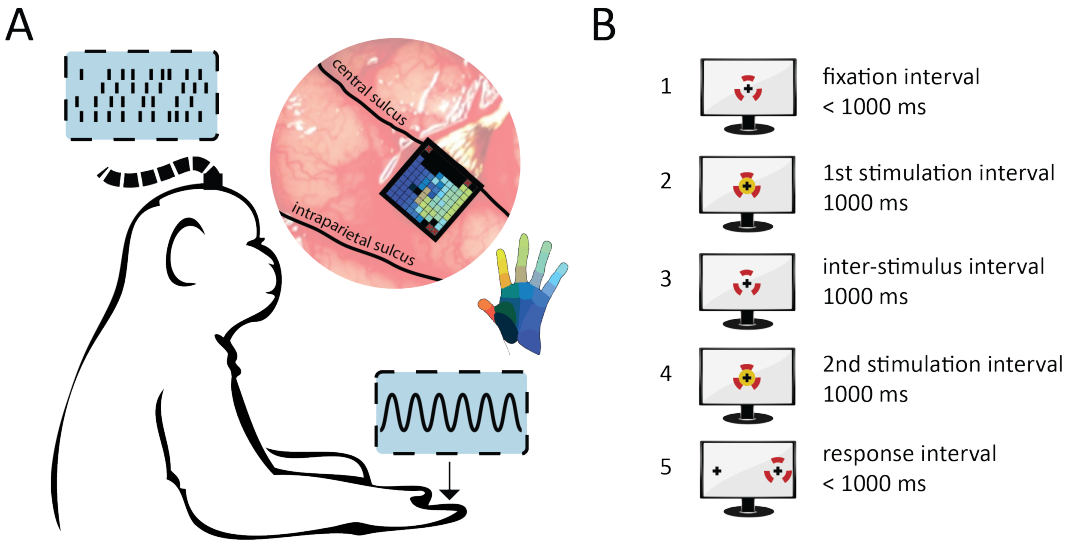

Figure 2.1: Experiment. A — A multielectrode array was implanted on the hand representation of monkeys M3 and M4. During experiments, monkeys were seated facing a monitor with their palm facing upward. Sinusoidal vibrations were delivered to the hand via a punctate probe. For M3 and M4, stimuli were delivered to the receptive fields of neurons captured by the array and neural responses were recorded. During passive recordings, M3 and M4 simply had to remain still while stimuli were delivered in sequence. B — Task progression. M1, M2, and M3 performed the discrimination task shown in B, in which they had to judge whether the standard frequency presented in the first interval (step 2) was higher than the comparison frequency in the second interval (step 4). M4 performed a similar frequency classification task with a single stimulation interval. It had to determine whether the stimulus frequency was higher or lower than a separatrix learned through training. Very importantly, in both tasks the amplitudes of the stimuli was manipulated so that high frequencies could not reliably be identified by the intensity of sensations.

With both paradigms, we found that animals were able to discriminate frequency in the presence of fluctuations in amplitude (Figure 2.2A, Figure E.1A). Indeed, as the comparison frequency increased, the likelihood of judging it as higher in frequency increased systematically. However, even after extensive training, animals retained a bias toward judging higher amplitude vibrations as higher in frequency, as evidenced by the spread in the psychometric functions (upward shift as curves progress from cyan to purple). Low-amplitude, high-frequency stimuli and high-amplitude, low-frequency stimuli were overrepresented to train the monkeys to reduce this bias, even leading to a slight reversed bias in a single case,

when monkey M4 performed the classification task with a 100-Hz separatrix (Figure E.1B right panel, Figure 2.2C). The amplitude bias was more pronounced for some animals than others and was stronger at some frequencies than others (see below).

In humans, tactile frequency perception is more acute at the low than high frequencies (Goff, 1967). The same phenomenon was observed in monkeys, with JNDs increasing systematically as the standard frequency increased (Figure 2.2D). JNDs tended to increase faster than did the standard frequency, leading to a tendency for the Weber fraction to increase with frequency, as has been observed in human participants (Figure E.1C)(Goff, 1967). The JNDs (and Weber fractions) derived from the monkeys' performance were similar to their human counterparts when amplitudes were reduced with higher frequencies to obtain matched intensities (Goff, 1967; LaMotte and Mountcastle, 1975; Mahns et al., 2006; Mountcastle et al., 1990). Note that the task the animals were performing is more complex than was the task performed in these psychophysical experiments with humans, because instead of being matched, intensive cues varied widely and randomly.

As mentioned above, the magnitude of the amplitude bias – reflected in the spread between psychometric functions – varied across animals and frequencies. The bias was larger for the more difficult comparison frequencies (Figure E.1D, comparison stimuli with lower P(correct) tend to have higher performance spreads), suggesting the animals may have defaulted to using intensity when they could not confidently judge frequency. For the discrimination task, the bias was also more pronounced at the higher frequencies of each range (Figure E.1 A: compare the spreads to the left and right of the standards, and D: the more purple comparisons tend to have higher spreads), which were more difficult to distinguish especially for the higher standards, as evidenced by higher JNDs and Weber fractions. However, even with extreme differences in amplitudes, the monkeys could consistently make frequency judgements indicating that frequency could be discriminated semi-independently of amplitude.

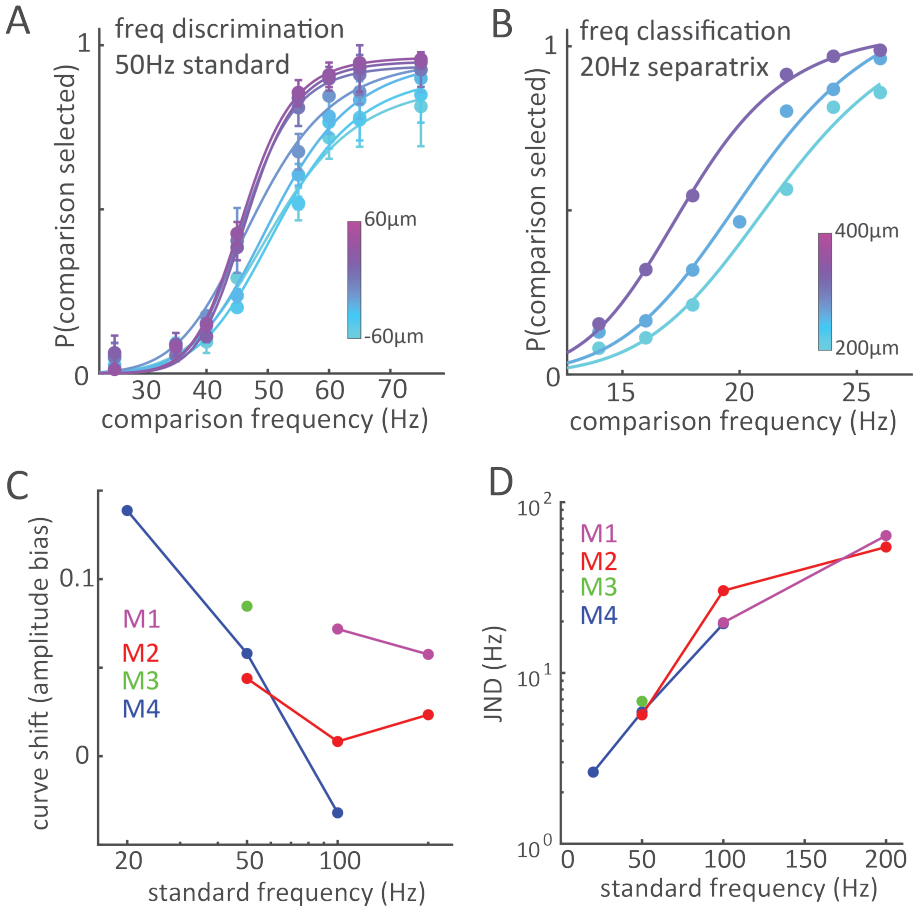

Figure 2.2: Psychophysics. A — one example of frequency discrimination psychophysical performance. This plot shows the performance of monkeys M2 and M3 with a 50Hz standard. The Y axis shows the proportion of trials on which the monkeys selected the comparison frequencies on the x axis as higher than the standard. The color legend corresponds to the amplitude differences between the comparison and standard frequencies. Performance plots for all standards are show in Figure E.1A. B — one example of frequency classification psychophysical performance. This plot shows the performance of monkey M4 with a 20Hz separatrix. Y axis shows the proportion of trials on which the monkeys selected the comparison frequencies on the x axis as higher than the separatrix. Color legend corresponds to the amplitude of the stimulus. Performance plots for all separatrixes are show in Figure E.1B. C — Amplitude bias on performance. For each monkey and frequency range, this shows the amplitude-related curve shift (see methods), which quantifies the tendency for higher-amplitude (more purple in A and B) curves to lie above lower-amplitude (more blue) curves. A positive number indicates the monkey had a bias for selecting higher amplitudes while a negative number indicates the inverse. D — JNDs of individual animals for discrimination (M1, M2, M3) and classification (M4) at each standard/separatrix. Note the y axis is on a log scale.

2.3.2 Neural responses to sinusoidal vibrations

While all neurons in somatosensory cortex (SC) responded vigorously to vibrations applied to their receptive fields, the dependence of the response on frequency varied across neurons. Indeed, some SC neurons exhibited a strong sensitivity to frequency in their response whereas others did not (Figure 2.3, Figure E.3A-C). For neurons whose firing rates were frequency-dependent, frequency dependence was very prominent at the low frequencies and disappeared at the high frequencies (Figure 2.3). In contrast, the responses of all neurons increased with amplitude at all frequencies (Figure E.3D-F). Most SC neurons also exhibited spiking responses that phase locked with the stimulus, producing one or more spikes within a restricted phase of each stimulus cycle (Figure 2.4A). This phase-locking was prominent and widespread at low frequencies and became less so at higher frequencies (Figure 2.4B,C, Figure E.4).

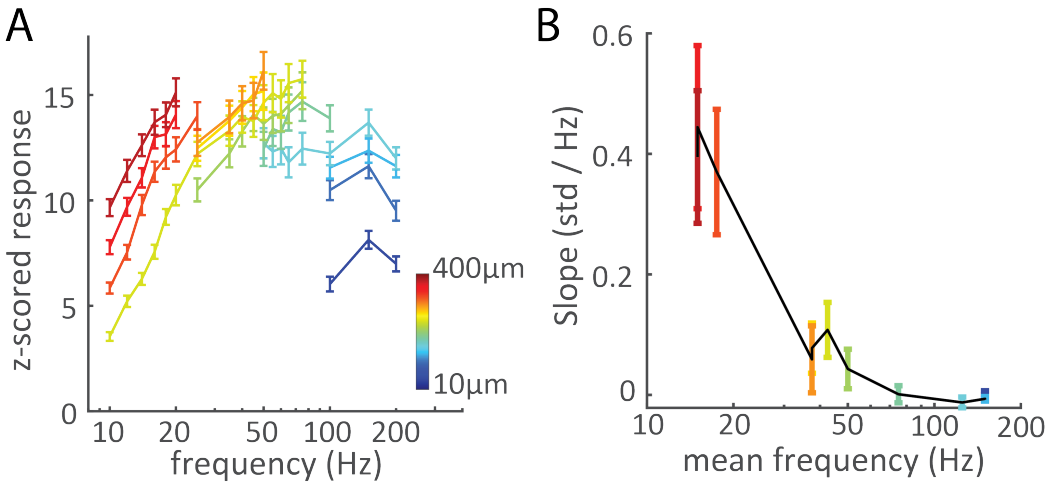

Figure 2.3: Firing rate and frequency A — Spike rate versus frequency for a representative neuron with a strong rate-frequency relationship. Rate rises with frequency in the low range but the slopes decrease at higher frequency ranges. B — Rate-versus-frequency slopes as a function of frequency for the most highly responsive neurons (see Figure E.2B for the distribution of responses). Each colored point corresponds to the slope of the matching line in panel A. The X-coordinate correspond to the mean frequency spanned by each of these lines.

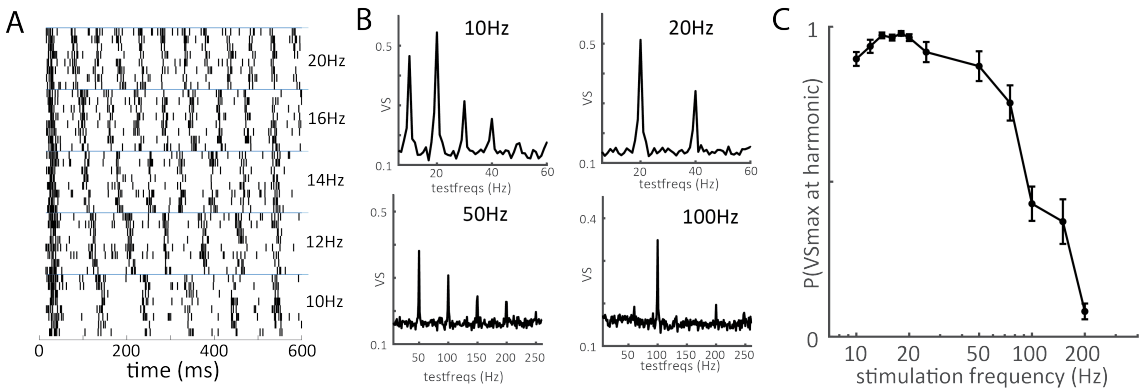

Figure 2.4: Timing in SC responses. A — Raster plot of responses to low frequency vibrations from an example neuron. B — Illustrative examples of spike train vector strengths at the stimulation frequencies indicated on each plot. Note the peaks at the stimulation frequencies and their harmonics, indicating stronger phase locking to these frequencies. C — Strength of phase locking across stimulation frequencies. The plot shows the proportion of trials on which the stimulus frequency or its harmonic have the highest VS of all test frequencies, as a function of stimulus frequency. The line shows the average results across test sessions of the most highly-phase-locked electrode in each session judged using this metric. Note the drop-off in the strength of phase locking at higher frequencies.

2.3.3 Neural coding of frequency – decoding

Having established (1) that animals can perform a vibratory frequency discrimination task across variations in amplitude and (2) that the rate and timing of the responses of SC neurons are both modulated by vibratory frequency, we sought to assess whether these two aspects of the neuronal response could account for the animals' discrimination behavior. To this end, we investigated the degree to which frequency could be decoded from the rate and timing of the neuronal response using linear discriminant analysis (LDA).

First, we gauged our ability to decode frequency when amplitude was constant, focusing on the low frequency range to replicate previous findings that firing rate carries frequency information under these conditions (Luna et al., 2005; Romo and Salinas, 2003; Salinas et al., 2000). Indeed, classification performance was nearly perfect under these conditions (Figure 2.5A). When this analysis was extended across the entire frequency range, however, the rate-based code was found to break down at high frequencies (Figure E.5A), consistent

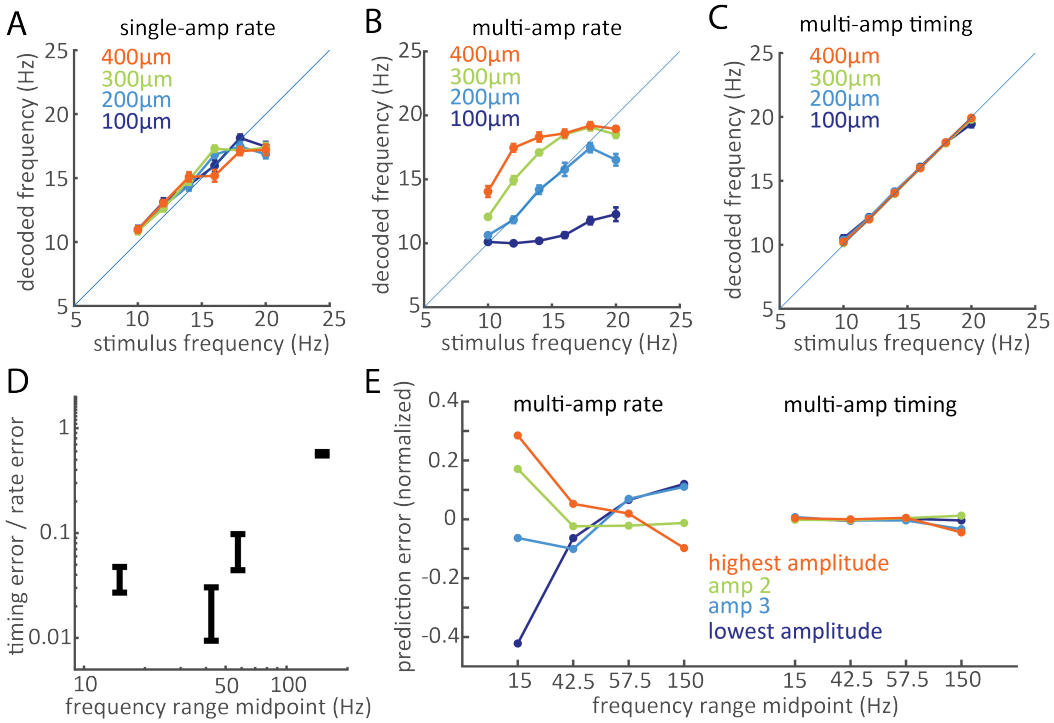

Figure 2.5: Effect of multiple amplitudes on frequency decoding. A-C — Decoded frequency versus stimulus frequency in the low frequency range, using (A) a rate decoder with constant amplitudes (neural responses were grouped by amplitude and a rate decoder was trained and tested for each separately, (B) a rate decoder with all amplitudes (a single rate decoder was trained and tested on neural responses from all amplitudes), and (C) a timing decoder with all amplitudes. See Figure E.5 for decoding of higher frequency ranges. D— Ratio of timing prediction error to multi-amp rate prediction error across frequency ranges. Note the log y scale. The prediction error is averaged across all frequencies and amplitudes in each frequency range. E — For the multi-amp decoder (left) and multi-amp timing decoder (right), prediction error for the 4 amplitudes in each frequency range, ranked from highest to lowest (see color legend). The error is computed as (decoded frequency – actual frequency) so the sign reflects the direction of any bias: a positive error means predictions were systematically too high, and a negative one means they were too low. Errors from each frequency range were computed separately for each amplitude but averaged across frequencies, and were normalized by the frequency range.

with the flat rate-frequency functions in this range (Figure 2.3B).

Next, we gauged our ability to decode frequency in the presence of variations in amplitude. Under these conditions, decoding performance was poor as decoded frequency was strongly dependent on amplitude (Figure 2.5B), reflecting the dependence of firing rate on amplitude (Figure E.3D-F). In contrast, a decoder that exploited phase locking in the response yielded near perfect performance for all frequencies below 100 Hz, and still outperformed a rate decoder at higher frequencies (Figure 2.5C, Figure E.5B,C). We compared the performance of rate and timing decoders across the ranges of frequencies and found not only that timing-based decoders systematically outperformed their rate-based counterparts (Figure 2.5D), but that only the errors of the rate decoder were highly biased by amplitude (Figure 2.5E). That is, the frequency signal conveyed by the temporal patterning was independent of amplitude whereas that conveyed by the rate was highly amplitude-dependent. The direction of the amplitude-related bias was inconsistent across frequency ranges (Figure 2.5E).

2.3.4 Neural coding of frequency – neurometrics

The classification analysis described above gauges the ability to recover frequency from the population response, averaged across repeated presentations of a stimulus. However, these analyses do not take into consideration the reliability of the frequency signal, precluding a comparison with the psychophysical performance of the animals. To fill this gap, we computed neurometric functions by using decoders to perform the same tasks as the monkeys had performed: judging whether the spike trains evoked by a single stimulus encode a lower or higher frequency than a standard frequency, either in a two alternative forced choice task or a binary classification task. In brief, the rate or timing signals from single stimuli were used to decode their vibration frequency, and the frequency judgment was then computed from these decoded values (by comparing two of them for the two alternative forced choice discrimination task, or by determining whether the decoded value was above the separatrix

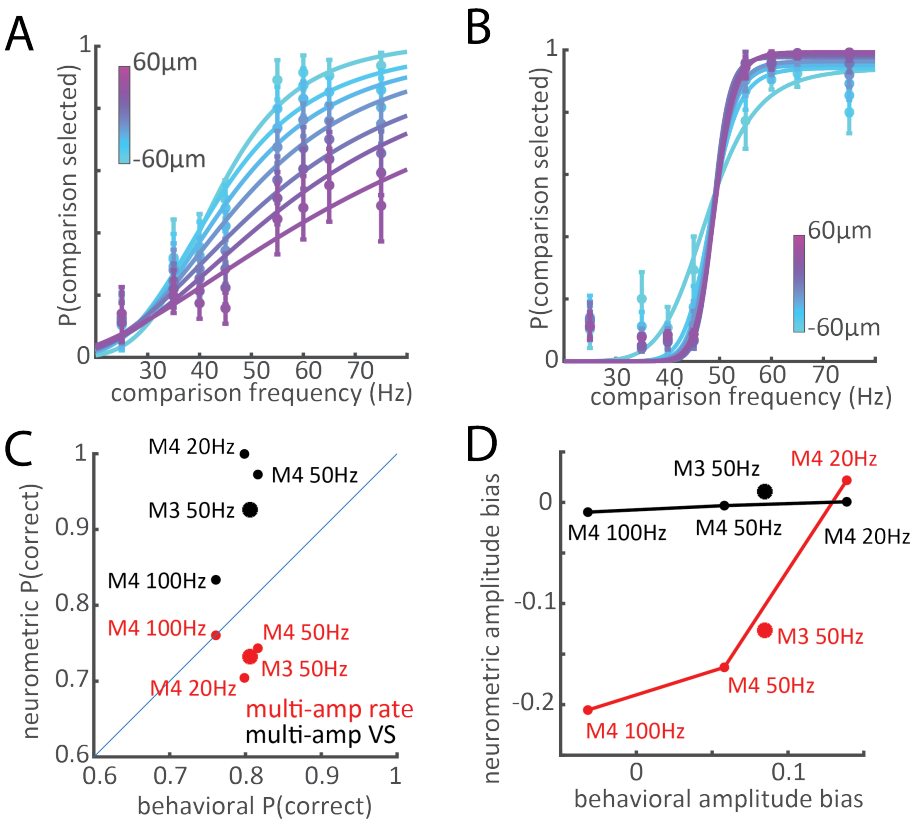

Figure 2.6: Neurometrics A and B — Neurometric performance of a multi-amp rate decoder (A) or multi-amp timing decoder (B) applied to the neural responses of M3 from the 2AFC discrimination task with a 50Hz standard. Color legend represents the difference between comparison and standard stimuli compared each trial. The neurometric performances of decoders applied to the neural responses of M4 from the frequency classification task are shown in Figure E.6A-F. C — For each monkey and standard/separatrix from which neural responses were recorded during the task (M3: 50Hz; M4: 20, 50, 100Hz), this plot shows overall neurometric percent correct for the timing (black) and rate (red) decoders versus the overall percent correct achieved by the animals. Each point corresponds to data from one animal at one standard/separatrix and is labeled. The animals outperformed the rate decoders, but not the timing decoders. D — Amplitude bias of the neurometric performance of each decoder versus the amplitude bias of the animal (as shown in Figure 2.1C). A positive bias indicates a tendency to select high-amplitude stimuli as higher in frequency. The timing decoders show negligible amplitude bias in all cases. The rate decoders show substantial biases that differ from those of the animals in magnitude and direction.

for the classification task).

For all animals and frequency conditions, the timing-based decoders yielded far superior performance than did the rate-based decoders (Figure 2.6A-C, Figure E.6). Importantly, differences in amplitude strongly influenced the performance of the rate decoders, typically to a higher degree than they influenced the performance of the animals (Figure 2.6D, and compare the left column of Figure E.6 to Figure E.1A,B). Furthermore, the direction of the amplitude bias of the rate decoders was often inconsistent with that of the animals (Figure 2.6D, observe the signs of points on each axis). At low frequencies, where rate generally rises fast with frequency, the rate decoder was biased toward judging higher-amplitude stimuli as being higher in frequency. At higher frequencies, where the rate-frequency functions become flat or even negatively sloped (Figure 2.3B, Figure E.3A-C), the amplitude bias progressively shifts toward lower frequencies (Figure 2.6D). The monkeys, on the other hand, generally maintained a bias toward higher amplitudes (the only exception being M4 with the 100-Hz separatrix, whose slight negative bias is shown in Figure E.1B, right panel).

In conclusion, the rate-based frequency decoders are far more susceptible to changes in amplitude than are the timing-based ones. If the animals' frequency judgments were driven solely by neuronal firing rates, their performance on the discrimination task would be more amplitude-dependent than it is.

2.3.5 Single trial covariance of neural responses and behavior

Having examined whether the rate and timing of the neuronal response could account for the animals' trial-averaged performance, we next investigated whether fluctuations in the neuronal responses covaried with the animals' choice on a trial-by-trial basis. In other words, do momentary fluctuations in the neuronal response correlate with the animals' behavior for any given experimental condition? To test this possibility, we repeated the decoding analysis described above, but split trials according to the binary judgments of the animals for each

stimulus pair (M3 discrimination) or stimulus (M4 classification). We reasoned that, if fluctuations in the firing rate or strength of phase locking resulted in fluctuations in the perceived frequency, these fluctuations would also be reflected in the animals' judgments. As a result, decoded frequency would then to be higher for stimuli selected by the animal than for those not selected.

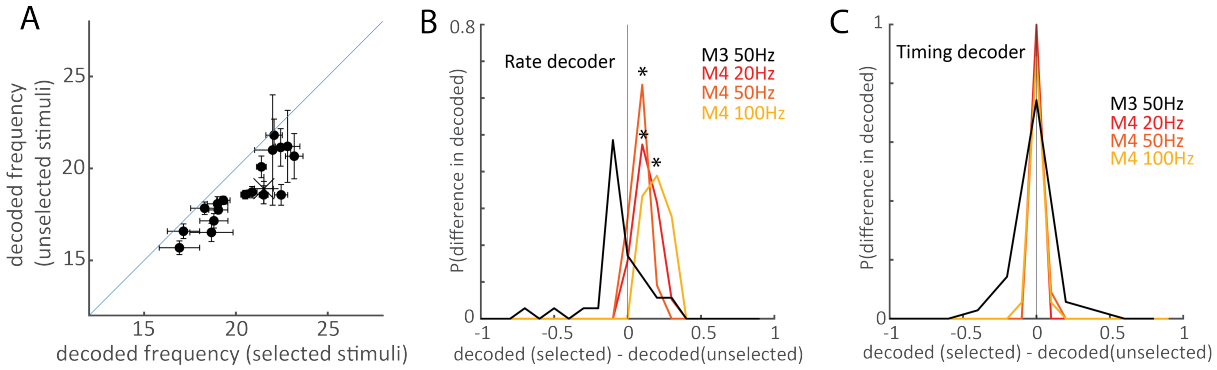

Figure 2.7: Single trial covariation of neural responses and behavior. A — Mean rate-decoded frequency when M4 did not select a stimulus versus mean rate-decoded frequency when M4 did. Each point represents a unique comparison stimulus used with the 20Hz separatrix. The results were similar with the 50-Hz and 100-Hz separatrices (Figure E.7A-C). An analogous plot for M3 is shown in Figure E.7D. B — Probability distribution of differences in average decoded frequencies in the selected and unselected cases for each unique trial condition (i.e. difference in x and y axis values for individual points in A and Figure E.7A-D). Results from each monkey and separatrix are plotted in different colors. Asterisks denote distributions with means significantly different from 0 ($p = 0.01$). The three M4 distributions have significant non-zero positive means, indicating that identical stimuli are decoded as higher on average when selected by M4. The M3 distribution mean is not significantly different from 0, indicating no single trial covariance of rate and behavior. C — Probability distribution of differences in average timing-decoded frequencies in the selected and unselected cases for each unique trial condition. No significant relationship was found between behavior and the timing-decoded frequency across all monkeys and frequency ranges.

Frequencies decoded from rates covaried significantly with the behavior of M4 (Figure 2.7A, B, Figure E.7A-C): decoded frequencies were slightly higher for vibrations that were judged to be higher than the separatrix than were decoded frequencies that were not judged to be higher for each amplitude condition. This effect was most pronounced for frequencies near the standard, consistent with the hypothesis that amplitude biases were more

pronounced when the animal was uncertain. For M3, frequencies decoded based on rates evoked on individual trials tended to covary with behavior (though not significantly; $p = 0.08$), but in the wrong direction. That is, the decoded frequency tended to be lower when the animal judged the stimulus as higher in frequency (Figure 2.7B, Figure E.7D). To understand the relationship between decoded frequency and the animals' behavior, we analyzed the firing rates themselves, conditioning them according to the animals' behavioral choice. While firing rates and behavior covaried in both M3 and M4, the relationship was inconsistent across animals and difficult to interpret (see Supplementary Discussion in Appendix E).

We carried out similar analyses using timing decoders and found that decoded frequencies did not covary with behavior in any condition (Figure 2.7C).

2.4 Discussion

We show that animals can judge the pitch of tactile vibrations independent of concomitant and uninformative variations in sensation magnitude arising from variations in stimulus amplitude, although the animals exhibit some amplitude-dependent bias in their frequency judgments. We then find that frequencies decoded from neuronal firing rates are far more susceptible to variations in vibratory amplitude than are the corresponding pitch judgments. In contrast, decoding frequency from the temporal patterning in the response – reflecting phase locking to the vibration – yields more reliable and nearly amplitude-independent pitch discrimination judgments. We conclude that temporal spiking patterns in SC play a key role in the genesis of the pitch percept. However, trial-to-trial fluctuations in firing rate also covary with pitch judgments, suggesting that pitch perception may rely on a combination of spike timing and rate.

2.4.1 The perceptual correlates of changes in vibratory frequency

A major challenge in establishing a neural code is that stimulus dimensions are typically not encoded independently. In the sense of touch, for example, the neural representations of texture and scanning speed are entangled in the somatosensory nerves (Delhaye et al., 2019; Weber et al., 2013); texture and speed information is then disentangled via downstream processing (Lieber and Bensmaia, 2020), a process that culminates in a stable representation for texture but not for speed (Boundy-Singer et al., 2017; Delhaye et al., 2019; Dépeault et al., 2008). Even the two parameters that define a sinusoidal vibration – frequency and amplitude – modulate the resulting experience in non-orthogonal ways. While vibratory frequency is the major determinant of pitch and vibratory amplitude is the main determinant of perceived magnitude, magnitude is also strongly dependent on frequency (Verrillo et al., 1969) and pitch is somewhat dependent on amplitude (Prsa et al., 2021; Roy and Hollins, 1998). This interplay of the two stimulus parameters in shaping the sensory experience must then be taken into consideration in the search for neural codes. The challenge in the study of the neural underpinnings of pitch perception is that vibratory frequency has a strong impact on magnitude, so frequency judgments reflect changes in both pitch and magnitude.

2.4.2 Neural codes for vibratory frequency

We show that temporal spiking patterns convey information about vibratory frequency in an amplitude-independent way whereas rate responses convey far less information about vibratory frequency, particularly at the high frequencies (> 50 Hz), and do so in a highly amplitude-dependent way. Two findings argue against the temporal code for pitch. The first is that timing-based decoders outperform the animals, both in the acuity with which they can discriminate frequency and in the degree to which they do so independently of amplitude. The second is that frequencies decoded from phase-locked responses do not fluctuate with the animals' behaviors in the way that rate-based decoders do. The challenge

is that timing-based decoders – which rely on Fourier analysis or vector strength – do not take into consideration any neural implementation. These decoders therefore provide an estimate of the upper bound on the ability to discriminate frequency from temporal spiking patterns. To the extent that the extraction of pitch information from phase-locked responses (by downstream neurons) is not optimal, frequency discrimination performance will be lower than that derived from (nearly) optimal temporal decoders (cf. Figure 2.6B and (Salinas et al., 2000)). To the extent that the pitch extraction is contaminated by amplitude cues, as most biological plausible circuits are liable to be, the resulting pitch percepts will be contaminated by amplitude cues and covary with firing rate. The present results constrain models of how neural circuits convert temporal representations of frequency into rate-based representations ones that are robust (but not impervious) to variations in amplitude.

One possibility to explain the amplitude-dependence of pitch judgments is that pitch perception is not solely dependent on timing but also relies on firing rates. In this view, pitch discrimination relies on a combination of temporal and rate-based codes. Another possibility is that humans and animals fall back on magnitude cues when the pitch judgments are challenging and uncertain. That the covariation of rate and behavior is strongest for difficult comparisons is consistent with the latter interpretation. However, the integration of rate-based and timing-based signals has been observed in the context of texture perception and could play a role in the genesis of pitch percepts.

2.5 Methods

2.5.1 Animals

Four male Rhesus macaques (Macaca mulatta), 7-13 years old and weighting 9-12kg, participated in this study. Animal care and handling confirmed to the procedures approved by the University of Chicago Animal Care and Use Committee. Monkeys M1 and M2 were

implanted over four years before the beginning of the study so signal quality precluded any neural data collection. Accordingly, only behavioral data are reported for M1 and M2. Neurophysiological and behavioral data are reported for M3 and M4, who received implants at the onset of these experiments.

2.5.2 Implants

Each animal was implanted with one Utah electrode array (UEA)(Blackrock Microsystems, Inc., Salt Lake City, UT) in the hand representation of Brodmann's area 1 in somatosensory cortex (SC) (Figure 2.1A). Each UEA consists of 96 1.5mm-long electrodes with tips coated in iridium oxide, spaced 400µm apart, and spanning 4mm x 4mm of the cortical surface. The hand representation in area 1 was targeted based on anatomical landmarks. Given that the arrays were contiguous to the central sulcus and area 1 spans approximately 3-5mm of cortical surface from the sulcus (Pons et al., 1985), few if any electrodes were located in Brodmann's area 2. Given the length of the electrodes, their tips likely terminated in the infragranular layers of the somatosensory cortex if embedded to their base, as we have previously shown in postmortem histological analysis with other animals instrumented with identical arrays (Rajan et al., 2015).

2.5.3 Tactile stimuli

Stimuli consisted of 1-s long sinusoidal vibrations delivered at precisely controlled frequencies and amplitudes using a custom shaker motor (Westling et al., 1976) driving a 1-mm probe, pre-indented 0.5 mm into the skin (Figure 2.1A). The experimental decision to pre-indent was intended to mitigate the effects of small changes in the hand position of the animal, and predicated on the fact that afferent responses to pre-indentation decay within 10-20s (Leung et al., 2005), as does the resulting sensation, and afferent responses to indentation to the skin beyond the pre-indentation are identical to those with no pre-indentation (Vega-Bermudez

and Johnson, 1999). We mapped the receptive field of each electrode by identifying which areas of skin on the hand evoked significant multiunit activity when stimulated relative to baseline. Because an important goal of this research was to decode tactile stimuli using signals from multiple electrodes, we focused on skin locations whose somatotopic representation in area 1 was near the center of the array (i.e. the responses were not localized to the edge of the array, where some of the response might be outside the region upon which the array impinged). For M3 stimuli were delivered to the thumb pad, and for M4 they were delivered to the index fingertip pad.

2.5.4 Neurophysiological recordings

We simultaneously recorded from all 96 electrodes of the UEAs using a Cerebus system (Blackrock Microsystems, Salt Lake City, UT), passed the continuous voltage from each electrode, sampled at 30kHz, through at 250-Hz high-pass filter to reduce background noise, and recorded the timing of threshold-crossing events in each channel. Because we were interested in population responses, we analyzed the multi-unit responses (threshold crossings) from each electrode.

2.5.5 Passive recordings

Animals sat facing a monitor with their hand fixed palmar surface facing up – using Velcro starts and a drop of cyanoacrylate on the nail – to allow delivery of vibrotactile stimuli to the target skin location (Figure 2.1A). Eye movements were tracked with an optical eye-tracking system (MR PC60, Arrington Research, Scottsdale, AZ). For passive recordings, animals simply had to remain still while a series of 1-s long stimuli were sequentially delivered to the hand, each separated by 2 seconds. They performed a visual tracking task to keep them engaged and limit agitation and movement due to boredom. A large stimulus set was used, with frequencies ranging from 10 to 200 Hz and amplitudes from 10 to 400 microns.

2.5.6 Behavioral tasks – two-alternative forced-choice frequency discrimination

The animals were seated at the experimental table facing a monitor, which signaled the trial progression (Figure 2.1B). The animals initiated trials by directing their gaze to a cross in the center of the monitor. On each trial, 2 vibrotactile stimuli were sequentially delivered to the skin, each 1-s long and separated by a 1-s interstimulus interval. The first stimulus contained the standard stimulus and the second the comparison stimulus. The animals' task was to judge which of the two stimuli was higher in frequency. They responded by making a saccadic eye movement toward the left (selecting the first stimulus) or right (second stimulus) response targets that appeared after the second stimulus finished. A trial was aborted if the animal failed to maintain its gaze on the center until the appearance of the response targets. Correct responses were rewarded with juice. This task was performed by M1, M2, and M3.

2.5.7 Behavioral tasks – two-alternative forced choice frequency classification

This task was similar to the discrimination described above, except a single 1-s long vibrotactile stimulus was delivered on each trial. The animal had to judge whether the frequency of the stimulus was higher or lower than a separatrix learned over the first several hundred trials of training (with a constant separatrix). The animal made a saccade to the left to signal a lower stimulus frequency and to the right to signal a higher one. This task was performed by M4.

2.5.8 Experimental design – frequency discrimination

Three standard frequencies were used: 50 Hz (with comparisons ranging from 25 to 75 Hz), 100 Hz (with comparisons ranging from 50 to 300 Hz), and 200 Hz (with comparisons ranging

from 50 to 400 Hz). Only one standard was used per experimental session and behavioral and neurophysiological data collection with one standard was completed before moving on to another. Importantly, on each trial the amplitudes of the standard and comparison stimuli varied pseudo-randomly across large ranges, to preclude performing the task by judging the intensity of vibrations instead of their frequency. Amplitudes ranged between 55 and 115 microns for the 50-Hz standard and between 25 and 55 microns for the 100- and 200-Hz standards. Standards differing in amplitude were parametrically combined with comparisons differing in both amplitude and frequency and randomly interleaved in each experimental block. M1 performed the task with the 100- and 200-Hz standards, M2 performed the task with all three standards, and M3 performed it with just the 50-Hz standard.

2.5.9 Experimental design – frequency classification

Three separatrices were used: 20 Hz (with comparisons ranging from 14 to 26 Hz), 50 Hz (comparisons ranging from 35 to 65 Hz), and 100 Hz (comparisons ranging from 70 to 130 Hz). Only one separatrix was used per experimental sessions and all data were obtained with one before moving on to the next. As in the discrimination task, the amplitudes of the vibrations varied widely and randomly to prevent the animal from relying on intensive cues to make frequency judgments. Amplitudes ranged between 200 and 400 microns for the 20-Hz separatrix, between 67 and 150 microns for the 50-Hz separatrix, and between 30 and 70 microns for the 100-Hz separatrix.

2.5.10 Psychophysical data analysis

Just noticeable differences (JNDs) and Weber fractions: We built psychometric curves by fitting performance at each comparison frequency using a cumulative normal density function. For the discrimination task, we fit separate curves for each amplitude condition (i.e. combination of comparison and standard amplitudes)(Figure 2.2A, Figure E.1A). Similarly,

for the classification task, we fit separate curves for each comparison amplitude, given the absence of standard (Figure 2.2B, Figure E.1B). JNDs and Weber fractions were calculated using only trials in which both stimuli in the pair were of equal amplitude (for discrimination) or only trials in which the single comparison stimulus was at the middle amplitude (for classification), using a criterion performance of 75% correct.

Amplitude bias: The upward or downward shifts of psychometric curves representing different amplitude conditions reflected the dependence of animals' frequency judgments on the amplitude of stimuli. An upward shift indicates a bias toward judging more intense stimuli as being higher in frequency and vice versa. To quantify this bias, we computed the difference in the probability of being selected as higher in frequency (y axis values in Figure 2.1A,B) between every pair of comparisons with the same frequency but different amplitudes (e.g. the proportion of times a comparison of 55Hz at 60 microns minus the proportion of times a comparison of 55Hz at 40 microns, in Figure 2.1A). A positive value denotes a bias toward higher amplitudes, a negative value a bias toward lower amplitudes, a null value denotes no bias.

2.5.11 Neural data analysis

Standardizing neural responses: Multiunit activity varies widely from electrode to electrode, both at baseline when no stimulus is applied and in response to a stimulus, as might be expected given that different electrodes acquire signals from neuron groups that vary in size, sensitivity, and spontaneous activity. To compare rate responses across electrodes, we standardized stimulus-evoked responses according to the pre-stimulus baseline activity by subtracting the mean baseline rate and dividing by the standard deviation of the baseline rate across trials. That is, responses were converted to z-scores with respect to the baseline activity (Figure E.2A).

Rate-frequency relationships: We regressed mean firing rate on frequency at each ampli-

tude separately then averaged the resulting slopes of the lines. Neurons were then split into two groups depending on whether the resulting mean slopes were positive or negative.

Quantifying timing in the neural response: Consistent with previous results, we observed that SC neurons fire in phase with vibrotactile stimuli applied to their receptive fields: that is, their spike trains are phase locked to the frequency of the stimulus. We quantified the strength of this phase locking for by computing the vector strength (VS) of each stimulus-evoked spike trains across the relevant range of frequencies. To compare or combine phase locking signals across electrodes, we normalized the VS values from each spike train by the largest VS value across all test frequencies. Figure 2.4B and Figure E.4A show the results of this averaged across many repetitions of specific stimuli.

Decoding frequency from neural responses: We used linear discriminant analysis (LDA) to classify the frequency of stimuli from their evoked neural responses. As we recorded from 96 electrodes simultaneously, and there would be some daily variation in the strength of responses and their dependence on stimuli (though RFs were quite stable), we first computed the mutual information between the rates or vector strengths recorded at each electrode and stimulus frequency for each electrode, within each experimental session. We then selected the five most informative electrodes for rate and timing within each session for the classification analysis, having established that decoding performance was relatively insensitive to the number of electrodes, as long as it was more than 2.

Having selected the electrodes with the most informative rates, we computed the rate-frequency relationships and grouped electrodes according to whether they were positively or negatively sloped. We then averaged together the (z-scored) responses of the positive electrodes and did the same for the negative ones, yielding two inputs for the rate LDA. To generate the timing LDA input, we averaged the vectors of VS across test frequencies across the top timing electrodes. Once the decoder inputs for each stimulus were computed, we decoded the frequency of a given stimulus using a leave-one-out approach: the decoder

was trained on the inputs from every other stimulus, then applied to the held out one. This procedure was repeated for each stimulus in turn.

Decoding errors: Decoder errors were computed as the difference between the decoded and actual frequency for each stimulus. Negative errors corresponded to underestimates of the stimulus frequency.

Neurometric analyses: Neurometric functions were derived in the same manner as were their psychometric counterparts. For each stimulus pair in the discrimination task, the proportion of times the decoded frequency of the higher-frequency stimulus was greater than the decoded frequency of the lower-frequency stimulus was taken as the performance for that pair. For each stimulus in the classification task, performance was the proportion times the decoded frequency was higher or lower than the separatrix for the given experimental session. Once neurometric functions were obtained, the amplitude bias was computed as with their psychometric counterparts.

Covariance of decoded frequency and behavior: For each unique stimulus pair in each session of the discrimination task, trials were split according to whether or not the animal correctly selected the higher-frequency vibration. Stimulus conditions that were not repeated at least three times in the session or which did not yield at least one correct and one incorrect response were excluded from the analysis. The frequencies for each stimulus in each trial was decoded with rate- or timing-based LDAs and the mean decoded frequency was computed for each behavioral condition. For the classification task the approach was similar, but trials were split according to whether or not the animal selected the stimulus as higher than the separatrix.

Covariance of firing rate responses and behavior: This analysis was conducted as the one described above, except instead of analyzing decoded frequencies in each behavioral case, we compared firing rates conditioned on the two behavioral choices. Rates from electrodes with positive and negative rate-frequency relationships were analyzed separately.

Covariance of rate responses and behavior, pooling stimuli across parameters: We replicated a previous analysis (Luna et al., 2005) in which responses are pooled across all stimulus conditions before splitting them according to behavioral outcome. In brief, we z-scored the rates (classification) or rate differences (discrimination) of each trial for each stimulus condition in each session, then normalized each by dividing it by that conditions mean. The resulting normalized firing rate or firing rate differences were then pooled across trials, conditioned on the behavioral choice.

2.6 References

Birznieks, I., and Vickery, R. (2017). Spike Timing Matters in Novel Neuronal Code Involved in Vibrotactile Frequency Perception: Current Biology. Current Biology 27, 1485–1490.

Boundy-Singer, Z.M., Saal, H.P., and Bensmaia, S.J. (2017). Speed invariance of tactile texture perception. Journal of Neurophysiology 118, 2371–2377.

Britten, K.H., Newsome, W.T., Shadlen, M.N., Celebrini, S., and Movshon, J.A. (1996). A relationship between behavioral choice and the visual responses of neurons in macaque MT. Visual Neuroscience 13, 87–100.

Delhaye, B.P., O'Donnell, M.K., Lieber, J.D., McLellan, K.R., and Bensmaia, S.J. (2019). Feeling fooled: Texture contaminates the neural code for tactile speed. PLoS Biol 17.

Dépeault, A., Meftah, E.-M., and Chapman, C.E. (2008). Tactile Speed Scaling: Contributions of Time and Space. Journal of Neurophysiology 99, 1422–1434.

DiCarlo, J.J., Johnson, K.O., and Hsiao, S.S. (1998). Structure of Receptive Fields in Area 3b of Primary Somatosensory Cortex in the Alert Monkey. J. Neurosci. 18, 2626–2645.

Goff, G.D. (1967). Differential discrimination of frequency of cutaneous mechanical vibration. Journal of Experimental Psychology 74, 294–299.

Harvey, M.A., Saal, H.P., Dammann, J.F., and Bensmaia, S.J. (2013). Multiplexing Stimulus Information through Rate and Temporal Codes in Primate Somatosensory Cortex. PLoS

Biology 11, e1001558.

Hernandez, A., Zainos, A., and Romo, R. (2000). Neuronal correlates of sensory discrimination in the somatosensory cortex. Proceedings of the National Academy of Sciences 97, 6191–6196.

LaMotte, R.H., and Mountcastle, V.B. (1975). Capacities of humans and monkeys to discriminate vibratory stimuli of different frequency and amplitude: a correlation between neural events and psychological measurements. Journal of Neurophysiology 38, 539–559.

Leung, Y.Y., Bensmaïa, S.J., Hsiao, S.S., and Johnson, K.O. (2005). Time-Course of Vibratory Adaptation and Recovery in Cutaneous Mechanoreceptive Afferents. J Neurophysiol 94, 3037–3045.

Lieber, J.D., and Bensmaia, S.J. (2019). High-dimensional representation of texture in somatosensory cortex of primates. Proc Natl Acad Sci USA 116, 3268–3277.

Lieber, J.D., and Bensmaia, S.J. (2020). Emergence of an Invariant Representation of Texture in Primate Somatosensory Cortex. Cereb Cortex.

Lieber, J.D., Xia, X., Weber, A.I., and Bensmaia, S.J. (2017). The neural code for tactile roughness in the somatosensory nerves. Journal of Neurophysiology 118, 3107–3117.

Long, K.H., Lieber, J.D., and Bensmaia, S.J. (2021). Texture is encoded in precise temporal spiking patterns in primate somatosensory cortex (Neuroscience).

Luna, R., Hernández, A., Brody, C.D., and Romo, R. (2005). Neural codes for perceptual discrimination in primary somatosensory cortex. Nat Neurosci 8, 1210–1219.

Mackevicius, E.L., Best, M.D., Saal, H.P., and Bensmaia, S.J. (2012). Millisecond Precision Spike Timing Shapes Tactile Perception. Journal of Neuroscience 32, 15309–15317.

Mahns, D.A., Perkins, N.M., Sahai, V., Robinson, L., and Rowe, M.J. (2006). Vibrotactile Frequency Discrimination in Human Hairy Skin. Journal of Neurophysiology 95, 1442–1450.

Moore, J.D., Mercer Lindsay, N., Deschênes, M., and Kleinfeld, D. (2015). Vibrissa Self-Motion and Touch Are Reliably Encoded along the Same Somatosensory Pathway from

Brainstem through Thalamus. PLoS Biol 13, e1002253.

Mountcastle, V.B., and Steinmetz, M.A. (1990). Cortical Neuronal Periodicities and Frequency Discrimination in the Sense of Flutter. Cold Spring Harbor Symposia on Quantitative Biology 55, 861–872.

Mountcastle, V., Steinmetz, M., and Romo, R. (1990). Frequency discrimination in the sense of flutter: psychophysical measurements correlated with postcentral events in behaving monkeys. J. Neurosci. 10, 3032–3044.

Mountcastle, V.B., Talbot, W.H., Sakata, H., and Hyvärinen, J. (1969). Cortical neuronal mechanisms in flutter-vibration studied in unanesthetized monkeys. Neuronal periodicity and frequency discrimination. Journal of Neurophysiology 32, 452–484.

Pons, T.P., Garraghty, P.E., Cusick, C.G., and Kaas, J.H. (1985). A sequential representation of the occiput, arm, forearm and hand across the rostrocaudal dimension of areas 1, 2 and 5 in macaque monkeys. Brain Research 335, 350–353.

Prsa, M., Kilicel, D., Nourizonoz, A., Lee, K.-S., and Huber, D. (2021). A common computational principle for vibrotactile pitch perception in mouse and human. Nat Commun 12, 5336.

Rajan, A.T., Boback, J.L., Dammann, J.F., Tenore, F.V., Wester, B.A., Otto, K.J., Gaunt, R.A., and Bensmaia, S.J. (2015). The effects of chronic intracortical microstimulation on neural tissue and fine motor behavior. J. Neural Eng. 12, 066018.

Romo, R., and Salinas, E. (2003). Flutter Discrimination: neural codes, perception, memory and decision making. Nat Rev Neurosci 4, 203–218.

Roy, E.A., and Hollins, M. (1998). A ratio code for vibrotactile pitch. Somatosensory & Motor Research 15, 134–145.

Saal, H.P., Harvey, M.A., and Bensmaia, S.J. (2015). Rate and timing of cortical responses driven by separate sensory channels. ELife 4, e10450.

Salinas, E., Hernández, A., Zainos, A., and Romo, R. (2000). Periodicity and Firing Rate

As Candidate Neural Codes for the Frequency of Vibrotactile Stimuli. J. Neurosci. 20, 5503–5515.

Suresh, A.K., Greenspon, C.M., He, Q., Rosenow, J.M., Miller, L.E., and Bensmaia, S.J. (2021). Sensory computations in the cuneate nucleus of macaques. BioRxiv 2021.07.28.454185.

Talbot, W.H., Darian-Smith, I., Kornhuber, H.H., and Mountcastle, V.B. (1968). The sense of flutter-vibration: comparison of the human capacity with response patterns of mechanoreceptive afferents from the monkey hand. Journal of Neurophysiology 31, 301–334.

Urbain, N., Salin, P.A., Libourel, P.-A., Comte, J.-C., Gentet, L.J., and Petersen, C.C.H. (2015). Whisking-Related Changes in Neuronal Firing and Membrane Potential Dynamics in the Somatosensory Thalamus of Awake Mice. Cell Reports 13, 647–656.

Vega-Bermudez, F., and Johnson, K.O. (1999). SA1 and RA Receptive Fields, Response Variability, and Population Responses Mapped with a Probe Array. Journal of Neurophysiology 81, 2701–2710.

Verrillo, R., Fraioli, A., and Smith, R. (1969). Sensation magnitude of vibrotactile stimuli. Perception and Psychophyiscs 6, 366–372.

Weber, A.I., Saal, H.P., Lieber, J.D., Cheng, J.-W., Manfredi, L.R., Dammann, J.F., and Bensmaia, S.J. (2013). Spatial and temporal codes mediate the tactile perception of natural textures. Proceedings of the National Academy of Sciences 110, 17107–17112.

Westling, G., Johansson, R., and Vallbo, Å.B. (1976). A METHOD FOR MECHANICAL STIMULATION OF SKIN RECEPTORS. In Sensory Functions of the Skin in Primates, Y. Zotterman, ed. (Pergamon), pp. 151–158.

Chapter 3 | The frequency of cortical microstimulation shapes artificial touch

3.1 Abstract

Intracortical microstimulation (ICMS) of somatosensory cortex evokes vivid tactile sensations and can be used to convey sensory feedback from brain-controlled bionic hands. Changes in ICMS frequency lead to changes in the resulting sensation, but the discriminability of frequency has only been investigated over a narrow range of low frequencies. Furthermore, the sensory correlates of changes in ICMS frequency remain poorly understood. Specifically, it remains to be elucidated whether changes in frequency only modulate sensation magnitude – as do changes in amplitude – or whether they also modulate the quality of the sensation. To fill these gaps, we trained monkeys to discriminate the frequency of ICMS pulse trains over a wide range of frequencies (from 10 to 400 Hz). ICMS amplitude also varied across stimuli to dissociate sensation magnitude from ICMS frequency and ensure that animals could not make frequency judgments based on magnitude. We found that animals could consistently discriminate ICMS frequency up to approximately 200 Hz but that the sensory correlates of frequency were highly electrode dependent: on some electrodes changes in frequency were perceptually distinguishable from changes in amplitude – seemingly giving rise to a change in sensory quality –, on others they were not. We discuss the implications of our findings for neural coding and for brain-controlled bionic hands.

3.2 Introduction

Intracortical microstimulation (ICMS) delivered to somatosensory cortex has been shown to evoke tactile percepts the location and magnitude of which can be systematically manipu-

1. This chapter was published : Callier, T., Brantly, N. W., Caravelli, A., and Bensmaia, S. J. (2020). The frequency of cortical microstimulation shapes artificial touch. Proceedings of the National Academy of Sciences, 117(2), 1191–1200. https://doi.org/10.1073/pnas.1916453117.

lated (Berg et al., 2013; Flesher et al., 2016, 2017; Kim, Callier, Tabot, Gaunt, et al., 2015; Kim, Callier, Tabot, Tenore, et al., 2015; Tabot et al., 2013), a phenomenon that can be exploited to convey sensory feedback from sensorized bionic hands. The output of sensors on the prosthetic fingers can drive stimulation through electrodes located in the appropriate region of the somatosensory homunculus, thereby intuitively conveying information about contact location on the hand; -the strength of stimulation can be modulated to produce sensations whose magnitude depends on the output of the sensor, thereby intuitively conveying information about contact pressure (Tabot et al., 2013). Ideally, the electrically induced neuronal activity would mimic its mechanically induced counterpart in able bodied individuals, which would lead to completely natural sensation (Bensmaia, 2015; Bensmaia Miller, 2014). However, limitations inherent to electrical stimulation, in the number of stimulating channels, and in our understanding of cortical circuitry severely restrict our ability to produce naturalistic neuronal activity.

Despite its unnaturalness, however, ICMS leads to sensations that are reported by human subjects as being natural or nearly so (Flesher et al., 2016; Salas et al., 2018) and ICMS-based feedback leads to improved functionality for brain-controlled bionic hands(Flesher et al., 2019). In light of this, we seek to refine our understanding of how the parameters of ICMS shape the percept in the hopes of achieving increasingly intuitive and useful artificial touch. As alluded to above, the effects of ICMS amplitude on the evoked sensations have been extensively studied, as has the effect of stimulation location on the cortical sheet (i.e., through different electrodes)(Berg et al., 2013; Flesher et al., 2016; Kim, Callier, Tabot, Gaunt, et al., 2015; Salas et al., 2018; Tabot et al., 2013). Changes in ICMS frequency have been shown to evoke discriminable percepts in studies with non-human primates (Romo et al., 1998, 2000). However, the range of frequencies tested only spanned a small fraction of that relevant for neuroprosthetics (from 10 to 36 Hz).

Furthermore, the question remains how changes in frequency affect the evoked percept.

Indeed, sensitivity to ICMS increases with frequency (Kim, Callier, Tabot, Gaunt, et al., 2015) so the ability to discriminate frequency may rely on frequency-dependent changes in perceived magnitude. Alternatively, differences in the quality of the percept, which have been reported by human subjects to accompany changes in ICMS frequency (Lee et al., 2018; Salas et al., 2018), may serve as the basis for discriminating frequency. Of course, these two possibilities are not mutually exclusive, as subjects could use sensation magnitude, quality, or a combination of both to determine which of two stimuli (of equal amplitude) is higher in frequency. In theory, we could empirically distinguish one strategy from the other by equalizing the sensation magnitude across frequencies: the higher the frequency, the lower the amplitude (solid line in fig. 3.1A). In practice, this approach would require a precise, electrode-by-electrode characterization of the relative contribution of frequency and amplitude to perceptual magnitude. Any miscalculation in the trade-off between frequency and amplitude would allow the subject to use differences in magnitude to make frequency judgments (dashed lines in fig. 3.1A). An alternative approach is to vary ICMS amplitude independently of frequency: if the lower-frequency stimulus is sufficiently higher in amplitude than the higher-frequency stimulus to overcome the frequency-dependent difference in sensory magnitude, a strategy based on magnitude will lead to an incorrect frequency judgment. If stimulus amplitude varies unpredictably from stimulus to stimulus (green crosses in fig. 3.1A), reliance on magnitude thus leads to poor overall performance.

The objective of the present study, then, was to characterize the ability of non-human primates (Rhesus macaques) to discriminate the frequency of ICMS applied to somatosensory cortex over a wide range of frequencies (from 10 to 400 Hz) independently of amplitude and to assess the degree to which changes in frequency affect the magnitude and quality of the percept. Results from the present study provide a quantitative basis for the design of sensory feedback algorithms that modulate ICMS frequency and amplitude to shape artificial touch and complement previous and future subjective reports from humans.

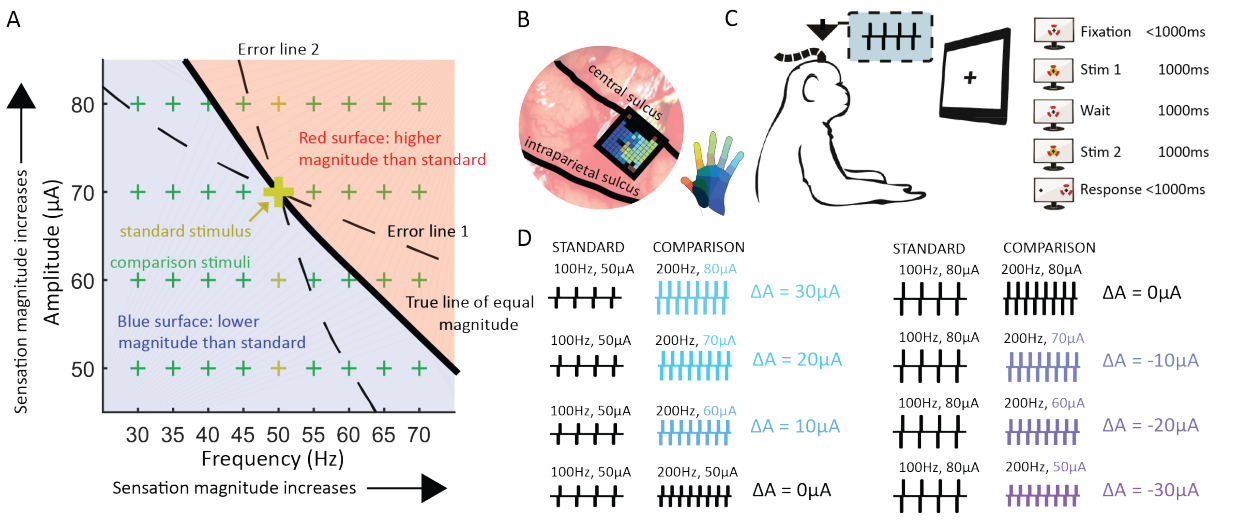

Figure 3.1: Experimental design. (A) Frequency/amplitude trade-off in perceived magnitude, illustrated with the stimuli used with a 50-Hz standard frequency. Each point on the surface represents a pair of stimulation parameters. Sensation magnitude increases with both frequency and amplitude. The thick black line describes stimuli whose sensory magnitude is equal to that of a 50-Hz, 70-μA stimulus (large gold +). In theory, the standard stimulus could then be paired with other comparison stimuli on the line and the animals could not discriminate frequency based on differences in magnitude. However, if the estimate of this line is incorrect (dashed lines), then the animals can still make frequency judgments based on differences in magnitude: Following error line 1, every comparison frequency greater than the standard frequency will feel more intense and every comparison frequency lower than the standard will feel less intense. The inverse is true for error line 2. As the relative contributions of frequency and amplitude to intensity vary across electrodes, characterizing the isointensity contour is challenging. The alternative approach is to present stimuli that tile the frequency and amplitude space (green +s), so that the magnitude of the higher-frequency stimulus is sometimes higher and sometimes lower than that of the lower-frequency stimulus. Reliance on magnitude will lead to poor overall performance and lower rewards. The separation between the blue and red regions will shift if the standard frequency is presented at other amplitudes (small gold +s). (B) A Utah electrode array (UEA) was implanted in the hand representation of area 1 (the implant of monkey C is shown). (C) The animal faced a monitor that signaled the trial sequence (shown on the right, red markers denote the gaze). The animal maintained fixation on a central target while 2 ICMS pulse trains were sequentially delivered and then reported its frequency judgment by making a saccade to one of 2 targets. The animal was rewarded if it selected the pulse train with the higher frequency (regardless of stimulus amplitude). (D) Example of standard-comparison frequency pair (not all amplitude combinations shown). Colors denote the difference in amplitude between the comparison and the standard stimulus. The largest amplitude difference was ± 30 μA.

3.3 Results

Three monkeys, implanted with electrode arrays (Utah electrode arrays, UEAs) in Brodmann's area 1 of somatosensory cortex, judged which of two 1-s long ICMS pulse trains was higher in pulse frequency (fig. 3.1B,C). On each experimental block, consisting of several hundred trials, a standard stimulus (at 20, 50, 100, or 200 Hz) was paired with several comparison stimuli whose frequencies varied around the standard frequency. The amplitudes of the standard and comparison stimuli also varied from trial to trial (50, 60, 70 or 80 μA presented in every possible combination in random order, all above typical detection thresholds)(fig. 3.1D; for all stimulus parameters see table F.1, frequency discrimination stimulus set 1). The animal was rewarded when it correctly reported which of the two stimuli was higher in frequency. As discussed above, the large, behaviorally irrelevant variations in amplitude were intended to reduce or abolish the informativeness of perceived magnitude, which is modulated by changes in both frequency and amplitude (fig. 3.1A).

3.3.1 Frequency Discrimination with Equal Amplitudes

On all electrodes tested, the animals were able to reliably discriminate the frequency of ICMS pulse trains when the amplitudes of the standard and comparison were equal, except over the highest frequency range (from 200 to 400 Hz)(fig. 3.2A). Indeed, the animals reached near perfect performance with the 20-, 50-, and 100-Hz standards and, with the 200-Hz standard, for frequencies below 200 Hz. However, when both frequencies were 200 Hz and above, performance leveled off, often below 75%, suggesting that further increases in frequency had no impact on the evoked sensation. To gauge the animals' sensitivity to changes in frequency, we computed the just noticeable difference (JND), which denotes the frequency increment or decrement required to achieve 75% discrimination performance. We found that JNDs increased with standard frequency from around 3 Hz for a 20-Hz standard to 95 Hz for the 200-Hz standard (fig. 3.2B). Weber fractions – the ratio of the JND to

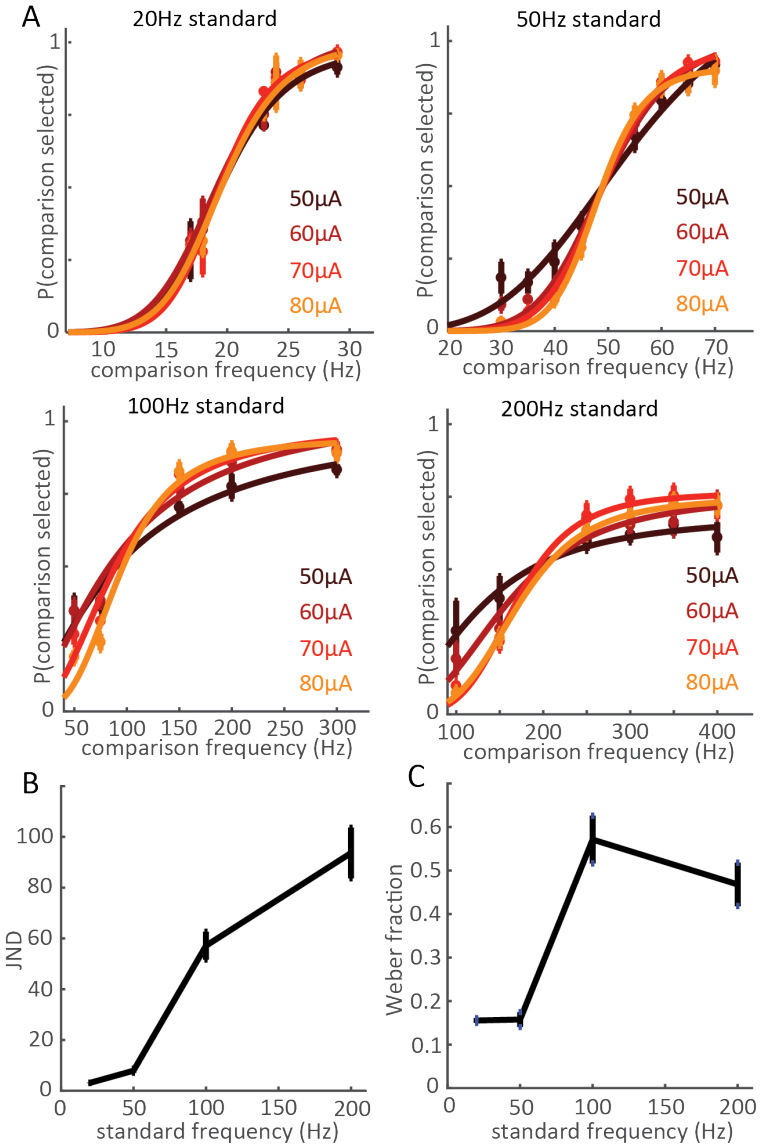

Figure 3.2: Frequency discrimination with equal amplitudes. (A) Performance on the frequency discrimination task when stimulus amplitudes were equal, averaged across all electrodes (n = 1 each from monkeys A and B for the 20- Hz standard; n = 5 from monkeys A and B for both the 50-Hz and 200-Hz standard; n = 8 from monkeys A, B, and C for the 100-Hz standard). Different colors denote different stimulus amplitudes. Error bars show the SEM across electrodes. The animals achieved high performance for frequencies below 200 Hz. (B) Just noticeable difference (JND) as a function of standard frequency. JNDs at each amplitude were averaged for each electrode. (C) Weber fractions as a function of standard frequency. Error bars in B and C denote the SEM across all electrodes tested at each standard.

the standard frequency – increased dramatically, from 0.15 to 0.5, between 50 and 100Hz, indicating a much higher sensitivity to changes in frequency in the low range (fig. 3.2C). Frequency discrimination performance was independent of stimulus amplitude at the low frequencies but improved somewhat with increasing amplitude at the high frequencies (fig. 3.2A, fig. F.1). Note that, while only trials with equal-amplitude pairs were included in this analysis, these trials were interleaved with many more trials on which the standard and comparison amplitudes differed. The monkeys therefore had to develop a strategy geared towards selecting the higher frequency in the face of task-irrelevant magnitude confounds. If the animals were trained with only equal amplitude pairs, sensation magnitude would be a reliable cue and the animals may have performed better by developing a strategy that exploits this cue.

3.3.2 Frequency Discrimination with Unequal Amplitudes

A central objective of the present study was to assess the extent to which changes in frequency shape the evoked percept beyond modulating its magnitude. Indeed, one might expect higher microstimulation frequencies to evoke stronger sensations given the increased sensitivity at higher frequencies as reflected in the detection thresholds (Kim, Callier, Tabot, Gaunt, et al., 2015). However, increases in microstimulation amplitude (charge per pulse) also evoke stronger sensations (Flesher et al., 2016; Tabot et al., 2013). To the extent that frequency discrimination judgments were based on intensive differences, then, we expected the psychometric functions to shift to lower or higher frequencies (i.e. left- or rightward) depending on the amplitude difference between the standard and comparison stimulus. As expected, animals exhibited a systematic bias towards selecting the higher-amplitude stimulus (fig. 3.3), as evidenced by a left- or rightward shift in the psychometric functions when the standard stimulus was lower or higher in amplitude than the comparison stimulus, respectively. The direction of the bias was consistent across standard frequencies and elec-

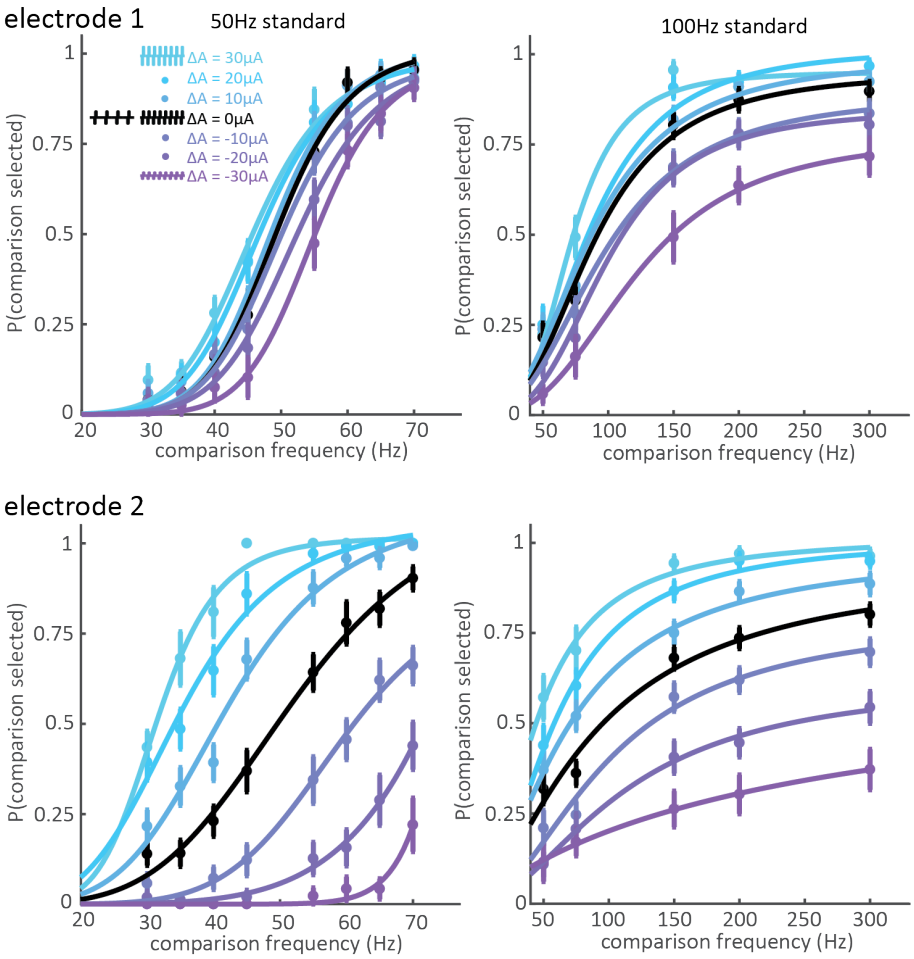

Figure 3.3: Frequency discrimination with unequal amplitudes. (A, Top) Behavioral performance at one electrode from monkey A for standard frequencies of 50 and 100 Hz. Colors indicate amplitude differences between the comparison and standard frequencies (blue indicates the comparison stimulus amplitude was higher and purple indicates it was lower). The animal's choices were slightly biased toward the higher amplitude. (A, Bottom) The same monkey's performance for a different electrode. The monkey could perform frequency discrimination with equal amplitudes at both electrodes (black), but amplitude exerted a powerful influence on its frequency judgments when stimulation was delivered through this electrode. Error bars show the SEM across training blocks. (B) Behavioral performance on one low-bias electrode in monkey B (Left) and one in monkey C (Right).

trodes and the magnitude of the bias increased monotonically as the difference between the comparison and standard amplitude increased. The magnitude of the bias also varied widely across electrodes: on some electrodes, amplitude differences only slightly contaminated frequency judgments (fig. 3.3, top row; fig. 3.4, electrodes on the left side of the x-axis); on others, amplitude differences dominated the animal's choices (fig. 3.3, bottom row; fig. 3.4, high-spread electrodes on the right side of the x-axis).

To maximize reward, the monkeys had to distinguish changes in frequency independently of amplitude. Implementation of this strategy would have yielded psychometric functions with different amplitudes that overlapped completely, and the minute amplitude-related biases at many electrodes demonstrate that the monkeys were capable of learning this strategy. The persistence of large amplitude-dependent biases on some electrodes, even after extensive training on those electrodes, indicates that changes in frequency could not be distinguished from changes in amplitude. We conclude that the sensory correlate of frequency changes on those electrodes was a change in sensory magnitude.

3.3.3 Differences Across Electrodes

After extensively testing a few electrodes as described above, we had the animals perform the frequency discrimination task using a more restricted set of stimuli to sample electrodes more widely across the arrays. In this set, the frequency difference between the two trial stimuli was always 100 Hz, with the low frequency stimulus spanning the range from 70 to 170 Hz, and the amplitudes were the same as those tested in the full set (table F.1, frequency discrimination stimulus set 2). The 25 electrodes tested yielded a wide range of amplitude biases (fig. 3.4, fig. F.2, 2-way ANOVA of performance with amplitude difference and stimulation electrode as factors; interaction term: $F(48,12660) = 12.2$, $p < 0.001$): performance was consistently high when the higher-frequency stimulus was also higher in amplitude (blue in fig. 3.4), whereas performance in the converse conditions – when the

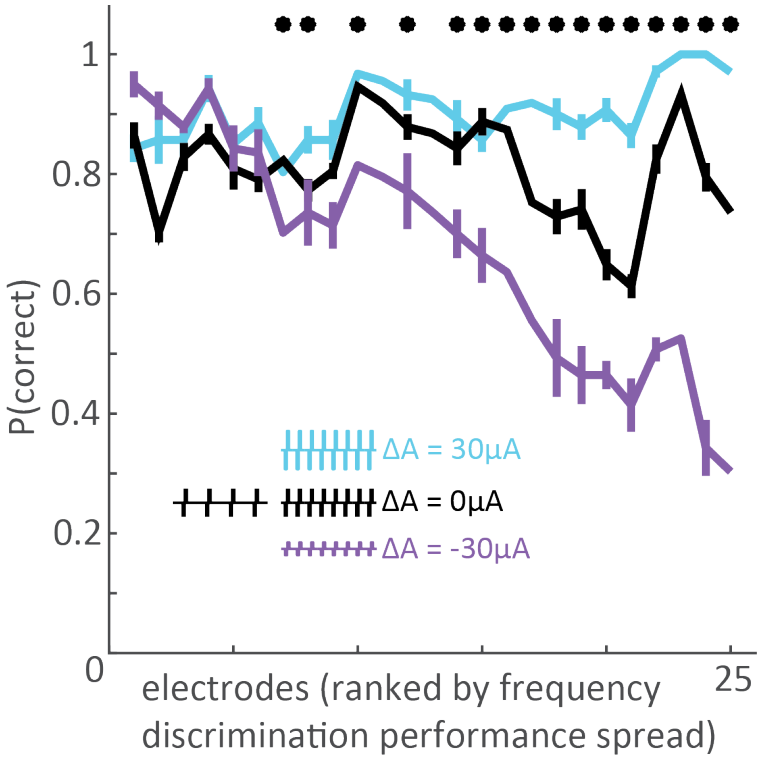

Figure 3.4: Magnitude of the amplitude bias across electrodes. For the 25 electrodes tested (5 from monkey A, 17 from monkey B, 3 from monkey C), asymptotic performance on the frequency discrimination task with a frequency difference of 100 Hz (with base frequency ranging from 70 to 170 Hz) and amplitude differences of -30, 0, and 30 μA. Electrodes are ranked by spread, computed as the difference in performance between the 2 amplitude extremes (cyan and purple). Error bars represent the SEM performance at each base frequency. Data points without error bars represent the 100-Hz vs. 200-Hz performance for the 8 electrodes that were extensively tested (full psychometric curves were obtained). Black dots indicate electrodes at which differences in amplitude had a significant effect on performance ($\chi 2$ test, $P < 0.01$). The effect of amplitude on performance differed significantly across electrodes (2-way ANOVA of performance with amplitude difference and stimulation electrode as factors, interaction term $P < 0.001$).

higher-frequency stimulus was lower in amplitude – varied widely (purple in fig. 3.4). Poor performance when the high-frequency stimulus was lower in amplitude indicated a reliance on intensity differences to perform the frequency discrimination task.

Next, we investigated the possible causes for differences in frequency sensitivity across electrodes. ICMS frequency discrimination has been previously hypothesized to be dependent on the response properties of the stimulated population: in area 3b, electrodes that impinged upon cortical neurons with rapidly adapting responses (RA-like, which exhibit responses to stimulus transients but not to sustained skin indentations) yielded better performance than did electrodes that impinged upon neurons with slowly adapting responses (SA-like, which exhibit sustained responses to static indentations)(Romo et al., 1998, 2000). Note that the distinction between RA- and SA-like responses has been called into question, as most cortical neurons exhibit intermediate responses, even in area 3b (Pei et al., 2009; Saal Bensmaia, 2014). Nonetheless, we tested this hypothesis by examining the responses to mechanical indentations delivered to the receptive field of the neurons surrounding each electrode tested. From these responses, we computed an adaptation index to gauge how "RA-like" the response was at each electrode (Callier et al., 2018; Pei et al., 2009)(a higher index value indicates more "RA-like" response properties: see Adaptation index in appendix F). We found no consistent relationship between adaptation index and the susceptibility to the amplitude confound (fig. F.3). Note, however, that the relationship between adaptation properties and frequency discrimination performance was observed for ICMS applied to area 3b, not area 1 as in the present study, which may explain the discrepancy with previous findings.

Another possibility is that differences in discrimination performance reflect differences in sensitivity to ICMS. To test this hypothesis, we measured the detection threshold amplitudes on a subset of 12 electrodes used in the frequency discrimination experiment (measured at 100 Hz; see table F.1, detection task) and found no relationship between frequency discrimination

performance and detection threshold (fig. F.4). In other words, the poor performance on frequency discrimination on some electrodes cannot be attributed to an inability to feel the stimulation.

3.3.4 Disentangling Frequency and Amplitude Effects

One possibility is that ICMS frequency and amplitude exert the same effect on the evoked percept, namely modulate its magnitude. If this were the case, any increase in frequency could be completely reversed by a concomitant decrease in amplitude (and vice versa). Under this assumption, we can estimate the relative impact of frequency and amplitude on sensory magnitude from the animals' behavioral performance (see "Gauging the relative contribution of amplitude and frequency to discrimination judgments" in the Methods). Discrimination performance for any given pair of stimuli is then determined by a weighted sum of the frequency and amplitude differences, and the ratio of the weights – which we will call the offset ratio – can be used as an index of the relative impact of frequency and amplitude on sensory magnitude. For an electrode with a very strong amplitude bias, the offset ratio was 0.96 Hz/μA (fig. 3.3, electrode 2 with the 50-Hz standard). That is, an increase of 0.96 Hz (from 50 Hz) was equivalent to an increase of 1 μA (from the standard amplitude) on this electrode. For an electrode with a weak amplitude bias, the offset ratio was 0.14 Hz/μA (fig. 3.3, electrode 1 with the 50-Hz standard). We could then compare these offset ratios, obtained from frequency discrimination performance when both frequency and amplitude varied, to offset ratios obtained from discrimination performance when one parameter varied while the other was held constant. Specifically, from amplitude discrimination experiments with frequency held constant (performed in an earlier study and published in (Kim, Callier, Tabot, Gaunt, et al., 2015)(Kim, Callier, Tabot, Gaunt, et al., 2015), we estimated sensitivity to changes in amplitude and, from frequency discrimination experiments (with amplitude held constant), we estimated sensitivity to changes in frequency (fig. F.6, see Generating equiv-

alent frequency-amplitude tradeoffs using single-variable discrimination in methods). We could then recalculate the offset ratio based on these measurements and assess the degree to which the relative sensitivities to frequency and amplitude derived from the single-parameter experiments matched those derived from the combined parameter experiments. If frequency and amplitude exert the same influence on perception (both only affecting sensation magnitude), the offset ratios computed for the single- and variable-parameter experiments should match. To the extent that frequency has a different impact on sensation than does amplitude, the offset ratio should be systematically lower for the combined-variable experiments than for the single-variable ones. If frequency impacts sensation quality, the single-variable experiments should lead to an underestimate of the discriminability of frequency in the presence of amplitude confounds because changes in quality are relatively robust to changes in sensory magnitude.

Consistent with the quality-modulation hypothesis, the offset ratios derived from combined-variable experiments were consistently and significantly lower (in Hz/μA) than were those derived from the single-variable discrimination experiments (fig. 3.5A; Mann-Whitney test, $p < 0.01$). That is, the effect of frequency relative to that of amplitude was systematically and strongly underestimated from single-variable experiments, especially for electrodes with a weak amplitude bias (compare iso-performance contours in fig. F.6). These results are thus inconsistent with the hypothesis that amplitude and frequency influence the percept in the same way and support the conclusion that changes in microstimulation frequency affect the evoked sensation beyond simply modulating its magnitude. However, the extent to which this is the case is highly electrode dependent. On some electrodes (those overlapping the unity line in fig. 3.5A), changes in frequency and changes in amplitude seem to be completely interchangeable.

To further test the hypothesis that frequency changes have non-intensive effects on perception, we introduced catch trials on which the two stimuli in the pair had the same fre-

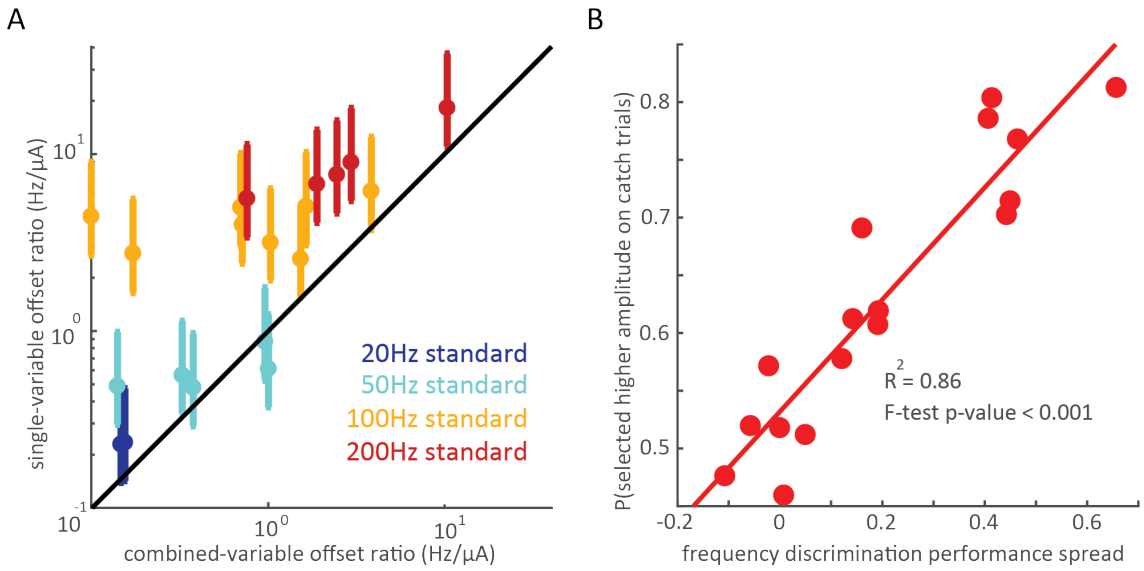

Figure 3.5: Disentangling the effects of ICMS frequency and amplitude. (A) Offset ratios (the equivalent trade-off between frequency and amplitude changes) computed from single-variable discrimination experiments versus the offset ratios computed from combined-variable discrimination experiments. Each data point represents 1 electrode at 1 standard frequency (2 points for the 20-Hz standard, 5 for the 50- and 200-Hz standards, and 8 for the 100-Hz standard). Different colors denote different standard frequencies. The y axis error bars show the range of offset rates obtained by pairing each electrode's same-amplitude frequency discrimination performance with the amplitude discrimination performance from all electrodes tested in the single-variable amplitude discrimination task (Data Analysis), and the marker shows the mean of these estimates. All but 2 electrodes at the 50-Hz standard are above the unity line, indicating that the relative effect of frequency is consistently greater in the combined-variable experiment. The single-variable offset ratios were significantly different from the combined-variable offset ratios (Mann–Whitney test, $P < 0.01$). (B) Proportion of catch trials in which the animal selected the higher amplitude stimulus versus spread, the difference in performance between the 2 amplitude extremes (+30 μA to -30 μA). Each data point represents 1 electrode from Monkey B. Probability of selecting the higher amplitude increased significantly with performance spread (linear regression $R2 = 0.86$, $P < 0.001$). The animal had negligible or no preference for the higher amplitude stimulus on catch trials at low-spread electrodes, confirming that the animal was not using sensation intensity to select higher frequencies. Catch trials represented ~5% of trials at each electrode. The number of catch trials performed at each electrode ranged from 49 to 161.

quency but different amplitudes (table F.1, catch trials). To the extent that the animal relied on intensive cues to make its judgment, it would select the higher amplitude stimulus. To the extent that it judged the stimuli along a frequency-specific continuum and ignored differences in intensity (as it was rewarded to do), it would be equally likely to select either stimulus, having no basis to choose one or the other. We found that, for electrodes with a weak amplitude bias, the animal was equally likely to pick either stimulus on catch trials. For electrodes with a strong amplitude bias, on which we hypothesized the animal was performing an intensity discrimination task, it was highly likely to pick the higher amplitude stimulus on catch trials (fig. 3.5B).

In fact, examination of the catch trials revealed that animals switched their behavioral strategy in a context-dependent manner. When the stimulus set was such that the task could be performed using sensation magnitude (when only same-amplitude pairs were presented, e.g.), the animals relied more heavily on intensive cues to perform the task on all electrodes, as evidenced by a strong tendency to pick the stronger stimulus on catch trials. When amplitude variations precluded a reliance on intensive cues, animals switched to a strategy that was less dependent on intensive cues as evidenced by a lack of preference for one stimulus over the other on catch trials, but only on electrodes with weak amplitude biases)(fig. F.7, also see "validation of catch trials" in appendix F).

3.3.5 Dependence of the Sensory Correlates of ICMS Frequency on the Spatial Pattern of Recruitment

Computational modeling suggests that the perceived magnitude of a stimulus can be predicted from the population spike count (Fridman et al., 2010; Kim et al., 2017). To the extent that animals were not solely relying on differences in sensory magnitude to discriminate frequency, however, this neural code is unlikely to exclusively mediate their behavioral performance. One possibility is that the stimulus can be decoded from the spatial layout of

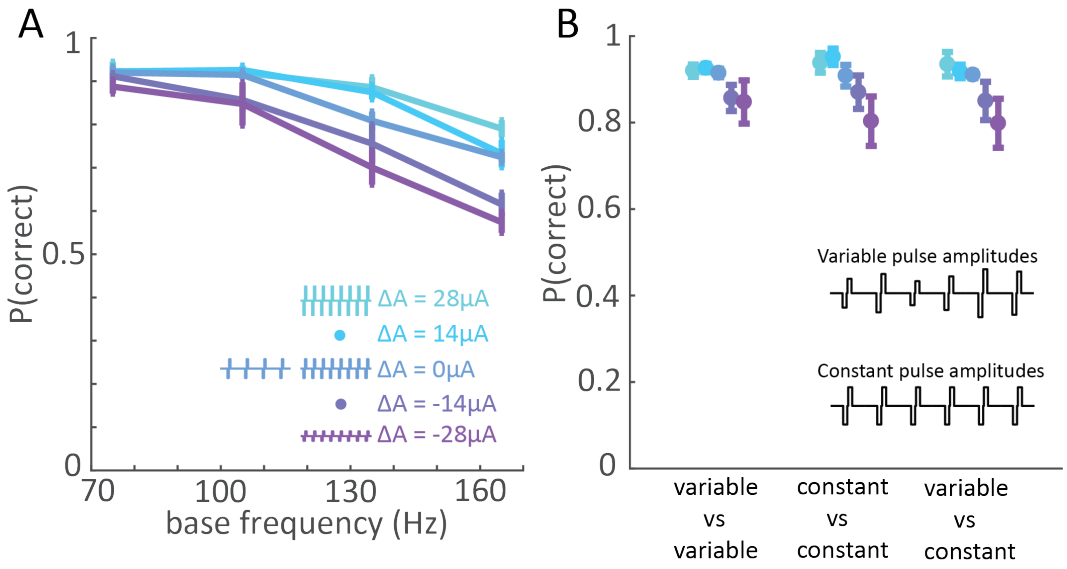

Figure 3.6: Varying individual pulse amplitude has a negligible effect on frequency discrimination performance. (A) Monkey B's performance vs. base frequency in the variable-amplitude experiment for a group of 4 electrodes with weak amplitude bias. The frequency difference was always 90 Hz for the variable-amplitude experiment due to hardware constraints (Methods). Error bars in A and B show the SEM across electrodes. (B) Performance when stimulus pulse trains were both variable-amplitude were split or were both constant-amplitude, for the same 4 electrodes with weak amplitude bias. The Inset illustrates variable-amplitude and constant-amplitude pulse trains. Changing spatial distribution of the ICMS-induced activity on a pulse-by-pulse basis had little to no effect on the animal's ability to discriminate frequency.

the cortical response. For example, frequency and amplitude may each shape in a systematic way the falloff in the response with distance from the electrode tip. Their individual contributions could then be untangled by sampling total evoked activity at several distances from the electrode tip. To investigate this possibility, we delivered pulse trains in which the amplitude varied from pulse to pulse over a range but were on average equal to the amplitudes of constant-amplitude pulse trains (table F.1, frequency discrimination stimulus set 3). The spatial extent of the response – the pattern of recruitment – thus varied from pulse to pulse, blurring the formerly sharp separation between distinct spatial patterns of recruitment, and so reliance on a spatial pattern of activation would lead to poor frequency discrimination performance. In individual experimental blocks, we randomly interleaved trials on which 1) both pulse trains had constant amplitudes as in previous experiments, 2) both pulse trains had variable amplitudes, and 3) one pulse train was constant in amplitude and the other was variable. We found that the pulse-by-pulse variability in amplitude had a negligible effect on performance (fig. 3.6, fig. F.8), suggesting that frequency discrimination does not rely on differences in spatial patterns of electrically evoked neural activation.

3.4 Discussion

In summary, we find that 1) animals can discriminate the frequency of ICMS up to ∼200 Hz, 2) changes in frequency affect both the magnitude and quality of the evoked sensation, 3) the degree to which frequency shapes sensory quality varies across electrodes, and 4) ICMS frequency discrimination does not depend on the spatial pattern of neural activation.

3.4.1 Microstimulation Frequency Can Be Discriminated up to ∼200 Hz

When stimuli differing in frequency but matched in amplitude were paired, animals were able to discriminate frequency up to approximately 200 Hz, beyond which performance declined considerably (fig. 3.2, fig. F.1), suggesting that increases in frequency beyond 200

Hz have a negligible impact on the evoked percept. This frequency cut-off coincides with the point at which detection thresholds for ICMS level off (Kim, Callier, Tabot, Gaunt, et al., 2015), beyond which intensive cues for frequency are likely no longer available. The steep decline in performance suggests that the neural code that mediates microstimulation frequency discrimination independent of amplitude also deteriorates (see below for discussion of neural codes).

3.4.2 Increased ICMS Frequency Leads to Increased Perceived Magnitude

Three lines of evidence suggest that higher ICMS frequencies give rise to more intense percepts. First, increasing frequency lowers detection thresholds, indicating increased sensitivity at higher frequencies (Kim, Callier, Tabot, Gaunt, et al., 2015). Second, animals exhibit a highly consistent bias to select the higher-amplitude stimulus as being higher in frequency, even though this leads to less reward (fig. 3.3, fig. 3.4, fig. F.7). This systematic bias implies a systematic relationship between frequency and perceived magnitude. Third, on experimental blocks comprising primarily equal-amplitude stimuli, catch trials – on which both stimuli had the same frequency but different amplitudes – resulted in the systematic selection of the higher-amplitude stimulus, consistent with the hypothesis that the animal relied in part on intensity to make these discrimination judgments (fig. F.7). Note that systematic selection biases on catch trials disappeared to the extent that animals judged frequency independently of amplitude (fig. 3.5B, fig. F.7, see validation of catch trials in Appendix F). Increased perceived magnitude at higher frequencies has also been reported for peripheral nerve stimulation (D'Anna et al., 2017; Graczyk et al., 2016; Valle et al., 2018) and is consistent with the hypothesis that intensity is determined by the spike rate evoked in the neuronal population (Fridman et al., 2010; Kim et al., 2017).

3.4.3 Changes in ICMS Frequency Can Lead to Changes in the Quality of the Evoked Percept

On a number of electrodes, animals could select the higher frequency stimulus even when (1) it was much lower in amplitude and perceived as less intense than the stimulus with which it was paired (points in the blue region of fig. 3.1A at which the frequency is higher than the standard) and (2) it was interleaved with other pairs in which the higher frequency stimulus was perceived as more intense (points in the red region). In these cases, when the animal was presented with catch trials – in which both stimuli were of equal frequency but different amplitude – animals did not exhibit a bias to select the higher-amplitude stimulus (fig. 3.5B, fig. F.7). The animal thus demonstrated that it was largely ignoring differences in magnitude in making its frequency judgments. Furthermore, on those electrodes, the animal's behavior was inconsistent with the hypothesis that frequency and amplitude affect only a common sensory continuum – magnitude – as evidenced by the significantly lower frequency/amplitude offset ratios derived from the combined-variable experiment compared to those derived from the single-variable experiments (fig. 3.5A, fig. F.6). Indeed, the amplitude bias was weaker than would be predicted based on single-parameter discrimination performance (amplitude or frequency).

Together, these observations are consistent with the hypothesis that changes in frequency also affect the quality of the evoked percept on some electrodes in a highly electrode-dependent way reflected in a wide range of frequency/amplitude offset ratios. That the animals were often able to transfer performance from one electrode to the next suggests that the effect of frequency on sensory quality was consistent across electrodes. Indeed, had the perceptual effect been very different from electrode to electrode, the animal would have had to discover the relevant sensory continuum on an electrode-by-electrode basis. The inability to distinguish frequency independently of amplitude on other electrodes indicates that the effect of frequency on those electrodes is indistinguishable from that of amplitude, is subtle

and drowned out by the fluctuations in amplitude, or does not lie on a discernible continuum.

3.4.4 Neural Codes

Any proposed neural code to explain the discrimination behavior must account for the animals' ability to distinguish increases in frequency from increases in amplitude despite the fact that both stimulation parameters affect the firing rate of neural populations near the electrode tip. While higher amplitudes lead to the recruitment of a larger volume of neurons (Tehovnik, 1996; Tolias et al., 2005) and to changes in the spatial distribution of neuronal activity (Histed et al., 2009), the precise shape of recruitment is frequency dependent (Michelson et al., 2018). In principle, then, the spatial pattern of neuronal activation may have shaped the resulting percept and mediated the animals' frequency discrimination behavior. We ruled out this possibility – and others positing that frequency discrimination relied on a spatial pattern of activation – by showing that performance is largely unhindered by random changes in amplitude from pulse to pulse, leading to a spatial pattern of activation that varies from pulse to pulse (fig. 3.6, fig. F.8).

Having excluded the population spike rate and spatial hypotheses, we hypothesize that frequency discrimination relies on the temporal structure of the ICMS-evoked activity. Indeed, each ICMS pulse synchronously activates a large population of neurons around the electrode tip (Tehovnik, 1996), so periodic stimulation results in synchronized periodic responses across a large swath of somatosensory cortex. The animals' ability to discriminate ICMS frequency relies on the ability to detect differences in the temporal patterning in the population response, which in turn result in differences in sensation quality along a continuum that is distinct from magnitude. According to this hypothesis, the drop-off in performance for frequencies above 200Hz is caused by an inability of neuronal populations to phase lock at these frequencies. Note that a small population of neurons in somatosensory cortex has been shown to phase lock to vibratory stimuli up to 800 Hz (Harvey et al., 2013),

but it is unlikely that hundreds or thousands of neurons – confined to a restricted volume – could do so. According to this hypothesis, differences across electrodes would be due to differences in the ability of local circuits to phase lock to stimulation, a hypothesis that can be tested by recording the electrically induced neuronal activity.

3.4.5 Implications for Neuroprosthetics

Regardless of the relevant perceptual continuum and neural mechanisms, ICMS frequency exerts a robust influence on the evoked percept. Indeed, we estimate that the perceptually relevant range of frequencies (from 10 to 200 Hz) accommodates 10 to 20 non-overlapping JNDs. That is, changes in frequency can lead to tens of mutually discriminable percepts. In contrast, amplitude JNDs – which range from 14 to 30 μA (Flesher et al., 2016; Kim, Callier, Tabot, Gaunt, et al., 2015) – provide at best 5 to 7 mutually discriminable percepts, from detection threshold (around 20-30 μA at 300 Hz) to the maximum amplitude used for human experiments (100 μA) (Flesher et al., 2016; Kim, Callier, Tabot, Gaunt, et al., 2015; Tabot et al., 2013). ICMS frequency manipulation may therefore enable more finely graded sensory feedback than does amplitude manipulation.

To the extent that ICMS frequency and amplitude have different sensory correlates, the perceptual space that can be achieved by changing these two stimulation parameters is vast ($\sim$100-150 discriminable percepts if we assume that the effects of frequency and amplitude are completely orthogonal). Note, however, that frequency and amplitude can never be completely dissociated, even after extensive training on the "best" electrodes. On many electrodes, frequency and amplitude cannot be dissociated at all. An ideal sensory encoding algorithm would take into consideration these electrode specific trade-offs between frequency and amplitude, which we gauge with the offset ratio. One approach to estimate the trade-offs would be to conduct extensive psychophysical testing on each human participant to assess frequency and amplitude sensitivity on an electrode by electrode basis, but this is unlikely

given the time and tedium this strategy entails. A more viable approach would be to discover response properties of neural tissue around electrodes that would be readily identified and diagnostic of that electrode's frequency and amplitude sensitivity. Regardless, the challenge will be to harness stimulation frequency and amplitude, as well as other simulation parameters, taking into consideration idiosyncratic differences across electrodes, to evoke meaningful tactile percepts.

3.5 Methods

3.5.1 Animals

Three male Rhesus macaques (Macaca mulatta), ranging in age from 7 to 9 years old and weighing between 9 and 10 kg, participated in this study. Animal care and handling procedures were approved by the University of Chicago Institutional Animal Care and Use Committee.

3.5.2 Implants

Each animal was implanted with one Utah electrode array (UEA, Blackrock Microsystems, Inc., Salt Lake City, UT) in the hand representation of area 1 (fig. 3.1B). Each UEA consists of 96 1.5 mm-long electrodes with tips coated in iridium oxide, spaced 400 μm apart, and spanning 4 mm x 4 mm of the cortical surface. The hand representation in area 1 was targeted based on anatomical landmarks. Given that the arrays were continuous to the central sulcus and area 1 spans approximately 3-5 mm of cortical surface from the sulcus (Pons et al., 1985), few if any electrodes were located in area 2. Given the length of the electrodes, their tips likely terminated in the infragranular layers of somatosensory cortex if embedded to their base, as we have previously shown in postmortem histological analysis with other animals instrumented with identical arrays (Rajan et al., 2015). We mapped the

receptive field of each electrode by identifying which areas of skin evoked significant z-scored multiunit activity (Callier et al., 2018). The age of the implanted arrays used in these studies ranged from 2 months to 4 years. The stability of sensitivity to ICMS in area 1 over multiple years has been documented (Callier et al., 2015).

3.5.3 Stimuli

Intracortical stimulation (ICMS) consisted of cathodal phase-leading symmetrical biphasic pulses delivered through a 96-channel neurostimulator (CereStim R96; Blackrock Microsystems Inc., Salt Lake City, UT). Across all tested stimulation regimes, pulse train frequencies ranged from 17 to 400 Hz, pulse amplitudes ranged from 44 to 100 μA, and phase durations equaled 200 or 400 μs. The interval between phases was always 53 μs. All biphasic pulses within the same stimulus were separated by the same time interval (pulse trains were periodic). In all experiments, pulse train duration was always 1 s. In some experiments, all of the pulses in a train had the same amplitude; in others, amplitude varied from pulse to pulse (see below).

3.5.4 Behavioral Task

The animals were seated at the experimental table facing a monitor, which signaled the trial progression (Fig. 3.1C). Eye movements were tracked with an optical eye-tracking system (MR PC60; Arrington Research, Scottsdale, AZ). The animals initiated trials by directing their gaze to a cross in the center of the monitor. A trial was aborted if the animal failed to maintain its gaze on the center until the appearance of response targets. Each trial comprised 2 successive stimulus intervals, each indicated by a circle on the video monitor, lasting 1 s, and separated by a 1-s interstimulus interval during which the circle disappeared, followed by a response interval during which 2 response targets appeared on either side of the gaze fixation point (Fig. 3.1C). The animals' task was to judge which of the 2 pulse trains was

higher in frequency. The animals responded by making a saccadic eye movement toward the left (selecting the first stimulus) or right (second stimulus) target. Correct responses were rewarded with juice. Psychophysical performance was calculated as the proportion of trials on which the higher frequency stimulus was selected.

3.5.5 Experimental Design

Stimulus set for detailed psychometric curves: We first performed extensive testing on a small group of electrodes, building psychometric curves spanning a wide range of frequencies. In each test block, consisting of several hundred trials, one stimulus of each pair had the same standard frequency (20, 50, 100, or 200 Hz) and the other stimulus was drawn from a set of comparison frequencies around the standard (comparisons for 20Hz standard: 17, 18, 22, 23, 26, 29 Hz; comparisons for 50Hz standard: 30, 35, 40, 45, 55, 60, 65, 70 Hz; comparisons for 100Hz standard: 50, 75, 150, 200, 250, 300 Hz; comparisons for 200Hz standard: 50, 100, 150, 250, 300, 350, 400 Hz)(table F.1). Phase duration during each pulse was 200 μs at the higher frequencies (100 and 200 Hz standards) and 400 μs at the lower ones (20 and 50 Hz standards) to ensure that the stimuli were detectable (Berg et al., 2013). Stimulus amplitudes were 50, 60, 70, or 80 μA, comfortably above expected detection threshold (Kim, Callier, Tabot, Gaunt, et al., 2015). Every possible combination of frequencies (standard vs. comparisons) and amplitudes, numbering hundreds of unique stimulus pairs, was presented in each test block, ensuring the animals had to perform frequency discrimination instead of memorizing the correct responses to individual pairs of stimuli. For each electrode/standard combination, animals were trained until they reached stable performance, a process which could take weeks or even months as we incrementally included harder stimulus pairs (those with small frequency differences and large amplitude confounds). To discourage the animals' reliance on perceptual magnitude in making their frequency judgments, we over-represented stimulus pairs in which the higher-frequency stimulus was lower in amplitude by 50%. That

way, the higher-frequency stimulus was lower in amplitude on ∼50% of trials, to compensate for the fact that the higher-frequency stimulus will feel more intense on equal-amplitude pairs. The psychometric curves were constructed after asymptotic performance was achieved. We extensively tested 5 electrodes (4 from monkey A, 1 from monkey B) at standard frequencies of 50, 100, and 200Hz. Only 1 electrode from each monkey was tested at the 20 Hz standard before testing was cut short by the failure of Monkey A's array. Three electrodes from monkey C were extensively tested at only the 100 Hz standard before testing was cut short by health issues that precluded water restriction.

Reduced stimulus set: After extensively testing a few electrodes, which took weeks or even months for each electrode and standard frequency, we developed a reduced stimulus set to test the animals' performance at a faster pace over a wide range of electrodes. In this stimulus set, the frequency difference was always 100 Hz, a salient difference according to the psychometric curves obtained from the full set, and the base (lower) frequency was 70, 80, 90, 100, 110, 120, 130, or 170 Hz. The amplitudes were the same as in the full set (50, 60, 70, or 80 μA) and, again, parametrically combined (table F.1). Here too, we over-represented stimulus pairs in which the higher frequency stimulus had a lower amplitude during the training phase to reduce the animals' reliance on intensive cues in making their frequency judgments. We tested 17 electrodes from monkey B with this stimulus set. Instead of first training to asymptotic performance while incrementally adding harder stimulus pairs, we had the animal complete several thousand trials (from 2500 to 6000) with the complete stimulus set at each electrode. On 4 of the 17 electrodes, the animal performed the frequency discrimination task on 2 subsets of stimuli in separate experimental blocks: one containing only pairs with equal amplitudes and one containing only pairs in which the base stimulus' amplitude was 30 μA higher than that of the comparison stimulus (fig. F.7, table F.1; see validation of catch trials in Appendix F).

Catch trials: Included in the reduced stimulus set was a small proportion of trials (∼5%)

on which the two stimuli in the pair were at the same frequencies but differed in amplitude by 30 μA. On these catch trials, all base frequencies were used. The animal was rewarded randomly during these trials. The animal's bias toward the higher or lower amplitude stimulus in the absence of frequency differences gauged its reliance on intensive cues (fig. 3.5B, fig. F.7).

Variable-amplitude pulse trains: The mean amplitudes of the pulse train were of 58, 72, and 86 μA but the amplitudes of individual pulses spanned a range around the mean (table F.1). For each stimulus, one of the following sets of individual pulse amplitudes was randomized, then repeated with the frequency-appropriate inter-pulse interval to complete a 1-s long stimulus: [44 to 72, in increments of 2] , [58 to 86, in increments of 2], [72 to 100, in increments of 2]. One of the stimuli in each pair was at 75, 105, 135, or 165 Hz and the other was 90 Hz higher. Our implementation was constrained by our stimulation hardware, which required that the frequency be a multiple of the number of different pulse amplitudes used (in order to last exactly 1s). The maximum number of different amplitudes was 15 so we used frequencies that were multiples of 15 for this experiment. For each pair of frequencies, every possible combination of amplitudes (variable or constant) was tested. Of the 17 electrodes tested with the reduced stimulus set, 4 showing small effects of amplitude on performance and 3 showing large amplitude effects were tested with variable amplitude pulse trains.

Detection threshold measurements: One interval on each trial contained a 100- Hz pulse train at 10, 25, 40, 55, or 70 μA, and the other interval was empty. The animal reported which interval contained the stimulus. Twelve electrodes from monkey B covering the range of susceptibilities to amplitude were tested. The animal was trained to perform the detection task only after all data collection for the frequency discrimination experiments was complete.

3.5.6 Data Analysis

Psychophysics: We built psychometric curves by fitting performance at each comparison frequency to a cumulative normal density function. Just noticeable differences (JNDs) and Weber fractions were calculated using only trials on which both the stimuli in the pair were equal in amplitude using a criterion performance of 75% correct (Fig. 3.2). JNDs were calculated as the average of the frequency differences required for threshold performance above and below the standard frequency. These were nearly equal for standard frequencies of 20 and 50 Hz but tended to be asymmetric at higher frequencies (with the upper JND greater than the lower one). If performance did not reach threshold for comparison frequencies above the standard for a given electrode and standard, only the frequency difference below the standard was used. This only occurred with the 200-Hz standard frequency.

Gauging the relative contribution of amplitude and frequency to discrimination judgments: The behavioral data show that the animals' judgments depended on both frequency and amplitude, but the relative contribution of these 2 stimulation parameters varied from electrode to electrode. To assess the relative contributions of frequency and amplitude to discrimination judgments, we modeled the position of each stimulus along the task-relevant sensory dimension as a weighted combination of the stimulus's frequency and amplitude. To predict performance we first subtracted the value of the standard stimulus from that of the comparison along this sensory continuum for each pair. The resulting differences then constituted the input to a sigmoid (cumulative normal density function). The resulting function comprised 3 free parameters: 2 regression weights (frequency and amplitude) and 1 sigmoid parameter (SD). For each of the 5 electrodes through which the complete stimulus set was delivered, the function was optimized to predict behavioral performance. The model provided an accurate fit of the behavioral data (R2 mean ± SEM) (Fig. F.5B). The regression weights gauge the relative contribution of frequency and amplitude in determining the animals' choices (Fig. F.5B). For example, to the extent that the regression weight

for amplitude was low, we concluded that the animal was able to discriminate frequency independent of amplitude on that electrode.

Generating equivalent frequency-amplitude trade-offs using single-variable discrimination: We wished to test the hypothesis that frequency discrimination performance was based entirely on intensive cues. That is, changes in frequency and changes in amplitude had the same effect on the evoked percept. To test this hypothesis, we first assessed discriminability when only frequency or only amplitude changed and then assessed whether the performance in these experiments could account for performance when both parameters varied (Fig. 3.5, Figs. F.5 and F.6). To gauge sensitivity to ICMS amplitude, we used previously collected behavioral data in amplitude discrimination task, published in (Kim, Callier, Tabot, Gaunt, et al., 2015). In these experiments, the standard amplitude was 70 μA, and the comparisons were 40, 50, 60, 80, 90, and 100 μA. Psychometric curves were built based on amplitude discrimination performance averaged across all frequencies (50, 100, 250, and 500 Hz) because we found that frequency had a negligible effect on amplitude JNDs (Kim, Callier, Tabot, Gaunt, et al., 2015). To gauge sensitivity to ICMS frequency, we restricted the analysis to trials in which both stimuli had amplitudes of 70 μA.

Using the psychometric functions derived from the single-parameter discrimination experiments, we computed equivalent frequency-amplitude trade-offs by equating changes in frequency and amplitude that resulted in equal discrimination performance. For example, if an amplitude difference of $\pm$10 μA and a frequency difference of $\pm$8 Hz both resulted in a discrimination performance of 65%, $\pm$10 μA and $\pm$8 Hz were considered to be perceptually equivalent. The resulting predicted equal intensity curves were smoothed, and the tangent to this curve (the rate of change in Hz/μA) was computed at the point corresponding to the standard frequency and 70 μA. The frequency/amplitude trade-off implied by this slope could then be compared to the trade-off obtained with the linear model above, which was derived without the assumption that the sensory consequences of amplitude and frequency

changes are indistinguishable. Because the amplitude discrimination data were collected for a separate experiment several years prior to this one (retraining animals from amplitude discrimination to frequency discrimination, or training new animals to perform frequency discrimination, was a very lengthy process and imposed a long delay before we could collect any of the frequency discrimination data presented here), it was performed on different electrodes (8 total, collectively the "amplitude electrodes") than the frequency experiment (the "frequency electrodes"). While it would have been preferable to have both amplitude discrimination and frequency discrimination data from the same electrodes, we mitigated this weakness in the design by matching each "frequency electrode" with each of the 8 "amplitude electrodes" in turn to carry out this analysis. This yielded a distribution of possible offset rates (Hz/μA) based on each amplitude sensitivity at each frequency electrode. If the frequency-amplitude trade-off computed from the model fell outside of this distribution, results from this analysis were inconsistent with the hypothesis that frequency and amplitude affect a common intensive continuum. Note that this approach constitutes a highly conservative characterization of the possible outcomes of the null hypothesis, in that electrodes that span the entire range of amplitude discrimination performance are included in the computation of the single-variable offset ratio. Strong performance on amplitude discrimination yields a lower ratio, which is thus more liable to support the null hypothesis (that frequency and amplitude exert the same effect on performance).

Statistical test of the effect of amplitude differences on performance within electrode: Restricting the analysis to trials on which amplitude difference between the comparison and standard stimuli was -30, 0, or 30 μA and the frequency difference was 100 Hz (Fig. 3.4), we tested the hypothesis that outcome was independent of amplitude difference with a $\chi 2$ test. The black dots in Fig. 3.4 denote electrodes for which the hypothesis was rejected with an alpha level of 0.01.

Statistical significance of differences in the effect of amplitude across electrodes: Re-

stricting the analysis to trials where the amplitude difference was -30, 0, or 30 μA and the frequency difference was 100 Hz (Fig. 3.4), we performed a 2-way ANOVA with electrode, amplitude difference, and their interaction as factors.

Statistical comparison of offset ratios from single-variable and combined-variable discrimination experiments: We used the Wilcoxon–Mann–Whitney test to assess the likelihood that offset rates derived from the combined-variable discrimination experiment (1 value per electrode-standard frequency combination) and the single-variable experiment (8 values per electrode-standard frequency combination, 1 for each electrode tested in the amplitude discrimination experiment) were drawn from the same distribution (alpha level = 0.01).

3.6 References

Bensmaia, S. J. (2015). Biological and bionic hands: Natural neural coding and artificial perception. Philosophical Transactions of the Royal Society B: Biological Sciences, 370(1677). https://doi.org/10.1098/rstb.2014.0209

Bensmaia, S. J., Miller, L. E. (2014). Restoring sensorimotor function through intracortical interfaces: Progress and looming challenges. Nature Publishing Group, 15(5), 313–325. https://doi.org/10.1038/nrn3724

Berg, J. A., Dammann, J. F., Tenore, F. V., Tabot, G. A., Boback, J. L., Manfredi, L. R., Peterson, M. L., Katyal, K. D., Johannes, M. S., Makhlin, A., Wilcox, R., Franklin, R. K., Vogelstein, R. J., Hatsopoulos, N. G., Bensmaia, S. J. (2013). Behavioral demonstration of a somatosensory neuroprosthesis. IEEE Transactions on Neural Systems and Rehabilitation Engineering, 21(3), 500–507. https://doi.org/10.1109/TNSRE.2013.2244616

Callier, T., Schluter, E. W., Tabot, G. A., Miller, L. E., Tenore, F. V., Bensmaia, S. J. (2015). Long-term stability of sensitivity to intracortical microstimulation of somatosensory cortex. Journal of Neural Engineering, 12(5).

Callier, T., Suresh, A. K., Bensmaia, S. J. (2018). Neural Coding of Contact Events in

Somatosensory Cortex. Cerebral Cortex, 1–15. https://doi.org/10.1093/cercor/bhy337

D'Anna, E., Petrini, F. M., Artoni, F., Popovic, I., Simanić, I., Raspopovic, S., Micera, S. (2017). A somatotopic bidirectional hand prosthesis with transcutaneous electrical nerve stimulation based sensory feedback. Scientific Reports, 7(1), 1–15.

Flesher, S., Collinger, J. L., Foldes, S. T., Weiss, J. M., Downey, J. E., Tyler-Kabara, E. C., Bensmaia, S. J., Schwartz, A. B., Boninger, M. L., Gaunt, R. A. (2016). Intracortical microstimulation of human somatosensory cortex. Sci. Transl. Med, 8, 361–141. https://doi.org/10.1126/scitranslmed.aaf8083

Flesher, S., Collinger, J., Weiss, J., Hughes, C., Bensmaia, S. J., Boninger, M., Gaunt, R. (2017). Restoring touch through intracortical microstimulation of human somatosensory cortex. Proceedings - 2017 1st New Generation of CAS, NGCAS 2017, 185–188. https://doi.org/10.1109/NGCAS.2017.68

Flesher, S., Downey, J. E., Weiss, J. M., Hughes, C., Herrera, A., Tyler-Kabara, E. C., Boninger, M. L., Collinger, J. L., Gaunt, R. A. (2019). Restored tactile sensation improves neuroprosthetic arm control. http://dx.doi.org/10.1101/653428

Fridman, G. Y., Blair, H. T., Blaisdell, A. P., Judy, J. W. (2010). Perceived intensity of somatosensory cortical electrical stimulation. Experimental Brain Research, 203(3), 499–515. https://doi.org/10.1007/s00221-010-2254-y

Graczyk, E. L., Schiefer, M. A., Saal, H. P., Delhaye, B. P., Bensmaia, S. J., Tyler, D. J. (2016). The neural basis of perceived intensity in natural and artificial touch. Science Translational Medicine, 8(362), 1–11. https://doi.org/10.1126/scitranslmed.aaf5187

Harvey, M. A., Saal, H. P., Dammann, J. F., Bensmaia, S. J. (2013). Multiplexing Stimulus Information through Rate and Temporal Codes in Primate Somatosensory Cortex. PLoS Biology, 11(5). https://doi.org/10.1371/journal.pbio.1001558

Histed, M. H., Bonin, V., Reid, R. C. (2009). Direct Activation of Sparse, Distributed Populations of Cortical Neurons by Electrical Microstimulation. Neuron, 63(4), 508–522.

https://doi.org/10.1016/j.neuron.2009.07.016

Kim, S., Callier, T., Bensmaia, S. J. (2017). A computational model that predicts behavioral sensitivity to intracortical microstimulation. Journal of Neural Engineering, 14(1). https://doi.org/10.1088/1741-2552/14/1/016012

Kim, S., Callier, T., Tabot, G. A., Gaunt, R. A., Tenore, F. V., Bensmaia, S. J. (2015). Behavioral assessment of sensitivity to intracortical microstimulation of primate somatosensory cortex. Proceedings of the National Academy of Sciences of the United States of America, 112(49), 15202–15207. https://doi.org/10.1073/pnas.1509265112

Kim, S., Callier, T., Tabot, G. A., Tenore, F. V., Bensmaia, S. J. (2015). Sensitivity to microstimulation of somatosensory cortex distributed over multiple electrodes. Frontiers in Systems Neuroscience, 9(APR). https://doi.org/10.3389/fnsys.2015.00047

Lee, B., Kramer, D., Armenta Salas, M., Kellis, S., Brown, D., Dobreva, T., Klaes, C., Heck, C., Liu, C., Andersen, R. A. (2018). Engineering Artificial Somatosensation Through Cortical Stimulation in Humans. Frontiers in Systems Neuroscience, 12(June), 1–11.

Michelson, N. J., Eles, J. R., Vazquez, A. L., Ludwig, K. A., Kozai, T. D. Y. (2018). Calcium activation of cortical neurons by continuous electrical stimulation: Frequency dependence, temporal fidelity, and activation density. Journal of Neuroscience Research, 97(September 2018), 620–638. https://doi.org/10.1002/jnr.24370

Pei, Y.-C., Denchev, P. V., Hsiao, S. S., Craig, J. C., Bensmaia, S. J. (2009). Convergence of Submodality-Specific Input Onto Neurons in Primary Somatosensory Cortex. Journal of Neurophysiology, 102(3), 1843–1853. https://doi.org/10.1152/jn.00235.2009

Pons, T. P., Garraghty, P. E., Cusick, C. G., Kaas, J. H. (1985). A sequential representation of the occiput, arm, forearm and hand across the rostrocaudal dimension of areas 1, 2 and 5 in macaque monkeys. Brain Research, 335(2), 350–353. https://doi.org/10.1016/0006-8993(85)90492-5

Rajan, A. T., Boback, J. L., Dammann, J. F., Tenore, F. V., Wester, B. A., Otto, K.

J., Gaunt, R. A., Bensmaia, S. J. (2015). The effects of chronic intracortical microstimulation on neural tissue and fine motor behavior. Journal of Neural Engineering, 12(6). https://doi.org/10.1088/1741-2560/12/6/066018

Romo, R., Hernandez, A., Zainos, A. (2000). Sensing without Touching: Somatosensory discrimination based on cortical microstimulation. Neuron, 26, 273–278.

Romo, R., Hernández, A., Zainos, A., Salinas, E. (1998). Somatosensory discrimination based on cortical microstimulation. Nature, 392(6674), 387–390.

Saal, H. P., Bensmaia, S. J. (2014). Touch is a team effort: Interplay of submodalities in cutaneous sensibility. Trends in Neurosciences, 37(12), 689–697.

Salas, M. A., Bashford, L., Kellis, S., Jafari, M., Jo, H., Kramer, D., Shanfield, K., Pejsa, K., Lee, B., Liu, C. Y., Andersen, R. A. (2018). Proprioceptive and cutaneous sensations in humans elicited by intracortical microstimulation. ELife, 7, 1–11.

Tabot, G. A., Dammann, J. F., Berg, J. A., Tenore, F. V., Boback, J. L., Vogelstein, R. J., Bensmaia, S. J. (2013). Restoring the sense of touch with a prosthetic hand through a brain interface. Proceedings of the National Academy of Sciences, 111(2), 875–875. https://doi.org/10.1073/pnas.1322627111

Tehovnik, E. J. (1996). Electrical stimulation of neural tissue to evoke behavioral responses. Journal of Neuroscience Methods, 65(1), 1–17. https://doi.org/10.1016/0165-0270(95)00131-X

Tolias, A. S., Sultan, F., Augath, M., Oeltermann, A., Tehovnik, E. J., Schiller, P. H., Logothetis, N. K. (2005). Mapping cortical activity elicited with electrical microstimulation using fMRI in the macaque. Neuron, 48(6), 901–911. https://doi.org/10.1016/j.neuron.2005.11.034

Valle, G., Mazzoni, A., Iberite, F., Petrini, F. M., Rossini, P. M., Micera, S., Valle, G., Mazzoni, A., Iberite, F., Anna, E. D., Strauss, I., Granata, G., Controzzi, M., Clemente, F., Rognini, G., Cipriani, C., Stieglitz, T., Petrini, F. M., Rossini, P. M., Micera, S. (2018). Biomimetic Intraneural Sensory Feedback Enhances Sensation Naturalness , Tactile Sensi-

tivity , and Manual Dexterity in a Bidirectional Prosthesis. Neuron, 100(1), 37–45.

Chapter 4 | Conclusions

4.1 Future investigations of timing in somatosensory cortex

The experiments presented in Chapter 2 add to a growing body of evidence showing that temporal spiking patterns in somatosensory cortex (SC) shape tactile perception. However, the precise and repeatable spiking patterns observed at the somatosensory periphery and in the early stages of cortical processing get progressively weaker and ultimately vanish as one ascends the somatosensory neuraxis (Harvey et al., 2013; Romo et al., 2002). We hypothesize that stimulus information carried in the timing of the response is converted into a rate-based representation but the neural circuits that mediate this transformation are unknown.

The responses of many somatosensory neurons in the central nervous system – including the cuneate nucleus (CN) and SC – have been shown to reflect a temporal computation on their inputs. Specifically, a subpopulation of CN and SC neurons implement a temporal differentiation of their inputs, conferring to them a selectivity for temporal features in their inputs (Saal et al., 2015; Suresh et al., 2021). To test whether this computation – applied to SC responses by downstream neurons – could give rise to a rate-based representation of vibratory frequency that was independent of amplitude, we simulated the responses of such neurons by convolving measured SC spike trains with balanced filters of different widths (Figure 4.1). To the extent that the period of the filter matches that of the signal, the rectified output of the convolution will be high. A bank of such filters, each designed to extract a narrow range of frequencies, results in a spectral mapping of the SC activity (Figure 4.2A).

When this approach is applied to SC responses presented in Chapter 2, vibratory frequency can be accurately decoded from spike trains (Figure 4.2B). This decoder, trained and tested on responses pooled across amplitude, matches the ability of the timing-based decoder (from Chapter 2) to extract frequency independent of amplitude, unlike the rate-

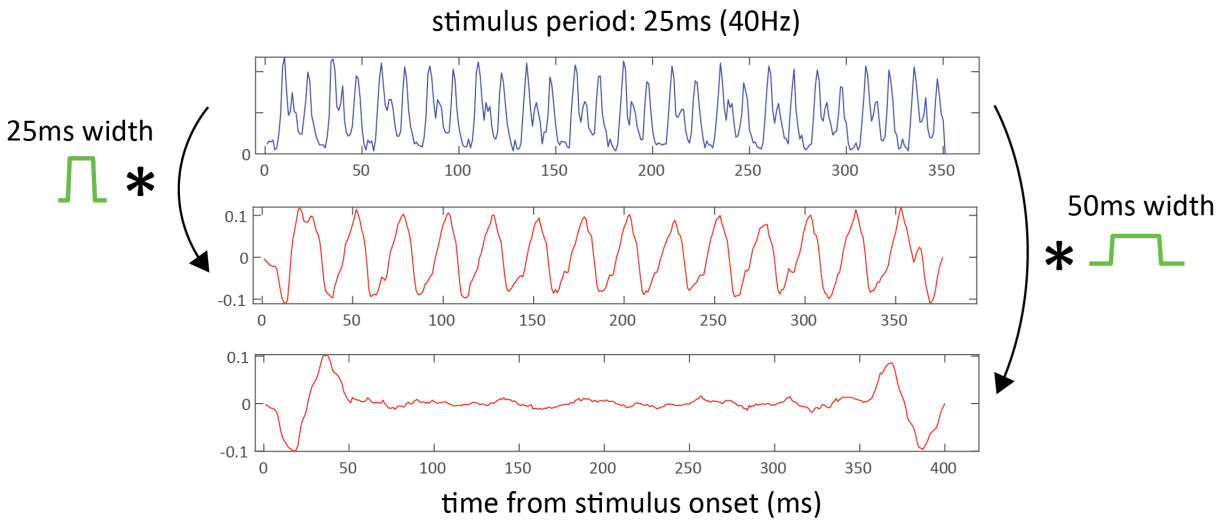

Figure 4.1: Convolution of the measured response with two temporal filters. The time-varying rate of the response of an SC neuron to a 40-Hz vibration (top row) is convolved with two filters, one 25 ms wide, the other 50 ms wide. The outputs of the convolutions depend on the width of the filters. The rectified output of the filter whose width matches the vibratory period (middle row) dwarfs that of the wider filter (bottom row).

based decoder. Thus, a known computation effected in the somatosensory system – temporal differentiation – could in principle give rise to an amplitude-independent representation of vibratory frequency. This hypothesis makes very clear predictions about vibratory responses in higher-order somatosensory cortices, including secondary somatosensory cortex (S2) and the parietal ventral area (PV). Such a filter bank could be constructed with coincidence detectors and systematically arranged delay lines, as famously employed by the barn owl to localize sound by computing interaural time differences (Carr & Konishi, 1990).

The next step in this line of inquiry will be to record vibratory responses in S2/PV and assess whether these match predictions from the filter bank hypothesis.

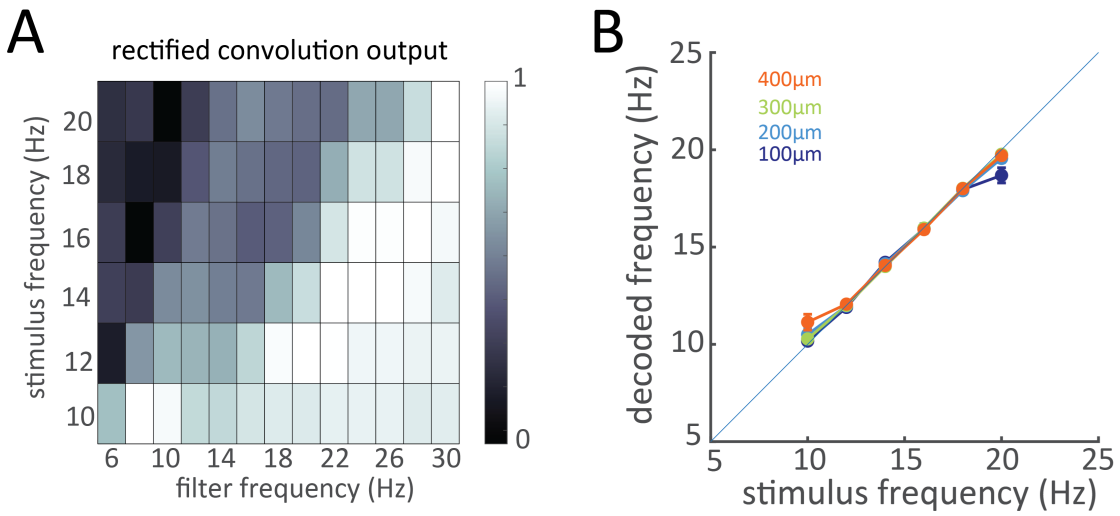

Figure 4.2: Convolution of neural signal with a bank of filters. A — Responses of an SC neuron to vibrations from 10 to 20 Hz (from the experiment presented in Chapter 2) are convolved with filters with different periods (equivalent frequencies shown on the x axis), and the rectified sums of the output of each convolution are shown in greyscale. B — The frequency of the stimulus on each trial is decoded from the outputs of convolutions with the filter bank. The decoder was trained and tested on all stimulus amplitudes grouped together.

4.2 Future horizons for touch neuroprosthetics

The restoration of touch – via stimulation of the peripheral nerves or somatosensory cortex – improves the dexterity of bionic hands despite the crudeness of current technologies used to activate neurons. The main limitation is the inability to reproduce specific spatiotemporal patterns of activity because electrical stimulation activates populations of neurons around the electrode synchronously and non-selectively. Nonetheless, a guiding principle in the development of artificial touch is that of biomimicry: to the extent that we can speak the language of the nervous system – reproduce aspects of natural neuronal response that play a key role in conveying specific sensory information –, the resulting percepts will be naturalistic and thus convey sensory information intuitively. While arbitrary mappings between sensor output and electrical stimulation can be used to convey sensory information (Dadarlat et al., 2015; Thomson et al., 2013), these require learning on the part of the user and are unlikely

to scale up to accommodate the bandwidth required to achieve dexterity that approaches that of the native limb (Delhaye et al., 2016).

However, as stimulating technology progresses beyond electrical stimulation and as the ability to selectively stimulate individual neurons improves, the potential to achieve naturalistic sensory feedback will grow. This selectivity will open the door to exploit explicit rate-based representations of specific object features in somatosensory cortex. For example, a subpopulation of neurons in Brodmann's area 1 is highly selective for direction of motion, responding preferentially to objects moving across the skin in a specific direction (Pei et al., 2010). Perhaps electrical activation of a population of such neurons would produce a percept of directed motion, a strategy that has shown promise in visual experiments; indeed, electrical stimulation of direction-selective neurons in medial temporal cortex biases the perceived direction of motion of a visual stimulus (Salzman et al., 1992). This strategy requires that direction-selective neurons are clustered together, and the topographical organization of direction selectivity in somatosensory cortex has not been investigated. However, electrical stimulation of certain patches of area 1 has been shown to occasionally evoke sensations of tactile motion (Armenta Salas et al., 2018), perhaps providing a proof of principle for the strategy.

As discussed in Chapter 2, some sensory information is encoded in the timing of the neuronal response, relying on a so-called temporal code. Accordingly, modulation of pulse timing – which in turn shapes spike timing in the activated population – can be used to convey stimulus information in a biomimetic way. For example, texture coding relies in part on temporal spiking patterns (Weber et al., 2013), and modulating pulse trains to mimic patterns of neuronal activation produced during the haptic exploration of textured surface can be used to convey information about surface texture in the nerve (Oddo et al., 2016) and in the brain (O'Doherty et al., 2019). While the quality of the evoked percepts is not one of texture per se, this strategy may convey some information about texture in an intuitive

way.

Beyond prosthetic applications, the ability to produce tactile sensations that convey specific stimulus information will set the stage for writing information into the brain through artificial means, bypassing our senses, in a variety of other contexts. While restoring other sensory modalities is an obvious extension, one might imagine interfacing with language structures to convey speech signals or with memory structures to implant memories, etc. While these ideas may seem outlandish given the primitive state of artificial touch, the private sector has begun to invest in them. In the meantime, sensitized bionic hands are on the cusp of clinical viability and may soon become part of our everyday experience.

4.3 References

Armenta Salas, M., Bashford, L., Kellis, S., Jafari, M., Jo, H., Kramer, D., Shanfield, K., Pejsa, K., Lee, B., Liu, C. Y., & Andersen, R. A. (2018). Proprioceptive and cutaneous sensations in humans elicited by intracortical microstimulation. ELife, 7, e32904. https://doi.org/10.7554/eLife.32904

Carr, C., & Konishi, M. (1990). A circuit for detection of interaural time differences in the brain stem of the barn owl. The Journal of Neuroscience, 10(10), 3227–3246.

Dadarlat, M. C., O'Doherty, J. E., & Sabes, P. N. (2015). A learning-based approach to artificial sensory feedback leads to optimal integration. Nature Neuroscience, 18(1), 138–144. https://doi.org/10.1038/nn.3883

Delhaye, B. P., Saal, H. P., & Bensmaia, S. J. (2016). Key considerations in designing a somatosensory neuroprosthesis. Journal of Physiology-Paris, 110(4, Part A), 402–408. https://doi.org/10.1016/j.jphysparis.2016.11.001

Harvey, M. A., Saal, H.P., Dammann, J.F., & Bensmaia, S.J. (2013). Multiplexing Stimulus Information through Rate and Temporal Codes in Primate Somatosensory Cortex. PLoS Biology, 11, e1001558.

Oddo, C. M., Raspopovic, S., Artoni, F., Mazzoni, A., Spigler, G., Petrini, F., Giambattistelli, F., Vecchio, F., Miraglia, F., Zollo, L., Di Pino, G., Camboni, D., Carrozza, M. C., Guglielmelli, E., Rossini, P. M., Faraguna, U., & Micera, S. (2016). Intraneural stimulation elicits discrimination of textural features by artificial fingertip in intact and amputee humans. ELife, 5. http://dx.doi.org/10.7554/eLife.09148

O'Doherty, J. E., Shokur, S., Medina, L. E., Lebedev, M. A., & Nicolelis, M. A. L. (2019). Creating a neuroprosthesis for active tactile exploration of textures. Proceedings of the National Academy of Sciences, 116(43), 21821–21827. https://doi.org/10.1073/pnas.1908008116

Pei, Y.-C., Hsiao, S. S., Craig, J. C., & Bensmaia, S. J. (2010). Shape Invariant Coding of Motion Direction in Somatosensory Cortex. PLoS Biology, 8(2), e1000305.

Romo, R., Hernández, A., Zainos, A., Lemus, L., & Brody, C. D. (2002). Neuronal correlates of decision-making in secondary somatosensory cortex. Nature Neuroscience, 5(11), 1217–1225. https://doi.org/10.1038/nn950

Saal, H. P., Harvey, M. A., & Bensmaia, S. J. (2015). Rate and timing of cortical responses driven by separate sensory channels. ELife, 4, e10450. https://doi.org/10.7554/eLife.10450

Salzman, C., Murasugi, C., Britten, K., & Newsome, W. (1992). Microstimulation in visual area MT: Effects on direction discrimination performance. The Journal of Neuroscience, 12(6), 2331–2355. https://doi.org/10.1523/JNEUROSCI.12-06-02331.1992

Suresh, A. K., Greenspon, C. M., He, Q., Rosenow, J. M., Miller, L. E., & Bensmaia, S. J. (2021). Sensory computations in the cuneate nucleus of macaques. BioRxiv, 2021.07.28.454185. https://doi.org/10.1101/2021.07.28.454185

Thomson, E. E., Carra, R., & Nicolelis, M. A. L. (2013). Perceiving invisible light through a somatosensory cortical prosthesis. Nature Communications, 4, 1482.

Weber, A. I., Saal, H. P., Lieber, J. D., Cheng, J.-W., Manfredi, L. R., Dammann, J. F., & Bensmaia, S. J. (2013). Spatial and temporal codes mediate the tactile perception of natural textures. Proceedings of the National Academy of Sciences, 110(42), 17107–17112.

Appendix A | Neural basis of touch

A.1 Tactile innervation of the skin

The palmar surface of the hand – where most object interactions take place – is innervated by 12,000 tactile nerve fibers (Johansson & Vallbo, 1979), each of which terminates in one of four types of mechanoreceptors embedded in the skin (Figure A.1A). These mechanoreceptors convert mechanical deformations of the skin into neural signals and different classes of receptors respond differently to skin deformations (Darian-Smith, 2011; Goodman & Bensmaia, 2020; Johansson & Flanagan, 2009; Johnson, 2001; Vallbo & Johansson, 1976) (Figure A.1 B). Slowly adapting type 1 (SA1) fibers produce a sustained response to a static indentation of the skin and, as a population, convey a spatial image of the pattern of skin deformation (Phillips et al., 1988; Phillips & Johnson, 1981). Rapidly adapting (RA) fibers respond only at the onset and offset of a skin indentation and are silent when the skin is not moving (Knibestöl, 1973). Their responses instead seem best suited to track dynamic force applications to the hand, such as the rapid sequence of contact events accompanying manipulation of objects. Pacinian corpuscle-associated (PC) fibers are exquisitely sensitive to skin vibrations, peaking in sensitivity around 250 Hz with thresholds measured in the hundreds of nanometers (Bell et al., 1994; Freeman & Johnson, 1982; Johansson et al., 1982; Muniak et al., 2007). These nerve fibers play an important role in the perception of fine textures (Weber et al., 2013) and of substrate borne vibrations, for example those transmitted through a tool (Brisben et al., 1999). Slowly adapting type 2 (SA2) fibers respond primarily to stretch and are most prevalent around the nails (Knibestöl, 1975), where they can sense forces applied on the fingertips (Birznieks et al., 2009). Tactile information about an object and about contact events is multiplexed in the responses of these four afferent populations

1. Excerpt from: Callier, T., and Bensmaia, S. J. (2021). Restoring the sense of touch with electrical stimulation of the nerve and brain. Somatosensory Feedback for Neuroprosthetics, edited by Burak Guclu, Academic Press, 2021, pp. 349-378.

and touch sensations typically involve the integration of signals from all four classes (Saal & Bensmaia, 2014; Weber et al., 2013).

A.2 Medial lemniscal pathway

Tactile nerve fibers innervating the palmar surface of the hand converge to form the median and ulnar nerves, which carry tactile signals up the arm and a short distance up the spinal cord before they synapse onto the cuneate nucleus in the brainstem (Figure A.1 A). The cell bodies of tactile nerve fibers are located in the dorsal root ganglia between the vertebrae, just outside of the spinal column. The nerve fibers synapse onto neurons in the cuneate nucleus, located in the brainstem, where afferent inputs are first integrated and processed. While the response properties of neurons in the cuneate nucleus were thought to be similar to those of their afferent inputs, recent work suggests that this neural structure may carry out some degree of feature extraction (Bengtsson et al., 2013; Hayward et al., 2014; Jörntell et al., 2014; Suresh, 2015, 2019; Suresh et al., 2017). The cuneate nucleus sends projections contralaterally to the ventroposterior nucleus (VPL) of the thalamus (Craig, 2006) (Figure A.1 A), which then projects mainly to somatosensory cortex, located in anterior parietal cortex.

A.3 Somatosensory cortex

Somatosensory cortex – sometimes mistakenly referred to as primary somatosensory cortex – comprises four cortical fields: Brodmann's areas 3a, 3b, 1, and 2 (Figure A.1 A). Neurons in area 3a exhibit proprioceptive responses, neurons in areas 3b and 1 exhibit cutaneous responses, and neurons in area 2 exhibit both. Each cutaneous neuron will only respond to touch within a restricted patch of skin, the so-called receptive field (RF). Brodmann's area 3b is primary somatosensory cortex proper as its structure and interconnectivity with other

brain structures are similar to primary sensory cortices in other modalities (Kaas, 1983). Somatosensory cortex is organized hierarchically – with area 3b at the bottom and area 2 at the top – as evidenced by the progressive increase in RF size and in response complexity (Delhaye et al., 2018). The most striking feature of somatosensory cortex is its somatotopic organization: nearby neurons respond to touch of nearby and partially overlapping patches of skin. Each cortical field within somatosensory cortex contains a full map of the contralateral side of the body, with greater cortical area dedicated to the representation of highly innervated regions of the body such as the hands (Sur et al., 1980) (Figure A.1 A).

In the hand representation within area 3b, neurons have small receptive fields, typically limited to a single finger pad or digit (DiCarlo et al., 1998), which comprise excitatory subfields flanked by inhibitory ones. Neurons display response properties that reflect those of multiple classes of nerve fibers (SA1, RA, and PC) (Pei et al., 2009), which implies that individual neurons receive convergent input from multiple tactile submodalities, though this integration begins to take place in the cuneate nucleus (Suresh, 2019). Neurons in area 1 tend to have larger RFs than do their counterparts in area 3b, sometimes spanning multiple digits (Iwamura et al., 1983) and they often exhibit selectivity for complex features, such as direction of tactile motion (Bensmaia et al., 2008; Delhaye et al., 2018; Hyvärinen & Poranen, 1978a; Iwamura et al., 1983). Neurons in area 2 exhibit both cutaneous and proprioceptive responses (Hyvärinen & Poranen, 1978b; Iwamura et al., 1993; Seelke et al., 2012), typically have large RFs spanning multiple fingers (Pons et al., 1985), and often exhibit selectivity for complex features, such as local curvature (Yau et al., 2013). Importantly, areas 1 and 2 lie on the post-central gyrus and thus can be surgically accessed far more easily than can area 3b, which lies almost entirely within the posterior bank of the central sulcus.

Secondary somatosensory cortex (S2) and the parietal ventral area (PV) receive input from the somatosensory cortical fields in anterior parietal cortex described above and carry high-level representations of touch (Delhaye et al., 2018). However, these structures have

never been targeted in neuroprosthetic applications so will not be discussed here.

A.4 References

Bell, J., Bolanowski, S., & Holmes, M. H. (1994). The structure and function of pacinian corpuscles: A review. Progress in Neurobiology, 42(1), 79–128. https://doi.org/10.1016/0301-0082(94)90022-1

Bengtsson, F., Brasselet, R., Johansson, R. S., Arleo, A., & Jörntell, H. (2013). Integration of Sensory Quanta in Cuneate Nucleus Neurons In Vivo. PLoS ONE, 8(2), e56630. https://doi.org/10.1371/journal.pone.0056630

Bensmaia, S. J., Denchev, P. V., Dammann, J. F., Craig, J. C., & Hsiao, S. S. (2008). The Representation of Stimulus Orientation in the Early Stages of Somatosensory Processing. Journal of Neuroscience, 28(3), 776–786. https://doi.org/10.1523/JNEUROSCI.4162-07.2008

Birznieks, I., Macefield, V. G., Westling, G., & Johansson, R. S. (2009). Slowly Adapting Mechanoreceptors in the Borders of the Human Fingernail Encode Fingertip Forces. Journal of Neuroscience, 29(29), 9370–9379. https://doi.org/10.1523/JNEUROSCI.0143-09.2009

Brisben, A. J., Hsiao, S. S., & Johnson, K. O. (1999). Detection of Vibration Transmitted Through an Object Grasped in the Hand — Journal of Neurophysiology. Journal of Neurophysiology, 81, 1548–1558.

Craig, A. D. (Bud). (2006). Retrograde analyses of spinothalamic projections in the macaque monkey: Input to ventral posterior nuclei. The Journal of Comparative Neurology, 499(6), 965–978. https://doi.org/10.1002/cne.21154

Darian-Smith, I. (2011). The Sense of Touch: Performance and Peripheral Neural Processes. In R. Terjung (Ed.), Comprehensive Physiology (p. cp010317). John Wiley & Sons, Inc. https://doi.org/10.1002/cphy.cp010317

Delhaye, B. P., Long, K. H., & Bensmaia, S. J. (2018). Neural Basis of Touch and Pro-

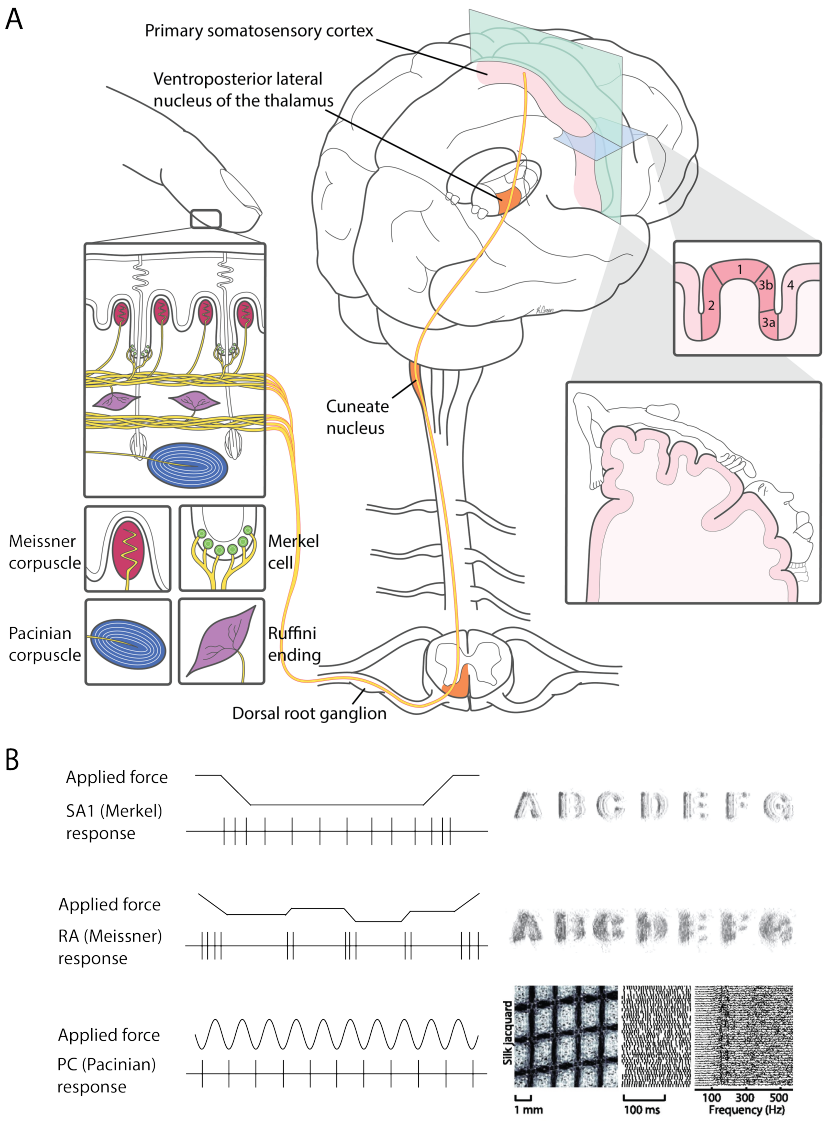

Figure A.1: Neuroanatomy of touch. A) The touch neuraxis from periphery to cortex. Mechanoreceptors embedded in the skin (left insets) facilitate the initiation of responses in afferent fibers. These bundle in fascicles that join to form nerves. The axons of afferent neurons ascend the spinal cord and synapse onto the cuneate nucleus in the brainstem. Axons from the cuneate project to the contralateral ventroposterior complex of the thalamus, which in turn projects to somatosensory cortex. Top right inset: somatosensory cortex comprises Brodmann's areas 3a, 3b, 1, and 2. Bottom right inset: each area is somatotopically organized. B) Response properties of afferent fibers. SA1 afferents produce a sustained response to static indentation of the skin. As a population, they convey a spatial image of the pattern of skin deformation, as shown in the reconstructed response of SA fibers to embossed letters scanned across the skin. RA afferents respond to changes in applied force and are silent when the force is constant. Their responses are well suited to track dynamic forces and also convey some information about the local geometric features of objects. PC fibers are sensitive to skin vibrations and become entrained to the frequencies of the vibrations. The timing or frequency composition of PC responses is texture-specific and plays an important role in the perception of fine textures. Modified from (Phillips et al., 1988; Weber et al., 2013).

prioception in Primate Cortex. In D. M. Pollock (Ed.), Comprehensive Physiology (pp. 1575–1602). John Wiley & Sons, Inc. https://doi.org/10.1002/cphy.c170033

DiCarlo, J. J., Johnson, K. O., & Hsiao, S. S. (1998). Structure of Receptive Fields in Area 3b of Primary Somatosensory Cortex in the Alert Monkey. The Journal of Neuroscience, 18(7), 2626–2645. https://doi.org/10.1523/JNEUROSCI.18-07-02626.1998

Freeman, A. W., & Johnson, K. O. (1982). A model accounting for effects of vibratory amplitude on responses of cutaneous mechanoreceptors in macaque monkey. The Journal of Physiology, 323(1), 43–64. https://doi.org/10.1113/jphysiol.1982.sp014060

Goodman, J. M., & Bensmaia, S. J. (2020). The Neural Mechanisms of Touch and Proprioception at the Somatosensory Periphery. In The Senses. Elsevier.

Hayward, V., Terekhov, A. V., Wong, S.-C., Geborek, P., Bengtsson, F., & Jörntell, H. (2014). Spatio-temporal skin strain distributions evoke low variability spike responses in cuneate neurons. Journal of The Royal Society Interface, 11(93), 20131015.

Hyvärinen, J., & Poranen, A. (1978a). Movement-sensitive and direction and orientation-selective cutaneous receptive fields in the hand area of the post-central gyrus in monkeys. The Journal of Physiology, 283(1), 523–537. https://doi.org/10.1113/jphysiol.1978.sp012517

Hyvärinen, J., & Poranen, A. (1978b). Receptive field integration and submodality convergence in the hand area of the post-central gyrus of the alert monkey. The Journal of Physiology, 283(1), 539–556. https://doi.org/10.1113/jphysiol.1978.sp012518

Iwamura, Y., Tanaka, M., Sakamoto, M., & Hikosaka, O. (1983). Converging patterns of finger representation and complex response properties of neurons in area 1 of the first somatosensory cortex of the conscious monkey. Experimental Brain Research, 51(3).

Iwamura, Y., Tanaka, M., Sakamoto, M., & Hikosaka, O. (1993). Rostrocaudal gradients in the neuronal receptive field complexity in the finger region of the alert monkey's postcentral gyrus. Experimental Brain Research, 92(3). https://doi.org/10.1007/BF00229023

Johansson, R. S., & Flanagan, J. R. (2009). Coding and use of tactile signals from the

fingertips in object manipulation tasks. Nature Reviews Neuroscience, 10(5), 345–359. https://doi.org/10.1038/nrn2621

Johansson, R. S., Landstro¨m, U., & Lundstro¨m, R. (1982). Responses of mechanoreceptive afferent units in the glabrous skin of the human hand to sinusoidal skin displacements. Brain Research, 244(1), 17–25. https://doi.org/10.1016/0006-8993(82)90899-X

Johansson, R. S., & Vallbo, A. B. (1979). Tactile sensibility in the human hand: Relative and absolute densities of four types of mechanoreceptive units in glabrous skin. The Journal of Physiology, 286(1), 283–300. https://doi.org/10.1113/jphysiol.1979.sp012619

Johnson, K. O. (2001). The roles and functions of cutaneous mechanoreceptors. Current Opinion in Neurobiology, 11(4), 455–461. https://doi.org/10.1016/S0959-4388(00)00234-8

Jörntell, H., Bengtsson, F., Geborek, P., Spanne, A., Terekhov, A. V., & Hayward, V. (2014). Segregation of Tactile Input Features in Neurons of the Cuneate Nucleus. Neuron, 83(6), 1444–1452. https://doi.org/10.1016/j.neuron.2014.07.038

Kaas, J. H. (1983). What, if anything, is SI? Organization of first somatosensory area of cortex. Physiological Reviews, 63(1), 206–231. https://doi.org/10.1152/physrev.1983.63.1.206

Knibestöl, M. (1973). Stimulus-response functions of rapidly adapting mechanoreceptors in the human glabrous skin area. The Journal of Physiology, 232(3), 427–452.

Knibestöl, M. (1975). Stimulus-response functions of slowly adapting mechanoreceptors in the human glabrous skin area. The Journal of Physiology, 245(1), 63–80.

Muniak, M. A., Ray, S., Hsiao, S. S., Dammann, J. F., & Bensmaia, S. J. (2007). The Neural Coding of Stimulus Intensity: Linking the Population Response of Mechanoreceptive Afferents with Psychophysical Behavior. Journal of Neuroscience, 27(43), 11687–11699. https://doi.org/10.1523/JNEUROSCI.1486-07.2007

Pei, Y.-C., Denchev, P. V., Hsiao, S. S., Craig, J. C., & Bensmaia, S. J. (2009). Convergence of Submodality-Specific Input Onto Neurons in Primary Somatosensory Cortex. Journal of Neurophysiology, 102(3), 1843–1853. https://doi.org/10.1152/jn.00235.2009

Phillips, J. R., & Johnson, K. O. (1981). Tactile spatial resolution. II. Neural representation of Bars, edges, and gratings in monkey primary afferents. Journal of Neurophysiology, 46(6), 1192–1203. https://doi.org/10.1152/jn.1981.46.6.1192

Phillips, J. R., Johnson, K. O., & Hsiao, S. S. (1988). Spatial pattern representation and transformation in monkey somatosensory cortex. Proceedings of the National Academy of Sciences, 85(4), 1317–1321. https://doi.org/10.1073/pnas.85.4.1317

Pons, T. P., Garraghty, P. E., Cusick, C. G., & Kaas, J. H. (1985). The somatotopic organization of area 2 in macaque monkeys. The Journal of Comparative Neurology, 241(4), 445–466. https://doi.org/10.1002/cne.902410405

Saal, H. P., & Bensmaia, S. J. (2014). Touch is a team effort: Interplay of submodalities in cutaneous sensibility. Trends in Neurosciences, 37(12), 689–697.

Seelke, A. M. H., Padberg, J. J., Disbrow, E., Purnell, S. M., Recanzone, G., & Krubitzer, L. (2012). Topographic Maps within Brodmann's Area 5 of Macaque Monkeys. Cerebral Cortex, 22(8), 1834–1850. https://doi.org/10.1093/cercor/bhr257

Sur, M., Merzenich, M. M., & Kaas, J. H. (1980). Magnification, receptive-field area, and "hypercolumn" size in areas 3b and 1 of somatosensory cortex in owl monkeys. Journal of Neurophysiology, 44(2), 295–311. https://doi.org/10.1152/jn.1980.44.2.295

Suresh, A. K. (2015, October 21). Tactile coding in the cuneate nucleus of macaques [Poster]. Society for Neuroscience 2015, Chicago, Illinois.

Suresh, A. K. (2019, October 23). Sensory computations in the cuneate nucleus of macaques [Poster]. Society for Neuroscienc 2019, Chicago, Illinois.

Suresh, A. K., Winberry, J. E., Versteeg, C., Chowdhury, R., Tomlinson, T., Rosenow, J. M., Miller, L. E., & Bensmaia, S. J. (2017). Methodological considerations for a chronic neural interface with the cuneate nucleus of macaques. Journal of Neurophysiology, 118(6), 3271–3281. https://doi.org/10.1152/jn.00436.2017

Vallbo, Å. B., & Johansson, R. S. (1976). Skin mechanoreceptors in the human hand: Neural

and psychophysical thresholds. In Sensory Functions of the Skin in Primates (pp. 185–199). Elsevier. https://doi.org/10.1016/B978-0-08-021208-1.50021-7

Weber, A. I., Saal, H. P., Lieber, J. D., Cheng, J.-W., Manfredi, L. R., Dammann, J. F., & Bensmaia, S. J. (2013). Spatial and temporal codes mediate the tactile perception of natural textures. Proceedings of the National Academy of Sciences, 110(42), 17107–17112. https://doi.org/10.1073/pnas.1305509110

Yau, J. M., Connor, C. E., & Hsiao, S. S. (2013). Representation of tactile curvature in macaque somatosensory area 2. Journal of Neurophysiology, 109(12), 2999–3012.

Appendix B | Electrical interfaces with the nervous system

B.1 Interface hardware - peripheral

Nerves in the hand and arm consist of bundles of sensory and motor nerve fibers called fascicles. The proportion of motor nerve fibers decreases as one proceeds distally (toward the hand), as might be expected given that these innervate muscles (Downey et al., 2020). For sensory restoration, distal targets are thus preferable. Chronically implanted electrical interfaces with the nerve can be divided into two broad categories, each with its advantages and disadvantages: extrafascicular or epineural electrodes, which surround the nerve, and intrafascicular or intraneural electrodes, which penetrate it (Figure B.1A).

Epineural electrodes sit on the outside surface of the nerve without breaching its surrounding sheath. As such they are less invasive than intraneural interfaces, but the separation between electrical contacts and fascicles requires higher stimulation currents to achieve sensation than with intraneural electrodes (Saal & Bensmaia, 2015). Higher currents lead to a broader spatial spread, which activates larger afferent populations and lowers selectivity – the ability to activate only a target population of afferents and not others. Two common examples are the spiral cuff electrode (Tan et al., 2014), which wraps around the nerve and provides a number of distinct contacts around its surface, and the flat interface nerve electrode (Charkhkar et al., 2018; Freeberg et al., 2017; Graczyk et al., 2016), which flattens the nerve to improve access to fascicles farther from the surface of the nerve. A major advantage of these interfaces is their demonstrated stability over the span of years (Graczyk et al., 2018; Ortiz-Catalan et al., 2014).

Intraneural interfaces are inserted into the nerve to achieve direct contact with nerve fibers. Some intraneural implants consist of wire-like electrodes that run parallel to the

1. Excerpt from: Callier, T., and Bensmaia, S. J. (2021). Restoring the sense of touch with electrical stimulation of the nerve and brain. Somatosensory Feedback for Neuroprosthetics, edited by Burak Guclu, Academic Press, 2021, pp. 349-378.

nerve (Lawrence et al., 2004; Yoshida & Stein, 1999) or traverse it (Boretius et al., 2010), each with multiple contacts to impinge upon several fascicles. Other intraneural implants consist of an array of microelectrodes laid out in a grid that are driven into the nerve like a bed of nails, with the tip of each electrode providing an electrical contact (Page et al., 2018; Wendelken et al., 2017). For these, electrodes get progressively longer along the axis of the nerve to ensure that the electrical contacts impinge on different fascicles (Figure B.1A). The advantage of intraneural approaches over their epineural counterparts is that lower currents are required to achieve sensation given the closer proximity of the electrical contact to the nerve fibers (Saal & Bensmaia, 2015), which limits current spread and, in principle, allows for the selective stimulation of small groups of fibers (Branner et al., 2001) and even individual fibers. However, intraneural electrodes are more liable to move within the nerve, which may limit their stability, and, in practice, the currents delivered to achieve robust sensations preclude a high degree of selectivity. Whether intraneural electrodes can lead to stable percepts over the span of years has yet to be demonstrated (Rossini et al., 2010; Wendelken et al., 2017).

One of the main disadvantages of interfacing with the peripheral nerve is that arm movements result in movement of the nerve inside the arm, which leads to instability in the interface. An alternative approach to interface with the peripheral nervous system is to target the dorsal root ganglia (DRG) near the spinal cord (Gaunt et al., 2009), where the cell bodies of tactile nerve fibers are located. Given its encasement in bone, the DRG is far less mobile than is the nerve and offers the additional advantage that it only comprises sensory nerve fibers. However, the implant surgery is far more challenging and invasive, and surgical innovation is ongoing.

B.2 Interface hardware - central

The two common interfaces used to deliver sensory feedback to the central nervous system are electrocorticography (ECoG) electrodes (Collins et al., 2017; Hiremath et al., 2017; Johnson et al., 2013; Lee et al., 2018) and penetrating microelectrode arrays (Armenta Salas et al., 2018; Flesher et al., 2016) (Figure B.1B). ECoG arrays consist of small metal disks (2-3mm diameter), arranged in a grid configuration with electrodes spaced 3 to 10 mm apart, implanted on the surface of the brain (Downey et al., 2020). Because ECoG electrodes are placed outside of the (insulating) pia mater (but under the dura mater), eliciting detectable sensations requires large stimulation currents, which leads to spatial spread and limited selectivity (Hiremath et al., 2017; Lee et al., 2018). Furthermore, ECoG stimulation preferentially activates the superficial layers of cortex, where horizontal connectivity is most extensive, thereby leading to even more diffuse neuronal activation. The advantage of ECoG arrays is that they are less invasive, in that they do not penetrate the gray matter, and seem to be more stable (Degenhart et al., 2016; Pels et al., 2019), though this has not been conclusively demonstrated.

In contrast to ECoG arrays and as their name suggests, penetrating microelectrode arrays (MEAs) penetrate the brain to bring electrodes in direct contact with neurons (Figure B.1B). The most common MEA is the Utah Electrode Array, which is largely identical to the intraneural array described above for the peripheral nerve except that the 96 electrodes are of equal length rather than tapered (1 or 1.5 mm). MEAs are more invasive than ECoG electrodes, but the close proximity of neurons and electrodes makes it possible to elicit sensations at far lower currents. As a result, MEAs offer better selectivity: microelectrodes separated by less than one millimeter can activate largely non-overlapping populations, while a single ECoG electrode can be roughly the size of an entire MEA. While MEAs can be used to elicit stable percepts for years (Callier et al., 2015), they inevitably fail catastrophically (Barrese et al., 2013), which severely limits their viability as clinical devices.

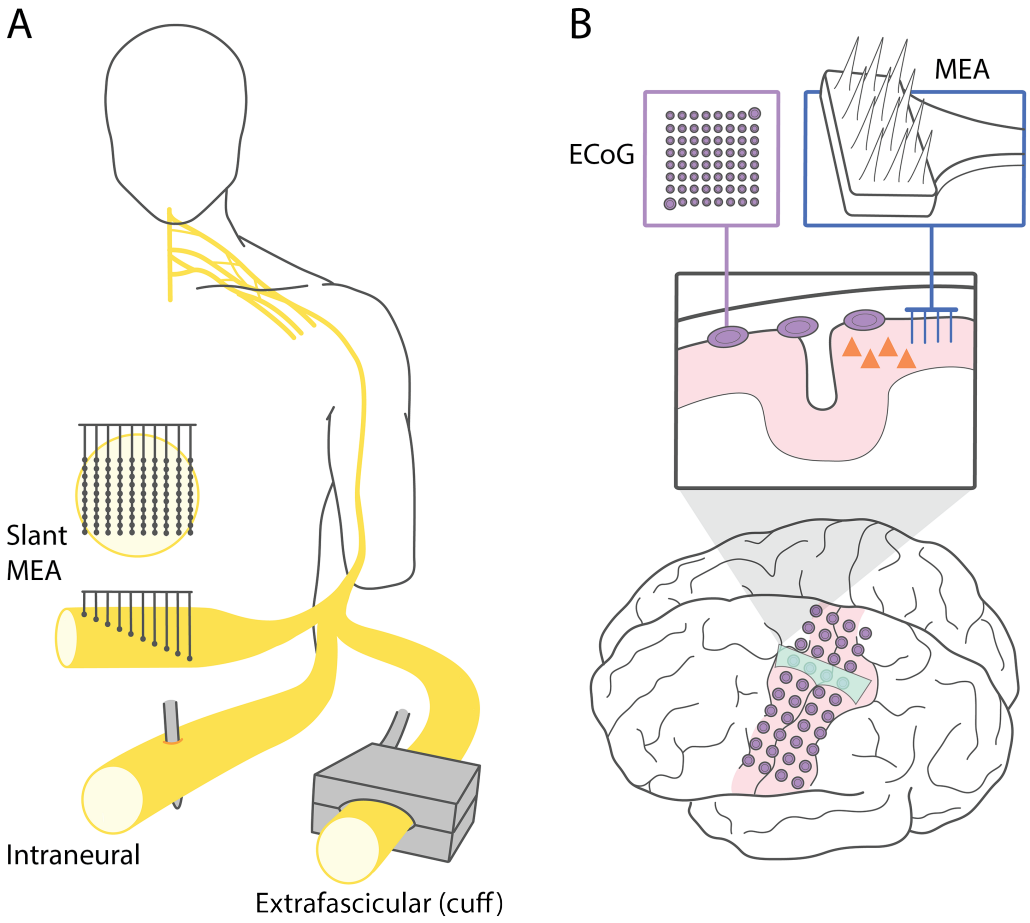

Figure B.1: Interface hardware. A) Examples of peripheral nerve interfaces. Extrafascicular or epineural electrodes such as cuff electrodes sit outside of the nerve. Intrafascicular or intraneural electrodes penetrate the nerve to bring electrodes in direct contact with axons. The transverse intrafascicular electrode shown here has multiple electrical contacts so it can stimulate different afferent fibers. Slant microelectrode arrays (MEAs) penetrate the nerve at varying depths across the width of the nerve to establish contacts with different afferent fibers. B) Two common interfaces with the central nervous system are electrocorticography (ECoG) electrodes and MEAs. ECoG arrays consist of small metal disks (2-3 mm in diameter) that are implanted on the surface of the brain, while penetrating MEAs are driven into the brain to bring electrodes in direct contact with neurons. MEAs are only a few millimeters wide, the size of a single ECoG electrode. As a result, they offer far higher spatial resolution than do ECoG arrays.

B.3 References

Armenta Salas, M., Bashford, L., Kellis, S., Jafari, M., Jo, H., Kramer, D., Shanfield, K., Pejsa, K., Lee, B., Liu, C. Y., & Andersen, R. A. (2018). Proprioceptive and cutaneous sensations in humans elicited by intracortical microstimulation. ELife, 7, e32904. https://doi.org/10.7554/eLife.32904

Barrese, J. C., Rao, N., Paroo, K., Triebwasser, C., Vargas-Irwin, C., Franquemont, L., & Donoghue, J. P. (2013). Failure mode analysis of silicon-based intracortical microelectrode arrays in non-human primates. Journal of Neural Engineering, 10(6), 066014.

Boretius, T., Badia, J., Pascual-Font, A., Schuettler, M., Navarro, X., Yoshida, K., & Stieglitz, T. (2010). A transverse intrafascicular multichannel electrode (TIME) to interface with the peripheral nerve. Biosensors and Bioelectronics, 26(1), 62–69.

Branner, A., Stein, R. B., & Normann, R. A. (2001). Selective Stimulation of Cat Sciatic Nerve Using an Array of Varying-Length Microelectrodes. Journal of Neurophysiology, 85(4), 1585–1594. https://doi.org/10.1152/jn.2001.85.4.1585

Callier, T., Schluter, E. W., Tabot, G. A., Miller, L. E., Tenore, F. V., & Bensmaia, S. J. (2015). Long-term stability of sensitivity to intracortical microstimulation of somatosensory cortex. Journal of Neural Engineering, 12(5), 056010. https://doi.org/10.1088/1741-2560/12/5/056010

Charkhkar, H., Shell, C. E., Marasco, P. D., Pinault, G. J., Tyler, D. J., & Triolo, R. J. (2018). High-density peripheral nerve cuffs restore natural sensation to individuals with lower-limb amputations. Journal of Neural Engineering, 15(5), 056002.

Collins, K. L., Guterstam, A., Cronin, J., Olson, J. D., Ehrsson, H. H., & Ojemann, J. G. (2017). Ownership of an artificial limb induced by electrical brain stimulation. Proceedings of the National Academy of Sciences, 114(1), 166–171.

Degenhart, A. D., Eles, J., Dum, R., Mischel, J. L., Smalianchuk, I., Endler, B., Ashmore, R. C., Tyler-Kabara, E. C., Hatsopoulos, N. G., Wang, W., Batista, A. P., & Cui, X. T. (2016).

Histological evaluation of a chronically-implanted electrocorticographic electrode grid in a non-human primate. Journal of Neural Engineering, 13(4), 046019.

Downey, J. E., Brooks, J., & Bensmaia, S. J. (2020). Artificial sensory feedback for bionic hands. In Intelligent Biomechatronics in Neurorehabilitation (pp. 131–145).

Flesher, S. N., Collinger, J. L., Foldes, S. T., Weiss, J. M., Downey, J. E., Tyler-Kabara, E. C., Bensmaia, S. J., Schwartz, A. B., Boninger, M. L., & Gaunt, R. A. (2016). Intracortical microstimulation of human somatosensory cortex. Science Translational Medicine, 8(361), 361ra141-361ra141. https://doi.org/10.1126/scitranslmed.aaf8083

Freeberg, M. J., Stone, M. A., Triolo, R. J., & Tyler, D. J. (2017). The design of and chronic tissue response to a composite nerve electrode with patterned stiffness. Journal of Neural Engineering, 14(3), 036022. https://doi.org/10.1088/1741-2552/aa6632

Gaunt, R. A., Hokanson, J. A., & Weber, D. J. (2009). Microstimulation of primary afferent neurons in the L7 dorsal root ganglia using multielectrode arrays in anesthetized cats: Thresholds and recruitment properties. Journal of Neural Engineering, 6(5), 055009. https://doi.org/10.1088/1741-2560/6/5/055009

Graczyk, E. L., Delhaye, B. P., Schiefer, M. A., Bensmaia, S. J., & Tyler, D. J. (2018). Sensory adaptation to electrical stimulation of the somatosensory nerves. Journal of Neural Engineering, 15(4), 046002. https://doi.org/10.1088/1741-2552/aab790

Graczyk, E. L., Schiefer, M. A., Saal, H. P., Delhaye, B. P., Bensmaia, S. J., & Tyler, D. J. (2016). The neural basis of perceived intensity in natural and artificial touch. Science Translational Medicine, 8(362), 362ra142-362ra142. https://doi.org/10.1126/scitranslmed.aaf5187

Hiremath, S. V., Tyler-Kabara, E. C., Wheeler, J. J., Moran, D. W., Gaunt, R. A., Collinger, J. L., Foldes, S. T., Weber, D. J., Chen, W., Boninger, M. L., & Wang, W. (2017). Human perception of electrical stimulation on the surface of somatosensory cortex. PLOS ONE, 12(5), e0176020. https://doi.org/10.1371/journal.pone.0176020

Johnson, L. A., Wander, J. D., Sarma, D., Su, D. K., Fetz, E. E., & Ojemann, J. G. (2013).

Direct electrical stimulation of the somatosensory cortex in humans using electrocorticography electrodes: A qualitative and quantitative report. Journal of Neural Engineering, 10(3), 036021. https://doi.org/10.1088/1741-2560/10/3/036021

Lawrence, S. M., Dhillon, G. S., Jensen, W., Yoshida, K., & Horch, K. W. (2004). Acute Peripheral Nerve Recording Characteristics of Polymer-Based Longitudinal Intrafascicular Electrodes. IEEE Transactions on Neural Systems and Rehabilitation Engineering, 12(3), 345–348. https://doi.org/10.1109/TNSRE.2004.831491

Lee, B., Kramer, D., Armenta Salas, M., Kellis, S., Brown, D., Dobreva, T., Klaes, C., Heck, C., Liu, C., & Andersen, R. A. (2018). Engineering Artificial Somatosensation Through Cortical Stimulation in Humans. Frontiers in Systems Neuroscience, 12, 24.

Ortiz-Catalan, M., Håkansson, B., & Brånemark, R. (2014). An osseointegrated human-machine gateway for long-term sensory feedback and motor control of artificial limbs. Science Translational Medicine, 6(257), 257re6-257re6. https://doi.org/10.1126/scitranslmed.3008933

Page, D. M., George, J. A., Kluger, D. T., Duncan, C., Wendelken, S., Davis, T., Hutchinson, D. T., & Clark, G. A. (2018). Motor Control and Sensory Feedback Enhance Prosthesis Embodiment and Reduce Phantom Pain After Long-Term Hand Amputation. Frontiers in Human Neuroscience, 12, 352. https://doi.org/10.3389/fnhum.2018.00352

Pels, E. G. M., Aarnoutse, E. J., Leinders, S., Freudenburg, Z. V., Branco, M. P., van der Vijgh, B. H., Snijders, T. J., Denison, T., Vansteensel, M. J., & Ramsey, N. F. (2019). Stability of a chronic implanted brain-computer interface in late-stage amyotrophic lateral sclerosis. Clinical Neurophysiology, 130(10), 1798–1803. https://doi.org/10.1016/j.clinph.2019.07.020

Rossini, P. M., Micera, S., Benvenuto, A., Carpaneto, J., Cavallo, G., Citi, L., Cipriani, C., Denaro, L., Denaro, V., Di Pino, G., Ferreri, F., Guglielmelli, E., Hoffmann, K.-P., Raspopovic, S., Rigosa, J., Rossini, L., Tombini, M., & Dario, P. (2010). Double nerve intraneural interface implant on a human amputee for robotic hand control. Clinical Neurophysiology, 121(5), 777–783. https://doi.org/10.1016/j.clinph.2010.01.001

Saal, H. P., & Bensmaia, S. J. (2015). Biomimetic approaches to bionic touch through a peripheral nerve interface. Neuropsychologia, 79, 344–353.

Tan, D. W., Schiefer, M. A., Keith, M. W., Anderson, J. R., Tyler, J., & Tyler, D. J. (2014). A neural interface provides long-term stable natural touch perception. Science Translational Medicine, 6(257), 257ra138-257ra138. https://doi.org/10.1126/scitranslmed.3008669

Wendelken, S., Page, D. M., Davis, T., Wark, H. A. C., Kluger, D. T., Duncan, C., Warren, D. J., Hutchinson, D. T., & Clark, G. A. (2017). Restoration of motor control and proprioceptive and cutaneous sensation in humans with prior upper-limb amputation via multiple Utah Slanted Electrode Arrays (USEAs) implanted in residual peripheral arm nerves. Journal of NeuroEngineering and Rehabilitation, 14(1), 121.

Yoshida, K., & Stein, R. B. (1999). Characterization of signals and noise rejection with bipolar longitudinal intrafascicular electrodes. IEEE Transactions on Biomedical Engineering, 46(2), 226–234.

Appendix C | Neural Coding of Contact Events in Somatosensory Cortex

C.1 Abstract

Manual interactions with objects require precise and rapid feedback about contact events. These tactile signals are integrated with motor plans throughout the neuraxis to achieve dexterous object manipulation. To better understand the role of somatosensory cortex in interactions with objects, we measured, using chronically implanted arrays of electrodes, the responses of populations of somatosensory neurons to skin indentations designed to simulate the initiation, maintenance, and termination of contact with an object. First, we find that the responses of somatosensory neurons to contact onset and offset dwarf their responses to maintenance of contact. Second, we show that these responses rapidly and reliably encode features of the simulated contact events—their timing, location, and strength—and can account for the animals' performance in an amplitude discrimination task. Third, we demonstrate that the spatiotemporal dynamics of the population response in cortex mirror those of the population response in the nerves. We conclude that the responses of populations of somatosensory neurons are well suited to encode contact transients and are consistent with a role of somatosensory cortex in signaling transitions between task subgoals.

C.2 Introduction

During manual interactions with an object, tactile signals provide precise and rapid feedback about the interface between hand and object. Several populations of mechanoreceptors in the skin convey detailed information about the timing, location, and nature of the contacts,

1. This appendix was published : Callier, T., Suresh, A. K., and Bensmaia, S. J. (2019). Neural Coding of Contact Events in Somatosensory Cortex. Cerebral Cortex, 29(11), 4613–4627. https://doi.org/10.1093/cercor/bhy337

and these signals are critical to our ability to dexterously manipulate objects (Augurelle et al. 2003; Witney et al. 2004; Johansson and Flanagan 2009). While tactile signals inform behavior at various stages of processing along the neuraxis, somatosensory cortex plays an important role in dexterous manipulation as evidenced by the fact that lesions thereof lead to severe and permanent deficits in hand use (Carlson 1981; Hikosaka et al. 1985; Xerri et al. 1998; Brochier et al. 1999; Duque et al. 2003; Schabrun et al. 2008). The precise role of somatosensory cortex in object interactions is unknown, however. For example, whether somatosensory cortex is involved in the online control of movement is unclear, and, to the extent that it is, the time scale over which somatosensory signals inform hand movements remains to be elucidated. One role of somatosensory cortex may be to guide motor learning by conveying information about the consequences of movement (Ostry et al. 2010; Mathis et al. 2017).

To help elucidate the role of somatosensory cortex in object manipulation, we examined the responses of populations of somatosensory neurons to simulated contact events, and the dependence of these responses on the features of contact. To this end, we delivered precisely controlled indentations, designed to mimic contact with an object, to the palmar surface of the hand of Rhesus macaques while recording the activity evoked in somatosensory cortex using chronically implanted arrays of electrodes. Our goal was to understand how the onset and offset of contact—during which the object moves into or retracts from the skin—and its maintenance—during which contact is approximately static—are encoded in the response of populations of somatosensory neurons, and how indentation depth and indentation rate modulate neuronal responses to contact. We also investigated the degree to which the spatiotemporal dynamics of the population responses in cortex reflect their inputs from the periphery by examining the simulated response of populations of tactile fibers to these same contact events.

C.3 Materials and methods

C.3.1 Animals

Three male Rhesus macaques (Macaca mulatta), 7–9 years old and weighing 9–10 kg, participated in this study. Animal care and handling conformed to the procedures approved by the University of Chicago Animal Care and Use Committee.

C.3.2 Implants

Each animal was implanted with one Utah electrode array at a time (UEA, Blackrock Microsystems, Inc., Salt Lake City, UT) in the hand representation of area 1 (Figs C.1B and C.2). Monkeys A and C were implanted with one array each, whereas monkey B was implanted with a second array after the first one failed. Each UEA consists of 96 electrodes, each 1.5mm long, with tips coated with iridium oxide, spaced 400 μm apart, and spanning 4mm $\times$ 4mm of the cortical surface. The hand representation in area 1 was targeted based on anatomical landmarks. Given that the arrays were contiguous to the central sulcus and area 1 spans approximately 3–5mm of cortical surface from the sulcus (Pons et al. 1985), few if any electrodes were located in area 2. Given the length of the electrodes, their tips terminated in the infragranular layers of somatosensory cortex, as we have previously shown in postmortem histological analysis with other animals instrumented with identical arrays (Rajan et al. 2015).

C.3.3 Stimuli

Mechanical stimuli consisted of 1-s long trapezoidal indentations delivered to the palmar surface of the hand using a high-precision custom-made tactile stimulator (Fig. C.1A) (similar to the one described in detail in Tabot et al. 2013). Initially, we delivered the stimuli by measuring the position of the hand along the vertical axis using a high-precision range finder

(Accurange 200–25; Acuity Lasers, Portland, OR) and having the indenting probe traverse this distance before it followed the desired indentation trajectory. Because the monkey's hand does not remain perfectly still, however, the position of the hand relative to the indenting stimulator changed over time in unpredictable ways by tens or hundreds of microns. These gradual shifts in hand position thus made it impossible to deliver indentations at a precisely controlled depth and resulted in fluctuations in the time at which the probe made contact with the skin.

To achieve well controlled skin deflections, then, we elected to preindent the stimulator tip 500 μm into the skin throughout the duration of each experimental session, and the indentation trajectory was delivered beyond this preindentation. This experimental decision is predicated on the fact that afferent responses to the preindentation decay away within 10–20 s, as does the resulting sensation, and afferent responses to indentations of the skin beyond the preindentation are identical to those with no preindentation (Vega-Bermudez and Johnson 1999). We compared cortical responses to actual contact events (from no contact to contact, with the probe starting position 0.5–1mm above the finger) to the cortical responses to simulated contact (with the preindentation) and found that, while the strength and timing of the latter was more variable than that of the former, the response profiles were otherwise virtually identical (see the section entitled "Preindentation vs. actual contact" in Appendix D and Fig. D.1 for a detailed comparison). Indentation depths ranged from 150 to 2000 μm, indentation rates from 5 to 50 mm/s, and probe diameter was 2 mm. All stimuli were reliably detectable for the animals (Callier et al. 2015), and were presented in pseudorandom order.

C.3.4 Behavioral Task

Monkeys A and B performed a tactile discrimination task in a 2-alternative forced choice paradigm. In these experiments, the animals sat facing a monitor, with their hand fixed

palmar surface facing up—using Velcro straps and a drop of cyanoacrylate on the nail—to allow a custom-designed tactile stimulator to indent their skin (Fig. C.1A). Eye movements were tracked with an optical eye-tracking system (MR PC60, Arrington Research, Scottsdale, AZ). On each trial, 2 indentations (10mm/s, 2-mm diameter) were sequentially delivered to the skin, each 1-s long and separated by a 1-s interstimulus interval. One stimulus interval contained the standard stimulus, whose amplitude was either 150 or 2000 μm; and the other contained a comparison stimulus whose amplitude varied from 150 to 2000 μm (excluding the standard amplitude). The order of presentation of the standard and comparison stimuli was randomized across trials. The monkey maintained fixation on a cross on the monitor until the end of the second stimulus presentation otherwise the trial was aborted. The animal's task was to judge which of the 2 stimuli was more intense (higher amplitude) by making a saccade to 1 of 2 visual targets placed on the left or the right of the fixation cross. Correct responses were rewarded with a drop of juice. Psychophysical performance was calculated as the proportion of trials on which the higher amplitude stimulus was correctly judged as more intense.

Additional recordings were obtained from monkeys B and C under similar circumstances, except that the animals performed a visual motion tracking task to keep them alert (see Fig. D.2 for the stimulations sites used in these experiments). The goal of these recordings was to investigate the effects of indentation rate on cortical responses. For these measurements, the stimulator probe tip was 2mm in diameter and indentation rates were 5, 10, 20, or 50 mm/s, thereby spanning the range of typical interactions with objects during activities of daily living (estimated from previously published interaction data (Kim et al. 2011)). To verify that responses evoked when tactile stimuli were behaviorally irrelevant were similar to those evoked with the animal engaged in a tactile discrimination task (for those stimulus conditions that were common to the 2 behavioral conditions), we compared the peristimulus time histograms obtained from the 2 conditions and the respective ratios of the transient

response to the sustained response (see section entitled "Heterogeneity of cortical responses" in the Supplementary Methods in Appendix D for details on this metric). We found the response dynamics to be virtually identical and the ratio to be statistically indistinguishable across conditions (2 sample t-test: t[110] = 1.72, P ¿ 0.05), in keeping with the expectation that attention exerts a negligible influence on neuronal responses in this area of cortex (Hyvarinen et al. 1980; Meftah et al. 2002). An experimental block consisted of a session, usually consisting of a few hundred trials, in which a single skin location was stimulated, with or without the behavioral task.

C.3.5 Electrophysiology Recording

We simultaneously recorded from all 96 electrodes of the UEAs using a Cerebus system (Blackrock Microsystems, Salt Lake City, UT), passed the continuous voltage signal from each electrode, sampled at 30 kHz, through a 100-Hz high-pass filter to reduce background noise, and recorded the timing of thresholdcrossing events in each channel. Because we were interested in population responses, we analyzed multiunit (rather than single- unit) activity.

C.3.6 Standardizing Neuronal Responses

Multiunit activity varies widely from electrode to electrode, both at baseline when no stimulus is applied, and in response to a stimulus, as might be expected given that different electrodes acquire signals from neuron groups that vary in size, sensitivity, and spontaneous firing rate. Counting spikes is therefore an inadequate gauge of evoked activity if one wishes to compare across electrodes. If the objective is to build an activation map across the cortical surface, it is necessary to correct for this source of variability. To this end, we standardized the evoked response according to the baseline activity (i.e., converted it to a z-score):

$$Rs(t) = (R(t) - BaselineMean)/BaselineStd$$

where R(t) is the spike count in time bin t (whose width differed across analyses and ranged from 1 to 1200 ms), BaselineMean is the mean spike count per bin during baseline, and BaselineStd is the standard deviation (s.d.) of the spike count per bin during baseline. Baseline spike count distributions were estimated from the response in the 500-ms time window preceding the first stimulus of each trial. Baseline levels were computed for each electrode and experimental block separately. Thus, Rs(t) = 3 indicates a spike rate at time t that is 3 s.d. above the mean baseline spike rate for that electrode on that experimental block. We quantified the spatial extent of cortical activation by tracking the area of the array over which the neuronal activity exceeded a threshold (2 s.d. above baseline unless otherwise specified).

C.3.7 Encoding Model

To quantify the relative contributions of indentation depth and indentation rate to the neural response, we fit a linear model relating the mean (time-varying) response at the hotzone electrode— that is, the electrode at which the strongest activity was observed when stimulating a specific skin location (Britten et al. 1992)—and the mean (time-varying) activated cortical surface area (threshold = 2 s.d. above baseline) for each of 12 indentations (0.5, 1, and 2mm at 5, 10, 20, or 50 mm/s) to linear combinations of (time-varying) indentation depth and indentation rate at different time lags using least-sum-of-squares optimization. The shortest time lag allowed was 20 ms after stimulus onset to account for conduction latency from periphery to cortex, and the longest was 50 ms. The model was fit using responses beginning 500 ms before stimulus onset and ending 500 ms after stimulus offset, sampled at 100 Hz then averaged across 8 stimulation sites from monkeys B and C (4603 trials total) for each stimulus. Model parameters were fit to the responses to 11 stimuli using indentation depth only, indentation rate only, or both, then used to reconstruct the neural response to the 12th stimulus using the same stimulus values (depth, rate, or both). This procedure

was repeated with each stimulus left out, yielding 12 (cross-validated) R2 values for each model. From these models, we could assess the degree to which neural responses tracked indentation depth and/or indentation rate. Including acceleration into the model yielded only a modest improvement over indentation depth and/or indentation rate. Note, however, that most firing rate profiles featured bursts during acceleration events that likely reflect a sensitivity to acceleration. The lack of improvement in the model fit with the inclusion of acceleration is due to the fact that acceleration events in these stimuli are impulse functions at the beginning and end of the indentation and retraction ramps. The inclusion of acceleration has been shown to significantly improve model predictions of afferent firing rates to sinusoidal vibrations and band-pass noise, but the contribution of acceleration to firing rate is dwarfed by that of indentation rate (Okorokova et al. 2018).

C.3.8 Signaling of Contact Timing

To study timing on a trial-by-trial basis, we examined how rapidly contact onset could be detected from neuronal responses. Because our neuronal sample was restricted to a small fraction of the activated population, results from this analysis constitute a floor on timing precision in cortex. First, we pooled single-trial activity from the 20 most responsive electrodes at a temporal resolution of one millisecond and smoothed these pooled responses over a causal time window (10 ms wide) (Fig. C.6A). For each trial, responses were analyzed over a 1 second window centered on stimulus onset, and the first time bin in which the aggregate response exceeded a threshold of 14 s.d. above baseline was taken to be the time of detection for that contact event (Fig. C.6B). Trials on which detection occurred before stimulus onset were counted as false alarms, and trials in which no contact event was detected were counted as misses. The timing results were robust to changes in threshold value over a range (from 8 to 22, but the lowest combined error rate—false alarms and misses—occurred close to 14) (Fig. D.6). For this analysis, we combined trials with amplitude 500, 1000, and

2000 μm and analyzed them separately by indentation rate and skin location (4603 trials from 8 skin locations).

C.3.9 Signaling of Contact Location

We assessed how rapidly information about contact location can be read out from the cortical response by tracing the evolution of the centroid of neural activity on the array over expanding integration time windows (Fig. C.6C,D). On a trial-by-trial basis and for each integration time window beginning at stimulus onset, we computed the responses measured at each electrode, normalized these responses across electrodes to a maximum of 1, and selected all the electrodes that yielded responses above 0.65 (an arbitrary threshold, the value of which did not meaningfully affect the results as long as it was above 0.5). The position vectors of the remaining electrodes were weighted by their respective responses then averaged to obtain the centroid of neuronal activation on that trial. We used trials with amplitude 500, 1000, or 2000 μm and analyzed them separately by indentation rate and skin location (4603 trials from 8 skin locations). We then computed the position of the mean centroid by averaging across trials at each indentation rate and skin location then computed the distance between these mean centroids and the reference centroid (calculated using an integration time window of 300 ms after response onset over all trials). This distance was used as a measure of localization error for each integration time window. The 300-ms time window used to calculate the reference centroid is highly robust, encompassing the bulk of the neural response to stimulus onset at all indentation rates. For this analysis, we computed centroids across trials to mitigate our massive under-sampling of the response. The time course over which centroids stabilized was similar when these were computed based on single trials responses, but the errors were significantly higher. The trial-averaged centroid is still based on far fewer responses (hundreds per skin location) than are included over the relevant neuronal volume (tens of thousands).

C.3.10 Neurometric Analysis

We wished to assess the degree to which neuronal responses evoked during the behavioral task could account for the animals' perceptual judgments. To this end, we performed 2 ideal observer analyses. In one, we computed the proportion of times the strong stimulus (standard or comparison) evoked the stronger response at the hotzone electrode. In the second, we computed the proportion of times the stronger stimulus (standard or comparison) elicited the more widespread response. For this analysis, we used a low threshold (0.5 s.d. above baseline) to achieve a more graded metric since estimates of recruitment are limited by the spatial resolution of the array; that being said, results were robust to changes in threshold over a range. These analyses yielded performance metrics that could be directly compared with those of the animals' behavior. We used 2 time windows to perform these analyses: 1) The response over a 300-ms period following stimulus onset, which encompassed the indentation ramp (200-ms duration at the largest indentation) and captured any residual phasic activity, and 2) the response during the sustained epoch, encompassing the 300-ms period beginning 400ms after stimulus onset (at which time the phasic response had subsided). For both time windows, we corrected for response latency, 20ms) (Fig. C.7). In addition, we performed the ideal observer analysis using a time window that spanned only probe movement for each indentation amplitude (the width of which thus varied with amplitude) to isolate the contribution of the phasic response (Fig. D.11).

C.3.11 Simulations of Whole Nerve Responses

We wished to compare the responses to contact events in somatosensory cortex and in the somatosensory nerves. To this end, we reconstructed the responses of all tactile nerve fibers—slowly adapting type 1 (SA1), rapidly adapting (RA), and Pacinian corpuscle-associated (PC)—that innervate the palmar surface of the hand to each of the stimuli presented in the cortical experiments. Specifically, we used a recently developed simulation of the nerve that

can accurately reproduce afferent responses with near millisecond accuracy (Saal et al. 2017). In brief, the model first computes the skin's response to a time-varying stimulus impinging upon it, then generates the spiking response evoked in nerve fibers whose receptive fields (RFs) tile the skin at measured innervation densities. This simulation has been extensively validated using a variety of psychophysical and neurophysiological data sets (Goodman and Bensmaia 2017; Saal et al. 2017). Using this model, we simulated the nerve responses to the mechanical stimuli used in the cortical experiments, described above, and compared these simulated responses to their measured cortical counterparts. We delivered the simulated indentations at each location that was mechanically stimulated in the cortical experiments (see Fig. D.2). For finger sites, we simulated responses over each respective finger, and for palm sites, we simulated responses over the entire palm (mean = 2498 fibers, stdev = 1369 fibers). For recruitment calculations, we only included SA1 and RA afferent responses. To validate the simulation, we compared simulated afferent responses to a skin indentation to their measured counterparts (see section entitled "Single unit recordings from the nerve" in the Appendix D and Fig. D.7).

To compare simulated responses of tactile nerve fibers to the measured responses of cortical neurons, we computed the cross-correlation between their respective peristimulus time histograms (PSTHs) using an average for each stimulus across locations (distal finger, proximal finger, and palm; see Fig. D.10). Specifically, for each stimulus condition (12 pairs varying in indentation depth and indentation rate), we smoothed the responses, starting 500 ms before stimulus onset to 500 ms after stimulus offset, with a 20ms Gaussian kernel and computed the correlation coefficient at the optimal lag.

To verify that the indentations were ethologically valid, we simulated the response to a time-varying indentation that resembles the skin deflection produced when an object is grasped, lifted up, and released (see section entitled "Simulating the response of the nerve during a manual interaction with an object" in Appendix D). We then compared the sim-

ulated responses of tactile nerve fibers to this naturalistic stimulus and to the trapezoidal indentations.

C.4 Results

Using chronically implanted electrode arrays, we recorded the multiunit responses evoked across populations of neurons in area 1 when the palmar surface of the hand was indented with a punctate probe at different locations, to different depths, and at different indentation rates (Fig. C.1).

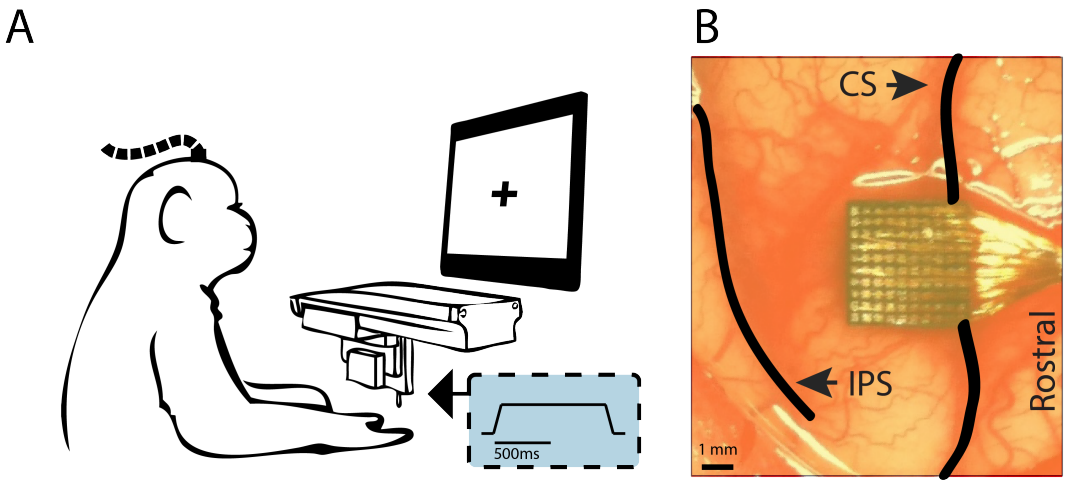

Figure C.1: Experimental design. (A) Experimental set-up. A monkey, with head fixed and hand with palmar surface facing upwards, receives indentations to the glabrous skin. Inset: temporal profile of the mechanical indentations (depicting depth). (B) Location of monkey A's array relative to the central sulcus (CS) and intraparietal sulcus (IPS), representative of the location of all the implanted arrays.

C.4.1 Spatial Layout of the Cortical Response

Indentation at different locations on the skin evoked activity that was localized to different regions of somatosensory cortex, usually with some overlap for adjacent skin locations (Penfield et al. 1937; Iwamura et al. 1983; Kaas 1983; Reed et al. 2008) (Fig. C.2). While the magnitude of the neural response varied greatly over the course of a stimulation event and

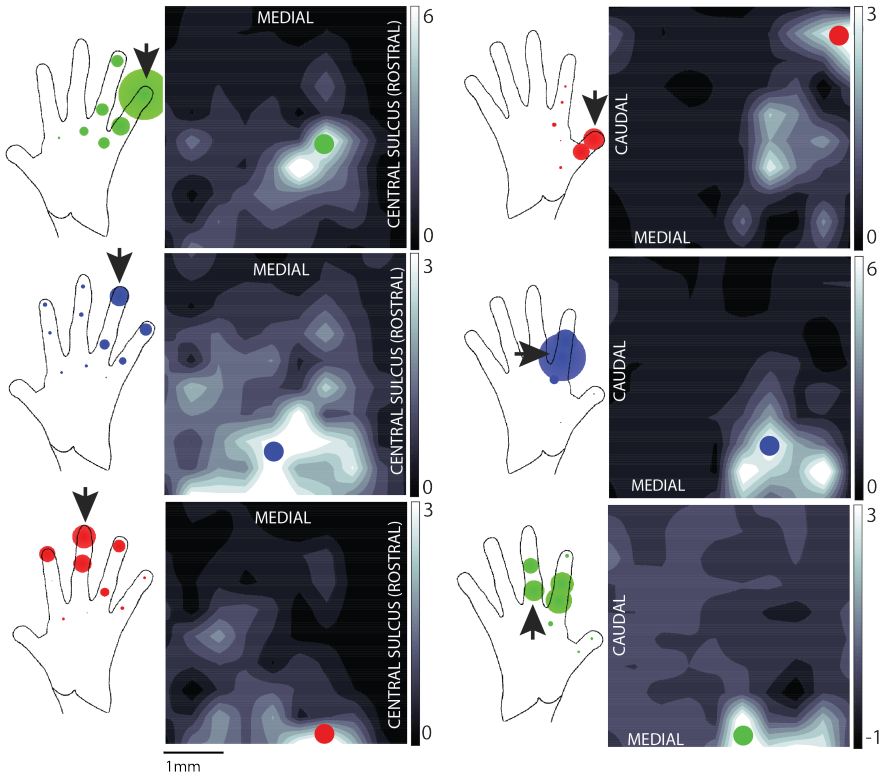

Figure C.2: Hand representation in area 1. Distribution of neural activity on 2 different arrays (array of monkey A and the first array of monkey B in the left and right columns, respectively) evoked by stimulation at 3 skin locations (rows). The neural activity is integrated over 1200 ms following the onset of a 2-mm, 10-mm/s indentation (lasting a total of 1 s) delivered to the location indicated by an arrow on the hand diagram to the left of the heat map. The colored dot on the array represents the location of the hotzone (highest responding) electrode for that skin location. As the site of stimulation shifts in the ulnar direction (red to blue to green), the hotzone of cortical activity shifts in the medial direction, consistent with the previously established somatotopy of the hand in area 1. In the hand diagram to the left of each heat map, each colored dot represents a different site of stimulation, with the dot radius proportional to the response of the electrode marked on the array when that skin location was stimulated. The response at the electrode tends to decrease as the stimulation site moves farther from the arrow, as expected. Responses are averaged over 75+ trials in each condition.

with stimulation parameters, the locus of activity remained unchanged, generally centered on a single electrode, to which we will refer as the hotzone electrode (the converse of the hotspot, or point of maximum sensitivity, of an RF). The location of the hotzone electrode followed the well-known somatotopic organization of somatosensory cortex, progressing medially and posterior along the central sulcus from the first to fifth digit. Typically, a given array would impinge upon the representation of 2–4 digits.

C.4.2 Temporal Profile of the Cortical Response

First, we examined the time course of neuronal activation recorded from the hotzone electrode. Here, we focused on a single mechanical stimulus, namely a probe with a diameter of 2mm indented 2mm into the skin at 10mm/s, held for 600ms, and then retracted at 10mm/s. In all cases, activity rose sharply, with a latency of about 20ms after stimulus onset and remained high as long as the probe continued to move into the skin. As soon as the probe stopped moving, however, neuronal activity abruptly dropped, often nearly to baseline despite the sustainment of the indentation (Fig. C.3A,B). Probe retraction also evoked a strong response, albeit weaker than during indentation.

To quantify the magnitude of the difference between the initial burst of activity (transient response evoked during probe movement), and subsequent tonic activity (sustained response while probe is statically indented into the skin), we computed the ratio between the spike rate over the first 200 ms of the response to that over a 200-ms window beginning 200 ms after the probe had stopped moving. We found that the response at the hotzone electrode during the onset transient was on average more than 15 times stronger than its counterpart during the static period and that this ratio varied widely across electrodes/ skin locations (range: 2.2 to 42.4, median: 12.0 over 28 skin locations from 4 arrays) (Fig. C.3B, Fig. D.3, Table D.1; see section entitled "Heterogeneity of cortical responses" in the Appendix D). Similarly, the response at the hotzone electrode during the offset transient was on average

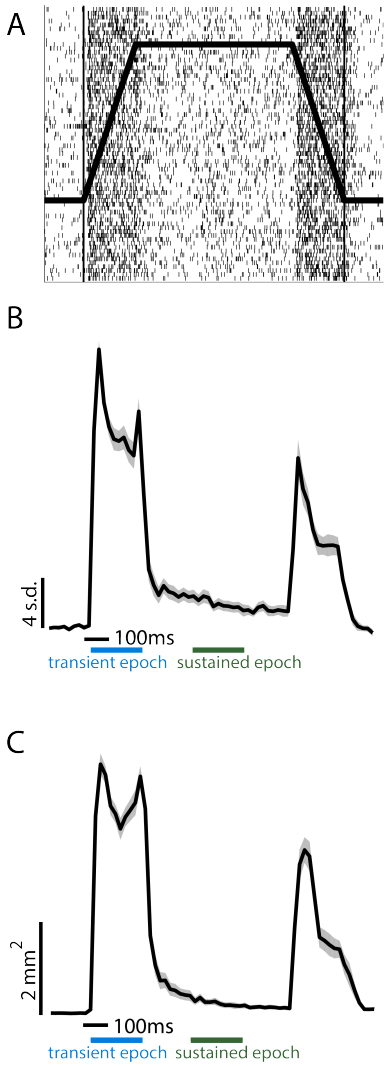

Figure C.3: Spatiotemporal dynamics of the response. (A) Multiunit raster of the response at the hotzone electrode to 70 repeated presentations of a 2-mm, 10- mm/s indentation delivered to the little finger (Fig. C.1A, top left), the profile of which is superimposed on the raster. (B) Peristimulus time histogram of the response (standard deviations above baseline mean) at the hotzone electrode to the same stimulus, averaged over 3408 trials from 28 palmar skin locations across the 4 arrays from the 3 animals (see Fig. C.2 and Fig. D.2 for all contact locations). Responses were normalized to a maximum of 1 within electrodes, averaged across electrodes, then multiplied by the mean peak response across electrodes. Shaded area denotes the standard error of the mean (SEM, N = 28 skin locations, time bin = 20 ms). Blue and green bars indicate transient and sustained epochs, respectively. The leftmost edge of the time scale bar indicates stimulus onset. The response to contact transients is far more prominent than that to static contact. (C) Dynamics of the spatial extent of cortical activation (surface with response greater than 2 std above baseline) as a function of time (3408 trials from 28 palmar skin locations across 4 arrays). Activation area was normalized to a maximum of 1 within skin locations, averaged across locations, then multiplied by the average peak activation area across skin locations. Leftmost edge of the time scale bar indicates stimulus onset, shaded area is SEM (N = 28 skin locations, time bin = 20 ms). The extent of activation is far greater during contact transients than during static contact.

more than 8 times stronger than the sustained response (range: 0.76 to 35.0, median 6.0; Table D.1, Fig. D.3). Ratios spanned a wide range and, while they overlapped largely across skin locations, electrodes with RFs on the palm tended to exhibit relatively weaker sustained responses (Fig. D.4, Table D.1). The variation in the ratio of transient to sustained response likely reflects variation in the relative strength of the input from different classes of nerve fibers across the cortical sheet (Sur et al. 1981). For instance, the relatively weaker sustained responses in palm cortex likely reflects the lower density of slowly adapting fibers on the palm relative to their rapidly adapting counterparts (Johansson and Vallbo 1979). Heterogeneity in these and other response metrics derived from cortical responses is documented in greater detail in Tables D1–D5.

C.4.3 Spatiotemporal Dynamics of the Cortical Response

As mentioned above, activation was not limited to a single electrode but rather was distributed over an area of cortex that spanned multiple electrodes. In light of this, we examined how the spatial pattern of activation evolved over time. We found that large swaths of cortex were activated as the probe moved into the skin (Fig. C.3C, Fig. D.3B). For example, a 10-mm/s indentation activated on average around 5mm^2 of somatosensory cortex. During the sustained portion of the indentation, however, the area of activation was limited to a small area (a fraction of a square millimeter) centered on the hotzone electrode. As was the case with response strength, recruitment also exhibited heterogeneity in its dynamics (Table D.5). Indeed, the extent of activation at stimulus onset and offset varied over the cortical sheet, though recruitment during the transients always dwarfed its counterpart during the sustained epoch. Recruitment was more restricted for palm stimulation than for digit stimulation (Table D.5), but the comparison is limited by the small number of stimulation sites.

C.4.4 Dependence of the Cortical Response on Contact Parameters

Next, we examined the degree to which the spatiotemporal dynamics of the response depend on the features of the simulated contact event.

First, we investigated the dependence of transient responses on indentation rate. Restricting our analysis to the period of time when the probe is moving, we found that both the firing rate at the hotzone electrode and the spatial extent of the activation increased monotonically with indentation rate (Fig. C.4A–F) but the spatial distribution did not change shape—responses scaled by roughly the same amount over the extent of the array (Fig. C.4G). Here, we restricted the time window over which responses were integrated to 40ms, the duration of the transient at the highest indentation rate (2mm traveled at 50mm/s), so that the initial burst of activity would not be weighted more heavily for the higher velocities. This meant, however, that the total indentation depth varied with indentation rate. The results were not meaningfully changed when responses were integrated over the full transient at each indentation rate, so that total indentation depth was constant but ramp duration decreased as speed increased (see colored traces in Fig. C.5C,D). To confirm that our firing response measures did not simply reflect increased recruitment around the electrode, we analyzed single-unit cortical data, and found that individual units increased their firing with increases in indentation rate (see section entitled "Single-electrode recordings from cortex" in Appendix D, Fig. D.5).

Next, we examined the dependence of the response on indentation depth (Fig. C.5). Restricting our analysis to the sustained response period, after the transient response had subsided, we found that both the firing rate at the hotzone electrode and the spatial extent of activation increased monotonically as the amplitude increased from 500 to 2000 μm (Fig. C.5A, dashed line in Fig. C.5C,D). During the transients, the modulation of firing rate and recruitment by indentation depth was weak compared with the modulation of firing rate and recruitment by indentation rate (colored traces in Fig. C.5C,D). If anything, firing rate

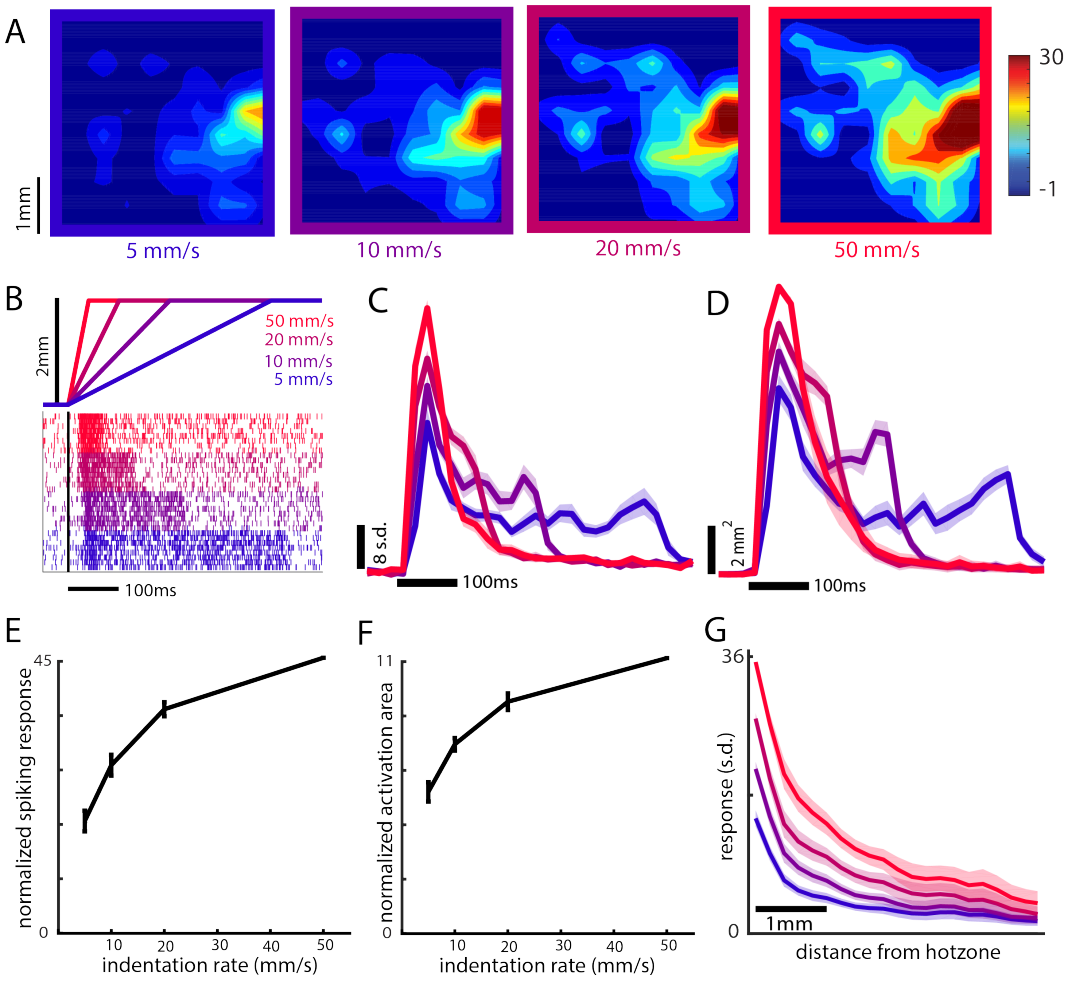

Figure C.4: Effect of indentation rate on the transient response. A) Heat map of neural activity during the first 40 ms of the response (starting 20 ms after stimulus onset to account for response latency) to a 2-mm indentation delivered to the second palmar pad of monkey C at indentation rates of 5, 10, 20, and 50 mm/s (40 ms is the probe movement time at the highest indentation rate; data averaged across 54 trials per indentation rate). (B) Indentation traces (top), along with the (color-matched) cortical responses (bottom). Indentation depth is constant so ramp durations increase as indentation rate decreases, as do the corresponding transient responses. (C) Time course of the response at the hotzone electrode to a 2-mm indentation at each indentation rate, averaged over 1535 trials across 8 skin locations from 2 arrays (second array of Monkey B and monkey C, same data for C–G). In panels C–G, responses were normalized as in Figure C.3 (N = 8 skin locations). Leftmost edge of the time scale bar indicates stimulus onset. (D) Dynamics of the spatial extent of activation evoked by a 2-mm indentation at each indentation rate. Peak activated area was normalized as in Figure C.3. Leftmost edge of the scale bar indicates stimulus onset. Shaded area shows the SEM (N = 8). Responses in C and D were calculated in 20-ms bins. (E) Mean and SEM of the cortical response at the hotzone electrode versus indentation rate during the transient for a 2-mm indentation. We used the same integration time window for each indentation rate (first 40 ms of the response starting 20 ms after stimulus onset). (F) Mean and SEM of the activated area versus probe indentation rate during the transient for a 2-mm indentation. We used the same integration time window at each indentation rate. (G) Response as a function of distance from the hotzone at the different indentation rates.

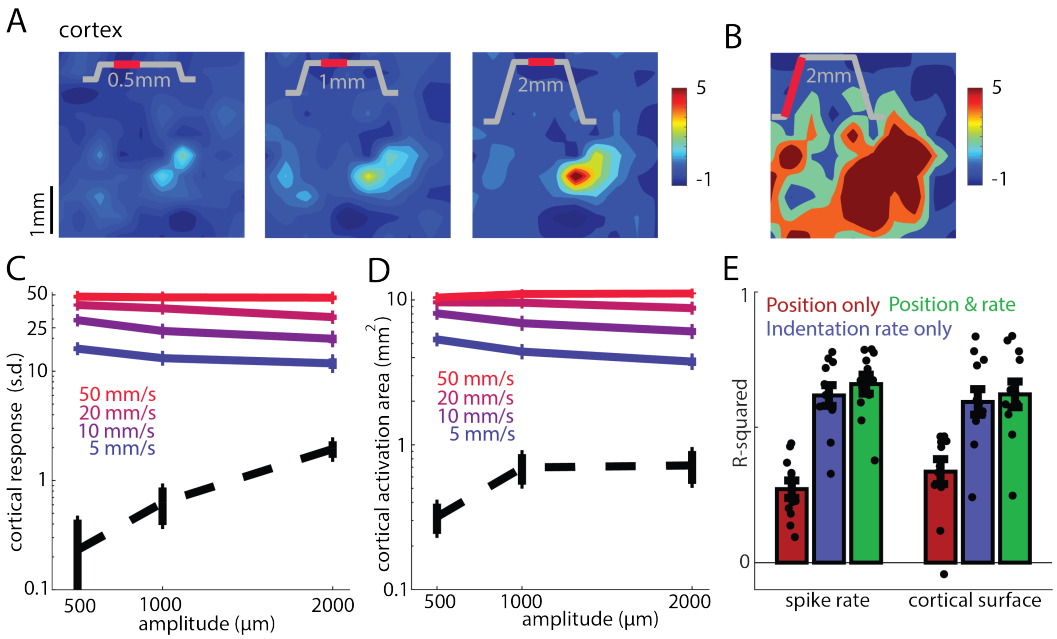

Figure C.5: Effect of indentation depth on the sustained and transient responses.

(A) Top: Spatial layout of the sustained response to 0.5-, 1-, and 2-mm indentations delivered to the little fingertip of monkey A at 10 mm/s (min 40 trials per amplitude). The inset shows the stimulus trace, the red section the relevant stimulus epoch (200 ms beginning 200 ms after the probe stopped moving, the only exception being the 2-mm, 5 mm/s indentation, for which the sustained epoch represents only the last 150 ms before probe retraction begins). (B) For comparison, spatial layout of the cortical response during contact onset of the same stimulation (the first 200 ms of the response). (C) Standardized firing rate at the hotzone electrode versus indentation depth during the transient phase (solid lines) and the sustained phase (dashed line) of the stimulus (4603 trials averaged across 8 skin locations from monkey B's second array and monkey C, same for C–E). The solid lines correspond to indentation velocities of 5, 10, 20, and 50 mm/s, and the dashed line to the sustained response averaged across trials at all velocities. Error bars show the SEM (N = 8). Responses were integrated over the full duration of the stimulus ramp. Note the logarithmically scaled ordinate. (D) Activation area versus indentation depth for the same stimuli and epochs as in C. (E) Fit of linear models relating spike rate at the hotzone electrode (left 3 bars) and activated cortical surface (right 3 bars) to time-varying indentation depth and rate. Neuronal responses primarily track indentation rate. Dots show the individual stimuli, and error bars show the SEM (n = 12 stimuli). Each color denotes different inputs used for both model training and reconstruction of the response.

seems to decrease as amplitude increases because, as the ramp gets longer, the strong initial burst (possibly driven by an acceleration event) gets washed out and this effect counteracts the weak amplitude-dependent increase in firing rate.

To quantify the relative contributions of indentation depth and indentation rate to the neural response, we fit linear models relating time-varying firing rate at the hotzone electrode and the time-varying spatial extent of activation (threshold = 2 s.d.) to time-varying indentation depth and indentation rate over a causal time window. For both hotzone firing rate and activated cortical area, models that included indentation depth and indentation rate yielded the best reconstruction of the neuronal response (firing rate: $R2 = 0.66 \pm 0.12$; activated area: $R2 = 0.62 \pm 0.17$). The reconstruction based on indentation rate only performed nearly as well (0.62 ± 0.13; 0.59 ± 0.16), while the reconstruction based on depth alone performed far worse (0.27 ± 0.11; 0.33 ± 0.16), highlighting that neuronal responses primarily track indentation rate rather than indentation depth (Fig. C.5E). Models yielded marginally better performance if acceleration was taken into consideration (firing rate: $R2 = 0.67 \pm 0.15$; activated area: $R2 = 0.64 \pm 0.18$). Note, however, that acceleration has been shown to drive afferent responses, though to a far lesser extent than does indentation rate (Dong et al. 2013; Saal et al. 2017; Okorokova et al. 2018), but ramp-and-hold stimuli are ill suited to reveal the contribution of acceleration (see Materials and Methods).

C.4.5 Rapid and Precise Signaling of Contact Timing

The rapid rise of the cortical response upon object contact (Fig. C.6A) yields a representation that is well suited to provide precise information about the timing of contact. With this in mind, we wished to estimate how rapidly contact with an object can be detected. To this end, we assessed when the aggregate cortical activity passes a (rather stringent) threshold on a trial by trial basis. We found that we could reliably detect the stimulus less than 30ms after onset for the most rapid indentation (Fig. C.6B). Given that the time for neuronal

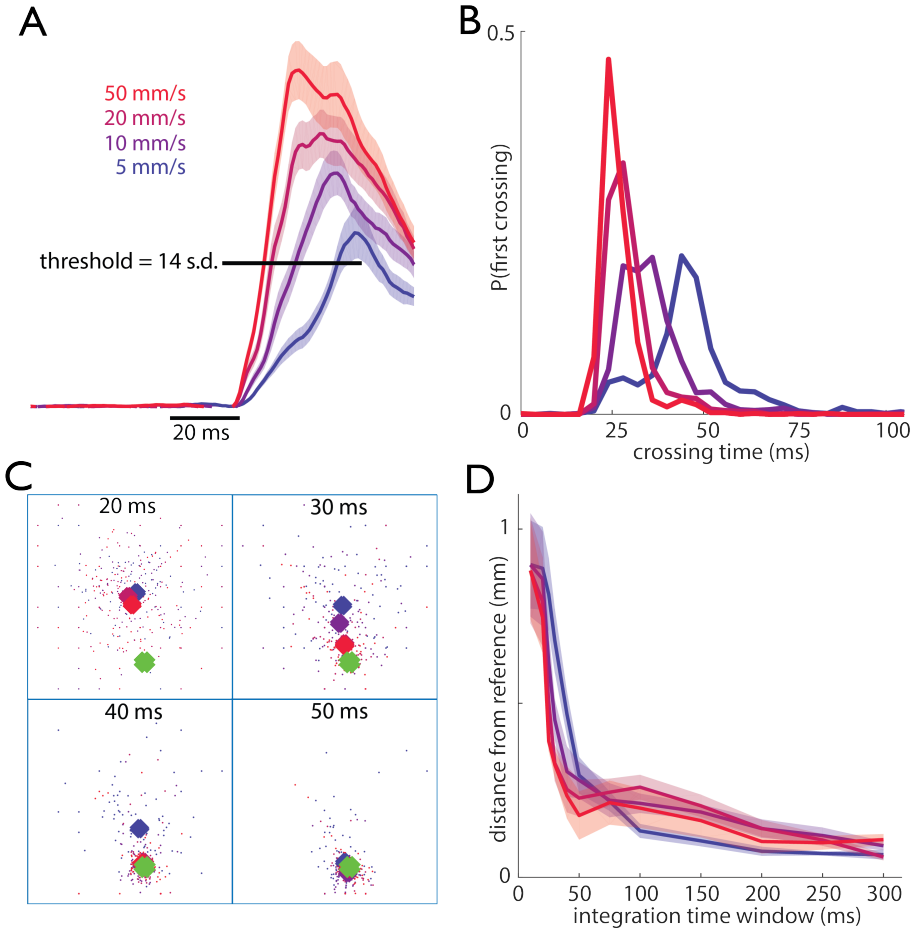

Figure C.6: Rapid detection and localization of contact events. (A) Pooled response of the 20 most responsive electrodes (for each skin location) around stimulus onset (smoothed over a 10-ms causal window). Shaded area shows the SEM (4603 total trials across 8 stimulation sites from monkey B's second array and monkey C). Leftmost edge of the time bar indicates stimulus onset. The threshold bar indicates the minimum single-trial response to signal a contact event (used to obtain the distribution in panel B). (B) Distribution of threshold-crossing times for each indentation rate for the same trials as in panel A (grouped in 4-ms bins). (C) For one example skin location (first palmar pad of monkey C), scatter plot of centroids for single-trial responses (small dots, color-coded by indentation rate) and mean responses (large diamonds) at integration windows of 20, 30, 40, and 50 ms following stimulus onset. The square denotes the 4mm × 4mm array and the green diamonds shows the reference centroid (calculated using an integration time window of 300 ms across all trials). The average centroids migrate to the reference centroid location within 40–50 ms. (D) Mean distance (across same stimulation sites as in A) between the reference centroid and the average centroids (for each indentation rate) as a function of integration time. Shaded area shows SEM.

signals to propagate from the skin of the hand to the brain is around 20 ms (Sripati et al. 2006), this signal is nearly as rapid as it could be. Importantly, even with this minuscule subset of the true cortical response, detection time was tightly distributed around its mean (e.g., at 50 mm/s, 80% of the detection times were within 6ms of their modal value), which highlights the reliability of this contact signal. Changing the detection criterion within a wide range did not greatly affect the modal detection time, but a lower threshold led to more spurious detections while a higher threshold led to more failures to detect (Fig. D.6). A neuronal response that tracked indentation depth rather than indentation rate, and thus evolved more slowly, would yield a slower and less precise contact timing signal.

C.4.6 Rapid and Precise Signaling of Contact Location

The location of contact is known to be encoded in the location of the evoked activity in somatosensory cortex. The most convincing evidence for this neural code is that microstimulation of neurons with RFs at a specific location on the body evokes sensations referred to that location (Tabot et al. 2013; Flesher et al. 2016). However, the spatial extent of activation is dependent on stimulus parameters, especially indentation rate, while the perceived location of contact remains consistent (as long as the stimulus is sufficiently above threshold (Johnson and Phillips 1981; Gibson and Craig 2006). We wished to assess the degree to which the centroid of neuronal activation evoked at a specific contact location was consistent across indentation rates and to characterize the time course over which it stabilized. We found that, at the highest indentation rate, the centroid of activation became stable within about 40 ms after contact (Fig. C.6C,D). In other words, the contact location was signaled almost as rapidly as it could be given the minimal response latency of around 20 ms. Given how dramatically the neuronal response was under-sampled, this constitutes an upper bound on timing and a lower bound on precision.

C.4.7 Relating Neuronal Responses to Behavior

Next, we assessed whether the responses of somatosensory neurons could account for the animals' amplitude discrimination performance. We used an ideal observer analysis to compute the discriminability based on neuronal responses measured as the animals performed the task. Specifically, we computed the proportion of times the comparison stimulus produced the stronger response and compared the resulting neurometric functions to the proportion of times the animal judged the comparison stimulus to be more intense. For the neurometric analysis, we used an epoch encompassing the transient response or one that included only the sustained response. We found that neurometric performance was best when we used a response epoch that included the transient phase and that it was comparable to the performance of the animal on the amplitude discrimination task (Fig. C.7A,B, compare red trace to blue trace). In contrast, neurometric performance was poor when only the sustained period was used (Fig. C.7A,B, green trace). In other words, more information about the stimulus is conveyed in the transient response than in the sustained one. Note that, because the indentation rate was the same at all amplitudes, increases in amplitude were associated with increases in the duration of the ramp. In principle, then, the animals could have performed this task by estimating the duration of the ramp. However, human subjects have been shown to have a poor sense of the temporal profile of an indentation and feel as though the indentation continues even after the probe has stopped moving (Poulos et al. 1984). Furthermore, after having performed a mechanical discrimination task, Monkeys A and B switched to a task in which they judged the relative amplitude of intracortical microstimulation (ICMS) trains—which did not have onset or offset ramps—and generalized to this new modality instantly (Tabot et al. 2013). In light of these observations, it is unlikely the animals used ramp duration to make their discrimination judgments. Neurometric performance based on responses restricted to probe movement far exceeded the behavioral performance as might be expected given that the duration of the response epoch increases

with amplitude (Fig. D.11).

We find, then, that the best discrimination performance is supported by integrating indentation rate—encoded in the phasic response—rather than by directly encoding indentation depth—reflected in the tonic response. Indeed, the phasic burst during the on-ramp is longer—and thus comprises more spikes —at long ramp durations, and the strength of that burst can account for the animal's performance. We performed the same analysis using area of activation rather than firing rate and obtained analogous results (Fig. C.7B), though firing rate yielded better performance than did activation area.

Note that, from these behavioral data, we cannot conclusively establish the neural code that underlies task performance. Indeed, the animals' judgments could rely on a combination of population spike rate and recruitment, for example, and the choice of integration time window—300ms—was quasi arbitrary (chosen to span the duration of the longest ramp and any residual phasic activity). The important conclusions is that the transient response information conveys far more information about stimulus intensity than does the sustained one.

C.4.8 Spatiotemporal Dynamics of the Response in the Peripheral Nerve

Finally, we wished to assess the degree to which cortical responses reflect their peripheral inputs. To this end, we simulated the response to all afferents activated by an indentation with identical parameters as the ones described above for the cortical experiment. We found that hundreds of afferents were activated, and that their aggregate response during the transients dwarfed that during the sustained portion of the stimulus, which was, again, remarkably weak (Fig. C.8A, also shown for measured responses in Fig. D.7A). The dominance of the transient response is due to the fact that RA and PC fibers only respond to changes in skin indentation, leaving only SA1 fibers to respond to the sustained indentation, and even these fibers respond more strongly to skin deflections (Knibestöl 1973, 1975). We also computed

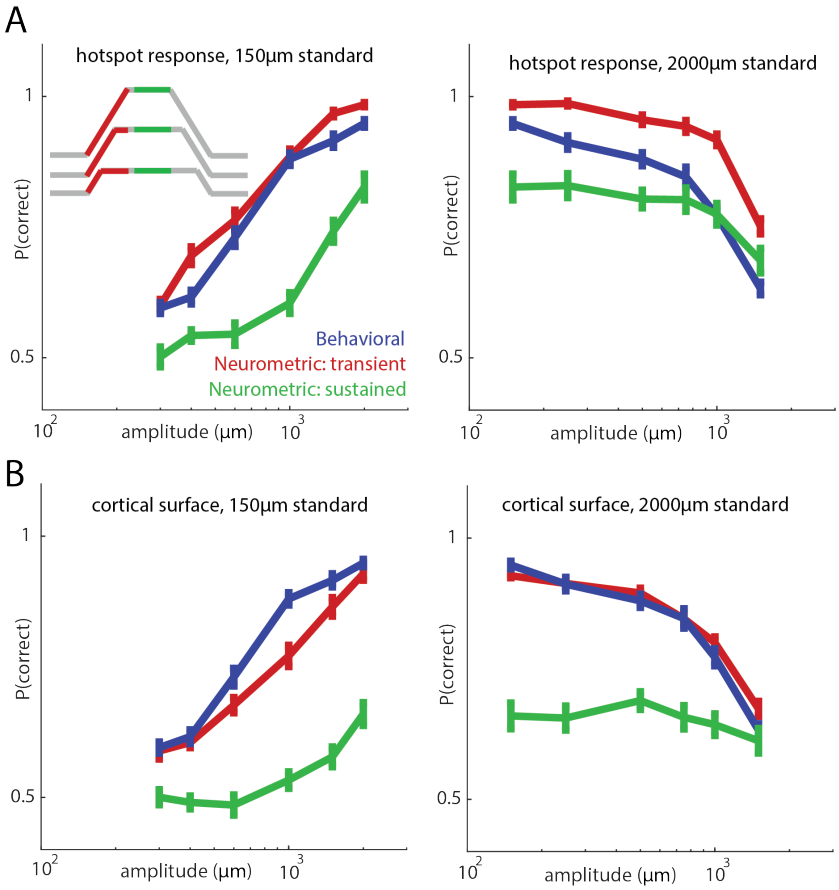

Figure C.7: Relating neuronal responses to behavioral performance. (A) Performance of the animals (blue) and that of an ideal observer based on the onset transient response (red, 300 ms window for all stimuli) and the sustained response (green, 300 ms window for all stimuli) at the hotzone electrode for a 150-μm standard stimulus (left, 5645 trials from 17 skin locations from monkey A and monkey B's first array) and 2000-μm standard stimulus (right, 6546 trials from 17 skin locations over the same 2 arrays). Inset shows the stimulus trace with color-coded stimulus epochs for 3 example stimuli (not drawn to scale). All stimuli in the behavioral task were delivered at 10 mm/s. Error bars denote the standard error of the mean (n = 17 skin locations). Behavioral performance approximately matches the neurometric performance based on the onset responses but is underestimated from the sustained response. If only the transient response is used, performance is even better (Fig. D.11). (B) Analogous ideal observer analysis based on activated cortical surface (number of channels with neuronal response above 0.5 s.d.).

the transient-to-sustained-response ratio for aggregate peripheral responses to a probe with a diameter of 2mm indented 2mm into the skin at 10mm/s, and found that transient responses were on average nearly 12 times (range 5.12–45.37, median 9.2, see Table D.6) stronger at stimulus onset and more than 5 times stronger at stimulus offset than sustained responses, similar to their cortical counterparts (means of around 15 and 8 for onset and offset, respectively, see above). As was found in the cortical responses, these ratios tended to be larger for the palm than for the distal digits, reflecting differences in the relative proportions of slowly adapting and rapidly adapting nerve fibers terminating in the different hand regions.

We then examined how the spatial pattern of activation evoked in nerve fibers by a skin indentation evolved over time. To this end, we computed the area of a polygon that contains all (simulated) SA1 and RA afferents activated by the stimulus as a function of time. We excluded PC fibers in this computation because their RFs are so large as to span most of the hand, and a given PC fiber is activated by touch almost anywhere on the hand. As was found in cortex, afferent activation during stimulus transients was distributed across wide swaths of skin around the probe, while activation during the static phase was localized to a small patch of skin under the probe (Fig. C.8B,C).

Next, we examined the dependence of the nerve response on the features of the contact event. We found that the strength and spatial extent of simulated afferent responses during the transient phase of the stimulus were only weakly modulated by indentation depth, whereas the afferent responses during the transient phase were strongly modulated by indentation rate (Figs D.8 and D.9), as was found in cortex.

To quantify the similarity between peripheral and cortical responses, we computed the cross-correlation between peripheral and cortical PSTHs to the same stimuli and found these to be high (mean $\pm$ s.d.: 0.92 ± 0.03) (Fig. D.10). In conclusion, then, the spatiotemporal dynamics of cortical responses to simulated contact events are highly similar to their peripheral counterparts.

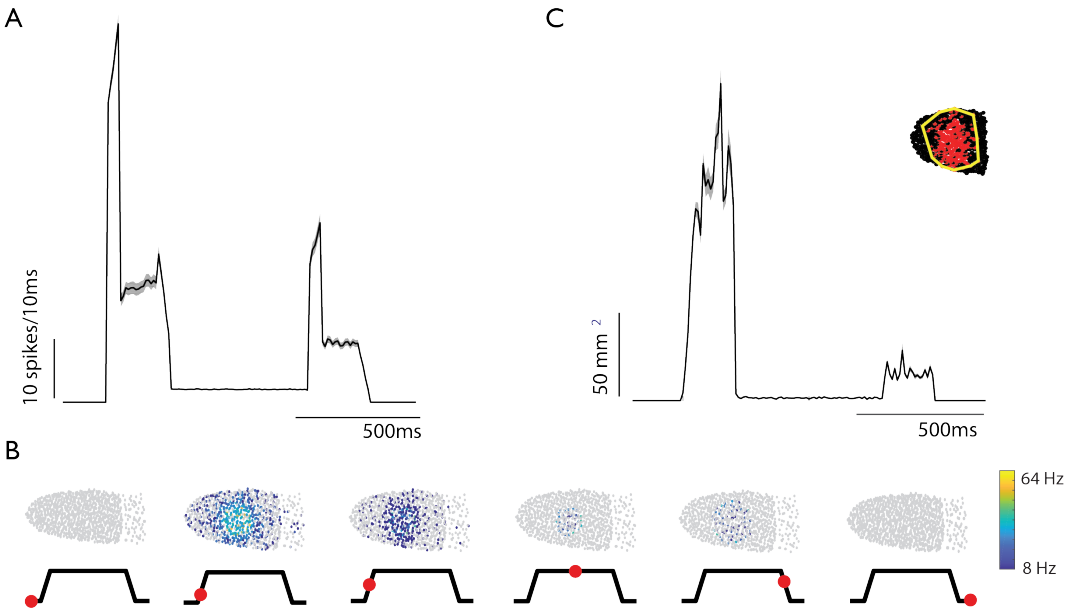

Figure C.8: Spatiotemporal dynamics of peripheral responses to skin indentations. (A) Simulated aggregate afferent responses (SA1, RA, and PC fibers) to a 2-mm, 10-mm/s indentation delivered to various locations on the hand, matched to those used in the cortical experiments (see Fig. D.2). Spike count represents summed spikes over the afferent population, in 10-ms bins, averaged across locations (Fig. D.2: mean = 2498 fibers, stdev = 1369 fibers). Shaded area represents standard error of the mean over all locations (n = 16). (B) Spatial pattern of the (stimulated) afferent activation during each epoch (indicated on the trace below). Each dot represents a the receptive field of a tactile nerve fiber (SA1 and RA fibers only) on the distal index finger pad and the color of the dot denotes the fiber's firing rate during the corresponding epoch. (C) Dynamics of the spatial extent of simulated afferent activation for 20-ms bins. Area was set to 0 for time points where less than 3 afferents were recruited, inset shows an example diagram of the polygon-based area computation.

C.5 Discussion

In summary, then, we found that population responses during the initiation and termination of contact dwarf responses during static contact both in the nerve and in cortex, so these responses signal primarily contact transients—changes in skin deformation— rather than tracking indentation depth. Furthermore, contact events are encoded in both the time-varying response of activated neurons as well as the time-varying size of the activated population. While responses to contact transients are strong and diffuse, responses to sustained contact are weak and highly localized. Information about the features of contact—its timing, location, and strength—are rapidly and faithfully conveyed by these phasic responses and can account for the ability of animals to discriminate indentations of varying strength. The spatiotemporal profile of the population response to contact in cortex mirrors its counterpart in the nerve.

C.5.1 Encoding of Contact Location

As indentation rate or depth increases, the volume of activated neurons in somatosensory cortex increases, a phenomenon that has also been observed for increases in vibratory amplitude using optical intrinsic signal imaging (Simons et al. 2005). The recruitment of neurons during contact transients may seem to render localization more difficult if stimulus location is encoded in the spatial location of neuronal activity within the somatosensory homunculus. For example, 2 spatially restricted and minimally overlapping activation patterns would in principle be more distinguishable from one another than more diffuse, highly overlapping ones. Consistent with this, reducing the activated area through vibrotactile adaptation results in better localization performance (Tanan et al. 2006). However, we show that the centroid of neural activity remains consistent as the spatial extent of activation increases, so the hotzone remains consistent and dependent on contact location regardless of the other stimulation parameters (indentation depth and indentation rate). The stability of the hot-

zone provides a neural basis for the documented robustness of localization performance across changes in applied pressure (Gibson and Craig 2006) despite the concomitant changes in activated area. Thus, while increased activated area is intrinsically deleterious to localization, this effect is mitigated by the consistency of the hotzone location.

C.5.2 Encoding of Indentation Rate

Increases in the rate at which the skin is indented results both in a systematic increase in firing rate of cortical neurons at the hotzone and in the recruitment of nearby neurons. The effect of indentation rate on the hotzone firing rate can be attributed primarily to RA and PC fibers whose responses are restricted to dynamic stimulus phases and increase as indentation rate increases, but SA1 afferents also respond more strongly to faster indentations (Knibestöl 1975; Pubols and Pubols 1976). That increases in indentation rate also result in an increase in the number of activated nerve fibers has been previously documented (Johnson 1974; Cohen and Vierck 1993; Muniak et al. 2008) and can be attributed to the increased sensitivity of rapidly adapting fibers at higher speeds (Knibestöl 1973). That indentation rate is a major determinant of cortical responses is consistent with results from psychophysical experiments with human observers showing that indentation rate drives to a large extent the perceived intensity of an indentation (Poulos et al. 1984).

C.5.3 Similarity of Peripheral and Cortical Response Dynamics

The aggregate response of cortical neurons to contact events is very similar to that of their peripheral inputs. First, the coarse temporal profiles of the spiking response is nearly identical to its cortical counterpart, featuring a prominent phasic response during contact transients and a weak tonic response during maintained contact. As alluded to above, a major source of the strong transient response in the nerve is the population of rapidly adapting afferents, including RA and PC fibers, which respond exclusively during the transients, and the stronger

response of SA1 fibers during the indentation phase. Second, the dynamics of recruitment observed in cortex also seem to mirror those at the periphery. Indeed, phasic recruitment of nerve fibers originating from afferents close to but not under the probe is observed during the transient periods and only a small population of SA1 fibers with RFs just under the probe is activated during sustained contact. Not only are the relative strengths of the transient and sustained responses similar in periphery and cortex, but their dependence on the locus of stimulation is also consistent (with weaker sustained responses from the palm). Finally, the dependence of the spatiotemporal dynamics of nerve responses on stimulus parameters—including indentation depth and indentation rate—largely mirrors its cortical counterpart (Fig. D10).

That the aggregate response in cortex resembles that in the nerve does not imply that no information processing occurs between nerve and cortex. Indeed, individual cortical neurons have complex RFs with excitatory and inhibitory subfields (DiCarlo et al. 1998), often exhibit feature selectively (to edge orientation (Bensmaia et al. 2008) or direction of motion (Pei et al. 2010)), and integrate their inputs nonlinearly (Chung et al. 2002; Katz et al. 2006; Thakur et al. 2006; Reed et al. 2010, 2011; Brouwer et al. 2015; Saal et al. 2015) to name a few properties that are largely absent in tactile nerve fibers. Interestingly, however, this processing is largely obscured when pooling responses to contact events across populations of neurons.

C.5.4 Active Versus Passive Touch

One might argue that the neuronal activity when stimuli are passively presented to the skin may not be representative of that evoked during active manipulation of objects. However, several lines of evidence suggest otherwise.

First, while the temporal profile of the indentations, following a trapezoidal trajectory, is highly contrived and may not match that of natural contact event, afferent responses to

a natural indentation profile, corresponding to grasping and releasing a coffee cup, exhibit very similar spatiotemporal dynamics (Fig. D.7B).

Second, tactile discrimination and pattern recognition are similar for active and passive touch (Lamotte and Whitehouse 1986; Vega-Bermudez et al. 1991), suggesting that the processing of cutaneous information is similar under these 2 conditions.

Third, studies explicitly comparing responses of somatosensory neurons to active and passive touch have found weak or no differences in firing rates, and any observed differences could be attributed to differences in the contact events themselves or in the attentional state of the animal (Chapman and Ageranioti-Belanger 1991; Jiang et al. 1991; Ageranioti-Bélanger and Chapman 1992; Williams and Chapman 2002). Regarding the former confound, comparing the neuronal responses to active and passive touch is challenging because it is impossible to exactly match how the skin is deformed in the 2 conditions and the sense of touch is exquisitely sensitive to any differences in skin deformation (down to the level of single-digit microns). Indeed, as discussed above, even under passive conditions, skin deflections produced by an identical stimulus are highly variable given the slights movements of the (restrained) hand, a challenge we circumvent by imposing a preindentation.

Fourth, while single-unit cortical responses evoked during grasping (Wannier et al. 1986, 1991; Gardner et al. 1999; Salimi et al. 1999; Ro et al. 2000; Debowy et al. 2001) are difficult to compare to aggregate cortical responses presented here, somatosensory neurons with RFs on the glabrous skin have been found to exhibit properties qualitatively consistent with those described here, often characterized by strong phasic responses at initiation and termination of contact and weak responses during maintenance of contact. Another component of active touch that may influence tactile responses in somatosensory cortex is movementgating, a phenomenon that has been documented for the balance sense, vision, and touch (Cullen et al. 2004). However, while cortical responses to touch on the proximal limb are suppressed during movement, the response dynamics seem to be preserved (Jiang et al. 1990, 1991). Moreover,

the function of movement gating of touch on the proximal limb may be to reduce tactile signals produced by skin stretch during movement (Rincon-Gonzalez et al. 2011), which, in some cases, may be behaviorally irrelevant and distracting. In this view, it is unlikely that tactile responses on the glabrous skin would be suppressed during object manipulation as these signals are the ones critical to behavior.

In light of these considerations and previous findings, we expect that the cutaneous responses to object contact in somatosensory cortex are unlikely to be fundamentally altered under conditions of active touch and that passive stimulation reveals the main characteristics of the representation of contact events at this stage of processing along the somatosensory neuraxis.

C.5.5 Functional Significance of the Phasic Response to Contact Transients

Object manipulation can be broken down into a sequence of action phases delimited by mechanical events associated with subgoals of the task. In reach and grasp, for example, contact with an object marks the end of the reach phase and signals the beginning of the grasp phase (Johansson and Flanagan 2009). Consistent with this view, disruption of somatosensory cortex with a pulse of transcranial magnetic stimulation (TMS) just before contact results in delayed initiation of the grasp (Lemon et al. 1995). Moreover, contact timing between object and fingers drives the online adaptation of grasp aperture during active grasping movements (Säfström and Edin 2008). The prominence of contact transients in cortex is consistent with a role for tactile feedback in signaling transitions between task goals rather than providing continuous feedback about object interactions (Johansson and Edin 1993; Johansson and Flanagan 2009). We would therefore expect that these phasic transients are key components of sensorimotor integration during object manipulation.

This is not to say that sustained responses are not useful and informative. Indeed, stimulus features—local object shape, for example,—may be most prominently encoded in

cortical responses during sustained contact (Bensmaia et al. 2008; Yau et al. 2013). However, this slower signal may be less important for onlinemotor control and play a greater role in haptic perception (Yau et al. 2016).

C.5.6 Implications for Neuroprosthetics

Characterization of the spatiotemporal dynamics of the response to contact events not only sheds light on the neural coding of tactile information and the role of touch in guiding object interactions but also has implications for the design of sensory feedback algorithms for use in upper limb neuroprostheses. Indeed, a basic design principle of such algorithms is to evoke patterns of neuronal activation through electrical stimulation that mimic natural patterns as much as possible (Bensmaia 2015; Delhaye et al. 2016). To the extent that electrically induced neuronal activation matches its natural counterpart, the resulting percepts will be naturalistic and intuitive, so little to no training will be required to learn to interpret them.

The standard sensory encoding algorithm converts the output of pressure (or force) sensors on the bionic hand into trains of electrical stimulation whose frequency or amplitude is modulated according to the sensory output. Within this framework, the rate of change of pressure does not influence the stimulation regime. Our results suggest that, to mimic natural responses to contact events, both in the periphery and in cortex, it is preferable to track changes in pressure while only weakly weighting the instantaneous pressure in the determination of stimulation parameters. Furthermore, the encoding algorithm should not only yield an increase in firing rate at the hotzone electrode—perhaps achieved through an increase in stimulation frequency—but also in the recruitment of nearby neurons—achievable by modulating the amplitude of stimulation or by stimulating through a variable number of adjacent electrodes. The resulting electrically induced patterns of neuronal activation will have the merit of signaling contact timing with much greater precision than do the slowly evolving pressure-tracking algorithms (for the same reasons that the natural phasic

responses are more temporally precise). Furthermore, the spatiotemporal dynamics of the response are liable to be more effectively integrated into motor planning and execution in that they reproduce key features of a natural cortical response to contact. We anticipate that such biomimetic stimulation patterns will lead to improved dexterity for bionic hands.

Another important implication of the present results for neuroprosthetics is that, given the remarkable similarities in the spatiotemporal dynamics of the aggregate response in periphery and cortex, sensory encoding algorithms developed for cortical interfaces may be very similar to those developed for the peripheral nerve interfaces (Okorokova et al. 2018).

C.6 References

Ageranioti-Bélanger SA, Chapman CE. 1992. Discharge properties of neurones in the hand area of primary somatosensory cortex in monkeys in relation to the performance of an active tactile discrimination task. II. Area 2 as compared to areas 3b and 1. Exp Brain Res. 91:207–228.

Augurelle A-S, Smith AM, Lejeune T, Thonnard J-L. 2003. Importance of cutaneous feedback in maintaining a secure grip during manipulation of hand-held objects. J Neurophysiol. 89:665–671.

Bensmaia SJ. 2015. Biological and bionic hands: natural neural coding and artificial perception. Philos Trans R Soc B Biol Sci. 370:20140209.

Bensmaia SJ, Denchev PV, Dammann JF III, Craig JC, Hsiao SS. 2008. The representation of stimulus orientation in the early stages of somatosensory processing. J Neurosci. 28: 776–786.

Britten KH, Shadlen MN, Newsome WT, Movshon JA. 1992. The analysis of visual motion: a comparison of neuronal and psychophysical performance. J Neurosci. 12:4745–4765.

Brochier T, Boudreau MJ, Paré M, Smith AM. 1999. The effects of muscimol inactivation of small regions of motor and somatosensory cortex on independent finger movements and

force control in the precision grip. Exp Brain Res. 128:31–40.

Brouwer GJ, Arnedo V, Offen S, Heeger DJ, Grant AC. 2015. Normalization in human somatosensory cortex. J Neurophysiol. 114:2588–2599.

Callier T, Schluter EW, Tabot GA, Miller LE, Tenore FV, Bensmaia SJ. 2015. Long-term stability of sensitivity to intracortical microstimulation of somatosensory cortex. J Neural Eng. 12:056010.

Carlson M. 1981. Characteristics of sensory deficits following lesions of Brodmann's areas 1 and 2 in the postcentral gyrus of Mococo mulatto. Brain Res. 204:424–430.

Chapman CE, Ageranioti-Belanger A. 1991. Experimental brain research discharge properties of neurones in the hand area of primary somatosensory cortex in monkeys in relation to the performance of an active tactile discrimination task I. Areas 3b and 1. Exp Brain Res. 87:31–339.

Chung S, Li X, Nelson SB. 2002. Short-term depression at thalamocortical synapses contributes to rapid adaptation of cortical sensory responses in vivo. Neuron. 34:437–446.

Cohen R, Vierck C. 1993. Population estimates for responses of cutaneous mechanoreceptors to a vertically indenting probe on the glabrous skin of monkeys. Exp Brain Res. 94:105–119.

Cullen KE, Anderson ME, Kiehn O. 2004. Sensory signals during active versus passivemovement. Curr Opin Neurobiol. 14:698–706.

Debowy DJ, Ghosh S, Gardner EP, Ro JY. 2001. Comparison of neuronal firing rates in somatosensory and posterior parietal cortex during prehension. Exp Brain Res. 137:269–291.

Delhaye BP, Saal HP, Bensmaia SJ. 2016. Key considerations in designing a somatosensory neuroprosthesis. J Physiol. 110: 402–408.

DiCarlo JJ, Johnson KO, Hsiao SS. 1998. Structure of receptive fields in area 3b of primary somatosensory cortex in the alert monkey. J Neurosci. 18:2626–2645.

Dong Y, Mihalas S, Kim SS, Yoshioka T, Bensmaia S, Niebur E. 2013. A simple model of mechanotransduction in primate glabrous skin. J Neurophysiol. 109:1350–1359.

Duque J, Thonnard J, Vandermeeren Y, Sébire G, Cosnard G, Olivier E. 2003. Correlation between impaired dexterity and corticospinal tract dysgenesis in congenital hemiplegia. Brain. 126:732–747.

Flesher SN, Collinger JL, Foldes ST, Weiss JM, Downey JE, Tyler- Kabara EC, Bensmaia SJ, Schwartz AB, Boninger ML, Gaunt RA. 2016. Intracortical microstimulation of human somatosensory cortex. Sci Transl Med. 8:361ra141.

Gardner EP, Ro JY, Debowy D, Ghosh S. 1999. Facilitation of neuronal activity in somatosensory and posterior parietal cortex during prehension. Exp Brain Res. 127:329–354.

Gibson GO, Craig JC. 2006. The effect of force and conformance on tactile intensive and spatial sensitivity. Exp Brain Res. 170:172–181.

Goodman JM, Bensmaia SJ. 2017. A variation code accounts for the perceived roughness of coarsely textured surfaces. Sci Rep. 7:46699.

Hikosaka O, Tanaka M, Sakamoto M, Iwamura Y. 1985. Deficits in manipulative behaviors induced by local injections of muscimol in the first somatosensory cortex of the conscious monkey. Brain Res. 325:375–380.

Hyvarinen J, Poranen A, Jokinen Y. 1980. Influence of attentive behavior on neurond responses to vibration in primary somatosensory cortex of the monkey. 43.

Iwamura Y, Tanaka M, Sakamoto M, Hikosaka O. 1983. Converging patterns of finger representation and complex response properties of neurons in area 1 of the first somatosensory cortex of the conscious monkey. Exp Brain Res. 51: 327–337.

Jiang W, Chapman CE, Lamarre Y. 1990. Modulation of somatosensory evoked responses in the primary somatosensory cortex produced by intracortical microstimulation of the motor cortex in the monkey. Exp Brain Res. 80:333–344.

Jiang W, Chapman CE, Lamarre Y. 1991. Modulation of the cutaneous responsiveness of neurones in the primary somatosensory cortex during conditioned arm movements in the monkey. Exp Brain Res. 84:342–354.

Johansson RS, Edin BB. 1993. Predictive feed-forward sensory control during grasping and manipulation in man. Biomed Res. 14:95–106.

Johansson RS, Flanagan JR. 2009. Coding and use of tactile signals from the fingertips in object manipulation tasks. Nat Rev Neurosci. 10:345–359.

Johansson RS, Vallbo AB. 1979. Tactile sensibility in the human hand: relative and absolute densities of four types of mechanoreceptive units in glabrous skin. J Physiol. 286: 283–300.

Johnson KO. 1974. Reconstruction of population response to a vibratory stimulus in quickly adapting mechanoreceptive afferent fiber population innervating glabrous skin of the monkey. J Neurophysiol. 37:48–72.

Johnson KO, Phillips JR. 1981. Tactile spatial resolution. I. Twopoint discrimination, gap detection, grating resolution, and letter recognition. J Neurophysiol. 46:1177–1192.

Kaas JH. 1983. What, if anything, is SI? Organization of first somatosensory area of cortex. Physiol Rev. 63:206–231.

Katz Y, Heiss JE, Lampl I. 2006. Cross-whisker adaptation of neurons in the rat barrel cortex. J Neurosci. 26:13363–13372.

Kim SS, Mihalas S, Russell A, Dong Y, Bensmaia SJ. 2011. Does afferent heterogeneity matter in conveying tactile feedback through peripheral nerve stimulation? IEEE Trans Neural Syst Rehabil Eng. 19:514–520.

Knibestöl M. 1973. Stimulus-response functions of rapidly adapting mechanoreceptors in the human glabrous skin area. J Physiol. 232:427–452.

Knibestöl M. 1975. Stimulus-response functions of slowly adapting mechanoreceptors in the human glabrous skin area. J Physiol. 245:63–80.

Lamotte RH, Whitehouse J. 1986. Tactile detection of a dot on a smooth surface: peripheral neural events. J Neurophysiol. 56:1109–1128. Printed in USA.

Lemon RN, Johansson RS, Westling G. 1995. Corticospinal control during reach, grasp, and precision lift in man. J Neurosci. 15:6145–6156.

Mathis MW, Mathis A, Uchida N. 2017. Somatosensory cortex plays an essential role in forelimb motor adaptation in mice. Neuron. 93:1493–1503.e6.

Muniak MA, Ray S, Hsiao SS, Dammann JF, Bensmaia SJ. 2008. The neural coding of stimulus of mechanoreceptive afferents with psychophysical behavior. J Neurosci. 27: 11687–11699.

Meftah E-M, Shenasa J, Chapman CE. 2002. Effects of a crossmodal manipulation of attention on somatosensory cortical neuronal responses to tactile stimuli in the monkey. J Neurophysiol. 88:3133–3149.

Okorokova L, He Q, Bensmaia SJ. 2018. Biomimetic encoding model for restoring touch in bionic hands through a nerve interface. J Neural Eng. 15:066033.

Ostry DJ, Darainy M, Mattar AAG, Wong J, Gribble PL. 2010. Somatosensory plasticity and motor learning. J Neurosci. 30: 5384–5393.

Pei Y-C, Hsiao SS, Craig JC, Bensmaia SJ. 2010. Shape invariant coding of motion direction in somatosensory cortex. PLoS Biol. 8:e1000305.

Penfield W, Brain E. 1937. Somatic motor and sensory representation in the cerebral cortex of man as studied by electrical stimulation. Brain. 60:389–443.

Pons TP, Garraghty PE, Cusick CG, Kaas JH. 1985. A sequential representation of the occiput, arm, forearm and hand across the rostrocaudal dimension of areas 1, 2 and 5 in macaque monkeys. Brain Res. 335:350–353.

Poulos DA, Mei J, Horch KW, Tuckett RP, Wei JY, Cornwall MC, Burgess PR, Evans B, Fisher J, Frederickson G, et al. 1984. The neural signal for the intensity of a tactile stimulus. J Neurosci. 4:2016–2024.

Pubols BH, Pubols LM. 1976. Coding of mechanical stimulus velocity and indentation depth by squirrel monkey and raccoon glabrous skin mechanoreceptors. J Neurophysiol. 39:773–787.

Rajan AT, Boback JL, Dammann JF, Tenore FV, Wester BA, Otto KJ, Gaunt RA, Bens-

maia SJ. 2015. The effects of chronic intracortical microstimulation on neural tissue and fine motor behavior. J Neural Eng. 12:066018.

Reed JL, Pouget P, Qi H-X, Zhou Z, Bernard MR, Burish MJ, Haitas J, Bonds AB, Kaas JH. 2008. Widespread spatial integration in primary somatosensory cortex. Proc Natl Acad Sci USA. 105:10233–10237.

Reed JL, Qi H-X, Kaas JH. 2011. Spatiotemporal properties of neuron response suppression in owl monkey primary somatosensory cortex when stimuli are presented to both hands. J Neurosci. 31:3589–3601.

Reed JL, Qi H-X, Zhou Z, Bernard MR, Burish MJ, Bonds AB, Kaas JH. 2010. Response properties of neurons in primary somatosensory cortex of owl monkeys reflect widespread spatiotemporal integration. J Neurophysiol. 103:2139–2157.

Rincon-Gonzalez L, Warren JP, Meller DM, Helms Tillery S. 2011. Haptic interaction of touch and proprioception: implications for neuroprosthetics. IEEE Trans Neural Syst Rehabil Eng. 19:490–500.

Ro JY, Debowy D, Ghosh S, Gardner EP. 2000. Depression of neuronal firing rates in somatosensory and posterior parietal cortex during object acquisition in a prehension task. Exp Brain Res. 135:1–11.

Saal HP, Delhaye BP, Rayhaun BC, Bensmaia SJ. 2017. Simulating tactile signals from the whole hand with millisecond precision. Proc Natl Acad Sci USA. 114:E5693–E5702.

Saal HP, Harvey MA, Bensmaia SJ. 2015. Rate and timing of cortical responses driven by separate sensory channels. Elife. 4:e10450.

Salimi I, Brochier T, Smith AM. 1999. Neuronal activity in somatosensory cortex of monkeys using a precision grip. I. Receptive fields and discharge patterns. J Neurophysiol. 81:825–834.

Schabrun SM, Ridding MC, Miles TS. 2008. Role of the primary motor and sensory cortex in precision grasping: a transcranial magnetic stimulation study. Eur J Neurosci. 27:750–756.

Simons SB, Tannan V, Chiu J, Favorov OV, Whitsel BL, Tommerdahl M. 2005. Amplitude-dependency of response of SI cortex to flutter stimulation. BMC Neurosci. 6:43.

Sripati AP, Yoshioka T, Denchev P, Hsiao SS, Johnson KO. 2006. Spatiotemporal receptive fields of peripheral afferents and cortical area 3b and 1 neurons in the primate somatosensory system. J Neurosci. 26:2101–2114.

Sur M, Wall JT, Kaas JH. 1981. Modular segregation of functional cell classes within the postcentral somatosensory cortex of monkeys. Science. 212:1059–1061.

Säfström D, Edin BB. 2008. Prediction of object contact during grasping. Exp Brain Res. 190:265–277.

Tabot GA, Dammann JF, Berg JA, Tenore FV, Boback JL, Vogelstein RJ, Bensmaia SJ. 2013. Restoring the sense of touch with a prosthetic hand through a brain interface. Proc Natl Acad Sci USA. 110:18279–18284.

Tanan V, Whitsel BL, tommerdahl M. 2006. Vibrotactile adaptation enhances spatial localization. Brain Res. 1102:109–116.

Thakur PH, Fitzgerald PJ, Lane JW, Hsiao SS. 2006. Receptive field properties of the macaque second somatosensory cortex: nonlinear mechanisms underlying the representation of orientation within a finger pad. J Neurosci. 26:13567–13575.

Vega-Bermudez F, Johnson KO. 1999. Surround suppression in the responses of primate SA1 and RA mechanoreceptive afferents mapped with a probe array. J Neurophysiol. 81:2711–2719.

Vega-Bermudez F, Johnson KO, Hsiao SS. 1991. Human tactile pattern recognition: active versus passive touch, velocity effects, and patterns of confusion. J Neurophysiol. 65: 531–546.

Wannier TM, Maier MA, Hepp-Reymond MC. 1991. Contrasting properties of monkey somatosensory and motor cortex neurons activated during the control of force in precision grip. J Neurophysiol. 65:572–589.

Wannier TMJ, Töltl M, Hepp-Reymond M-C. 1986. Neuronal activity in the postcentral cortex related to force regulation during a precision grip task. Brain Res. 382:427–432.

Williams SR, Chapman CE. 2002. Time course and magnitude of movement-related gating of tactile detection in humans. III. Effect of motor tasks. J Neurophysiol. 88:1968–1979.

Witney AG, Wing A, Thonnard J-L, Smith AM. 2004. The cutaneous contribution to adaptive precision grip. Trends Neurosci. 27:637–643.

Xerri C, Merzenich MM, Peterson BE, Jenkins W. 1998. Plasticity of primary somatosensory cortex paralleling sensorimotor skill recovery from stroke in adult monkeys. J Neurophysiol. 79:2119–2148.

Yau JM, Connor CE, Hsiao SS. 2013. Representation of tactile curvature in macaque somatosensory area 2. J Neurophysiol. 109:2999–3012.

Yau JM, Kim SS, Thakur PH, Bensmaia SJ. 2016. Feeling form: the neural basis of haptic shape perception. J Neurophysiol. 115:631–642.

Appendix D | Supplementary material: neural Coding of Contact Events in Somatosensory Cortex

D.1 Supplementary Methods

D.1.1 Pre-indentation vs actual contact

In preliminary experiments, we discovered that establishing contact with the skin results in unreliable contact timing and indentation trajectories due to movements of the hand relative to the stimulator, as discussed briefly in the main Methods section. In light of these observations, we opted to deliver indentations beyond a pre-indentation. This experimental decision is premised on the finding that afferent responses are independent of the pre-indentation (Vega-Bermudez and Johnson 1999). Having collected data with and without pre-indentation, we wished to assess the degree to which neuronal responses to indentations with a pre-indentation were similar to those without.

When time-locked to stimulus onset, the average responses had similar dynamics but appeared slightly depressed and with lower peaks for the actual contact events (Figure D.1A and B). In the actual contact case, however, the probe did not indent the skin immediately upon stimulus onset but rather did so at a delay, determined by the indentation rate of the probe and the initial distance between the probe and skin (unknown given small fluctuations in the position of the hand along the vertical axis). Under conditions of actual contact, then, the duration of the onset transient, when the probe is actively moving into the skin, and the final indentation depth both changed with changes in the initial distance between probe and skin. Accordingly, the response averaged over many trials appeared to be lower and more distributed over time without than with pre-indentation. We confirmed the increased

1. This appendix was published : Callier, T., Suresh, A. K., and Bensmaia, S. J. (2019). Neural Coding of Contact Events in Somatosensory Cortex. Cerebral Cortex, 29(11), 4613–4627. https://doi.org/10.1093/cercor/bhy337

variation in the timing of the response by tracking the time on each trial when the aggregate response passed a threshold of 10 standard deviations above baseline (see Signaling of Contact Timing in the methods for a detailed description). The times at which contact was detected were grouped more tightly around the mean with pre-indentation than without (Figure D.1C). When single trial responses were aligned to response onset rather than stimulus onset, the difference in mean responses between contact and pre-indentation became negligible (Figure D.1D). Note that the indentation rate is equivalent with and without pre-indentation, regardless of the distance between probe and skin. Given the strong dependence of the neuronal response on indentation rate (and its relative insensitivity to indentation depth), we would expect responses aligned at response onset to be approximately equivalent in the two conditions.

D.1.2 Heterogeneity of cortical responses

The spatiotemporal dynamics of the response varied across electrodes and stimulated skin locations (figure 3 A and B). To document this heterogeneity, we computed response metrics for the 4 most responsive electrodes from each stimulation site (112 electrodes from 28 sites across the 4 arrays). First, we tested whether the response during each epoch of a 2-mm, 10 mm/s indentation (onset transient: 20-220 ms, sustained: 500-700 ms, offset transient: 820-1020 ms) was significantly different from baseline (table 2, two-sample t-test, p ¡ 0.01) and assessed whether this metric differed across stimulation sites on the hand (figure 2). Second, we compared the responses across different stimulus epochs (figure 3C, figure 4A and B; Tables 1 and 3). Third, we characterized the dynamics of recruitment by counting the number of electrodes with average responses greater than 0.5 s.d. above baseline during each epoch (table 5). We selected a low threshold to achieve a more graded measure of the spread, but the results are not sensitive to the threshold (except that high thresholds yield more denominators of zero in the computation of transient/sustained response ratios).

Finally, we developed an adaptation Index to quantify the relative contributions of slowly adapting and rapidly adapting signals to the multi-unit responses at each electrode (table 4), as has been previously done (Pei, Denchev, Hsiao, Craig, & Bensmaia, 2009). For this calculation, we normalized the sustained and offset responses to their respective grand means across electrodes. The adaptation index was then computed by dividing the normalized offset response by the sum of the normalized sustained and normalized offset responses for each electrode separately. An index of 0 denoted a pure SA1-like response, an index of 1 a pure RA-like response.

D.1.3 Single-electrode recordings from cortex

To investigate the effect of amplitude on the responses of individual neurons, we analyzed data collected in a separate experiment in which we recorded the responses of single units to probes indented into the skin. Results from this analysis are shown in Figure D.5.

Stimuli: In brief, stimuli were delivered using a dense array tactile stimulator consisting of 400 probes arrayed in a 20 by 20 grid spanning 1 cm x 1 cm (Killebrew et al. 2007). Each probe was driven along the axis perpendicular to the skin's surface by a dedicated motor. The stimulator is the tactile equivalent of a video monitor, conferring to the experimenter the ability to activate each pin independently to create arbitrary spatiotemporal patterns over an area of 1 cm2. Each probe had a diameter of 0.3 mm, and the spacing between the center of each pin was 0.5 mm.. Stimuli consisted of a single pin indented onto the neuron's hotspot for 250 ms at amplitudes ranging from 250 to 700µm, 30 times each, in pseudorandom order, with a consistent ramp duration of 20ms.

Neurophysiology: All experimental protocols complied with the guidelines of The Johns Hopkins University Animal Care and Use Committee and the National Institutes of Health's Guide for the Care and Use of Laboratory Animals. Extracellular recordings were made in the postcentral gyri of three hemispheres of two macaque monkeys using standard methods

as previously described in detail (Bensmaia et al. 2008; Pei et al. 2010, 2011). Briefly, animals were trained to sit in a primate chair with their hands and arms restrained while tactile stimuli were applied to the distal pads of digits 2-5. Recordings were performed in the awake state, with quartz-coated platinum/tungsten (90/10) electrodes. For this control experiment, recordings were obtained from 6 neurons in area 3b (6 units) and 10 neurons in area 1.

D.1.4 Single unit recording from the nerve

To validate results from the nerve simulation (described in the main Methods), we analyzed data collected in a separate experiment in which we recorded the responses of individual afferents to half-spheres indented into the skin. Our neurophysiological data consists of a small sample of afferent fibers, while the simulation accounts for all afferents innervating the hand. Results from this analysis are shown in Figure D.7A.

Stimuli: Stimuli were delivered using the dense array tactile stimulator described above. Stimuli consisted of half spheres with a 2 mm diameter and an amplitude of 0.3 mm at their apex, and a rate of 10 mm/s. The stimulus was presented for 100 ms, centered on the afferent's hotspot. Stimuli were presented 8 times.

Neurophysiology: All experimental protocols complied with the guidelines of The Johns Hopkins University Animal Care and Use Committee and the National Institutes of Health's Guide for the Care and Use of Laboratory Animals. We recorded single units from the median and ulnar nerves of four anaesthetized macaque monkeys using standard methods (Mountcastle et al. 1967; Talbot et al. 1968) as previously described in detail (Bensmaia et al. 2008). In brief, the forearm and hand were fixed by a clamp, and the ulnar or median nerve was exposed in the upper or lower arm. Next, a skin flap pool was formed, and a small bundle of axons was separated from the nerve trunk and wrapped around a silver electrode. Each animal contributed up to eight recording sessions – upper and lower sites on median

and ulnar nerve – separated by two or more weeks.

A nerve fiber was classified as slowly adapting type 1 (SA1) if it had a small receptive field (RF) and produced a sustained response to a skin indentation, as rapidly adapting (RA) if it had a small RF and responded only at the onset and offset of the indentation, and as Pacinian (PC) if it had a large, diffuse RF and was activated by air blown gently over the hand. The point of maximum sensitivity (hotspot) was located using a handheld probe and the stimulus was centered on the hotspot. In these experiments, data were only collected from SA1 and RA fibers.

D.1.5 Simulating the response of the nerve during a manual interaction with an object

To verify that the simulated and measured neural responses to the trapezoidal indentation were representative of those evoked during an object interaction, we simulated the responses to the pressure profile measured during the grasp, hold, and release of an object. Specifically, we used a sensorized glove (FingerTPS, PPS, Inc., Los Angeles, CA) with six pressure sensors – one on each fingertip and one on the palm – to measure pressure exerted when a coffee cup is grasped, lifted, then put down (for a detailed description, see (Kim, Mihalas, Russell, Dong, & Bensmaia, 2011)). Given that indentation depth is approximately linear with contact pressure over a range, we converted the output of the index finger sensor into indentation depths by scaling the pressure trace to a maximum of 3 mm. The pressure trace exhibited a similar profile to the simple ramp indentations tested, but the trace extended over a much longer duration (50 seconds). Finally, we rescaled the indentation output from 64 to 512 Hz, and input this trace into TouchSim to simulate the aggregate afferent response (Figure D.7B).

D.2 Supplementary Tables

		Onset/sustained	Offset/sustained
All (28)	**Mean**	15.28	8.22
	Range	2.16-42.44	0.76-35.01
	Median	12.01	5.96
Digit distal pads (9)	**Mean**	10.41	7.0
	Range	2.16-17.91	0.76-19.05
	Median	10.47	5.76
Other digit locations (9)	**Mean**	11.88	6.49
	Range	2.36-30.99	0.85-17.96
	Median	8.26	5.13
Palm (10)	**Mean**	22.71	10.9
	Range	5.95-42.44	1.95-35.01
	Median	21.12	6.54

Table D.1: Transient/sustained response ratios at the hotzone electrode by stimulus location. Distributions of onset/sustained and offset/sustained response ratios for the hotzone electrode of each of the 28 stimulation sites across the 4 arrays for a 2-mm, 10-mm/s indentation.

	Onset	Sustained	Offset
Digit distal pads (36 electrodes from 9 stimulation sites)	1	0.86	1
Other digit locations (36 electrodes from 9 stimulation sites)	1	0.92	1
Palm (40 electrodes from 10 stimulation sites)	1	0.63	1

Table D.2: Significant on-, sustained-, and off-responses by stimulus location. Proportions of electrodes that yielded responses to a 2-mm, 10-mm/s indentation that were significantly different from baseline, separated by response epoch and hand location. Firing rates during the onset and offset transients were significantly different from baseline (pre-stimulus) firing rates for all 112 electrodes and 28 stimulated locations across the 4 arrays (p ¡ 0.01). The fraction of significant sustained responses were higher in the digits than the palm, as might be expected given the gradient of relative densities of innervation of slowly and rapidly adapting fibers across the hand.

		Onset	Sustained	Offset
All hand locations (28)	**Mean**	14.8	1.73	7.27
	Range	6.87-44.11	0.34-7.83	1.18-17.87
	Median	12.81	1.31	6.11
Digit distal pads (9)	**Mean**	12.81	2.32	6.84
	Range	8.03-19.45	0.45-7.83	4.69-10.95
	Median	12.02	1.19	5.95
Other digit locations (9)	**Mean**	17.13	2.1	8.41
	Range	8.68-44.11	0.34-3.93	3.12-16.96
	Median	14.02	1.87	8.01
Palm (10)	**Mean**	14.5	0.86	6.65
	Range	6.87-21.66	0.34-1.46	1.18-17.87
	Median	15.58	0.66	5.82

Table D.3: Response heterogeneity at the hotzone electrode by epoch and stimulus location. Metrics (mean, range, median) characterizing the distribution of hotzone electrode responses across all stimulated locations (from the 4 arrays) during different epochs of a 2-mm, 10-mm/s indentation. Onset responses are generally stronger than offset responses, and sustained responses are always considerably weaker than both. The ranges for the different hand locations are wide and largely overlapping. Sustained responses tend to be weaker in the palm than the digits, consistent with the sparser density of slowly adapting fibers innervating the palm compared to their rapidly adapting counterparts.

	Mean	Median	Range
ALL (28)	0.50	0.55	0.04-0.84
Distal (9)	0.41	0.30	0.04-0.84
Other digit (9)	0.52	0.57	0.09-0.75
Palm (10)	0.57	0.59	0.33-0.83

Table D.4: Adaptation index at the hotzone electrode by stimulus location. Distribution of Adaptation Index values for the hotzone electrode for each of the 28 stimulation sites across the 4 arrays. Indices overlap across hand regions, but responses tend to be more RA-like in the palm, reflecting differences in the relative innervation density of slowly and rapidly adapting fibers in the palm and digits.

		Onset	Sustained	Offset
All hand locations (28)	Mean	52.79	14.93	37.4
	Range	19-91	3-53	11-85
	Median	54	10.5	34
Digit distal pads (9)	Mean	64.22	17.56	48.44
	Range	49-91	3-37	24-85
	Median	58	14	45
Other digit locations (9)	Mean	45.78	19.11	28.77
	Range	19-64	4-53	11-43
	median	51	17	31
Palm (10)	Mean	48.8	8.8	35.2
	Range	26-63	4-16	18-48
	Median	50.5	8.5	35

Table D.5: Recruitment by epoch and stimulus location. Metrics (mean, range, median) characterizing the spread of cortical activity across all stimulated locations (28 sites from the 4 arrays) during different epochs of a 2-mm, 10-mm/s indentation. The number of electrodes with responses above 0.5 s.d. is used as a metric of recruitment. A low threshold was selected to achieve a more graded response. The spread is greatest during onset and lowest during the sustained epoch. The ranges for the different hand locations are wide and largely overlapping so no obvious pattern emerges. Recruitment is somewhat lower in the palm than in the digits during sustained indentation, consistent with the sparser innervation of slowly adapting fibers in the palm.

		Onset/sustained	Offset/sustained
ALL	Mean	11.76	5.47
	Range	5.12-45.37	2.15-19.4
	Median	9.2	4.2
DISTAL	Mean	9.96	5.42
	Range	8.70-12.33	3.90 – 8.0
	Median	8.86	4.37
PALM	Mean	17.90	7.69
	Range	8.16-45.37	3.96-19.4
	Median	11.66	5.21

Table D.6: Transient/Sustained ratios for simulated afferent responses by stimulus location. Metrics (mean, range, median) characterizing the distribution of onset/sustained and offset/sustained firing rate ratios for simulated afferents at the hand locations for which cortical data was collected. The stimulus was a 2-mm, 10-mm/s indentation. As is the case in cortical responses, responses are more transient in the palm than in the digits, reflecting differences in innervation patterns.

D.3 Supplementary Figures

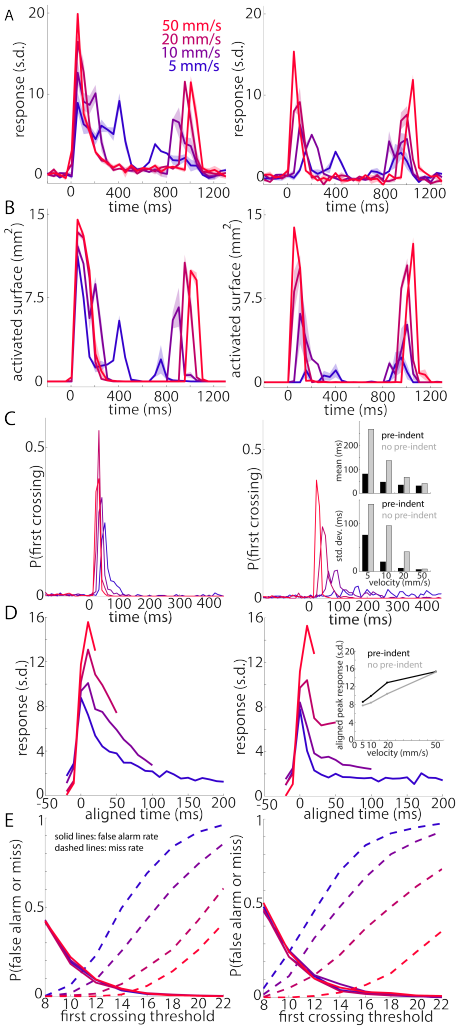

Figure D.1: Pre-indentation vs. contact initiation. Left column shows results from experimental sessions when the probe was pre-indented into the skin, and the right column shows results from sessions when the probe starting position was 0.5 mm above the skin surface (± changes in the position of the hand over time). The same two skin sites were used in the two stimulation conditions (the second array of monkey B, distal pad of digits 3 and 4; 520 trials with pre-indention, 360 trials without). A— Time course of the response at the hotzone electrode to a 2-mm indentation at indentation rates of 5, 10, 20, and 50 mm/s (50ms bins). B— Time course of recruitment (surface with response ¿ 2 s.d. above baseline) (50 ms bins). C— Distribution of threshold-crossing times for each indentation rate using a threshold of 10 standard deviations above the mean. Top inset in the right panel shows the mean crossing times (excluding false alarms) in the pre-indent (black) and no pre-indent (grey) conditions. Bottom inset shows the standard deviations of the crossing times in the two conditions. The higher means observed without pre-indentation are due to the extra time it typically takes for contact to be initiated. The larger standard deviations are due to variations in time it takes for contact to be initiated due to changes in resting hand position. D — Time course of the response at the hotzone electrode with the response aligned to its threshold-crossing time (10-ms bins). The inset on the right shows the aligned-response peak for each velocity in both conditions. The magnitudes of responses evoked with and without pre-indentation are comparable when responses are aligned to onset. E — False alarm rates (solid lines) and miss rates (dashed lines) for each indentation rate in both conditions. Miss and false alarm rates are higher without pre-indentation.

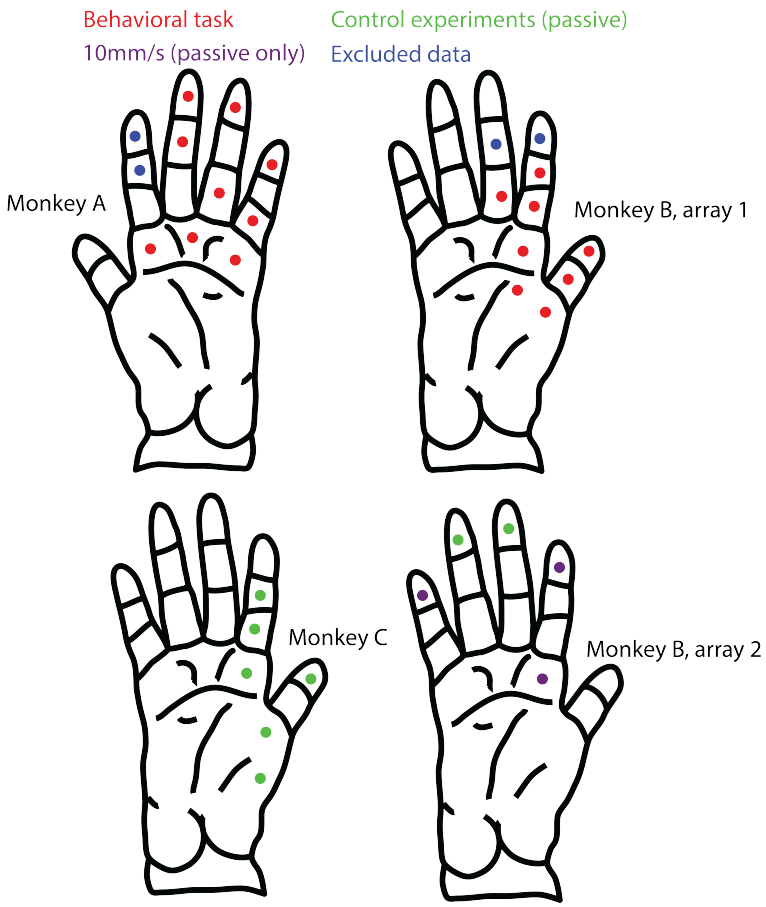

Figure D.2: Stimulation sites for each array. Every dot indicates a skin site that was stimulated. Blue dots indicate sites that were not included in any analyses because the associated hotzone was off the array.

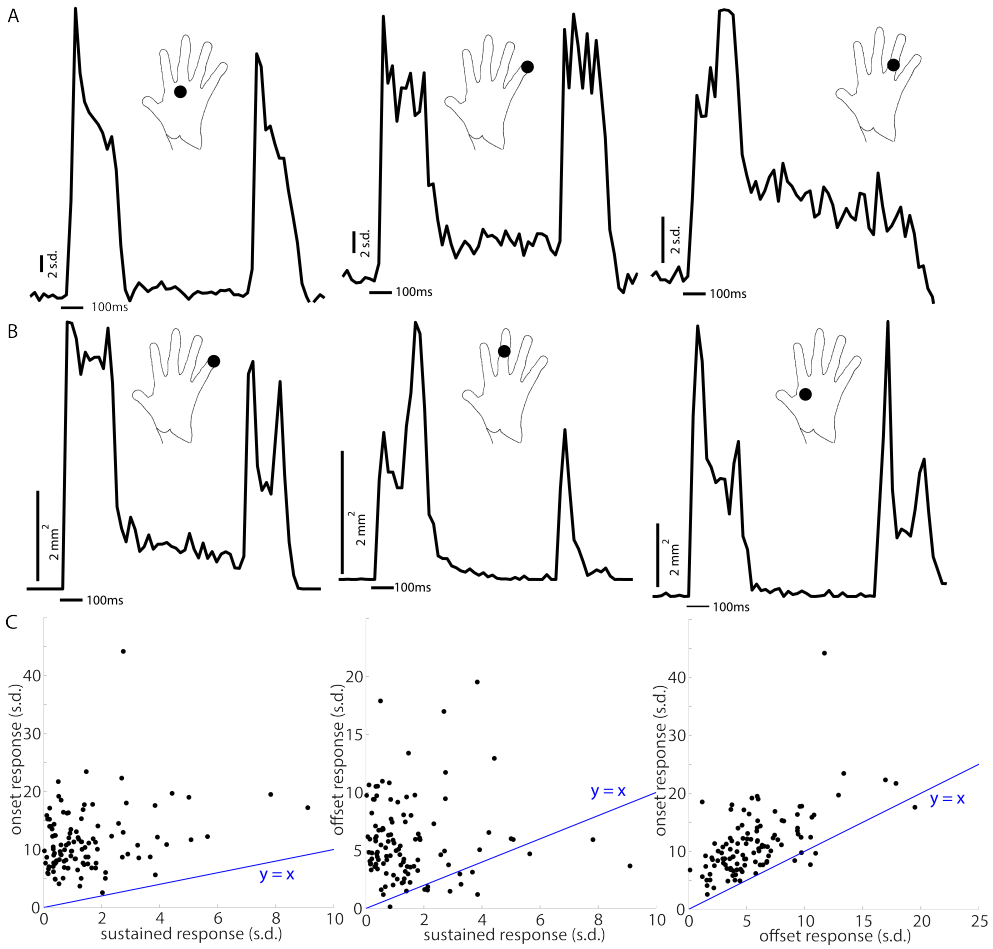

Figure D.3: Heterogeneity of response dynamics. A —Time course of the response at the hotzone electrode to a 2 mm, 10 mm/s indentation for different stimulation sites (from monkeys B, A, and A). From left to right, the magnitude of the sustained response relative to the transient response increases. The dot on the hand in each inset indicates the stimulation site. The spatiotemporal dynamics of the transients vary across electrodes. The same stimulus is used for B and C. B — Time course of the activation area for stimulation at different skin locations (monkeys A, A, and C). C — For 112 highly responsive electrodes from 28 stimulation sites across the 4 arrays, scatter plots of responses during onset vs sustained epochs (left), offset vs sustained epochs (middle), and onset vs offset epochs (right). The blue line is the unity line. Onset and offset responses are almost always stronger than the sustained response. Onset responses are typically stronger than offset responses.

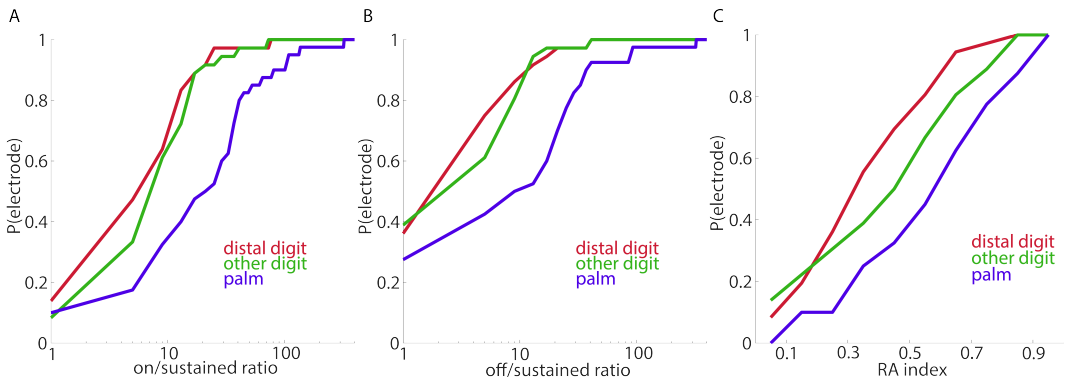

Figure D.4: Comparing Transient and Sustained Epochs. A— Cumulative probability distribution of the ratio of onset epoch response to sustained response to a 2-mm, 10-mm/s indentation for the 112 highly responsive electrodes across 28 stimulation sites from 4 arrays. B— Cumulative probability distribution of the ratio of offset epoch response to sustained epoch response for the same responses. The hand location distributions are largely overlapping, but the palm locations tend to yield larger ratios, reflecting weaker sustained responses. C— Distribution of RA Index values for the population of highly responsive electrodes, by hand location. The Adaptation Index is lower (more slowly adapting) for distal digits than for the palm.

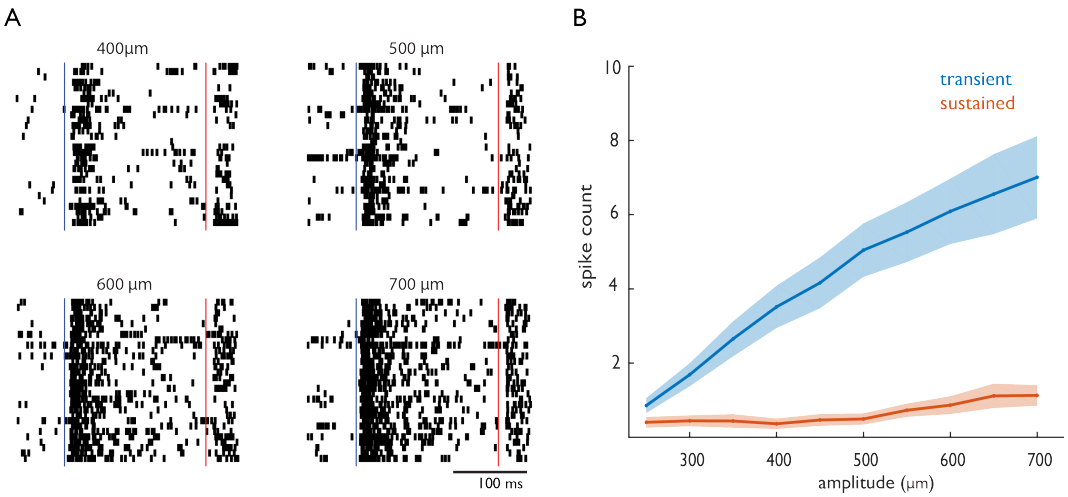

Figure D.5: Responses of single units in somatosensory cortex to indentations at different depths. A— Responses of a single representative neuron in somatosensory cortex to punctate indentations lasting 250 ms at 4 (of 10) amplitudes (ramp duration = 20 ms, indentation rates of 20, 25, 30, and 35 mm/s, with indentation rate increasing in proportion to amplitude given the constant ramp duration). The blue vertical line denotes the beginning of the indentation, and the red line denotes the beginning of the retraction. B— Spike count over 100 ms after stimulus onset (which encompasses the onset ramp for all stimuli), and sustained stimulus duration (subsequent 100 ms) of 16 single somatosensory cortical neurons (area 1, n=10; area 3b, n=6) in response to stimuli differing in indentation depth. As amplitude increases (as does indentation rate since the ramp duration was constant in these measurements), firing rate increases for the transient portion of the stimulus, but very weakly for the sustained portion. Shaded area represents SEM. Single-unit responses show that rate modulation observed in the multi-unit data reflects an increase in the firing rate of recorded units and not just local recruitment around the electrode.

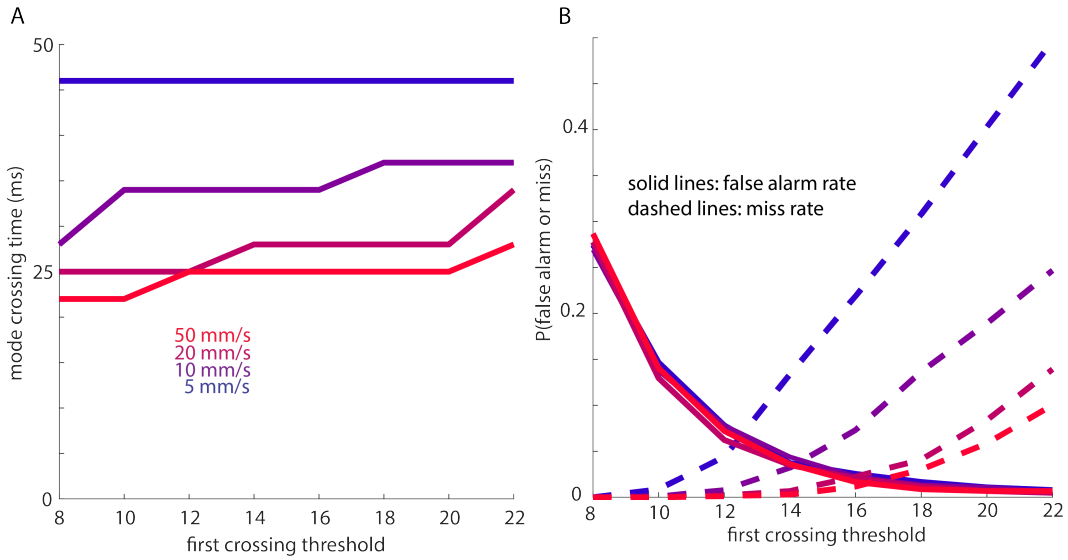

Figure D.6: Impact of threshold on contact timing signals. A— Modal time at which contact is detected (peaks of each velocity's histogram in Figure C.6B) as a function of threshold. As the threshold becomes more stringent, the modal detection time increases, but only slightly. The trials in this figure are the same used in Figure C.6 in the main text. B— Proportion of trials that yield spurious detections (occurring before stimulus onset, solid lines) and misses (no detection of signal up to 500 ms after stimulus onset, dashed lines). As the threshold becomes more stringent, the false alarm rate decreases and the miss rate increases.

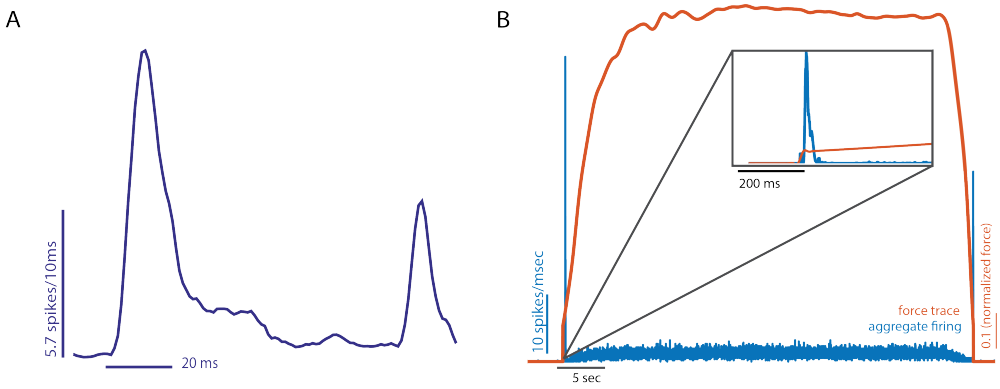

Figure D.7: Validation of nerve stimulation and of mechanical stimulation paradigm. A— Aggregate spike count of (measured) SA1 and RA responses (n=6 and 10 respectively, group sizes were selected to match the ratio of innervation densities found at the fingertip) to a skin indentation (0.3 mm, 10 mm/s, 100 ms). Measured responses are analogous to simulated ones but the latter can be tailored to the stimuli used in the cortical experiments and can reconstruct the spatio-temporal response of the entire nerve. B— Aggregate afferent response to grasping and releasing a coffee cup. Orange trace represents load on the index finger as a coffee cup is grasped, lifted, and put down. The simulated population response is shown in blue (binned at 5 ms). Inset shows a close up of the initial transient response. Simulated afferent response to an actual contact event is similar to the response to a skin indentation.

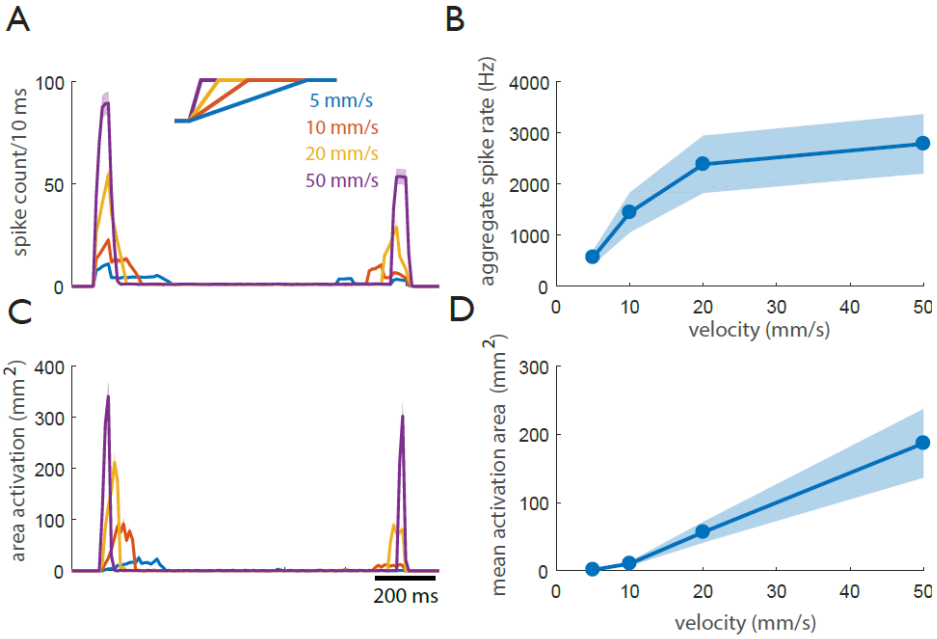

Figure D.8: Effect of indentation rate on the afferent response. A— Aggregate afferent response (spike count) to indentations at different rates (indentation depth = 1.0 mm). Transient responses scale with indentation rate. See timescale bar in panel C. B— Population firing rate during transient (first 20 ms) as a function of indentation rate. C— Area of activated afferents for different indentation rates. The area of activation during the transient response scales with indentation rate. D— Mean area of activation as a function of indentation rate over the transient interval (first 20 ms). Shaded areas represent standard error of the mean over multiple skin locations (n=16, specified in Figure D.2).

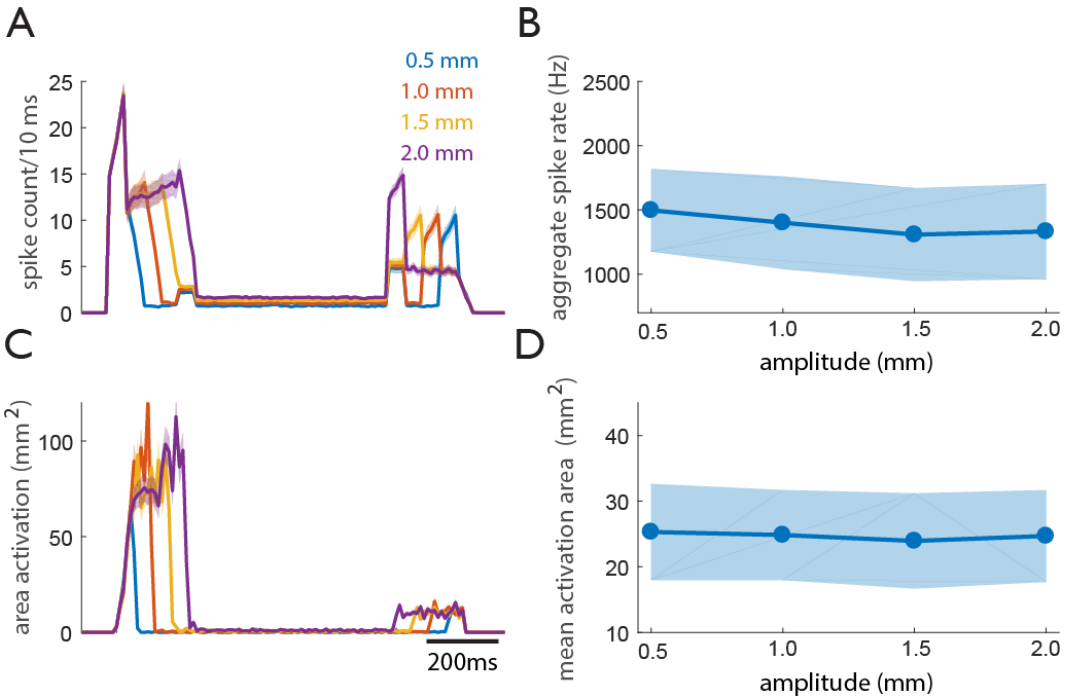

Figure D.9: Effect of indentation depth on the sustained and transient responses in the nerve. A— Time course of the simulated population response to indentations at 4 indentation depths: 0.5, 1.0, 1.5, and 2.0 mm with a fixed indentation rate of 10 mm/s. See timescale in C. B— Aggregate spike rate during transient phase (while the probe is moving) as a function of indentation depth. Firing rates are independent of amplitude during the transient phase (spike rate computed over respective ramp durations). C— Time course of the activated area for four indentation depths. D— Mean area of afferent activation as a function of indentation depth over the transient phase (mean area computed over respective ramp durations). Increases in amplitude have a negligible effect on recruitment. Shaded areas represent standard error of the mean over multiple skin locations (n=16, specified in Figure D.2).

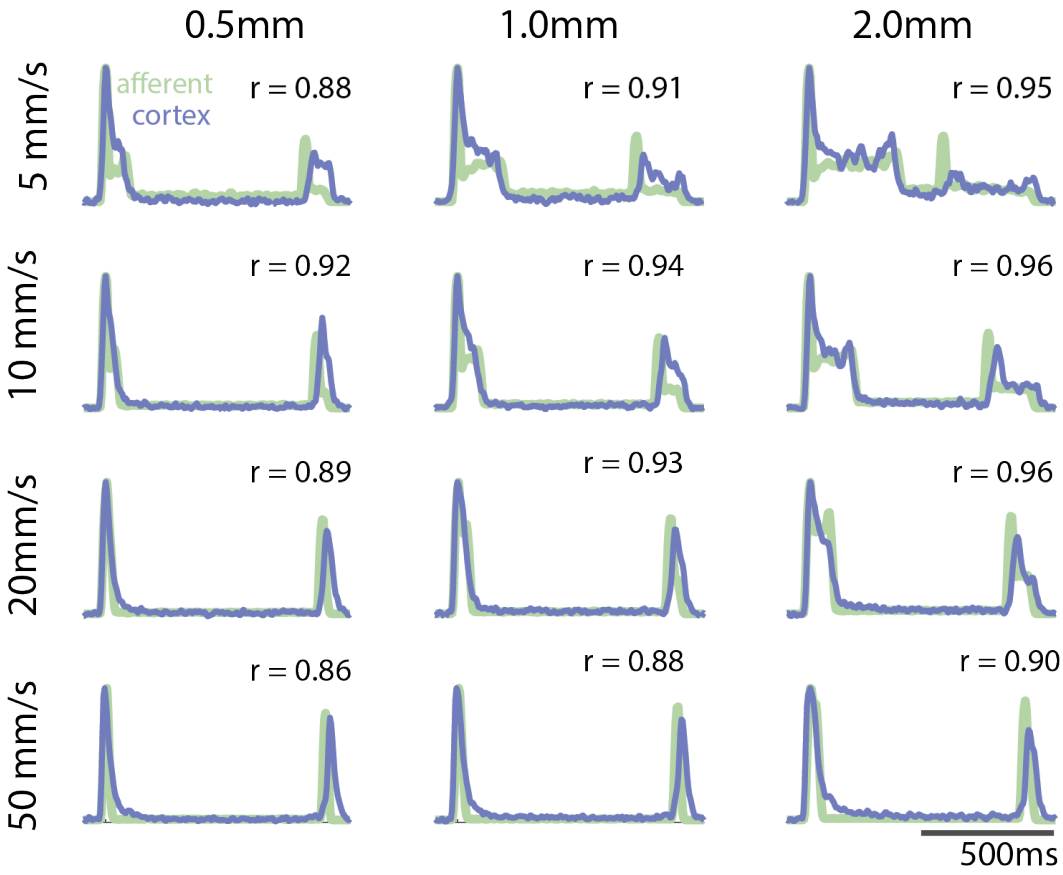

Figure D.10: Correlation between afferent and cortical responses. For each indentation rate/depth pair (12 total conditions), (simulated) afferent traces across 3 locations (distal fingerpad, proximal fingerpad, and palm) are shown in green, and (measured) cortical traces across the same 3 stimulation locations from monkey B's second array and monkey C (Figures C.2 and D.2) are shown in blue. Traces were smoothed with a Gaussian kernel width of 20 ms, and aligned to correct for conduction latency. Mean correlation over all 12 conditions is 0.92, (s.d. = .033).

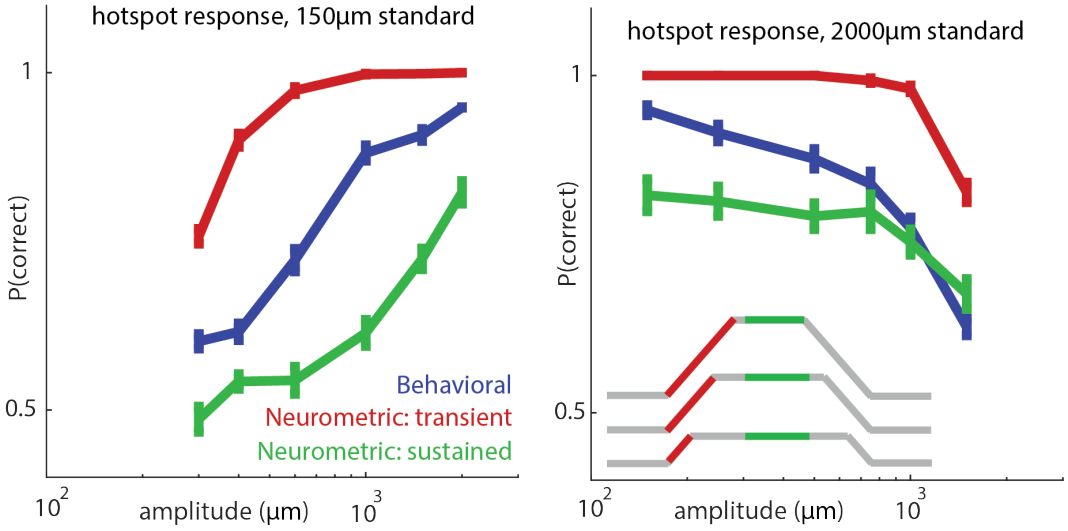

Figure D.11: Relating neuronal responses to behavioral performance using a variable transient time window. Performance of the animals (blue) and that of an ideal observer based on the spike count during the onset transient (red, time window equal to transient duration for each indentation amplitude) and based on the spike count during the sustained response (green, 300ms window for all stimuli) at the hotzone electrode for a 150-μm standard stimulus (left, 5645 trials from 17 skin locations from monkey A and monkey B's first array) and 2000-μm standard stimulus (right, 6546 trials from 17 skin locations over the same 2 arrays). Inset shows the stimulus trace with color-coded stimulus epochs for 3 example stimuli (not drawn to scale). All stimuli in the behavioral task were delivered at 10 mm/s. Error bars denote the standard error of the mean (n = 17 skin locations). Neurometric performance based on the burst of spikes elicited by probe indentation far exceeds behavioral performance. However, to exploit this code would require the animal count spikes only during probe movement, which is highly improbable. A more likely scenario is that the animal integrates the response over a fixed time window after onset, when the response is most informative about the stimulus (see Figure C.7 in the main text).

Appendix E | Supplementary material: spike timing in somatosensory cortex supports frequency perception

E.1 Supplemental discussion: covariance of neural responses and behavior

Analyzing the trial-by-trial covaration of neural responses and the animals' frequency judgments may offer insight into the neural coding of pitch. Indeed, covariation between trial-to-trial fluctuations in one feature of the neural response (e.g., firing rate) and the animal's behavior can be interpreted as evidence for a causal link between that neural feature and perception (Britten et al., 1996).

For M4, the frequency decoded based on firing rates tended to be higher when the animal selected a stimulus as higher in frequency than when it did not (Figure E.7, Figure 2.7A,B). For M3, the difference in frequencies decoded from the rates of all neurons was actually lower when the monkey correctly selected the higher frequency, though this effect did not reach statistical significance ($p = 0.08$, (Figure 2.7)). These findings imply a covariation between firing rates and behavioral choice. Given that the relationship between frequency and mean firing rate can be positively (+) or negatively sloped (-) (cf. (Salinas et al., 2000)), we expect that the relationship between frequency and behavioral choice should differ between these two populations of neurons. The responses of + neurons should be higher when the frequency is selected and lower when it is not, and vice versa for the - neurons. Another possibility is that monkeys defaulted to perceived magnitude when in doubt, in which case the responses of all neurons (+ and -) should be higher for the selected frequency, and this effect would be most prominent for difficult discriminations.

We found that the covariations between rate and behavioral choice followed neither of these scenarios. For M4, the rates was of – neurons was higher for selected than unselected stimuli (Figures E.8 and E.9), which accounts for the effect of behavioral choice on decoded

frequency and is consistent with a rate code for frequency (Figure 2.7). In contrast, the rates of the + neurons did not significantly covary with behavioral choice (Figures E.8 and E.9), except very weakly for one of the separatrices (50 Hz). For M3, the covariation with rate was generally much weaker. When the firing rates of + or – neurons for each stimulus condition were split by behavioral choice, no obvious trend emerged (Figure E.8). Pooling across all stimulus conditions, however, there was a slight but significant tendency for the responses of - neurons to be stronger when the animal correctly selected the higher frequency (Figure E.9), which accounts for the decoding effects and violates expectations from the rate code hypothesis. Indeed, higher firing rates in - neurons in principle will make stimuli be perceived as lower in frequency. That the responses of - neurons in M3 are higher on correct trials is consistent with the hypothesis that the animal defaulted to the more intense stimulus when in doubt. However, this hypothesis would also entail that the responses of + neurons would be higher on correct trials, which was not the case.

For M4, one frequency was decoded from single-trial responses. For M3, the frequency of each stimulus was decoded and their difference was taken to predict behavioral choice, as has been previously done for two-alternative force choice designs (Salinas et al., 2000). The latter difference computation (1) assumes that both stimuli in a pair are weighted equally in shaping the behavioral choice; (2) yields a noisier metric as it reflects noise from two neuronal responses rather than one; and (3) involves many more stimulus conditions (combinations of standard and comparison amplitudes), yielding fewer observations per condition. Consequently, the analyses of the covariation between firing rates and behavior for M3 have less statistical power than those for M4.

In conclusion, we find that firing rates significantly covary with behavior but do so in different ways for the two animals. The picture that emerges from this analysis of response/behavior covariation is thus muddled and hard to interpret.

E.2 Supplemental figures

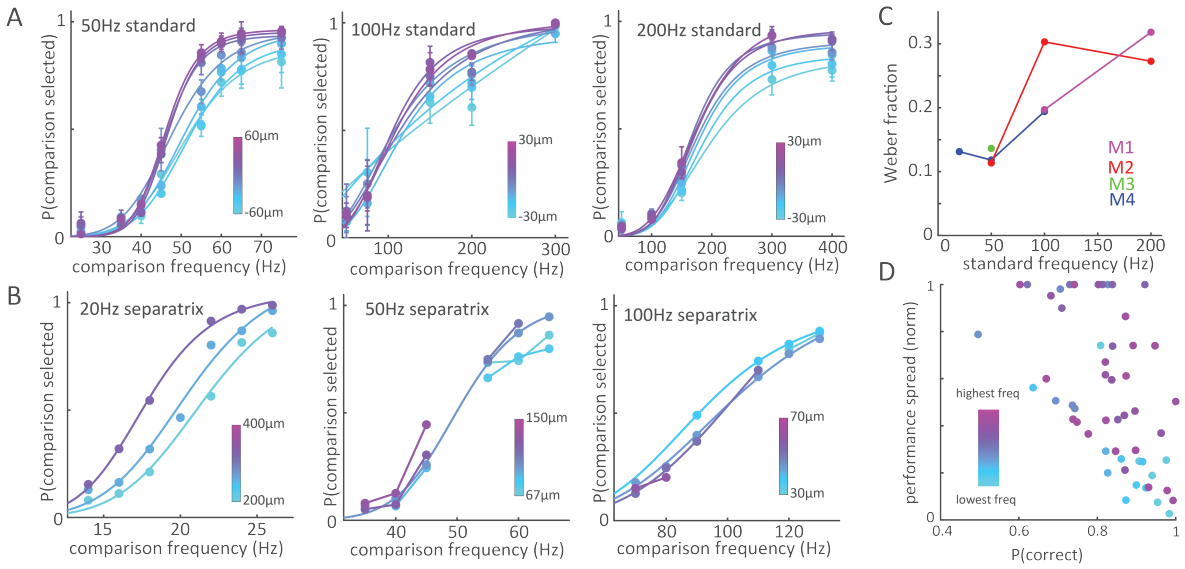

Figure E.1: psychophysics. A — Frequency discrimination performance for each standard frequency. Left: performance of M2 and M3 with a 50Hz standard. Middle: performance of M1 and M2 with a 100Hz standard. Right: performance of M1 and M2 with a 200Hz standard. B — frequency classification performance of M4 with separatrixes of 20Hz (left), 50Hz (middle), and 100Hz (right). C — Weber fractions for each animal at each standard/separatrix. D — amplitude-related spread as a function of performance. This shows, for each comparison frequency on each plot in A and B, the spread (largest difference between any 2 amplitudes at that frequency) as a function of average performance at that frequency (across amplitudes). The spread values are normalized to 1 within each animal/standard pair. Though each plot in A shows the performances of 2 monkeys averaged together, data from each individual monkey is shown in D. The color legend represents the ranking of frequencies from low (blue) to high (purple) within each frequency range. Performance spreads tend to be higher for lower-performance comparison frequencies. They also tend to be higher for higher frequencies within each range (more purple), an effect that is more pronounced for discrimination than classification.

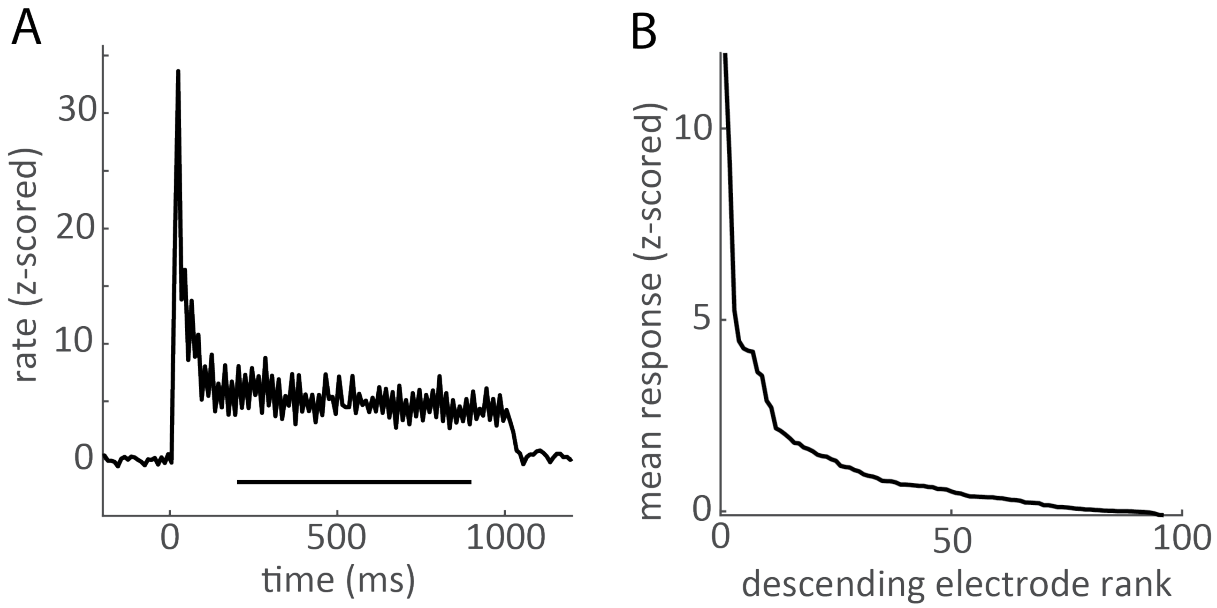

Figure E.2: Representative neural responses A — Peristimulus time histogram of a neuron's response to a 50Hz stimulus. Note the large transient at the onset of stimulation (t = 0ms), a consistent feature of SC responses to vibrations. As onset (and sometimes offset) transients are likely to contaminate stimulus-specific signals, we limited our analyses of rates and timing to the time interval indicated by the horizontal line. B — Multi-unit responses from each M4 electrode during passive recordings, sorted by overall firing rate response (averaged across all stimuli). All analyses of rate and timing were limited to the left tail of most highly responsive electrodes.

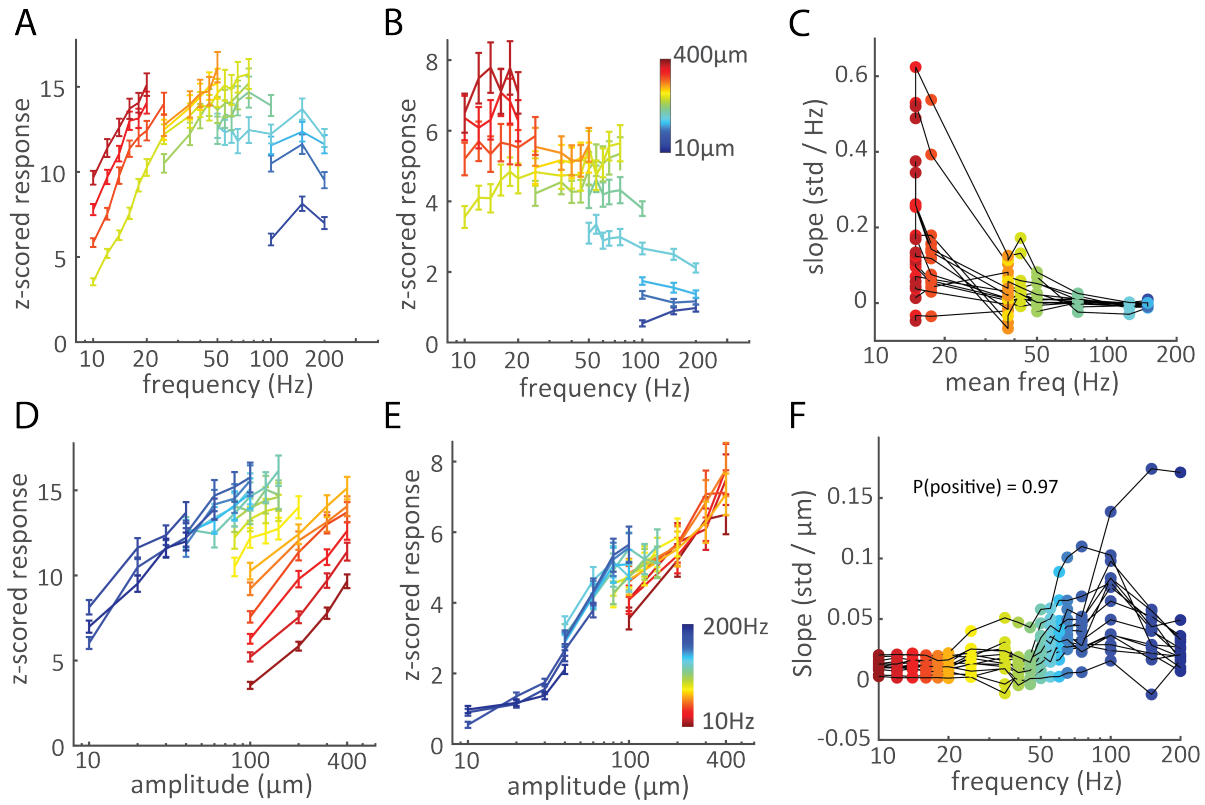

Figure E.3: Response dependence on frequency and amplitude. A and B — Spike rate versus frequency for two electrodes illustrating different rate-frequency relationships. In A, rate rises with frequency in the low range but the slopes decrease at higher frequency ranges. In B, the rate-frequency relationship is weak, with slopes close to zero and even negative. C — Rate-versus-frequency slopes as a function of frequency for the 15 most highly responsive electrodes (see Figure E.2B for ranked responses). Each colored point corresponds to the slope of the matching line in the examples in A and B for one electrode. X-axis points correspond to the mean frequency spanned by each of these lines. D and E — Spike rate versus amplitude for the same two electrodes in A and B. Rate rises monotonically with amplitude for both. F — Rate-versus-amplitude slopes as a function of frequency for the 15 most highly responsive electrodes (see Figure E.2B for responses). Each colored point corresponds to the slope of the matching line in the examples in D and E. X-axis points correspond to the frequency represented by each of these lines. The slopes across electrodes and frequencies are almost universally positive (97%).

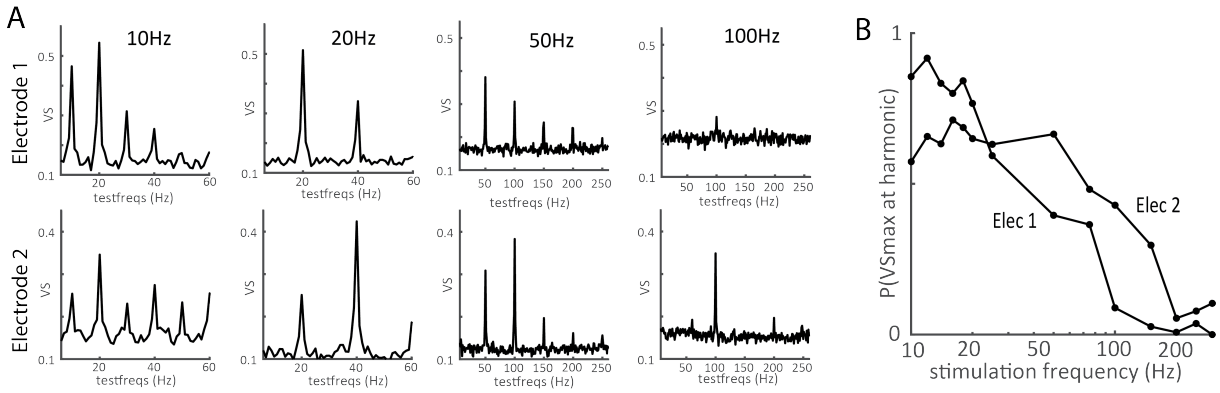

Figure E.4: Timing. A — Spike train vector strengths at various stimulation frequencies for multi-unit activity recorded at two example electrodes (in each row). B — Strength of phase locking across stimulation frequencies for the electrodes in A. The plot shows the proportion of trials on which the stimulus frequency or its harmonic have the highest VS of all test frequencies, as a function of stimulus frequency. The phase locking at low frequencies is stronger for electrode 1, but electrode 2 maintains better phase locking at higher frequencies, illustrating the variability in the timing of SC neural populations.

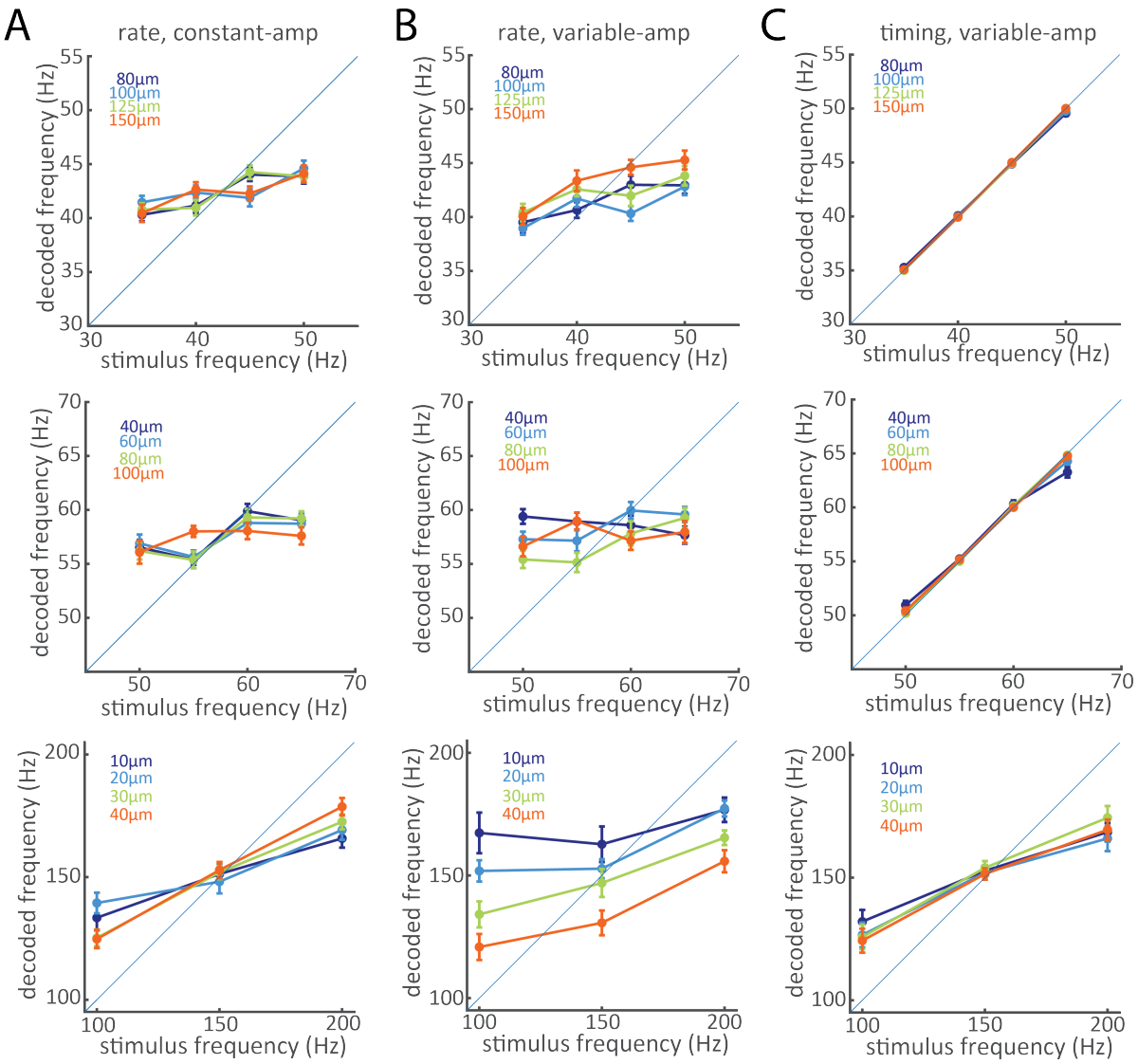

Figure E.5: Effect of multiple amps on decoding from 30 to 200Hz, from passive recordings of M4. Rows correspond to different frequency ranges within which the same amplitudes were used. A — Rate decoder with constant amplitudes: neural responses were grouped by amplitude and a rate decoder was trained and tested for each. B — Rate decoder with all amplitudes: a single rate decoder was trained and tested on neural responses from all amplitudes. C — Timing decoder with all amplitudes.

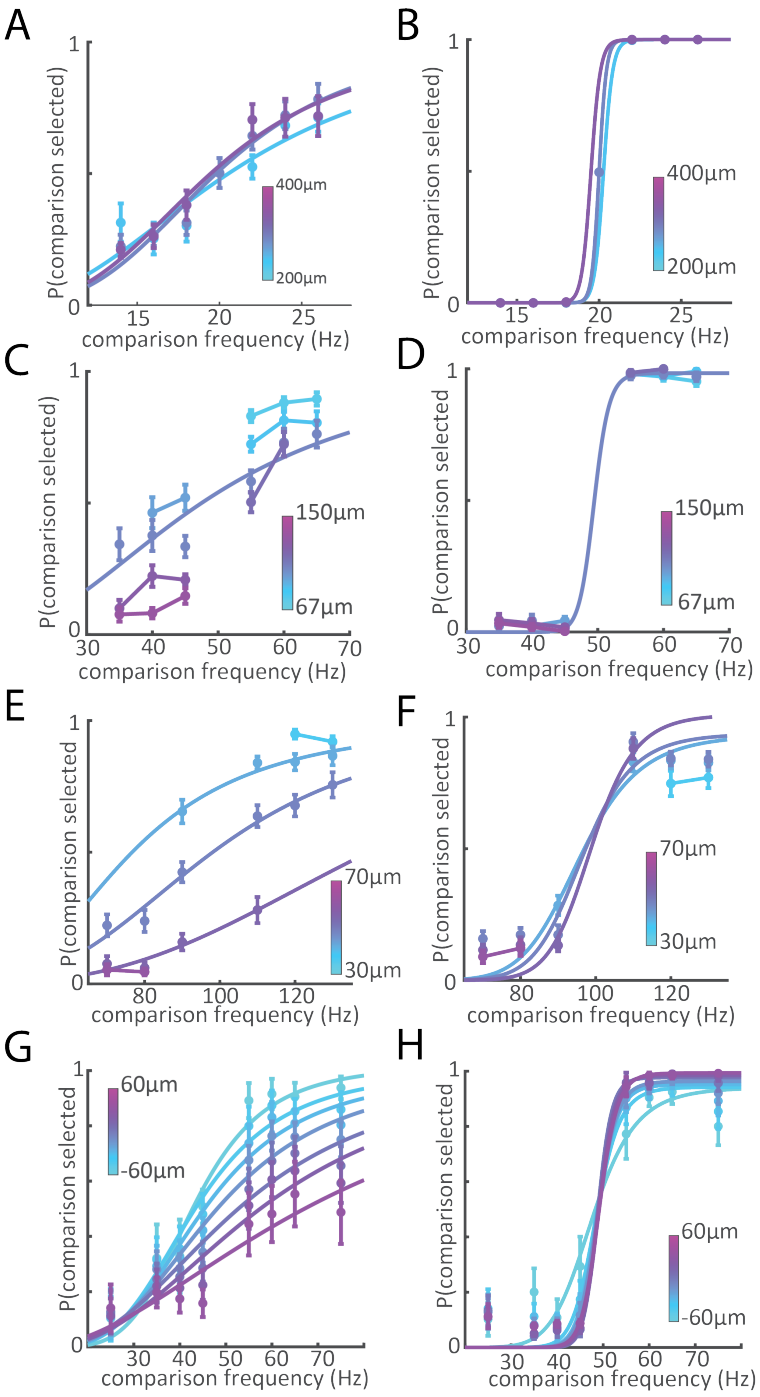

Figure E.6: Neurometric performance of rate (left) and timing (right) decoders for all monkeys and standards/separatrixes. A-B — decoders applied to data from M4 frequency classification with a 20Hz separatrix. C-D — decoders applied to data from M4 frequency classification with a 50Hz separatrix. E-F — decoders applied to data from M4 frequency classification data with a 100Hz separatrix. G-H — decoders applied to data from M3 frequency discrimination with a 50Hz separatrix (also shown in Figure 2.6A-B).

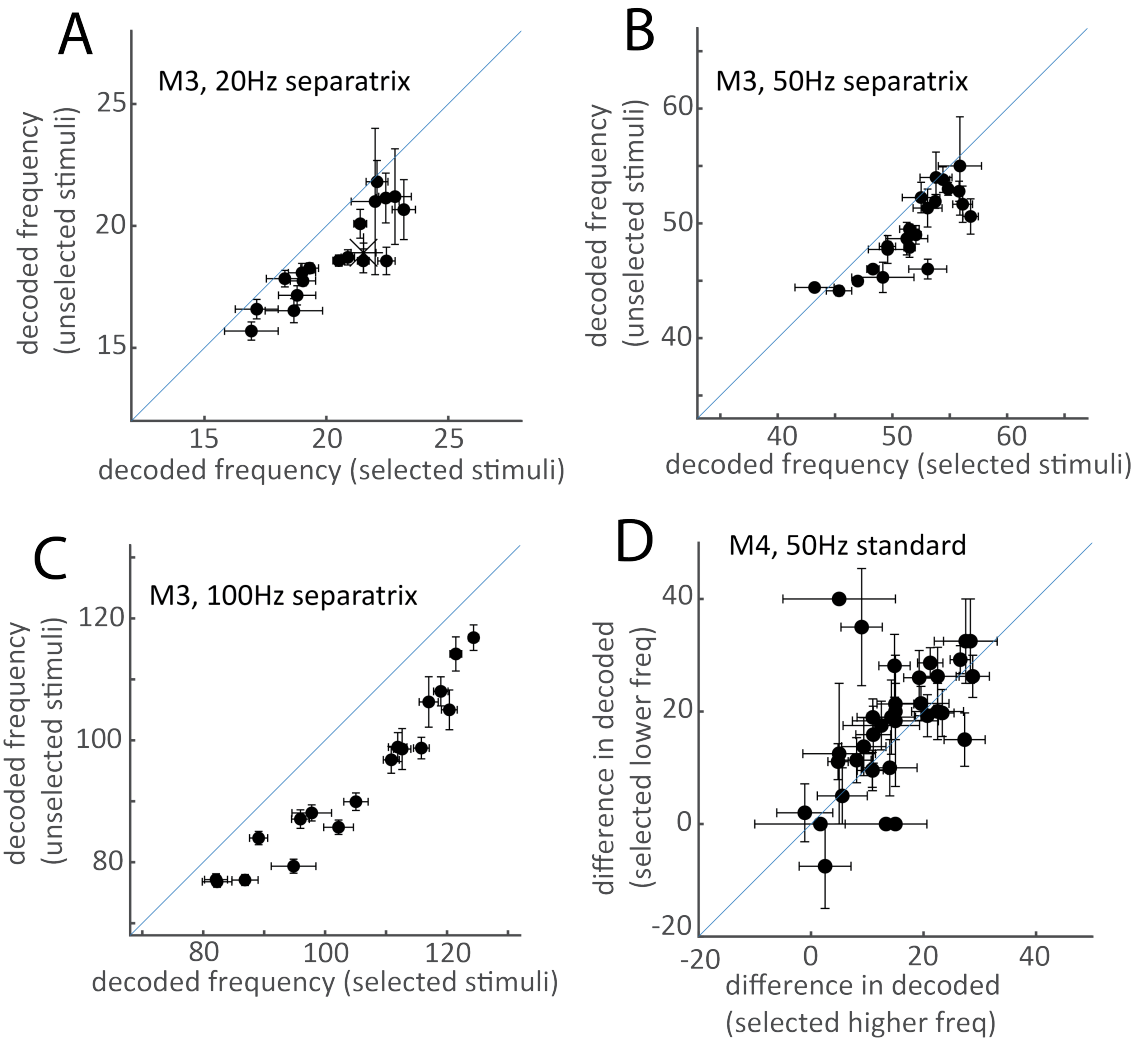

Figure E.7: Covariance of decoded frequency and behavior A-C — Covariance of decoded frequency and behavior, M4 classification task. Average rate-decoded frequency for every frequency/amplitude combination in the frequency classification task when M4 selected the stimulus (x axis) and when it did not (y axis). The decoded frequency is higher when the animal selected the stimulus. D — Covariance of response and behavior, M3 discrimination task. Each frequency in a trial is decoded and the difference between them is computed. The plot shows this difference when M3 selected the higher frequency (x-axis) and when it did not (y-axis). Each point represents a unique pair of stimuli. If rate fluctuations play a significant role in frequency perception, one would expect the difference to be larger in the case where the animal correctly selected the higher frequency.

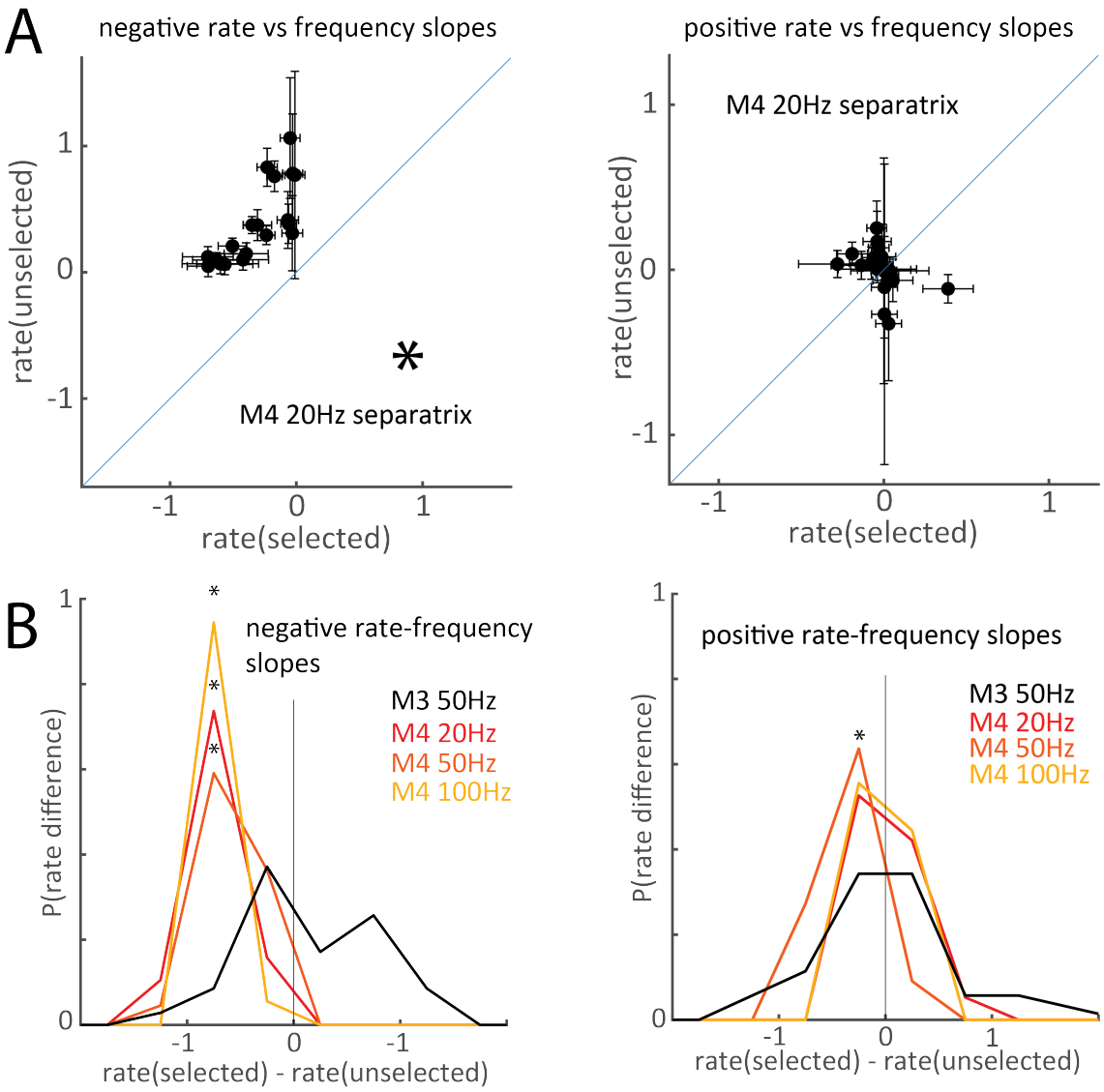

Figure E.8: Covariance of spike rate and behavior. A — As an example, firing rates when M4 did not select a stimulus versus average rate when M4 did select it. Each point represents a unique stimulus condition. The rates are z-scored within each stimulus condition. The left column shows rates for neurons with negative rate-frequency relationships and the right column shows rates for neurons with positive rate-frequency relationships. Asterisk denotes a significant difference between the mean rate when selected (x axis) and unselected (y axis). B — Probability distributions of differences in average firing rate in the selected and unselected cases for each trial condition (i.e. difference in x and y axis values for individual points in A). The left plot shows results from neurons with negative rate-frequency relationships while the right shows rates for neurons with positive rate-frequency relationships. On the left the three M4 distribution means are significantly below 0, indicating that rates were slightly higher when the animal did not pick the stimulus as higher. On the right this effect is seen for only the 50-Hz separatrix. No significant effect was found for M3.

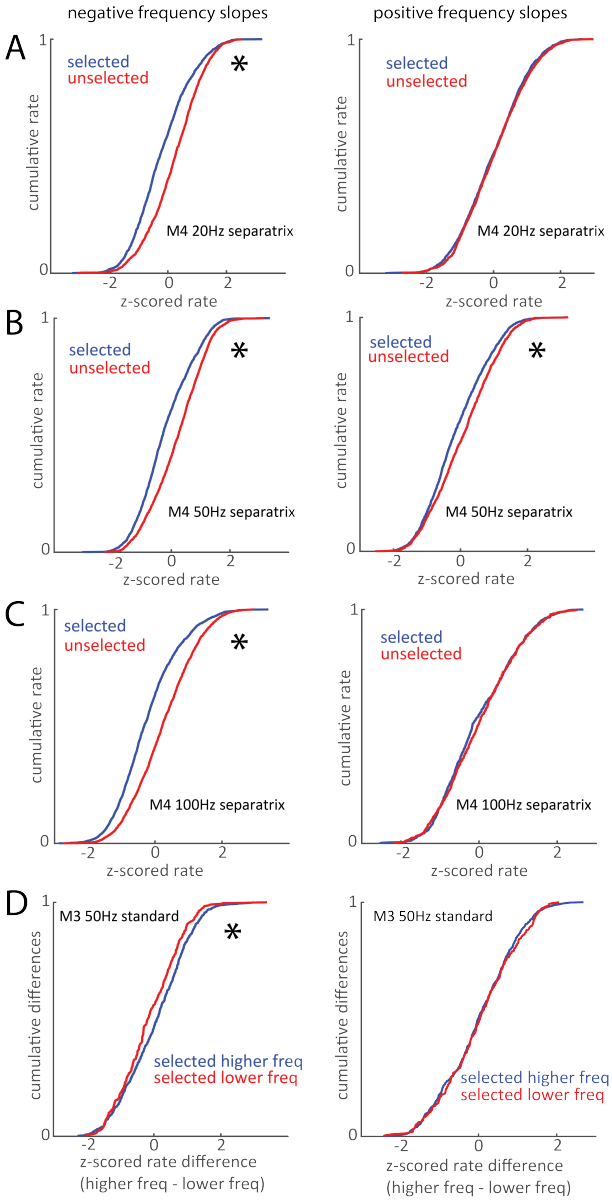

Figure E.9: Covariance of rate and behavior, pooling all stimuli. A-C — Cumulative distribution of firing rates across all selected (red) and unselected (blue) stimuli for M4 classification at the three separatrices (rows), for neurons with negative (left) and positive (right) rate-frequency relationships. Rates were z-scored within presentations of each unique stimulus in each experimental session before being pooled. Asterisks denote significant rate differences between the selected and unselected populations, with higher rates for the right-shifted curve. D — M3 cumulative distribution of rate differences (higher freq – lower freq) of neurons with negative (left) and positive (right) rate-frequency slopes. This analysis found that rate differences were significantly larger when the M3 correctly selected the higher frequency, but only for neurons with negative rate-frequency slopes.

Appendix F | Supplementary material: the frequency of cortical microstimulation shapes artificial touch

F.1 SI appendix text

F.1.1 Validation of catch trials

On four electrodes, we trained monkey B to perform frequency discrimination on 2 subsets of stimuli before using the full stimulus set: one with both stimuli in the pair of equal amplitude and one in which the higher frequency stimulus always was at a much lower amplitude. High performance was achieved on all four electrodes for these two subsets (Fig. F.7). However, catch trials revealed that the animal was biased toward more intense stimulus in the first set but toward less intense stimuli in the second set. These results are consistent with the hypothesis that catch trials reveal the animal's reliance on intensive cues and indicate that the 30-μA amplitude difference was sufficient to overcome the 100-Hz frequency difference such that the higher frequency stimulus felt less intense than the lower frequency one. When the animal was faced with the full set (which comprised stimuli from the first two), the animal was able to perform the task correctly regardless of amplitude differences on only two of the four electrodes (Fig. F.7).

F.1.2 Learning during task transfer

All the data described above reflect monkey B's asymptotic performance, sometime after weeks of training on each electrode and standard frequency. Next, we examined how the animal's performance evolved during training. We found that, on some electrodes, the animal appeared unable to overcome the amplitude confound over the course of up to 6000 trials

1. This chapter was published : Callier, T., Brantly, N. W., Caravelli, A., and Bensmaia, S. J. (2020). The frequency of cortical microstimulation shapes artificial touch. Proceedings of the National Academy of Sciences, 117(2), 1191–1200. https://doi.org/10.1073/pnas.1916453117.

(Fig. F.9B). On other electrodes, the animal relied on intensity cues at first, but learned over an extended period to discriminate frequency independent of amplitude (example 1). On yet other electrodes, the animal's performance was initially high but somewhat amplitude-dependent and became, relatively rapidly, independent of amplitude (example 3). We found that the majority of electrodes yielded good performance immediately (above criterion of 75% at all amplitude differences) or never yielded good performance (the animal did not learn to perform above criterion at all amplitude differences within 6000 trials)(Fig. F.9B).

F.1.3 Adaptation index

We developed an adaptation Index to quantify the relative contributions of slowly adapting and rapidly adapting signals to the multi-unit responses to skin indentations at each electrode (Fig. F.3), as has been previously done (1, 2). For this calculation, we normalized neural responses during sustained indentation and indentation offset to their respective grand means across electrodes. The adaptation index was then computed by dividing the normalized offset response by the sum of the normalized sustained and normalized offset responses for each electrode separately. An index of 0 denoted a pure SA1-like response, an index of 1 a pure RA-like response.

F.2 SI appendix references

1. Y.-C. Pei, P. V. Denchev, S. S. Hsiao, J. C. Craig, S. J. Bensmaia, Convergence of Submodality-Specific Input Onto Neurons in Primary Somatosensory Cortex. J. Neurophysiol. 102, 1843–1853 (2009).

2. T. Callier, A. K. Suresh, S. J. Bensmaia, Neural Coding of Contact Events in Somatosensory Cortex. Cereb. Cortex, 1–15 (2018).

F.3 SI appendix tables and figures

Frequency discrimination stimulus set 1: constant pulse amplitude, full stimulus set for detailed psychometric curves				
Standard stimulus frequency (Hz)	Standard stimulus amplitude (μA)	Comparison stimulus frequency (Hz)	Comparison stimulus amplitude (μA)	Phase duration (μs)
20	50, 60, 70, 80	16, 18, 22, 23, 26 29	50, 60, 70, 80	400
50	50, 60, 70, 80	30, 35, 40, 45, 55, 60, 65, 70	50, 60, 70, 80	400
100	50, 60, 70, 80	50, 75, 150, 200, 300	50, 60, 70, 80	200
200	50, 60, 70, 80	100, 150, 250, 300, 350, 400	50, 60, 70, 80	200
Frequency discrimination stimulus set 2: with constant pulse amplitude, reduced stimulus set. Row 1: subset 1, row 2: subset 2, row 3: mixed subset (in Fig. S7)				
Standard stimulus frequency (Hz)	Standard stimulus amplitude (μA)	Comparison stimulus frequency (Hz)	Comparison stimulus amplitude (μA)	Phase duration (μs)
70, 80, 90, 100, 110, 120, 130, 170	50, 60, 70, 80	Always equal to standard frequency + 100	Always equal to standard amplitude	200
70, 80, 90, 100, 110, 120, 130, 170	80	Always equal to standard frequency + 100	50	200
70, 80, 90, 100, 110, 120, 130, 170	50, 60, 70, 80	Always equal to standard frequency + 100	50, 60, 70, 80	200
Catch trials in reduced stimulus set for frequency discrimination (interleaved in frequency discrimination stimulus set 2)				
Standard stimulus frequency (Hz)	Standard stimulus amplitude (μA)	Comparison stimulus frequency (Hz)	Comparison stimulus amplitude (μA)	Phase duration (μs)
70, 80, 90, 100, 110, 120, 130, 170	50	Always equal to standard frequency	80	200
Frequency discrimination stimulus set 3: variable pulse amplitude				
Standard stimulus frequency (Hz)	Standard stimulus amplitude (μA)	Comparison stimulus frequency (Hz)	Comparison stimulus amplitude (μA)	Phase duration (μs)
75, 105, 135, 165	For each stimulus, one of the following sets of individual pulse amplitudes was randomized, then repeated with the frequency-appropriate inter-pulse interval to complete a 1-s long stimulus: [44 to 72, in increments of 2] , [58 to 86, in increments of 2], [72 to 100, in increments of 2]. Average pulse train amplitudes were 58, 72, or 86.	Always equal to standard frequency + 90	For each stimulus, one of the following sets of individual pulse amplitudes was randomized, then repeated with the frequency-appropriate inter-pulse interval to complete a 1-s long stimulus: [44 to 72, in increments of 2] , [58 to 86, in increments of 2], [72 to 100, in increments of 2]. Average pulse train amplitudes were 58, 72, or 86.	200
Detection task				
Standard stimulus frequency (Hz)	Standard stimulus amplitude (μA)	Comparison stimulus frequency (Hz)	Comparison stimulus amplitude (μA)	Phase duration (μs)
100	10, 25, 40, 55, 70	0	0	200
Amplitude discrimination task (previously performed experiment, results published in (5))				
Standard stimulus frequency (Hz)	Standard stimulus amplitude (μA)	Comparison stimulus frequency (Hz)	Comparison stimulus amplitude (μA)	Phase duration (μs)
50, 100, 250, 500	70	50, 100, 250, 500	40, 50, 60, 80, 90, 100	200

Table F.1: Stimulus parameters for each experiment. Each trial in the discrimination task consisted of a standard stimulus and a comparison stimulus. In an experimental block, every combination of amplitudes was used and the standard frequency was paired with every comparison frequency. For example, with the 50-Hz standard stimulus, 4 different standard stimuli (50Hz at 50, 60, 70, and 80 microamps) were tested against 32 different comparison stimuli (8 different frequencies at 4 different amplitudes each), at both presentation orders, yielding 256 unique trials in a block (4 standards * 32 comparisons * 2 possible orders).

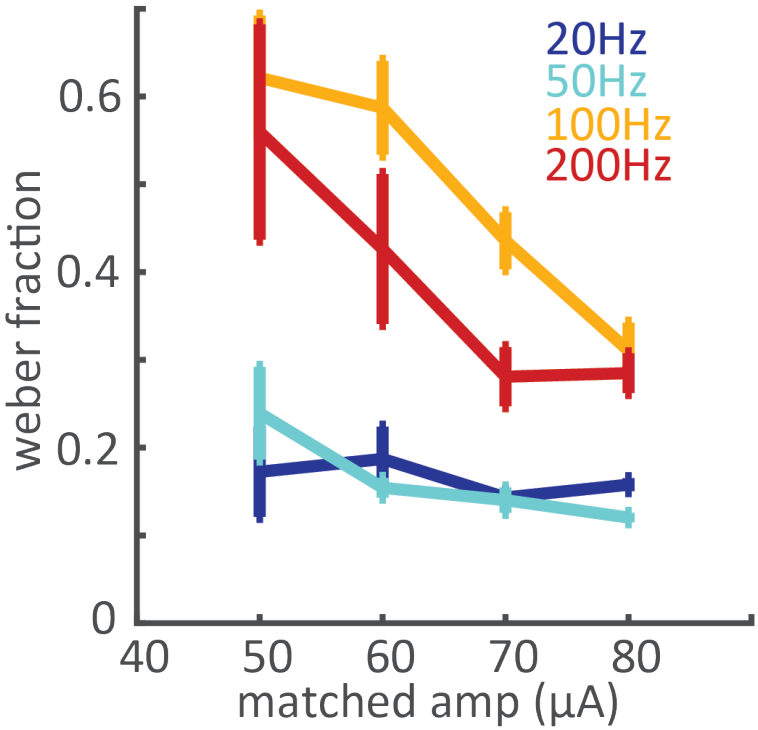

Figure F.1: Weber fraction as a function of amplitude. Performance at each standard frequency is shown in a different color. Error bars show the standard error of the mean across the extensively tested electrodes from the three monkeys (2 electrodes from monkeys A and B for the 20-Hz standard, 5 from monkeys A and B for the 50- and 200-Hz standards, 8 electrodes the three monkeys for the 100-Hz standard). Weber fractions were independent of amplitude in the lower frequency range, but decreased with amplitude for frequencies above 100 Hz.

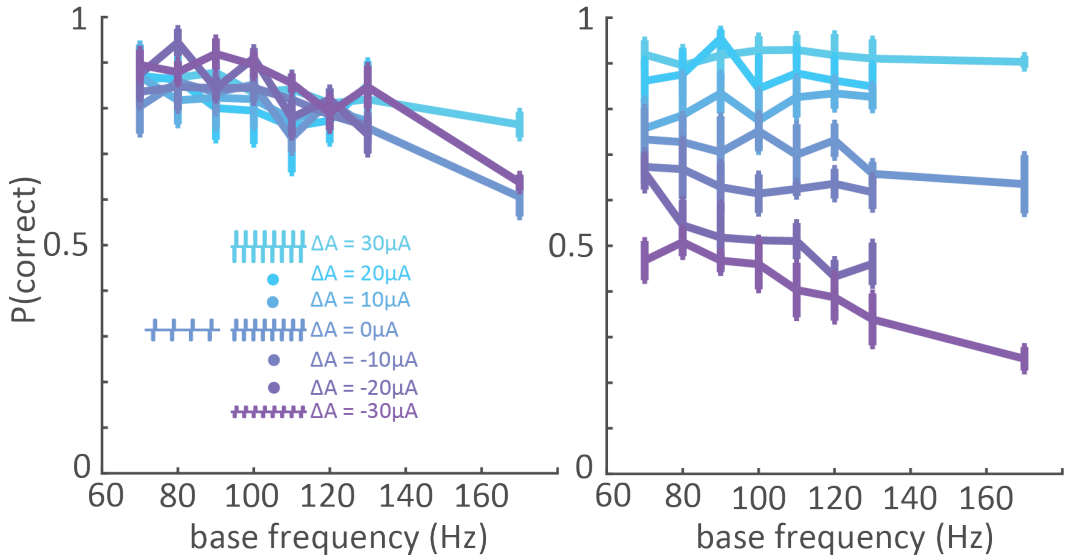

Figure F.2: Wide range of amplitude biases. Frequency discrimination performance as a function of base frequency for the 4 electrodes with the lowest spread (averaged across 4 electrodes) and the 4 electrodes with the greatest spread (average across 4 electrodes). The difference between base and comparison frequencies was always 100 Hz. Performance decreased slightly at higher frequencies, as expected. Error bars show the standard error of the mean across electrodes.

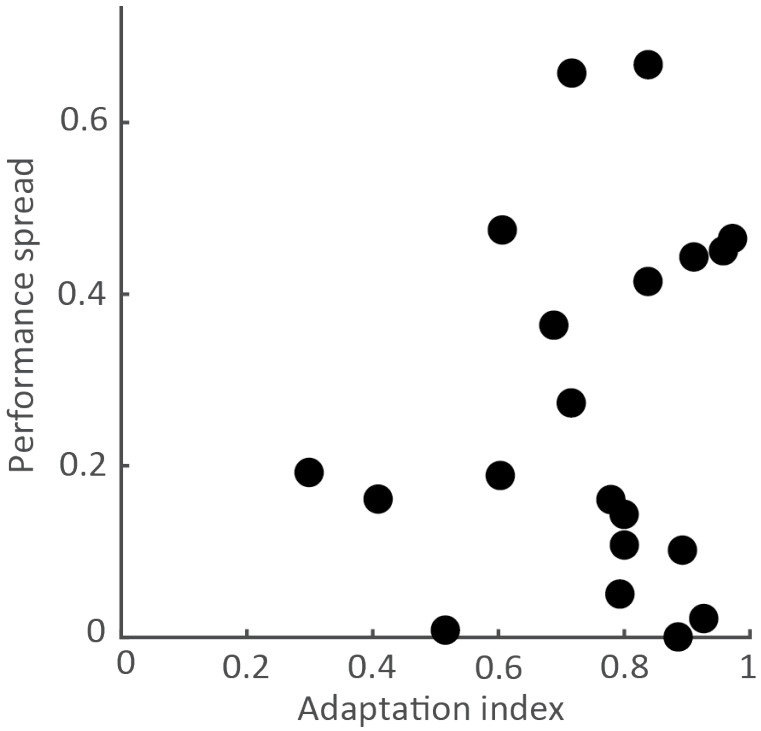

Figure F.3: Susceptibility to amplitude differences vs. adaptation index. Susceptibility is gauged by the difference in performances at the two amplitude difference extrema (purple and cyan in Fig. 3.4). A lower spread indicates a greater ability to distinguish the effects of frequency and amplitude. There is no apparent relationship between performance at an electrode and the adaptation properties of the corresponding neural response (how "RA-like" it is). Adaptation index values could only be computed for 20 of the 25 electrodes shown in Fig. 3.4 because the signal quality was too poor at the other 5 electrodes to record the responses of neurons.

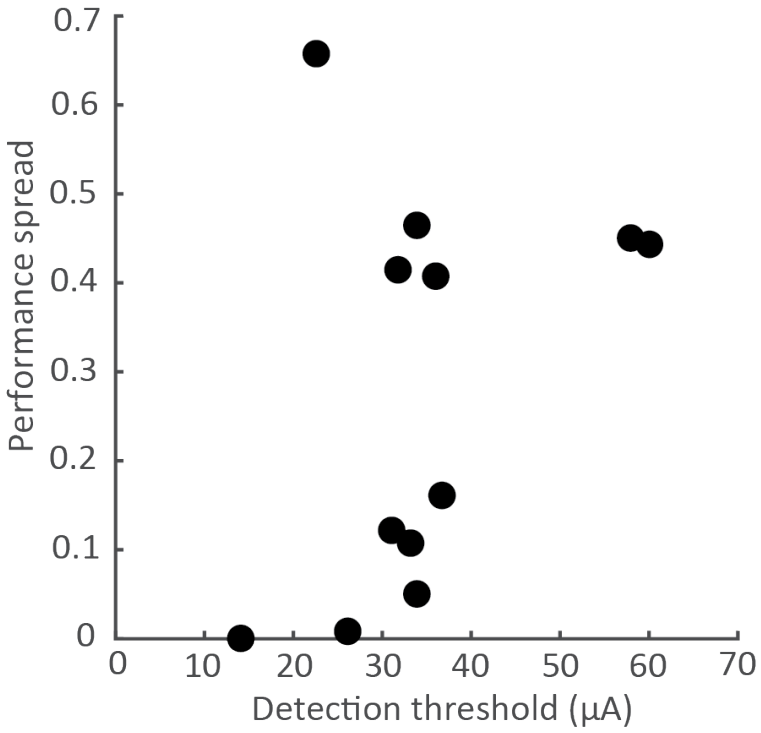

Figure F.4: Susceptibility to amplitude differences in the frequency discrimination task vs. detection threshold (measured at 100-Hz). The threshold is the minimum amplitude at which the animal detects the stimulus 75% of the time. Animals performed the detection task after all frequency discrimination experiments were complete to avoid any confusion due to task changes. The detection task was performed for 12 electrodes of the 25 electrodes shown in Fig. 3.4, 6 of which were selected from among low-spread electrodes (left side Fig. 3.4) and 6 of which were selected from among high-spread electrodes (right side).

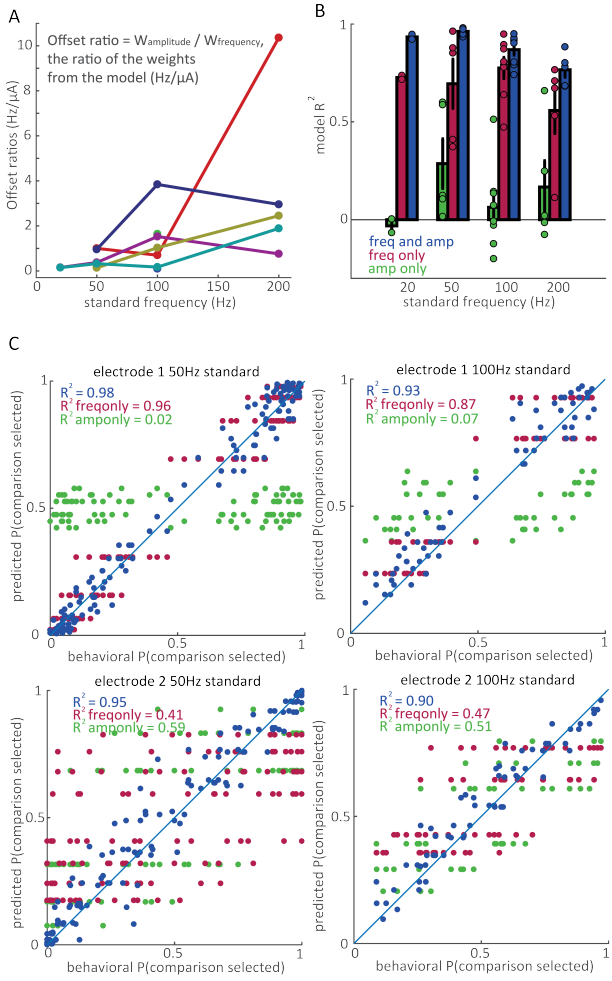

Figure F.5: Contribution of frequency and amplitude to frequency discrimination performance. A— Slopes of equivalent frequency-amplitude tradeoffs (the number of Hz equivalent to a 1μA change), derived from the model fit, for each standard frequency. We refer to these slopes as offset ratios. Different colors denote different electrodes. B— Goodness of fit of the model (R2 = 1 - RSS/TSS, where RSS is the residual sum of squares and TSS is the total sum of squares) when using amplitude only (green), frequency only (red), or both (blue) as predictors. Bars denote the mean R2, error bars the standard error of the mean and dots the value for individual electrodes. C— For the same two electrodes and standard frequencies shown in Fig. 3.3, model predictions for each unique stimulus pair vs. actual performance. Amplitude dominated the animal's choices on the bottom electrode to the point that the reconstruction using amplitude only is superior to the reconstruction using frequency only.

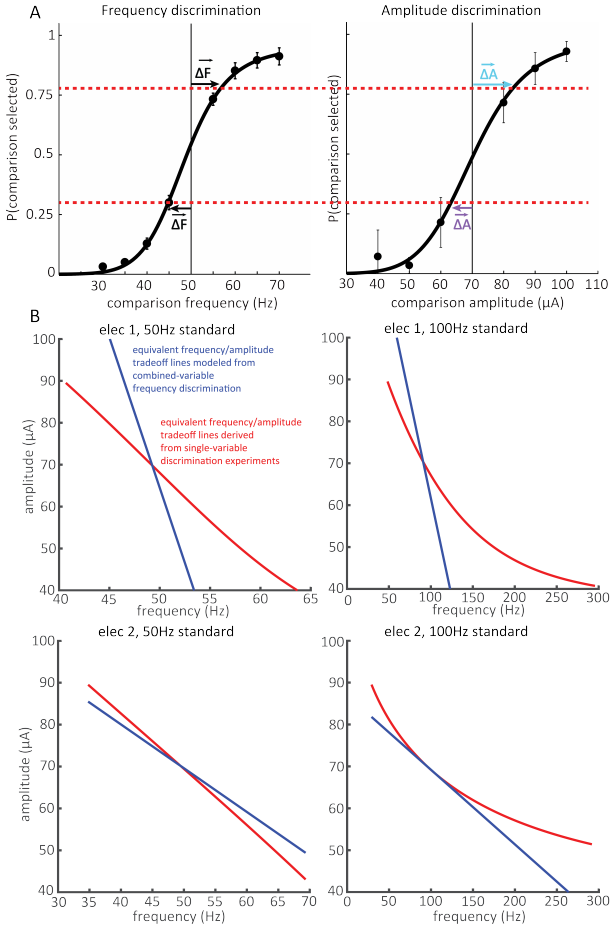

Figure F.6: disentangling frequency and amplitude. A— Construction of iso-intensity lines from single-variable discrimination experiments (see Generating equivalent frequency-amplitude tradeoffs using single-variable discrimination in methods). Frequency differences in a frequency discrimination task (left) and amplitude differences in an amplitude discrimination task (right) that yield the same discrimination performance are used to obtain perceptual equivalence (red, below). Note that this methodology assumes that differences in amplitude and frequency affect the percept along the same sensory continuum. B— For the two electrodes and standards in Fig. 3.3, equivalence lines were derived from single-variable discrimination (red) and from the full stimulus (blue, see Fig. F.5). At the standard stimulus, the equivalence line predicted from the single-variable experiments has a very different slope than observed equivalence relationship (blue) for electrode 1, but not for electrode 2. The relative importance of frequency is much greater for electrode 1 than what could be expected from the single-variable experiment, indicating that amplitude and frequency affect the elicited sensation along different perceptual axes.

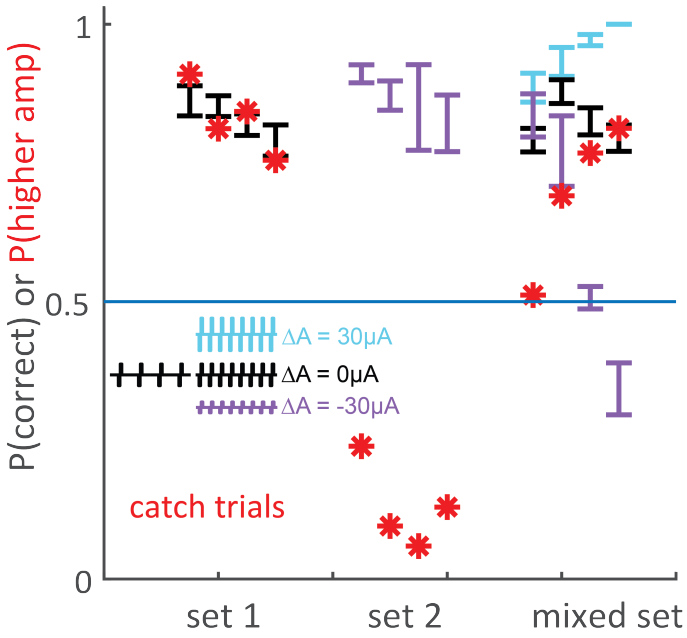

Figure F.7: Catch trials betray the animal's reliance on sensory magnitude. For four electrodes, p(correct) in the frequency discrimination task when amplitudes are matched (subset 1, black), when the higher frequency always has a lower amplitude (subset 2, purple), or when the full set is used (mixed subset, only the -30, 0, and 30 microamp differences are shown for the sake of clarity). The ordering of the four electrodes remains the same in each stimulus set. Two of the selected electrodes had low amplitude-related performance spreads and two had higher ones (as can be seen in the mixed set results in this figure). Red asterisks for each electrode in each condition denote the probability of selecting the higher amplitude on catch trials in which stimulus frequencies were equal (so the frequency discrimination task had no correct answer). Catch trials represented less than 5% of total trials in each condition. The probability of selecting the higher amplitude on catch trials was well above 50% for all four electrodes when the animal was trained on the first stimulus set (in which both stimuli always have equal amplitudes in non-catch trials), indicating that the animal was biased toward selecting the more intense stimulus. This is consistent with perceived intensity increasing with increases in frequency. The probability of selecting the higher amplitude on catch trials was well below 50% for all four electrodes when the animal was trained on the second stimulus set (in which the higher frequency always has much lower amplitude on non-catch trials), indicating that the animal was biased toward selecting the less intense stimulus. This suggests that the amplitude difference of 30 μA was sufficient to ensure that the higher-frequency stimulus was the less intense one. The mixed stimulus set therefore contained some trials in which the higher frequency stimulus was more intense, and some trials in which the higher frequency stimulus was less intense, randomly interleaved. To perform well on both types of trials, the animal could not rely on intensity as it could with the first two stimulus sets. On the first electrode in the mixed set, the animal could reliably select the higher frequency stimulus whether it had the higher or lower amplitude, yet the catch trial results indicate the animal's decisions were not biased toward higher or lower intensities. The animal therefore must have been using a non-intensive cue to perform the task. The number of catch trials performed at each electrode and in each condition ranged from 84 to 152. Error bars show the standard error of the mean across training blocks.

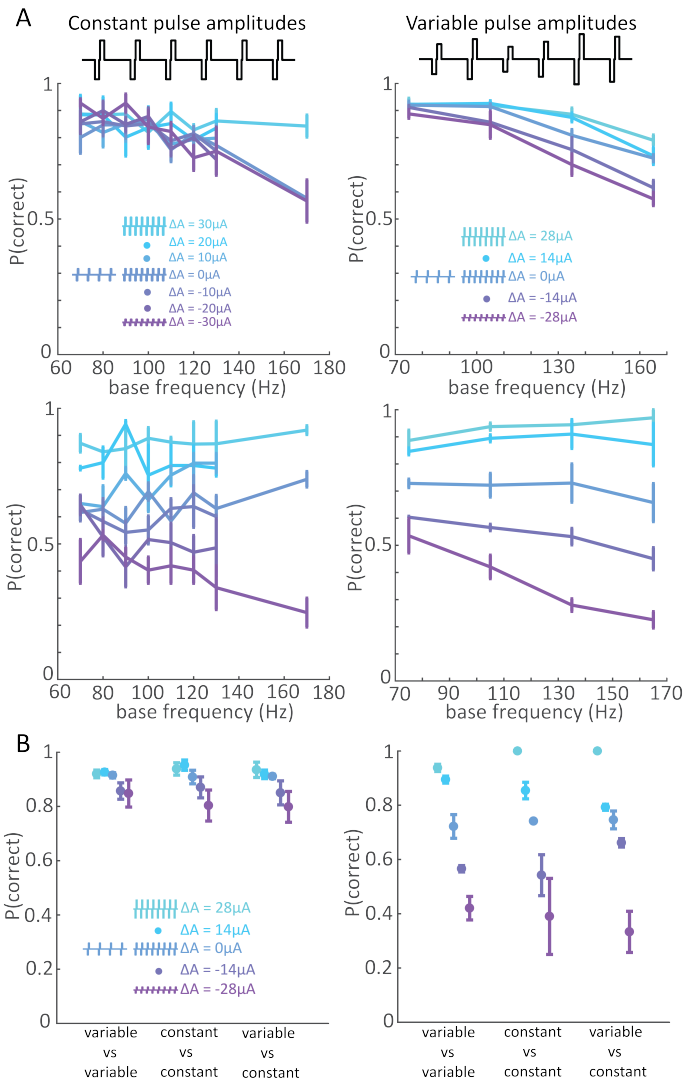

Figure F.8: Varying individual pulse amplitude has a negligible effect on frequency discrimination performance. This figure extends Fig. 3.6. A— Monkey B's performance vs. base frequency in the constant-amplitude experiment (left column) and the variable-amplitude experiment (right column) for the 4 electrodes with weak amplitude bias (top row) and the 2 electrodes with strong amplitude bias (bottom row). The frequency difference was always 100 Hz for the constant-amplitude experiment and 90 Hz for the variable-amplitude experiment due to hardware constraints (see Methods). B— Performance when stimulus pulse trains were both variable-amplitude, were split, or were both constant-amplitude, for the 4 electrodes with weak amplitude bias (left) and the two with strong amplitude bias (right). Changing the spatial distribution of the ICMS-induced activity on a pulse-by-pulse basis had little to no effect on the animal's ability to discriminate frequency. The top right panel in A and the left panel in B are taken from Fig. 3.6. Error bars in A and B show the standard error of the mean across electrodes.

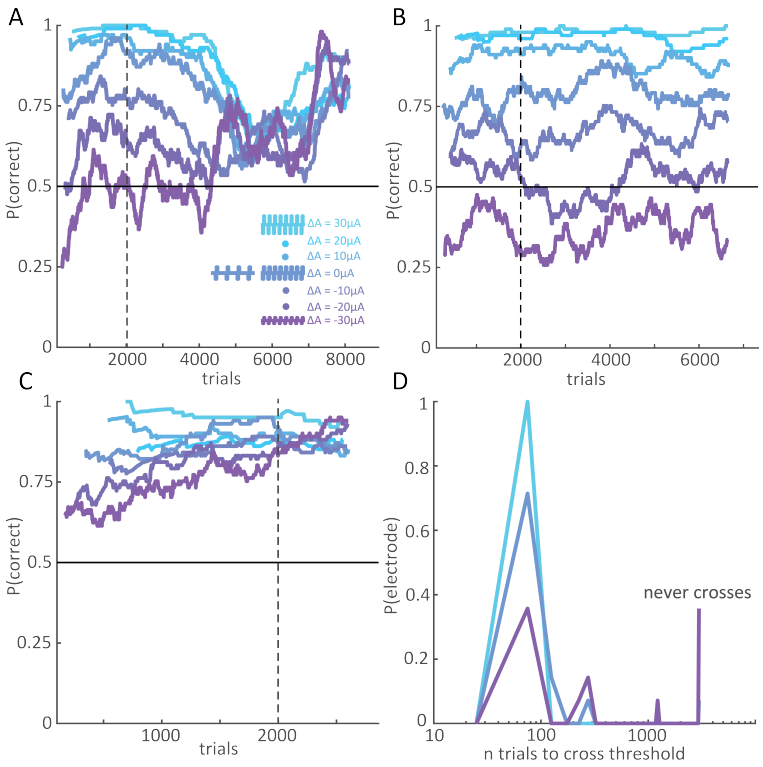

Figure F.9: Learning rate. A— Performance over time for an electrode at which the monkey first relied on intensity before learning to judge frequency independently. B— Example of an electrode at which the animal continued to rely on intensity. C— Example of an electrode at which the animal immediately performed well at all amplitude differences. D— Probability histogram of the number of trials of each condition required to achieve performance above a 75% threshold at amplitude differences of -30, 0, and 30 μA (for the 17 electrodes tested with the reduced stimulus set). When amplitudes were matched or the higher frequency had a higher amplitude, performance was above threshold immediately for all electrodes. When the lower frequency had a higher amplitude, at the vast majority of electrodes performance was either above threshold after little training, or never reached threshold. There were only a few electrodes for which performance in this condition was initially low but eventually met criterion performance.